SYNTHESIS OF POLYOLEFINS WITH CONTROLLED DISTRIBUTIONS OF MOLECULAR WEIGHT AND CHEMICAL COMPOSITION BY SELECTIVE COMBINATION OF SUPPORTED METALLOCENE / MAO CATALYSTS

by

Jung Dae Kim

A thesis
presented to the University of Waterloo
in fulfillment of the
thesis requirement for the degree of
Doctor of Philosophy
in
Chemical Engineering

Waterloo, Ontario, Canada, 1999

The University of Waterloo requires the signatures of all person using or photocopying this thesis. Please sign below, and give address and date.

ABSTRACT

The mechanical and physical properties of polyolefins are closely correlated to their chemical composition distributions (CCD) and molecular weight distributions (MWD). Until recently, control of these distributions was difficult due to the limitations involved with conventional polyolefin catalyst such as Ziegler-Natta catalysts. However, with the aid of the new metallocene catalysts, these microstructural distributions can now be customized to fit the requirements of several polymer applications. In this thesis, the MWD of polyethylene and the CCD-MWD of poly(ethylene-co-1-hexene) were customized through the selective combination of metallocene catalysts immobilized on a single silica support.

For the case of homopolymers, the MWDs of polyethylenes produced with combined catalysts were represented as the superposition of the MWDs of polymers produced with individually supported catalysts. It was shown that the bimodal MWDs could be deconvoluted into two Flory's most probable distributions with polydispersity indexes of two for each peak. It was found that the molecular weight of polyethylene produced with $Et[Ind]_2ZrCl_2$ did not change with increasing ethylene pressure or hydrogen concentration in the reactor when ethylene pressure was higher than approximately 100 psi at polymerization temperatures of 40 and 50 °C. When lower ethylene pressures were used, the molecular weight of polyethylene produced with $Et[Ind]_2ZrCl_2$ decreased with increasing hydrogen concentration. Surprisingly, the molecular weights also decreased with increasing ethylene pressure up to 100 psi in the absence of hydrogen.

This behavior provided easy ways of controlling MWD of polyethylene produced with bimetallic supported catalysts, when $Et[Ind]_2ZrCl_2$ was combined with other metallocene catalysts. The supported catalyst obtained by the combination of $Et[Ind]_2ZrCl_2$ and Cp_2HfCl_2 was able to produce polyethylene with MWDs ranging from broad and bimodal to narrow and unimodal by simply changing ethylene pressure or hydrogen concentration.

For the case of copolymers, it was shown that some supported metallocenes could produce polymers with broad and/or bimodal CCDs depending on the method involved in the

treatment of the inert carrier. Before this research, the effect of support treatment on polyolefin microstructure was mainly concentrated on MWD.

The trends observed in homopolymerization for the influence of polymerization conditions on the MWD were also observed in copolymerization, i.e. the MWD of copolymers produced with $Et[Ind]_2ZrCl_2$ showed the least sensitivity toward polymerization conditions. It was demonstrated that control of CCD and MWD could be simultaneously achieved to produce the kind of copolymers that are only made by reactor cascade technology when Ziegler-Natta catalysts are used.

Finally, a mathematical model was developed to provide useful insights on phenomena happening at microparticle levels, some of which cannot be observed directly. According to the model, the broadening of MWD or CCD seemed to be caused by the presence of multiple active site types rather than mass or heat transfer resistances. However, if the polymerization time is too short or the ratio of polymerization rate to diffusion rate of monomer in the catalyst particle is very large, mass transfer resistances can further broaden the distributions.

Acknowledgements

I would like to express my sincere gratitude to Professor João B. P. Soares for his guidance during the course of this work. Working with him was such a pleasure and I was greatly encouraged whenever we had discussions about a new result. Even though it might have been an insignificant discovery, he always maintained his curiosity and never failed to find something positive in it. Special thanks go to Ms. Maria Soares for preparing the wonderful occasional get-togethers.

I would like to thank Professor Garry L. Rempel for his support during this work. It was my special privilege as his student to have access to vast resources built over many years. Without them, I would not have been able to present many of the interesting results in this work.

Thanks are due to Luigi D'Agnillo, Daryoosh Beigzadeh, Catherine Cho, Colin Li, Karen Xiao, Deborah Sarzotti, and William Ripmeester for their interest in my research, support, encouragement, and friendship.

My sincere appreciation goes to my parents for their continuous support and ever increasing love.

Finally, I thank God for the awesome opportunity to study here in Waterloo toward my Ph.D. degree and for His never ending love and guidance. I also thank God for the precious gift of providing my beloved half, Sonia Clara Yoon. Support from her family during this study is also greatly appreciated.

The Spirit of the Sovereign Lord is on me,
because the Lord has anointed me
to preach good news to the poor.
He has sent me to bind up the brokenhearted,
to proclaim the year of the Lord's favor
and the day of vengeance of our God,
to comfort all who mourn,
and provide for those who grieve in Zion –
to bestow on them a crown of beauty
instead of ashes,
the oil of gladness instead of mourning
and a garment of praise instead of a spirit of despair.

Isaiah 61 : 1-3

TABLE OF CONTENTS

LIST OF TABLES

LIST OF FIGURES

CHAPTER 1
INTRODUCTION

1.1. BACKGROUND

The discovery of Ziegler-Natta catalysts in 1953 revolutionized the industry of polyolefin manufacture. Before Ziegler-Natta catalysts, linear high density polyethylene (HDPE) could only be made with Phillips catalysts. With Ziegler-Natta catalysts, the density and physical properties of polyethylene resins could be controlled better by copolymerizing ethylene with α-olefins. As a consequence, structure-property relationships in polyolefins attracted a lot of interest from academic and industrial researchers.

However, one of the disadvantages of Ziegler-Natta catalysts used for the commercial production of polyolefins is that they have several types of active sites that produce polymers with different average properties. It is very difficult to control the behavior of these sites separately. Polyolefins made with heterogeneous Ziegler-Natta catalysts have broad distributions of molecular weight (MWD) and chemical composition (CCD), and typically the shorter chains also have higher comonomer content.

Tandem reactor polymerization technology is used to overcome the behavior of heterogeneous Ziegler-Natta catalysts. In this method, two or more polymerization reactors are used in series to produce polyolefins with bimodal MWD and/or CCD. In a typical two-reactor cascade system, high molecular weight copolymer is produced in the first reactor in the absence of a chain transfer agent. The polymer is transferred to the second reactor where polymerization takes place in the presence of hydrogen, which is a commonly used chain transfer agent, to produce lower molecular weight homopolymer chains. The polyethylene produced with this technology has bimodal MWD with higher comonomer content in the high molecular weight chains. As a consequence, this polymer has the strength and stiffness of high-density polyethylene, while retaining the high stress crack resistance and processability of unimodal medium-density grades. However, reactor cascade technologies can be costly and the polymers produced by this technique may still need to be further homogenized.

The discovery of metallocene catalysts in the early 1980's once more revolutionized the polyolefin manufacture industry. These high-activity, single site catalysts are capable of producing polyolefins with well-controlled and uniform microstructures. This opens the doors to the production of polyolefins with entirely new and/or improved properties through microstructure control of the polymers. From the understanding of individual metallocene catalysts, the control of polymer microstructure might be possible by combination of different metallocenes onto a single support. If microstructures of polymers can be precisely controlled by a mixed metallocene catalyst, a variety of polymer resins can be produced to attend different applications at a reduced cost.

1.2. OBJECTIVES OF THE RESEARCH

The main objective of this research is to find new practical and versatile methods of customizing the microstructures of polyolefins made with metallocenes in a single reactor.

This thesis investigated several factors that influence both MWD and CCD of polyethylene and poly(ethylene-co-1-hexene) produced with bimetallic supported metallocene catalysts. It will be shown that differences in catalyst activation energy and chain transfer mechanisms, catalyst geometry, and polymerization rates determine how to combine metallocene catalysts to control MWD and CCD of polyolefins.

1.3. THESIS OUTLINE

Chapter 1 presents background information on olefin polymerization and the need for improved microstructural control in polyolefins

Chapter 2 reviews the literature on Ziegler-Natta catalysts, metallocene catalysts, polyolefin characterization methods, and mathematical modeling.

Chapter 3 describes the experimental methods used for polymerization and polymer characterization.

In Chapter 4, experimental results from ethylene homopolymerization using supported bimetallic metallocene catalysts are presented. Different ways of controlling MWDs and the effectiveness of these methods are demonstrated. The effects of polymerization conditions on MWD of the produced polymers, such as polymerization temperature and pressure, impurities, and chain transfer agents are investigated.

Chapter 5 is devoted to the investigation of the effects of catalyst support treatments on polymer properties by using various supports obtained from different sources or treated in different ways.

In Chapter 6, experimental results from the copolymerization of ethylene and 1-hexene are discussed. Some polymerization conditions can affect both MWD and CCD. Therefore, the effects of different polymerization conditions on the distributions of molecular weight and chemical composition are investigated in two levels of polymerization temperatures, four levels of ethylene pressures, and five levels of hydrogen concentrations. Fractionation results of industrial polymers obtained by preparative CRYSTAF are also discussed to study the correlation between microstructure of polymer chains and environmental stress crack resistance. Finally, a Monte-Carlo simulation was conducted to visualize the process of customizing MWD and CCD of copolymer by catalyst combination technology.

In Chapter 7, a mathematical model of ethylene and propylene copolymerization in a supported catalyst system is described. The model used is based on the multigrain polymerization model, and is able to deal with the multiplicity of the catalyst active site types, homo- and copolymerizations, inter- and intraparticle mass transfer resistances.

Finally, Chapter 8 presents the most significant contributions of this research and makes some recommendations for future work.

CHAPTER 2
LITERATURE REVIEW

2.1. BACKGROUND ON POLYOLEFIN CATALYSTS

Polyolefins can be produced by free-radical initiators, Phillips type catalysts, and Ziegler-Natta catalysts. Ziegler-Natta catalyst systems have been used most widely because of their broad range of applications.

2.1.1. Catalyst Structure

Ziegler-Natta catalysts can be used either in homogeneous, heterogeneous, or sometimes in colloidal forms. In heterogeneous system, polymers with different morphologies can be produced with a single supported catalyst, either by changing process conditions or by chemical modification of the catalyst (Wagner and Karol, 1989). The two components involved in conventional heterogeneous Ziegler-Natta catalyst are a transition metal-containing component and a support. Typical components which contains the transition metal are $TiCl_4$, $Ti(OR)_4$, or $VOCl_3$. $MgCl_2$, Mg(OH)Cl, and polymers with functional groups such as OH, COOH, etc. are used as support that might form bonds with the active sites. Some other supports, such as silica and polyethylene (PE), will not chemically interact with the active species. $MgCl_2$ or a functionalized polymer can serve both as an anchor for chemical bonding and an inert carrier (Nowlin *et al.*, 1988).

Metallocene catalysts, which are a new class of Ziegler-Natta catalyst systems, have the ability to produce polymer having narrower distributions of molecular weight (MWD) and chemical composition (CCD) than the ones produced with heterogeneous Ziegler-Natta catalysts. The general structure of metallocene catalysts is shown in Fig. 2.1.

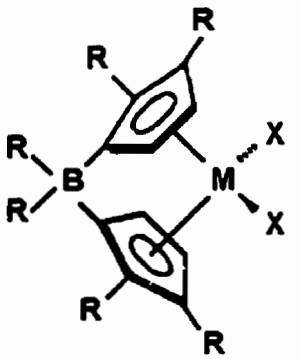

Figure 2.1 General structure of metallocene catalysts : B – bridge, R – alkyl group, M – metal center, X – halogen group

Common structures of rings include cyclopentadienyl, indenyl, and fluorenyl. Some metallocene catalysts have only a single ring, a metal center, and halogen groups. Constrained geometry catalysts are good examples of this type of catalyst. However, in most cases, metallocenes have two identical rings or combination of different types of rings. These two-ring metallocene catalysts can be further divided into bridged and unbridged. Ethylene or silanediyl bridges are most commonly found in the literature.

2.1.2. Polymerization Mechanism

The mechanism of catalyst activation is not fully understood. However, alkylation and reduction of the metal site by a cocatalyst (generally alkylaluminum or alkylaluminoxane) is believed to generate the active catalyst species. The initiation reaction takes place between the newly formed active species and a monomer unit to form a polymer chain with chain length one.

Propagation proceeds by coordination and insertion of new monomer units in the metal-carbon bond. The Cossee mechanism is still one of the most generally accepted polymerization mechanisms (Boor, 1979). In this mechanism, the polymer chain grows in two distinct steps. In the first step, monomer will form a complex with the vacant coordination site at the active catalyst center. Then through a four-point transition complex, bonds between the

monomer and metal center and between monomer and polymer chain are formed, increasing the length of the polymer chain by one monomer unit and generating another vacant site.

The trigger mechanism has been recently proposed for Ziegler-Natta and metallocene polymerization (Ystenes, 1993). In this model, two monomers interact with one active catalytic center in the transition state. A second monomer is required to form a new complex with the existing catalyst-monomer complex, thus triggering a chain propagation step. No vacant site is involved in this model. The trigger mechanism has been used to explain the rate enhancement effect observed when ethylene is copolymerized with α-olefins.

Finally, dead polymer chains can be formed by 1) β- hydride elimination, 2) transfer to monomer, 3) catalyst deactivation, 4) transfer to cocatalyst, and 5) transfer to chain transfer agents and impurities. The first two transfer reactions will form dead polymer chains containing terminal double bonds.

2.1.3. Cocatalysts

Both metallocene and Ziegler-Natta catalysts need to be activated by a cocatalyst. The most common types of cocatalysts are alkylalumiums including methylaluminoxane (MAO), triethylaluminum (TEA), trimethylaluminum (TMA), triisobutylaluminum (TIBA), and cation forming agents such as $(C_6H_5)_3C^-(C_6F_5)_4B^-$ and $B(C_6F_5)_3$. Among these, MAO is a very effective cocatalyst for metallocenes. However, due to the difficulties and costs involved in the synthesis of MAO, there has been considerable effort done to reduce or eliminate the use of MAO. Due to difficulties in separation, most commercially available MAO contains a significant fraction of TMA (about 10 – 30 %). Eisch *et al.* (1994) found that this TMA in MAO could substantially be eliminated by toluene-evaporations at 25 °C.

Cam and Giannini (1992) investigated the role of TMA present in MAO by a direct analysis of Cp_2ZrCl_2/MAO solution in toluene-d8 using ^{1}H-NMR. Their observation indicated that TMA might be the major alkylation agent and that MAO acted mainly as a polarizing agent. However, in general it is believed that MAO is the key cocatalyst in polymerizations involving metallocene catalysts. The role of MAO includes 1) alkylation of metallocene, thus

forming active catalyst species, 2) scavenging impurities, 3) stabilizing the cationic center by an ion-pair interaction, and 4) possibly the prevention of bimetallic deactivation of the active species.

A study of ion-pairs based on solvent polarity, temperature, and strength of Lewis acidity was conducted through combination of temperature-dependent multinuclear NMR, electrical conductivity measurements and polymerization activity assessments by Eisch *et al.* (1994). Higher polarity of solvent and higher dilution favored solvent-separated ion-pair, which is more active but less stereoselective in syndiotactic polymerization compared to its contact ion-pair isomer. The effects of temperature (above a threshold temperature) and Lewis acidity were relatively insignificant.

In general, homogeneous metallocene catalyst cannot be activated by common trialkylaluminiums only. However, Soga *et al.* (1993) were able to produce polyethylene with modified homogeneous Cp_2ZrCl_2 activated by common trialkylaluminiums in the presence of $Si(CH_2)_2OH$. Their results show that for an 'optimum' yield, aging of the catalyst and $Si(CH_2)_2OH$ mixture for four hours is required. However, MWD of the produced polymer is bimodal although the polymers obtained in the presence of MAO have a narrow MWD.

Chien *et al.* (1994) investigated propylene polymerization with $Et[Ind]_2Zr(CH_3)_2$ using $(C_6H_5)_3C^+(C_6F_5)_4B^-$ and $(C_6F_5)_3B$ as cocatalysts. TEA was also added in some cases to the polymerization system. Higher activity and stereoselectivity was obtained when the active site was formed with $(C_6F_5)_4B^-$ counter-ion. It was suggested that the relatively lower activities of the catalysts, when other cocatalysts were used, are due to the impurities and that TEA can scavenge them without adverse effects on polymerization rate and product quality. However, for some other metallocenes, additional TEA can form a different catalyst active species that will produce polymer chains with different microstructures.

Michiels and Munoz-Escalona (1995) mixed TEA, TIBA, and $B(C_6F_5)_3$ with MAO to find a correlation between the composition of mixed cocatalysts, polymerization activity, and the molecular weight of polymer produced. It was shown that TMA/MAO system has a local maximum in activity when the ratio is around 0.3-0.5 (mole/mole). The addition of TEA or TIBA to MAO reduced the polymerization activity. The molecular weight was decreased with

increasing ratio of AlR_3/MAO, however, for the case of $B(C_6F_5)_3$, the effect was less significant.

Ethylene/α-olefins copolymers with bimodal CCD were produced with homogeneous Cp_2ZrCl_2 with different cocatalysts such as MAO and mixture of TEA/borate or TIBA/borate (Katayama *et al.*, 1995). It seemed that the active species generated with different cocatalysts have different activities and produce polymers with different molecular weights.

Barron (1995) related the cocatalyst activity to ion-pair complex formation in Cp_2ZrMe_2 catalyzed ethylene polymerizations. They compared $[(^tBu)_2Al\{OAl(^tBu)_2\}]_2$ to $[(^tBu)AlO]_n$ (n=6, 7, 8, 9). Only the closed cage compound $[(^tBu)AlO]_n$ reacted reversibly with Cp_2ZrMe_2 to form the ion pair complex $[Cp_2ZrMe][(^tBu)_6Al_6O_6Me]$, which is active for ethylene polymerization.

The reactions of tetraalkyldialumoxanes $(R_2Al\text{-}O\text{-}AlR_2)_n$ or alkylalumoxane $(AlOR)_n$ with acetylacetone, alcohols, and electron donors such as ethers, amines, nitriles are discussed by Pasynkiewicz (1995). The structure of alumoxanes depends on many parameters such as kind of ligands, synthetic conditions including solvent types, reaction temperature, molar ratio of reactants, methods of isolation, etc. Even though there has been numerous studies, the structures of aluminoxanes are still not clear.

Some efforts were made to substitute MAO with other non-coordinating, bulky counter anions or some inorganic components exhibiting Lewis acidity. Soga *et al.* (1995a) used heteropolyacids ($H_3[PMo_{12}O_{40}]$ and $H_5[PMo_{10}V_2O_{40}]$) as the counter-anion and were able to produce polyethylene without use of MAO. However, the polymers exhibited very broad molecular weight distributions (PDI: 10 – 44).

Naga and Mizunuma (1997) demonstrated how the mixtures of MAO and TEA/$Ph_3CB(C_6F_5)_4$ vs. TIBA/ $Ph_3CB(C_6F_5)_4$ can affect the ratios of polymerization rates between rac- and meso-dimethylsilylenebis(2,3,5-trimethylcyclopentadienyl)zirconium dichloride used in α-olefin polymerization.

A general review on homogeneous metallocene-methylaluminoxane catalyst system for ethylene polymerization can be found in Reddy and Sivaram (1995).

2.1.4. Catalyst Activity

Cihlar *et al.* (1978, 1980) used $Cp_2TiEtCl/AlEtCl_2$ and $Cp_2TiEtCl/(AlEtCl_2 + H_2O)$ for ethylene polymerization. The hydrolyzed $AlEtCl_2$ cocatalyst, due to the formation of aluminoxane, increased the rate of polymerization. The polymerization rate showed a stationary period at the beginning of the polymerization when $AlEtCl_2$ was used as a cocatalyst. However, when the hydrolyzed $AlEtCl_2$ was used as a cocatalyst, a maximum rate was observed immediately upon the start of polymerizations. When the ratio of $H_2O/AlEtCl_2$ was around 0.5, the number average molecular weight of polyethylene was 70 times greater than that of polyethylene produced without H_2O. The use of hydrolyzed cocatalyst enhanced the propagation rate drastically. The $H_2O/AlEtCl_2$ ratio influenced the shape of MWD and even produced bimodal MWD. A possible explanation is the co-existence of $Cp_2TiEtCl/AlEtCl_2$ and $Cp_2TiEtCl$/aluminoxane catalytic sites. Each site type may produce polymers with different average properties.

Lee *et al.* (1992) investigated the electronic effects of ligand substitution in metallocene catalysts for ethylene and propylene polymerization using $(\eta^5\text{-}5,6\text{-}X_2C_9H_5)_2ZrCl_2$ /MAO (X = H, CH_3, OCH_3, or Cl). The produced polymers showed differences in molecular weight and stereorigidity. It was found that electron-withdrawing substituents on the indenyl ring decreased both polymer molecular weight and catalyst activity during ethylene polymerization. For propylene polymerization, an increase in electron density at the metal center of the catalyst decreased the stereoselectivity. The ethylene-bridged catalysts produced lower molecular weight polymers compared to their non-bridged counterparts, but the catalytic activity remained unaffected for ethylene polymerization. For propylene polymerization, both molecular weight and catalytic activity were not affected significantly by using the ethylene-bridged catalysts. It was speculated that the different interactions between catalyst and aluminoxane might affect the molecular weights and stereoselectivity.

Siedle *et al.* (1993) studied the role of non-coordinating anions in homogeneous olefin polymerization where the catalyst form metallocenium ion, such as Cp_2ZrMe^+, produced by equilibrium or irreversible CH_2^- transfer. The molecular weights of polymers produced with different catalysts were correlated to metal-carbon bond enthalpies as well as the ligand steric

and electronic effects. For instance, the molecular weight of polymer produced with zirconocene is lower than that of polymer produced with its counterpart hafnocene due to lower metal-carbon bond enthalpy for zirconocene.

Fierro *et al.* (1994) synthesized an asymmetric precursor, anti-rac-ethylidene-(1-μ^5-2,3,4,5-tetramethylcyclopentadienyl)(1-μ^5-indenyl)dichlorotitanium and dimethyl derivatives to investigate the ligand effect on polymer kinetics. The synthesized catalysts showed poor activities compared to the simple Cp_2ZrCl_2/MAO. However, the produced polypropylene (PP) exhibited excellent thermo-plastic elastomeric properties, attributable to micro-phase separation of stereo-regular and stereo-irregular blocks into crystalline and amorphous domains.

Ciardelli *et al.* (1994) studied the effect of ligand type for Ti- and Zr-centered metallocene catalysts on polymerization activity. Depending on ligand types and cocatalysts, the activity varied from 0.1 to 372 kg PE/g metal atom/h.

Janiak *et al.* (1994) used zirconium beta-diketonate/MAO systems for ethylene polymerization. The polymers produced by this system were compared with the polymers produced with Cp_2ZrCl_2/MAO in terms of the weight- and number-average molecular weights, and polydispersity index (PDI). The zirconium beta-diketonate/MAO system showed lower catalytic activity compared to Cp_2ZrCl_2/MAO. However, when MAO was partially replaced by TMA, a significant increase in the catalytic activity was observed. However, TMA alone could not activate the catalyst. The polymers produced with zirconium beta-diketonate/MAO systems had significantly higher molecular weights, and the PDI values were similar to the values obtained from the polymers produced by Cp_2ZrCl_2/MAO system. No clear explanation on the increased catalytic activity in the presence of TMA was presented.

Rieger and Janiak (1994) presented quantitative analysis on the effects of MAO, Zr, and TMA concentrations on the catalysts activity and molecular weight of polyethylene. It was found that the addition of TMA ($Al_{MAO}/Al_{TMA} \cong 1.4$) at moderate concentrations of Zr (10^{-5} ~ 10^{-4} mol/L) in solution polymerization could drastically reduce the required MAO concentration ($Al_{MAO}/Zr < 1000$).

Jüngline *et al.* (1995) compared Me_2Si(Benz[e]Indenyl)$_2ZrCl_2$/MAO (BI) and Me_2Si(2-Me-Benz[e]Indenyl)$_2ZrCl_2$/MAO (MBI) for propene polymerization at 40 °C and 2

bar. At this temperature, BI showed higher activity and produced lower molecular weight polymer. However, at elevated temperatures (higher than 60°C), MBI showed higher activity due to its higher activation energy. When these catalysts are supported together, the shape of the overall molecular weight distribution can be controlled (by changing the reaction temperature) since each catalyst produce polymers with different average molecular weights.

Han *et al.* (1995a) compared the activity of ethylene and propylene polymerization over chiral ansa-dichloro[o-phenylenedimethylenebis(μ^5-1-indenyl)]zirconium (**1**)/MAO. For ethylene polymerization, meso-(**1**)/MAO was more active than rac-(**1**)/MAO. For rac-(**1**)/MAO, the activity increased as the temperature increased. For propylene polymerization, rac-(**1**)/MAO was active, but meso-(**1**)/MAO was almost inactive. Also, for same rac-(**1**)/MAO, the activity decreased as the temperature increased. The authors could not propose a definite explanation for these observations.

Pieters *et al.*(1995) characterized rac-Et[Ind]$_2$ZrCl$_2$/MAO using ultra-violet (UV) spectroscopy to distinguish between active and inactive polymerization sites. This method can easily and economically provide information about the conditions for the synthesized metallocenes to be active. Kaminsky (1995) used a similar UV technique to investigate the polymerization mechanism of $Cp_2Ti(CH_3)_2$/MAO.

Roos *et al.* (1997) showed that a first order model could reasonably describe the deactivation rate as a function of temperature in a gas phase polymerization of ethylene with a silica supported rac-Me_2Si[Ind]$_2$ZrCl$_2$/MAO.

Ban *et al.* (1998) synthesized dinuclear ansa-zirconocene catalysts to improve catalyst stability at higher polymerization temperatures. The new catalysts showed fairly good activities even at 150 °C for ethylene or ethylene/1-octene copolymerization. However, the stability of the catalyst at high temperature could not be estimated because the polymerization time was limited to 2 minutes. Rate-time profiles obtained at 40 °C for the same catalyst show very rapid deactivation at initial stage (up to 10 min. from the start) and a slower deactivation rates at later stage. Therefore, it is possible that the synthesized catalysts may deactivate even more rapidly at high temperatures. Polymerization conducted at 60 °C showed that the meso-dinuclear catalyst has higher activity but produces polymers with lower molecular weights when compared rac-dinuclear catalysts. When a high polymerization temperature was used,

the molecular weights of the polymer decreased drastically. In case of propene polymerization, the activities were poor for all the catalysts compared.

2.1.5. Copolymerization

By adding a small percentage of comonomer to the polymerization reactor, the final polymer characteristics can be dramatically changed. For example, the Unipol process for linear low density polyethylene (LLDPE) uses hexene and the British Petroleum process (BP) uses 4-methylpentene to produce high-performance copolymers. The comonomer can affect the overall crystallinity, melting point, softening range, transparency, and also, structural, thermo-chemical, and rheological properties of the formed polymer. Copolymers can also be used to enhance mechanical properties by improving the miscibility in polymer blending (Albano *et al.*, 1998).

Koivumäki *et al.* (1994) found that small addition of 1-hexene in the ethylene polymerization with Cp_2ZrCl_2/MAO could improve the control of viscosity and heat transfer during the polymerization. It was found that the apparent viscosity of the reaction medium was constant throughout the experiment in the presence of a comonomer. However, for homopolymerization, the viscosity increased significantly during the reaction causing temperature control problems. Since the polymer particles produced in copolymerization were 1/5 times smaller than the particles produced in homopolymerization, a more uniform reaction medium was obtained in copolymerization. If a small amount of comonomer is added at the beginning of polymerization, improved polymerization control could be achieved without altering polymer properties significantly.

Aaltonen and Seppälä (1994) used styrene as a comonomer for ethylene polymerization using $CpTiCl_3$/MAO. Severe composition drift was observed in this system and block copolymer was produced. Styrene did not seem to be a good choice as a comonomer for ethylene with this catalyst, because the reactivity of styrene to ethylene was very low (0.01).

The incorporation of comonomers in polyethylene was greatly improved by the discovery of constrained geometry catalysts. The "openness" of these catalysts allows not only higher content of comonomer incorporation but also allow it to incorporate bulky macro-monomers to the growing polyolefin chains. Depending on comonomer content, constrained geometry catalyst can produce polymers with wide range of applications such as polyolefin plastomers (< 20 wt.-% octene), polyolefin elastomers (> 20 wt.-% octene), high performance polyolefins, and polyethylenes. Characteristics of polymers produced with Dow Chemical Company's Insite® based polymers can be found in Swogger (1994) and Stevens (1994).

The effects of polymerization conditions and molecular structure of the catalyst on ethylene/α-olefin copolymerization have been investigated extensively. Pietikainen and Seppälä (1994) investigated the effect of polymerization temperature on catalyst activity and viscosity average molecular weights for low molecular weight ethylene/propylene copolymers produced with homogeneous Cp_2ZrCl_2. Soga and Kaminaka (1994) compared copolymerizations (ethylene/propylene, ethylene/1-hexene, and proplylen/1-hexene) with $Et[IndH_4]_2ZrCl_2$ supported on SiO_2, Al_2O_3, or $MgCl_2$. Broadness of MWD were found to be related to the combinations of support types and monomers. The effect of silica and magnesium supports on copolymerization characteristics was also investigated by Nowlin *et al.* (1988). Their results indicated that comonomer incorporation was significantly affected by the way the support was treated based on the reactivity ratio estimation calculated with simplified Finemann Ross method. However, it should be noted that Finemann Ross method could be misleading due to linear estimation of nonlinear systems. Giz (1998) developed two new error-in-variable methods (EVM) used for estimation of the reactivity ratios in copolymerization. From their simulation it was shown that even for the new EVM, depending on the range of reactivity ratios, different calculation methods should be used. Because of that, a pre-estimation of the reactivity ratios is essential. Only for the initial estimation, a linear method might be used.

Soga *et al.* (1995b) noted that some metallocene catalysts produce two-different types of copolymers in terms of crystallinity. They copolymerized ethylene and 1-alkenes using 6 different catalysts, such as Cp_2ZrCl_2, Cp_2TiCl_2, Cp_2HfCl_2, $Cp_2Zr(CH_2)_2$, $Et[Ind\ H_2]_2ZrCl_2$, and $iPr(Cp)(Flu)ZrCl_2$. Polymers with bimodal crystallinity distribution (as measured by TREF-

GPC analysis) were produced with some catalytic systems. Only Cp_2TiCl_2-MAO and $Et[H_4Ind]_2ZrCl_2$-MAO produced polymers that have unimodal crystallinity distribution. The results seem to indicate that more than one active site type is present in some of these catalysts. However, it is also possible that non steady-state polymerization conditions might have caused the broad distributions in their case, since their polymerization times were very short (5 minutes for most cases).

Studies on α-olefin homopolymerization using metallocene catalysts might be interesting for copolymerization research. Frauenrath *et al.* (1998) used Cp_2ZrCl_2/MAO system to polymerize 1-hexene, which is one of popular comonomers used with ethylene. They found that as the polymerization temperature increased the molecular weight and isotactic sequences of polyhexene decreased.

Bergström *et al.* (1997) found the relationship between the content of isolated, alternating, and block sequences of comonomer and polymerization conditions in norbornene/ethylene copolymerization produced with dimethylsilyl bis(indenyl)zirconium dichloride and ethylene bis(indenyl)zirconium dichloride. It was shown that the different sequences of comonomers are sensitive to Al/Zr ratios, polymerization temperatures, and the metallocene types.

Stereoregulation in copolymerization is one of the most important areas in copolymerization research. Jin *et al.* (1998) were able to produce an alternating poly(ethylene-co-propylene) with a proportion of [EP] sequences over 95 % using [ethylene(1-indenyl)(9-fluorenyl)]zirconium dichloride (Et[1-Ind][9-Flu]$ZrCl_2$) catalyst. The polymerization temperature was extremely low (-40 °C). However, the alternating copolymer was stereoregular and isotactic. A comprehensive review on stereospecific olefin polymerization can be found in Brintzinger *et al.* (1995).

2.2. HETEROGENEOUS SYSTEMS

The new metallocene/MAO systems offer more possibilities in olefin polymerization compared to the conventional Ziegler-Natta catalysts, such as narrow stereoregularity, molecular weight and chemical composition distributions through ligand design. However, only heterogeneous catalysts can be practically used for the modern gas phase and slurry polymerization processes. Without using a heterogeneous system, high bulk density and narrow size distribution of polymer particles cannot be achieved. The advantages of supporting catalysts includes improved morphology, less reactor fouling, lower Al/metal ratios required to obtain the maximum activities or in some case the elimination of the use of MAO, and improved stability of the catalyst due to much slower deactivation by bimolecular catalyst interactions. Therefore, developing heterogeneous metallocene catalysts, that still have all the advantages of homogeneous systems, became one of the main research objectives of applied metallocene catalysis.

Steinmets *et al.* (1997) examined the particle growth of polypropylene made with a supported metallocene catalyst using scanning electron microscopy (SEM). They noticed formation of a polymer layer only on the outer surface of catalyst particles during the initial induction period. As the polymerization continued, the whole particle was filled with polymer. Particle fragmentation pattern depended on the type of supported metallocene.

The morphology of polymer particles depends mainly on catalyst morphology, support structure, reaction kinetics, and types of polymer. Polymer morphology is also affected by process conditions during polymerization. Burkhard *et al.* (1989) showed the importance of proper control of polymerization conditions during various stages of polymer particle growth in industrial UNIPOL™ process. The factors that affect the morphology of particles are initiation, which sets the boundary conditions for subsequent polymerization, shattering of the silica support, particle annealing, and different polymerization rates during initial, intermediate, and final particle growth stages.

2.2.1. Catalyst Chemistry

The nature of the active sites affects the polymer morphology, catalyst stability and activity, and the characteristics of the polymer produced. However, structure and chemistry of the active sites in supported catalysts are not clearly understood. Catalytic activities for supported metallocenes are usually much lower than that of their counterpart homogeneous system. Formation of different active species, deactivation of catalyst during supporting procedure, and mass transfer resistance may contribute to decrease catalyst activity.

Chien and He (1991) prepared a supported catalyst for ethylene and propylene copolymerization in fluidized bed reactors. Significantly lower ratios of Al/Zr (670 compared to 2,000-3,000 in homogeneous systems) were used to get random ethylene/propylene copolymer.

Kaminaka and Soga (1991, 1992) compared Al_2O_3 and $MgCl_2$ as supports for iPr(Flu)(Cp)$ZrCl_2$ /TMA and Cp_2ZrCl_2/TMA systems for propene polymerization. When Al_2O_3 and $MgCl_2$ were used as the support, TMA alone could activate the catalysts, although the activities were significantly lower than when MAO was used. ^{13}C-NMR results show that iPr(Flu)(Cp)$ZrCl_2$/$Al(CH_3)_3$ and Cp_2ZrCl_2/$Al(CH_3)_3$ produced syndiotactic and atactic polypropylenes, respectively. Molecular weight data were not complete and the molecular weights were low (M_w less than 80,000).

Soga and Kaminaka (1992) used supported Et[$IndH_4$]$_2ZrCl_2$ with different types of AlR_3 (R : CH_3, C_2H_5) in propylene polymerization. Some catalyst/AlR_3 systems showed high activity and produced high molecular weight polymer. However, the activity of polymerization using AlR_3 as a cocatalyst was much lower than when MAO is used. In some cases, only trace of polymers were produced.

Satyanarayana and Sivaram (1993) speculated that for Cp_2TiCl_2/$MgCl_2$-trialkyaluminum catalyst system for ethylene polymerization, the active site is a cation-like complex of Cp_2TiR^+ adsorbed on $MgCl_2$, where the reactive sites are isolated on the support, thereby stabilizing the coordinately unsaturated monomeric titanium species as shown in Fig.2.2.

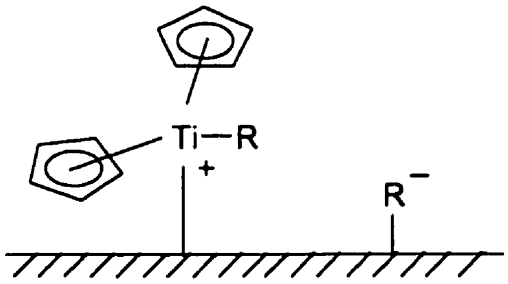

Figure 2.2 Structure of active sites for Cp_2TiCl_2 supported on $MgCl_2$

Ciardelli *et al.* (1994) studied the combined effect of ligand type and inorganic support type for Ti- and Zr-centered metallocene catalysts on ethylene polymerization activity. Depending on ligand types, cocatalysts, and support type, the activity varied from 2.4 to 41.3 kg PE/g metal atom/h. Steric and electric effects of ligands and support seemed to significantly contribute to catalyst performances.

Jin *et al.* (1995) supported neodymocene on SiO_2. Neodymocenes are known to be efficient catalysts for ethylene polymerization, although the homogeneous organolanthanide catalysts have a short lifetime. The lifetime of the supported catalysts was improved compared to the corresponding homogeneous catalyst systems, however, the polydispersities for the obtained polymers were very high (PDI = 2.9 ~ 10.5).

Tait *et al.* (1995,1996) reported general effects of support type, treatment, supporting procedure, and type of diluents on reaction kinetics and physical properties of polymer produced. Although the activities of supported catalysts are much lower compared to homogeneous systems, the activity of catalysts increased slightly when o-dichlorobenzene was introduced in toluene.

The catalytic activities of supported catalyst generally depend on the percentage of the incorporated metallocene (Quijada *et al.*, 1997). However, in the case of metallocenes supported on MAO pretreated silica, depending on how the surface-bound MAO can complex with the catalyst, the activity can be as high as that of homogeneous systems (Chen *et al.*, 1995). According to the experiment by Chen *et al.*, if a single MAO is attached to silica, it would complex with zirconocene and lowers its activity. On the other hand, if multiple MAOs are attached to the surface silanol, the supported zirconocene will not be further complexed with MAO and have higher activity.

Some review on methods and trends involved in supporting of metallocene catalysts, nature of the active sites, and mechanisms can be found in Ribeiro *et al.* (1997)

2.2.2. Supporting Methods

Metallocene immobilization methods can be divided into three main groups. The first method is the direct support of catalyst onto an inert support. The second method involves the pre-treatment of the inert support with MAO or other alkylaluminum followed by metallocene supporting. In the third method, the catalyst is chemically anchored to the support, which often involves in-situ catalyst synthesis. These methods produce catalysts with distinct activities, comonomer reactivity ratios, and stereospecificities.

Direct Supporting on Inert Material

Collins *et al.* (1992) reported that $Et[Ind]_2ZrCl_2$, when supported on partially dehydrated silica, reacted with surface hydroxyl groups during adsorption to form inactive catalyst precursors and free ligands (Fig. 2.3). Therefore, the activity is lower compared to the case of using dehydrated silica. Fig. 2.4 shows the proposed structure of inactive $Et[Ind]_2ZrCl_2$ supported on alumina. For the case of alumina, the activity of catalyst supported on dehydrated alumina is lower than the one supported on partially dehydrated alumina. The high Lewis acidity of aluminum sites on dehydroxylated alumina facilitates the formation of Al-Cl bonds and Zr-O bonded species when the metallocene compound is adsorbed on these sites. However, the metal sites in this case remain inactive even after MAO addition.

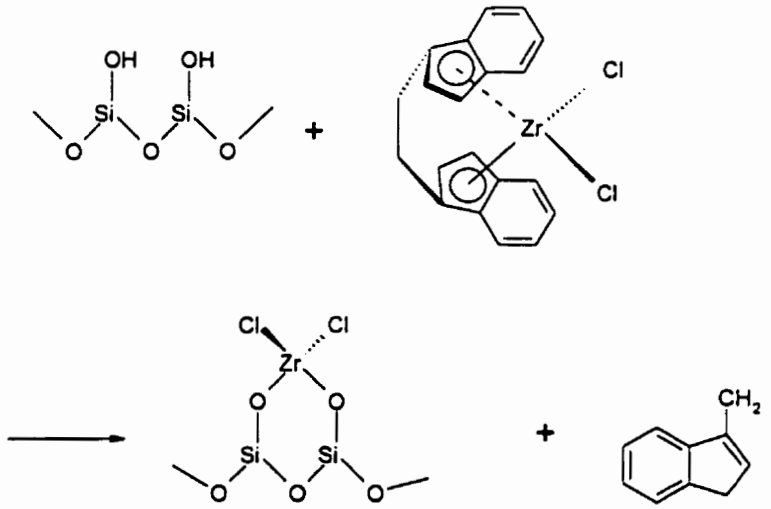

Figure 2.3 Formation of inactive site when $Et[Ind]_2ZrCl_2$ is supported on partially dehydrated silica

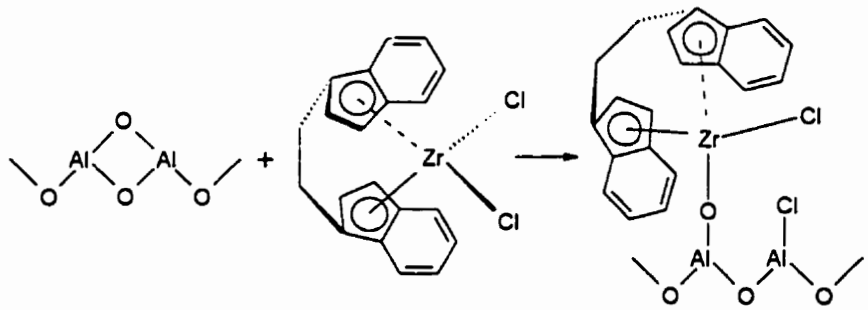

Figure 2.4 Formation of inactive site when $Et[Ind]_2ZrCl_2$ is supported on dehydrated alumina

Kaminsky *et al.* (1994) proposed a possible explanation for the different behavior of metallocenes supported directly onto silica, homogeneous systems, or supported onto MAO-pretreated silica. It is assumed that the supporting of metallocenes on silica takes place in three stages. First, the metallocene reacts with the OH groups of the silica as shown in Fig. 2.5 :

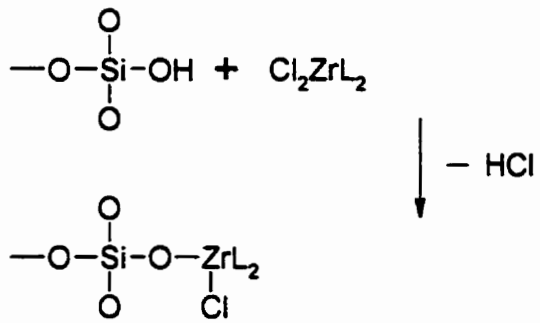

Figure 2.5 Reaction of silica and metallocene during catalyst supporting

where, L is a ligand (Cp, Ind)

The second step is the alkylation by MAO as shown in Fig. 2.6 :

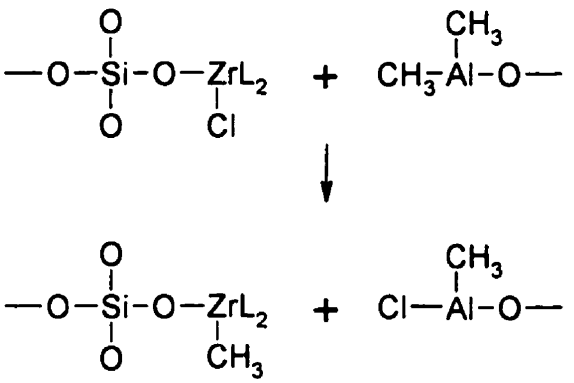

Figure 2.6 Alkylation of supported metallocene by MAO

The third step is the dissociation of the –Si–O–Zr– bond to an ion pair to form the cationic active center $(SiO^-)(Zr)^+$. The PDIs of polymers produced with these supported metallocenes are reported to be relatively high (5~8) due to different electronic and steric interactions between the silica surface and the metal active sites. The immobilization of the zirconocene on silica inhibits bimolecular deactivation processes because the active sites are separated from each other.

As a consequence less use of MAO is required, increased molecular weights are achieved due to the reduction of β-hydrogen transfer by a second zirconocene center, and polypropylene of higher isotacticity and melting points is formed.

When silica is pretreated with MAO, the supporting mechanism is different. The zirconocene is complexed to MAO supported on silica, which will make the catalyst similar to a homogeneous system. The polymers produced in this way have lower molecular weights.

Janiak and Rieger (1994) used silica to support Cp_2ZrCl_2/MAO for ethylene polymerization. It was found that when the catalyst was directly deposited on silica, the activity was much lower than when the sandwich structure of SiO_2/MAO/Cp_2ZrCl_2/MAO was used. The activity depended on the total Zr content. Supporting the catalyst significantly decreased its activity but increased molecular weights of the formed polymer. Reduced chain

transfer reactions between the immobilized Zr and Al centers is the possible cause of the increase in molecular weight. The decreased activity was explained by the partial activation of metallocene center at low Al/Zr ratios, as the Zr centers were set on the silica support. Also, intraparticle mass transfer resistances were considered as the cause of the decreased activity. Slight increases in polydispersity index of the produced polymers were observed, however no clear explanation was provided.

Sacchi *et al.*(1995) compared the stereochemical control of homogeneous and silica-supported Cp_2ZrCl_2. Ethylene polymerization rates with the supported catalyst were lower but more reproducible than the ones with the homogeneous system. Additionally, the heterogeneous system was activated by TIBA, which could not be achieved with the homogeneous system. Other interesting observation is the change of Cl/Zr mole ratios between supported and non-supported catalysts. When Cp_2ZrCl_2 was supported directly on SiO_2, the mole ratio of Cl/Zr decreased from the value of two, indicating a chemical composition change in the catalyst. However, if SiO_2 was pre-treated with MAO, the Cl/Zr mole ratio remained close to two. In propylene polymerization, the non-isospecific $[Ind]_2ZrCl_2$ became highly isospecific (as of $Et[Ind]_2ZrCl_2$ - SiO_2 system) when supported on SiO_2. No such improvement was found when the catalyst was supported on SiO_2 that was pre-treated with MAO. Therefore, when the metallocene is anchored directly onto silica, only isospecific centers may be formed independently of their chemical structure, because both $Et[Ind]_2ZrCl_2$ - SiO_2 and $[Ind]_2ZrCl_2$ - SiO_2 systems produced the same prevailingly isospecific polymer. The improvement in polymer morphology for supported catalyst was not mentioned.

Repo *et al.* (1997) were able to deposit $Zr(salen)Cl_2$ [salen = *N, N'*-ethylenebis(salicylideneiminato)] on to a silica support by heating $Zr(salen)Cl_2(THF)$ in toluene in the presence of SiO_2. The catalyst prepared in this method has acceptable activity for ethylene polymerization at 80 °C with low monomer pressure in the presence of MAO.

Supporting Catalyst on Materials Treated with Alkylaluminum

As shown in Fig. 2.7, for ionic metallocene catalyst, supporting of the aluminum-alkyl-free catalysts can cause (a) deactivation through coordination of Lewis-basic surface oxides to the

electrophilic metal center or (b) reaction of the ionic complex with residual surface hydroxyl groups (Hlatky and Upton, 1996).

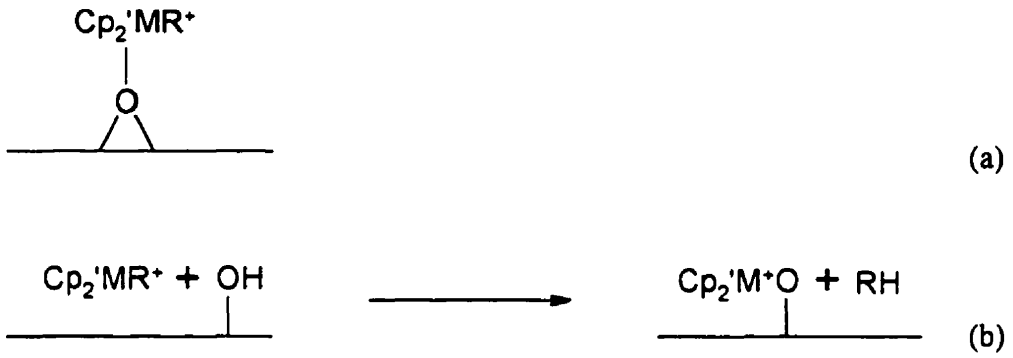

Figure 2.7 Effect of surface hydroxyl groups on ionic metallocene catalysts

However, highly active supported ionic metallocene catalysts for olefin polymerization can be prepared by pretreating the support with a scavenger. It is assumed that pretreatment of the support with a scavenger serves to passivate the support and compatibilize it with the ionic metallocene complex.

Kaminsky and Renner (1993) produced high melting polypropylenes with silica-supported zirconocene($Et[Ind]_2ZrCl_2$/MAO) catalysts. Three different approaches in supporting the catalyst were used. In the first method, silica was pretreated with MAO and then metallocenes were added. The second method did not use MAO during the supporting process, but for polymerization MAO was added. The third method is same as the second method, but the supported catalyst was pretreated with MAO before polymerization. No additional MAO was used during polymerization for the catalysts prepared by the third method. They noted that the pretreatment of silica with MAO (first method) causes the metallocene to interact mainly with MAO, resulting in a supported catalyst with behaviors similar to the equivalent homogeneous system. Compared to homogeneous systems, the supported catalysts produced polypropylenes with significantly higher molecular weights and melting points. The molecular weights of the polymers produced by the supported catalyst according to the second method showed increasing molecular weight as the Al/Zr ratio

increased. However, the opposite behavior was observed when catalysts supported by the third method were used for the polymerization.

Langhauser *et al.* (1994) supported metallocenes onto an inert support by physical or chemical means. Polypropylene, AlR_3-treated SiO_2, and chemically fixed MAO were used as the supports. The results were compared between the following four cases. I. $Me_2Si(H_4Ind)_2ZrCl_2$/MAO on SiO_2/TEA, II. Me_2Si(2-Me-4-tBu-Cp)$ZrCl_2$ on PP, III. $Me_2Si(Benz\text{-}inden)_2ZrCl_2$ on SiO_2/TEA, and IV. $TiCl_4/MgCl_2$ on SiO_2. Case II produced polypropylene that had the highest molecular weight (68,000), isotacticity, and crystallinity among the compared cases.

Lee *et al.* (1995) used TMA pretreated-silica as the support for metallocene catalysts. The activity of supported catalysts showed dependency to H_2O content in silica, H_2O/TMA ratio, metallocene, and cocatalyst. The supported catalyst was also able to polymerize ethylene in the absence of MAO when common alkyl aluminum was used as the cocatalyst.

Ernst *et al.* (1996) further cross-linked the MAO molecules supported on small size aluminum oxide using bisphenol A to create a support that had very low solubility of MAO in diluents. The polypropylenes produced with metallocene catalysts immobilized onto the cross-linked support were spheres with very broad particle size distribution including fines. However, when medium size silica was used for the support, the particle size distribution was comparable to polymers produced with conventional supported Ziegler-Natta catalysts.

The study of the surface aluminum and metallocene loading by Santos *et al.* (1997) reveals that about 7 wt.-% of MAO can be supported on silica when the initial amount of MAO in mixture of silica was ca. 10 wt.-%. Depending on silica type, saturation of MAO supported on silica can occur at lower MAO contents.

Harrison *et al.* (1998) compared a variety of silica and alumina supports with different degrees of surface hydroxylation as the supports. It was shown that as the concentration of OH groups on the surface of the support increased, more MAO could be impregnated and thus catalysts with more metallocene content could be produced. The most obvious benefit of supported catalyst with more metallocene was an increased activity compared to catalysts with lower concentration of surface hydroxyl groups (increased activities both in kg PE/mol Zr/hr and kg PE/g support/h). However, at high polymerization temperatures, leaching of

catalyst from the support was observed. At lower polymerization temperatures, leaching was less significant, however, the morphology and bulk density of the polymer formed were still unsuitable for use in gas-phase polymerization.

For the case of propylene polymerization, decrease in syndiotacticity was observed by Xu *et al.* (1998) when the metallocene catalyst was supported on pretreated silica.

Chemically Anchoring Catalyst on Support

Soga *et al.* (1994, 1995c) described a method to support zirconocenes more rigidly on SiO_2. The supporting steps are as follows : 1) Silica was treated with $SiCl_4$ to substitute the OH groups with chlorine atoms. 2) The resulting silica gel was filtered and washed with tetrahydrofuran (THF). 3) The solid was re-suspended in THF and a lithium salt of indene, dissolved in THF, was added drop-wise. 4) The resulting solid was filtered and washed again with THF. 4) To re-suspended solid in THF, $ZrCl_4 \cdot 2THF$ dissolved in THF was added. 4) The final solid part was separated by filtration, washed with THF and diethyl ether, and dried under vacuum. The supported catalyst produced in this way showed higher isospecificity than the corresponding homogeneous system for propylene polymerization. MAO or ordinary alkylaluminums were used as cocatalysts. The yield was higher when MAO was used as the cocatalyst, but the molecular weight of the polypropylene was half of the molecular weight obtained when TIBA was used as the cocatalyst (3.4×10^5 g/mol and 7.2×10^5 g/mol, respectively). Fig. 2.8, shows structures the silica supported metallocenes.

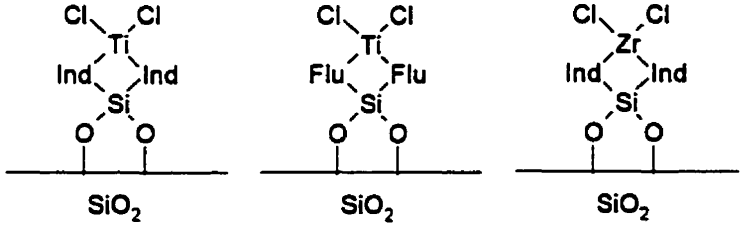

Figure 2.8 Structure of some silica supported metallocene catalysts (Soga *et al.*, 1995c)

Lee *et al.* (1997) used spacer molecules, where metallocene catalysts were attached to spacers supported on silica, to eliminate the steric hindrance near the active site caused by the silica surface (Fig. 2.9). By distancing the active site from the silica surface, higher catalytic activities but lower polymer molecular weights were obtained in comparison with analogous silica-supported catalysts without a spacer molecule. Trisiloxane and pentamethylene were used as spacer molecule between silica and $CpIndZrCl_2$.

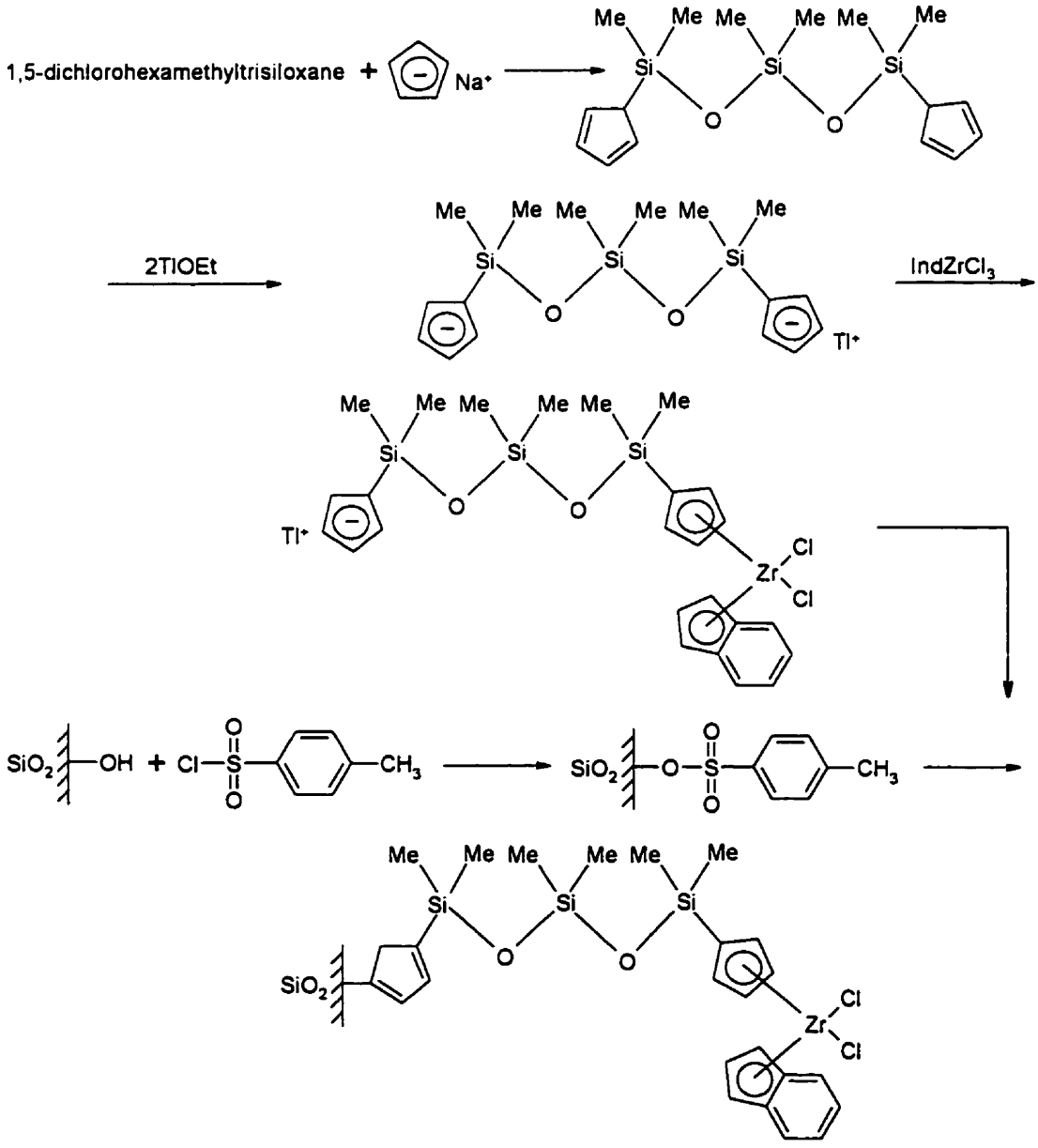

Figure 2.9 Mechanism for supporting metallocene catalysts on silica using spacer molecules

Iiskola *et al.* (1997) treated the surface of partially dehydroxylated silica with a silane coupling agent, $Cp(CH_2)_3Si(OCH_2CH_3)_3$, and then chemically supported $CpZrCl_3$ onto the modified silica to obtain a highly active catalyst (Fig. 2.10) for ethylene polymerization used in the presence of MAO. Depending on the calcination temperature and the modification methods, the catalysts showed different activities and produced polymers with different molecular weights. In general, when compared to homogeneous Cp_2ZrCl_2 systems, all the supported catalysts showed lower activities, but the polymers produced had higher molecular weights. On the other hand, when compared to homogeneous $CpZrCl_3$ systems, the activities of the supported catalysts were similar but the molecular weights of the polymer produced were lower and depended on the silica surface modification method used. The polydispersity index of the polymers ranged from 2.2 to 2.8

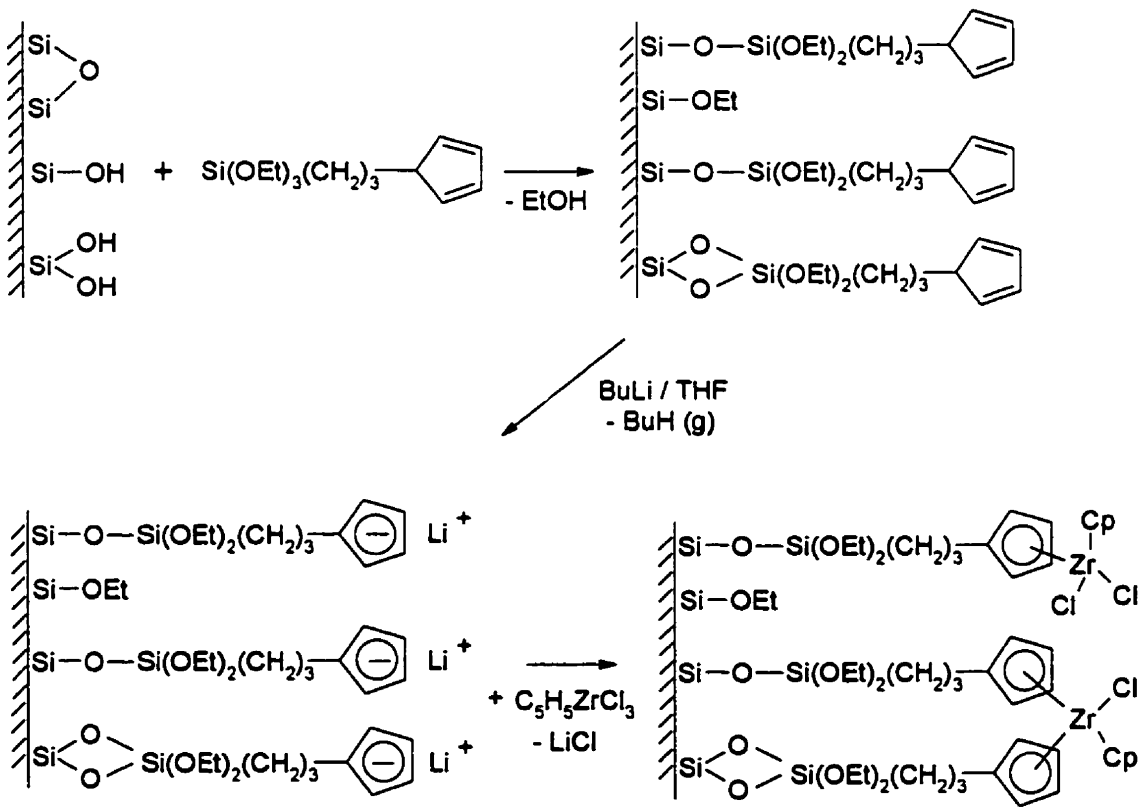

Figure 2.10 Modification of silica with $Cp(CH_2)_3Si(OCH_2CH_3)_3$ and preparation of supported metallocene catalysts, Iiskola *et al.* (1997)

In-Situ Technology

Galli *et al.* (1997) used an *in situ* impregnation technique to support metallocenes to spherical polypropylene particles made with Ti-based Ziegler-Natta catalysts to produce polymers with improved morphology. In their 'multi-catalyst reactor granule technology', they attempted to combine the excellent morphology control of Ziegler-Natta catalysts and unique properties of polyolefins made with metallocene catalysts. It was shown that for some reaction conditions the polymers were recovered as free-flowing particles with good morphology. The heterophasic PP/ethylene-propylene-rubber (EPR) copolymers seemed to have good dispersion of rubber inside the polymer granule, based on morphological characterization.

Incipient Wetness Method

Lately, a new "incipient wetness" method was demonstrated by Kamfjord *et al.* (1998). In this method, the catalyst is dissolved in liquid monomer (1-hexene, 1, 7-octadiene, and styrene) and then adsorbed on silica containing MAO, where the monomers are allowed to polymerize slowly to anchor the catalyst in the silica pores. The behavior of the supported catalysts prepared in this method depends on the type of monomer used during pre-polymerization. For instance, when 1,7-octadiene was used, the polyoctadiene-covered catalyst particle suffered possible mass transfer resistance due to the presence of the rigid pre-polymer. Because of this, when used for ethylene polymerization, the initial activity of the catalyst was low but gradually increased as more active sites were exposed as a result of particle fragmentation. When styrene was used during pre-polymerization, the activity was increased compared to the non pre-polymerized catalyst

Interestingly, the pre-polymer forms a protective layer around catalyst particles, which retards catalyst deactivation by poisons. Therefore, even after 5 hours of exposure to air, the catalysts retained some polymerization activity. For most polymerizations, the catalysts were activated with TEA. When the catalyst pre-polymerized with 1-hexene was activated with TIBA, the activity increased more than 100 %. However, TIBA appears to extract catalyst

and MAO from the support and thus the morphology of the polymer became somewhat similar to the one obtained in homogeneous systems.

Other Supports

Janiak *et al.* (1993) used polymeric MAO as support for metallocene catalysts. The characterization of polymeric MAO was performed by SEM, ^{13}C and ^{27}Al nuclear magnetic resonance (NMR), and Brunauer-Emmett-Teller (BET) method. Polymerization results using these metallocenes supported on polymeric MAO were not presented, although the authors claimed that their new catalyst showed higher yield on a *per gram* catalyst basis compared to their best silica supported catalyst.

Ti- based catalyst (from $TiCl_4$) was also supported on polymer such as poly(ethylene-co-acrylic acid). With the polymer supported catalyst, Sun *et al.* (1994) were able to produce polyethylene and poly(ethylene-co-1-hexene) with high melting point, high degrees of crystallinity, and high MW.

Lee and Yoon (1994) used α-cyclodextrin-supported Cp_2ZrCl_2/MAO for ethylene polymerization. Thermal properties, such as melting temperature and crystallization temperature, were increased when the catalysts were supported and also the polymerization was possible using only TMA as the cocatalyst.

Polysiloxanes have also been used as metallocene supports. Soga *et al.* (1995d) found that the activity and stereospecificity of metallocene catalysts supported on polysiloxanes were between those of corresponding homogeneous and SiO_2-supported catalysts. Arai *et al.* (1997) produced different types of polysiloxane-supported zirconocene catalysts by condensation of dichlorosilane with various side groups and water. The supported catalyst was more stable than equivalent homogeneous systems. The Zr content in the supported catalysts varied from 0.33 to 1.17 mmol/g. The activities of the catalysts depended significantly on the side groups. Unfortunately, the supported catalysts prepared by this method have both soluble and insoluble fractions in toluene depending on the molecular weight of the catalyst.

Nishda *et al.* (1995) used polystyrene as a support for metallocenes. The supported $Si[Ind]_2ZrCl_2$ and $Et[Ind]_2ZrCl_2$ on chemically modified polystyrene were stable at high temperatures (as high as 70 °C). Molecular weights of polypropylene produced with these catalysts was low (M_w = 23,000~27,000). The polydispersity indexes of the polymer obtained were between 2.1 and 5.1. SEM pictures show that the original polystyrene beads were not fractured during polymerization and that the polymer was produced mainly around the external surface of the beads. It was claimed that the polyethylene produced replicated the original shape of the polystyrene beads. However, based on these observations, it is possible that the polymer chains grow on the polystyrene surface only until all the active sites are blocked, when polymerization stops before significantly altering the shape of the supports. This seems to be confirmed by the fact the amount of polymer produced was very small compared to the original polystyrene support. Some SEM pictures also showed that polymer was formed only in some parts of the beads, which indicates irregular catalyst supporting.

Zeolites are used as catalyst supports in various applications other than polyolefin manufacturing due to their well-defined cage structure. Woo *et al.* (1995) used NaY zeolites, pre-treated with MAO or TMA, as the support for Cp_2ZrCl_2 and Cp_2TiCl_2. The molecular weight and melting point of polyethylene produced with the supported catalyst were higher in comparison to the ones obtained with its homogeneous counterpart. However, polymerization activities were significantly lower for the zeolite-supported system. Ko *et al.* (1996) used molecular sieves such as MCM-41 and VPI-5 as supports for $Et[Ind]_2ZrCl_2$ catalyst for propylene polymerization. The supported catalyst showed high activity toward propylene polymerization and the ability to produce superior polypropylene in terms of molecular weight, stereoregularity, and melting point compared to the homogeneous catalysts.

2.3. CONTROL OF POLYMER MICROSTRUCTURES

The mechanical and rheological properties of polymers depend not only on their average molecular weights and chemical compositions but also on their MWD and CCD. Polymers with broad MWD show great flowability in molten state at high shear rate, and thus can be

easily processed. Polymers with narrow MWD have greater dimensional stability, higher impact resistances, greater toughness at low temperatures, and higher resistance to environmental stress cracking. Polymers with high average molecular weights show better mechanical properties compared to polymers with low average molecular weights. However, narrower MWD causes low shear sensitivity and low melt tension, which make it difficult to process with conventional transformation machines. Especially, polymers with relatively narrow MWD with high average molecular weights will cause higher degree of extrusion defects such as melt fracture in addition to the decreased processability.

For copolymers, structural distribution caused by CCD will affect crystalline level such as a lamella thickness distribution. In general, the narrower CCD, the stronger the impact strength and less haze compared to copolymers with broader CCD. Overall, a narrow MWD and CCD will improve physical properties of polymer, however, processability of the polymer will suffer.

The disadvantages in processing can be greatly reduced by incorporating low molecular weight polymer chains to the polymer, which acts as lubricant during processing. Therefore, control of MWD and CCD becomes an important factor to determine the application of the produced polymer resin. The interest in producing designed polyolefins through single-site catalyst in industrial process is growing (Montagna, 1995) with the advent of metallocene catalysts.

Reactor cascade technology is commonly used to customize polymer microstructures in industrial process to produce polymers with CCD-MWD relationship shown in Fig. 2.11. Böhm *et al.* (1994) describe a process used to produce bimodal polyethylene with improved properties. The basic structure-property relation was qualitatively explained, such as the formation of tie molecules in a bimodal polymer alloy. Generally, the target of reactor cascade technology is to produce a mixture of polymers with two different microstructures. One comprises low molecular weight homopolymers and the other high molecular weight copolymers. The high molecular weight copolymers increase the probability of tie molecule formation that will physically connect different crystallites in a tri-dimensional network. Polymers produced in this way show high stiffness, high impact resistance, high resistance versus rapid crack propagation, and very high values of environmental stress crack resistance.

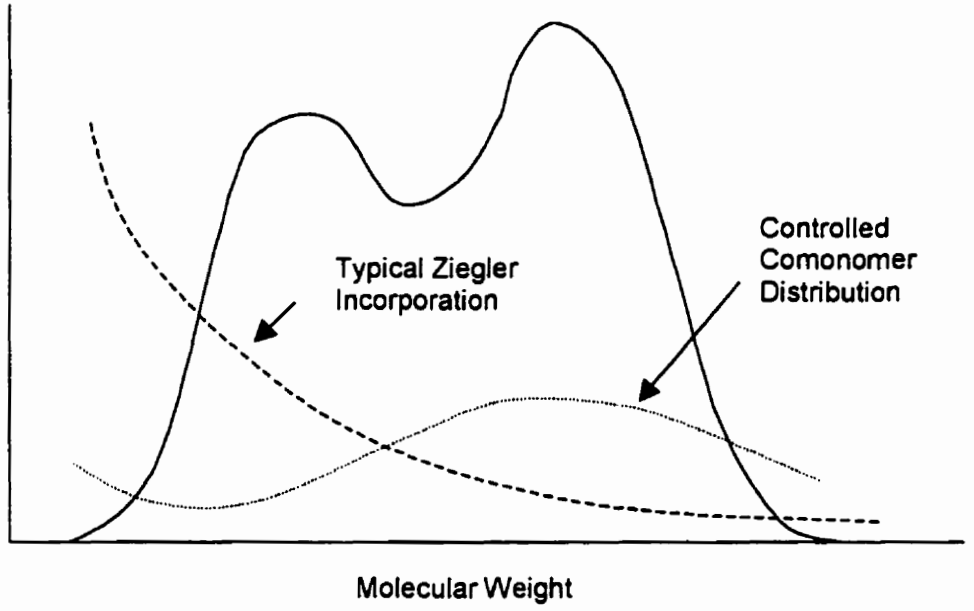

Figure 2.11 Bimodal HDPE with targeted comonomer incorporation (Equistar Chemicals., MetCon'98)

Another way to control MWD is to use combination of different catalysts. This technique became possible with the introduction of metallocene catalyst. Metallocene catalysts produce polymers with very uniform distributions, which were not attainable with the conventional heterogeneous Ziegler-Natta catalysts. MWD and CCD can be controlled by the selective combination of metallocene catalysts that differ in their ratios of chain transfer / propagation rates and comonomer reactivity ratios. The chain transfer / propagation controls average molecular weight and the comonomer reactivity ratio controls the average chemical composition of the produced polymer.

Heiland and Kaminsky (1992) compared rac-Et[Ind]$_2$HfCl$_2$/MAO and rac-Et[Ind]$_2$ZrCl$_2$/MAO for ethylene and ethylene/1-butene polymerizations. The hafnium catalyst had lower activity, but produced polymer with molecular weights 10 times higher than Et[Ind]$_2$ZrCl$_2$/MAO. Additionally, the comonomer incorporation increased significantly for the hafnium catalyst. They conducted polymerizations using a mixture of hafnocene and zirconocene (95% Hf, 5% Zr). The results showed that each catalyst produced its own

polymer independently, which indicated the possibility of producing a tailored molecular weight distribution by combination of different metallocene catalysts.

Spaleck *et al.* (1994, 1995) studied the possibility and limits of rational design of metallocene catalysts using aromatic substituents on different positions of the catalysts to control molecular weights for ethylene and propylene polymerizations. Significant change in molecular weight of produced polymer was observed when different aromatic substituted metallocenes were used. However, a rational design of catalysts was still limited according to their observations, because a detailed polymerization mechanism is still not established, especially for supported catalysts. Good descriptions of experimental techniques for metallocene catalyst synthesis were presented.

Ihm *et al.* (1994) noted that the shape of MWD of polyethylene made with silica-supported metallocene catalysts varies from narrow unimodal to bimodal depending on the method involved in preparing the supports. Cp_2MeCl_2 (Me = Ti, Zr, Hf) was supported onto the silica pretreated with MAO, TEA, or $(C_2H_5)MgCl$. The observed differences in MWD were attributed to differences in types of bonding between OH groups and alkylaluminum molecules used during the pretreatment of the surface. They speculated that the unusual formation of bimodal MWD polymers with Cp_2TiCl_2 supported on SiO_2/MAO was due to interaction among metallocene, MAO, and the pretreated support.

Han *et al.* (1995b) used mixtures of Cp_2TiCl_2, Cp_2ZrCl_2, $Et[Ind]_2ZrCl_2$ to produce unimodal or bimodal MWD polyethylenes by different combinations of metallocene mixtures under different polymerization conditions.

Ahn *et al.* (1998) attempted to control the MWD of polypropylene by sequential addition of Ziegler-Natta and metallocene catalysts during semibatch polymerization. By using different polymerization time segments for each catalyst after injection, different cocatalyst combinations, and varying the sequence of catalyst injection, they produced polymers with broad MWDs. However, this method cannot be easily adapted to industrial scale reactors due to the frequent change of reaction conditions.

There are numerous studies on polymer microstructure and physical property relationships, which in turn can be used in designing polyolefins with improved properties. Hosoda *et al.* (1994) correlated mechanical properties, such as impact strength, and CCD or

lamella thickness distribution of polyethylene. According to their results, copolymers with homogeneous structures have more efficient tie molecules than polymers with broad CCD, and thus exhibit a higher mechanical strength.

Kashiwa (1994) compared polymers produced with conventional Ziegler-Natta and metallocene catalysts to relate microstructure and the physical properties of polymer in the areas such as melting point vs. isotacticity, flexibility, CCD-MWD relationship, density vs. comonomer content, heat seal initiation temperature, haze vs. CCD, melt viscosity vs. shear rate, and melt tension vs. melt index. It was graphically illustrated how a well defined thin lamella favors the formation of tie-molecules.

The microstructure of polymers can also affect their thermal as well as physical properties significantly. Kim *et al.* (1996) show how the distributions of short chain branching in polyethylene can cause differences in melt flow index, environmental stress crack resistance (ESCR), and film dart drop impact strength, although all the samples have similar densities.

2.4. CHARACTERIZATION

2.4.1. Size Exclusion Chromatography (SEC)

Size exclusion chromatography (SEC) is also known as gel permeation chromatography (GPC). In this method, the polymer chains are fractionated based on their hydrodynamic volume in solution as they flow through column(s) packed with particles of varying porosity.

The MWD obtained by GPC can be modeled as a superposition of polymer chains produced at different catalyst site types. Therefore, by deconvoluting broad MWDs into narrower theoretical distributions, such as Flory's most probable distribution, information on active center types can be obtained in addition to the information on polymer chain length (Kissin, 1993; Soares and Hamielec, 1995a).

Information on long chain branching can be estimated through GPC coupled with multiangle laser light scattering photometer or differential viscometer (Podzimek, 1994). This

technique can be useful for analysis of polymers containing long chain branches such as low density polyethylene and certain metallocene-made polyethylene (Dayal, 1994).

2.4.2. Fractionation Methods Based on Polymer Crystallinity

Fractionation based on polymer crystallization in dilute solutions can be used to estimate the distribution of chemical composition and stereoregularity of polyolefins.

Temperature Rising Elution Fractionation (TREF)

The primary steps of preparation involved in TREF are 1) dissolution of polymer in a solvent at a high temperature, 2) precipitation of polymer onto an inert support under very slow cooling rate (not more than 0.1 °C / hr), and 3) elution and fractionation of polymer under slow heating to re-dissolve the precipitated polymer chains. TREF can be operated in analytical or preparative modes.

Polymers produced with conventional Ziegler-Natta catalyst have more comonomer content in lower molecular weight region. Analytical TREF results of these polymers show that samples with lower crystallization temperatures have broader CCDs than that with higher crystallization temperatures. Defoor *et al.* (1992) used preparative TREF to fractionate 1-octene LLDPE made with a Ziegler-Natta catalyst. Samples were separated into 8 fractions in the temperature interval from 25 to 105 °C and analyzed by GPC, DSC, and analytical TREF. The result show that as the fractionation temperature increases, the average molecular weight increases but the average number of short chain decreases.

An attempt to model the fractionation process on TREF based on a thermodynamic model was made by Borrajo *et al.* (1995). In addition to the Flory-Huggins theory, they considered effects of melting temperature, melting enthalpy, average crystallinity, average crystallizable sequence length, and polymer-solvent interactions. The thermodynamic model divides each chain by crystallizable homopolymer blocks and non-crystallizable highly branched copolymer blocks. Therefore, statistically, every individual chain has a distribution of

longest to shortest crystallizable lengths. Since the molecular weights of commercial copolymers are large enough for a single chain to form crystallites of different lamella thickness, the effect of chain length is not usually considered in this kind of approach. Their model further assumes that the crystallites have similar thickness. The model predicted the dependence of previously mentioned parameters in a reasonable manner when it was compared with experimental results.

Crystallization Analysis Fractionation (CRYSTAF)

Polymers with different ethylene sequence lengths will crystallize at different temperatures due to the differences in minimum crystallite thickness that can be formed in different temperatures. Unlike TREF, CRYSTAF analysis is conducted during the crystallization period by measuring polymer concentration in solution. Monrabal *et al.* (1999) used homogeneous ethylene/1-octene copolymers with narrow CCDs, made with a constrained geometry catalyst, to establish a correlation between CRYSTAF result and comonomer content in the polymer. The calibration curve obtained was linear and could be used for ethylene/1-octene copolymers for a weight fraction of 1-octene up to about 40 %.

CCDs obtained from these fractionation methods can be used to investigate the nature of catalyst active centers present during polymerization (Soares and Hamielec, 1995b, 1995c; Soares *et al.*, 1996).

2.4.3. Other Characterization Methods

Nuclear Magnetic Resonance (NMR)

NMR is an absolute method that does not require calibration. The location of the resonance peaks identifies type of branches or end-groups. Pooter *et al.* (1991) proposed a ^{13}C-NMR method for the analysis of polyethylene copolymers with propene, butene-1, hexene-1, octene-1, and 4-methyl pentene-1 in the composition range of 1-10 mol %. They showed detailed

calculations involved in estimation of the copolymer composition, based on the peak assignment and integration.

Randall (1989) wrote an extensive review on ^{13}C-NMR use for polyolefins, with detailed peak assignments and comonomer content calculations for ethylene polymerization with propylene, 1-butene, 1-hexene, 1-octene, and vinyl acetate copolymers.

Investigation of ^{13}C-NMR analysis results based on a statistical model can be useful for the study of polymerization mechanisms for model discrimination purposes (Bailey *et al.*, 1994).

Fourier Transformed - Infrared Spectroscopy (FT-IR)

FT-IR has some advantages over ^{13}C-NMR analysis of polyolefin in the areas of precision and analysis time. The disadvantage includes that the absorbance must be corrected due to interferences of the methylenes and other bands. The absorbance frequency and absorptivity of the methyl groups are also somewhat dependent upon the type of branch and upon crystallinity. Therefore, the quantitative analysis of branching in ethylene copolymers of two or more comonomers is problematic (Pooter *et al.*, 1991). Useful calibrations can be found for copolymer compositions for ethylene-propylene copolymers (Drushel and Iddings, 1963) and for ethylene/1-hexene copolymers (Nowlin *et al.*, 1988). Analysis of surface hydroxyl groups in catalyst support such as silica is also possible with FT-IR (Ihm *et al.*, 1994).

Differential Scanning Calorimetry (DSC)

Melting points and melting enthalpies can be determined by DSC. Depending on comonomer presence and polymerization conditions, the melting points of copolymers can change significantly. In addition to measuring melting points and fusion enthalpies, attempts were made to use DSC to get information on the distribution of microstructure of polymer samples. DSC can be used to determine rough chemical composition distributions based on the peak broadness in the DSC curve. To enhance this result, polymer samples can be slowly annealed

at different temperature ranges before the analysis (Adisson *et al.*, 1992) or by using more sensitive solution phase DSC (Mara and Menard, 1994).

2.5. MATHEMATICAL MODELING OF OLEFIN POLYMERIZATION WITH METALLOCENE AND ZIEGLER-NATTA CATALYSTS

Two different modeling approaches are generally taken to explain the observed decrease in polymerization rate with time and the broad MWD obtained with heterogeneous Ziegler-Natta and some supported metallocene catalysts. One is the chemical kinetic approach and the other is the mass and heat transfer approach. In the chemical kinetic approach, it is assumed that there are more than one distinctive active site types on the catalyst producing polymer chains with different average properties. For instance, overall MWDs are modeled as a superposition of individual narrow MWDs for each site type. In the mass and heat transfer approach, the broadening of the MWD is explained by mass and heat transfer resistances occurring during the polymerization, since radial monomer concentration gradients will result in radial gradients of polymer molecular weight.

For the modeling of the growing polymer particle, the multigrain model or its modified forms have been used extensively (Floyd *et al.*, 1987). In this model, the original catalyst particles become fragmented at the very beginning of the reaction and polymer will grow around each fragment, thus the overall particle size will increase. Another model is the polymeric flow model (Fig. 2.12). The polymeric flow model assumes that the active sites are uniformly dispersed in the polymer matrix.

Figure 2.12 Polymerization models

Galvan and Tirrell (1986) were the first to combine site heterogeneity and mass transfer resistance effects to model the broad distribution of polyolefin molecular weights made with heterogeneous Ziegler-Natta catalysts. It was shown that the multiplicity of site types played a more significant role in explaining broad molecular weight distributions than mass and heat transfer resistances.

Floyd *et al.*(1987) used the multigrain model to investigate the heat and mass transfer effects on polymerization behavior and polymer properties. They also investigated the effects of different site types present on the catalyst. Mass transfer resistances, catalyst physical properties (particle size, the microparticle size, and the porosity), temperature, and the external film resistances were investigated. From their research the following was concluded : 1) The initial acceleration behavior of a polymerization reaction becomes more pronounced as monomer diffusivity decreases and diffusion resistance becomes more severe, 2) the polymerization rate would be observed to be almost constant from the beginning of polymerization under conditions where microparticle diffusion was limiting, 3) under severe diffusion resistance influence, hybrid-type rate curves will result (combination of build up type and decay type), 4) increase in the catalyst site concentration may lead to highly diffusion-limited polymerizations, 5) little broadening in molecular weight distribution is induced by the catalyst particle size distribution, 6) the external film resistances exert a negligible effect on both the rate behavior and polymer properties in slurry polymerization, 7) polymers having large polydispersities will be produced only in the initial stages of polymerization. Therefore, with realistic diffusivity values, macroparticle concentration gradients alone cannot explain the breadth of the molecular weight distribution at typical reactor residence times.

The multiplicity of types of active sites offers a convincing explanation for both the polydispersity and the shape of the molecular weight distribution curves that are observed by GPC. Furthermore, diffusion resistances cannot explain the production of isotactic and atactic polypropylene on the same catalysts.

Rincon-Rubio *et al.*(1990) proposed a kinetic model for the slurry polymerization of propylene over a supported high activity Ziegler-Natta catalyst. In addition to the conventional polymerization mechanism, catalyst site transformation, monomer-assisted site deactivation, and hydrogen-assisted site deactivation steps were included in the model. Mass transfer limitation was not considered and it was assumed that all the active sites were instantaneously activated at the initial stage of the reaction. The transformation of the active sites and deactivation steps permitted effective correlations of the polymerization rate and total polymer properties in time for a given set of operating conditions. Polymerization rate, polymer yield, and number average molecular weight showed good agreement with experimental data.

Sau and Gupta (1993) modeled a semibatch polypropylene slurry reactor. The model extended the polymeric multigrain model (PMGM) to account for the presence of gas-liquid mass transfer resistances and the gradual build-up of the monomer concentration in the liquid medium in an isothermal, semibatch reactor. The incorporation of these effects significantly influenced the rate of polymerization, chain length, and polydispersity. Also, multiplicity of catalyst site types was found to be more important than diffusion effects in explaining the high polydispersity of the product.

Chan and Nascimento (1994) used the approach of back propagation neural networks for modeling of free radical olefin polymerization in high-pressure tubular reactors. This algorithm uses processing units called *neurons* which are connected to one another. By adjusting parameters in the coupling between neurons, the network is capable of learning from a set of numerical data corresponding to the input variables and the desired outputs. For this model to work, previous sets of results must be used to train the model. Based on the learned process information, the model can predict the output. Actual industrial tubular reactor process data were used for the training. The predictions for the temperature showed very good agreement with the experimental data and were comparable to or better than those

predicted by a mechanistic model published in the literature. The density, melt index, conversion, and molecular weights were also predicted reasonably well. The advantage of this alternative approach over the mechanistic modeling is the model's simplicity. The reliability of the network depends on the quality and range of the training data. However, the network training process can be tedious and time consuming, and in some cases, convergence can be slow and difficult. To our best knowledge, such approach has never been attempted for Ziegler-Natta or metallocene polymerizations.

Choi *et al.*(1994) used a population balance model for modeling a continuous gas phase olefin polymerization reactor. In this model, the catalyst particle size distribution was considered and the overall steady-state population balance equations were derived for a continuous flow, gas phase ethylene copolymerization reactor. For the modeling of each particle, the multigrain solid core model was incorporated into the population balance model. The effect of particle size distribution of the catalyst feed was not clear. However, the effect of catalyst site deactivation was significant. The site deactivation induced the particle size distribution to become asymmetric with a reduction in the amount of large polymer particles. Also, it narrowed the polymer particle size distribution as the deactivation occurs more rapidly.

Similar results were observed by Soares and Hamielec (1995a). Their model can be used to study the influence of any reactor residence time distribution on the polymer particle size distribution for olefin polymerization with heterogeneous catalysts.

Lee *et al.*(1994) used an analytic approach for the kinetic modeling of Ziegler-Natta polymerization of butadiene. Using simplified kinetic equations, moment and monomer concentration were solved analytically. The model prediction of conversion and molecular weights showed good agreement with the experimental data. The chain distribution and the weight average molecular weights were more accurately predicted when the dual active site model was used. This indicates the validity of the multiplicity of the catalytic site hypothesis.

Soares and Hamielec (1995b, 1995c) used a deconvolution method to determine the chain-length distributions of linear polymers made by multiple-site-type catalysts. Also, using the Stockmayer's bivariate distribution, TREF data were analyzed. The deconvolution method was shown to be very useful to analyze the multiplicity of active sites when mass and heat

transfer resistance effects are insignificant.

Bonini *et al.*(1995) proposed a new particle growth model. In their model, only the first external shell of the catalyst is supposed to be active in the initial stages of polymerization. The polymer growing in this shell fills the pores of the catalyst, which consequently results in the fragmentation of the shell, then a layer by layer growth and fragmentation takes place until all the catalyst is completely fragmented. The final stage is the same as the multigrain structure. The model showed good agreements with the experimental results except for the initial stage of the polymerization. However, their model could not predict large polydispersities.

Further reviews by Soares (1994) and by Subramanian and Chou (1995) deal with various modeling studies of the metallocene-catalyzed polymerization reactions.

CHAPTER 3
EXPERIMENTAL

3.1. REAGENTS AND APPARATUS

3.1.1. Reagents

Table 3.1 shows all the reagents used in the experiments. Every air sensitive compound was handled and stored in a dry box (Nexus, Vacuum/Atmospheres Co.) and/or Schlenk type glassware under ultra high purity (UHP) grade nitrogen atmosphere.

Table 3.1 Reagents used in experiments

Name	Formula/Abbr.	Grade	Supplier
Anti-Bumping Granule	N/A	N/A	BDH
Benzophenone	$C_6H_5COC_6H_5$	N/A	BAKER
n-Butyllithium	$CH_3(CH_2)_3Li$	2.5 M in Hexane	Aldrich
Diethyl zinc	$(C_2H_5)_2Zn$	1.1 M in Toluene	Aldrich
Ethanol	C_2H_5OH	Denatured	BDH
Heptane	C_7H_{16}	Distilled	EM Science
Hexane	C_6H_{14}	HPLC	EM Science
Hydrochloric Acid	HCl	ACS	BDH
Irganox 1010	$C_{73}H_{108}O_{12}$	N/A	CIBA-GEIGY
Methylaluminoxane	$(CH_3)_2Al(OAlCH_3)_nAl(CH_3)$ / MAO	10 % in Toluene	Albermarle
Sodium Metal	Na	99.8 %	BDH
Toluene	$CH_3C_6H_5$	ACS	BDH
1,2,4-Trichlorobenzene	$C_6H_3Cl_3$ / TCB	Distilled	EM Science
Triethylaluminum	$(C_2H_5)_3Al$ / TEA	1.9 M in Toluene	Aldrich
Triisobutylaluminum	$[(CH_3)_2CHCH_2]_3Al$ / TIBA	1.0 M in Toluene	Aldrich
Trimethylaluminum	$(CH_3)_3Al$ / TMA	2.0 M in Toluene	Aldrich

Some of the reagents were purified by the following methods. Reagents not mentioned below were used without further purification.

Hexane and Heptane

Ca. 150 g of activated type 4 A molecular sieves were added to 4 L solvent bottles capped with septa. Through a thin needle, ultra high purity nitrogen was bubbled in the solvents and purged through another needle connected to an oil bubbler. The solvents were purged for at least one day before usage and always kept under dry nitrogen atmosphere.

Toluene

Toluene was purified either by refluxing over n-butyl lithium/styrene oligomers or metallic sodium/benzophenone and by distillation in the apparatus shown in Fig. 3.1. For the n-butyl lithium/styrene method, toluene was added to the 4 L multi-neck round bottom flask located at the bottom of the apparatus. One spoonful of anti-bumping granules and 2 or 3 cylindrical solid sodium chunks were added to the system. After purging the system with nitrogen, ca. 20 mL of n-butyl lithium and 20 mL of distilled styrene were transferred to the system by a transfer needle using nitrogen pressure. The solvent temperature was brought up to its boiling point and the solvent was refluxed continuously. When there were enough n-butyl lithium/styrene oligomers, the solution turned to dark yellow, indicating that the solvent is free of oxygen. If not, more n-butyl lithium and styrene were added. Dry nitrogen was continuously bubbled through the top joint of the condenser as shown in Fig. 3.1 to provide an inert atmosphere to the system. When the toluene level in the still was low, more toluene was added under nitrogen pressure without adding extra amounts of sodium, n-butyl lithium, or styrene (up to 20 L of toluene before reinstalling the whole system). For the metallic sodium/benzophenone method, n-butyl lithium and styrene were replaced with enough benzophenone, which will turn the solution to dark blue when the solvent is dry. Both methods showed little difference as far as the solvent purity is concerned. However, when using benzophenone, the still needed to be emptied and reinstalled more frequently due to the decomposition of benzophenone and contamination by its byproducts. On the other hand,

benzophenone is much easier to deal with than n-butyl lithium that is extremely reactive toward oxygen and moisture.

When purified toluene was needed, the three-way valve (T-Valve in Fig. 3.1) was closed to collect distillate and the power to the heating mantle was increased slightly. When enough toluene was collected, the power was reduced and nitrogen flow to the condenser was increased to compensate the volume contraction as the gas cools down in the flasks. When the collected toluene approached room temperature, it was transferred to the side flask through the three-way valve where the solvent could be transferred to the polymerization reactor by a transfer needle under nitrogen pressure supplied by an attached gas line.

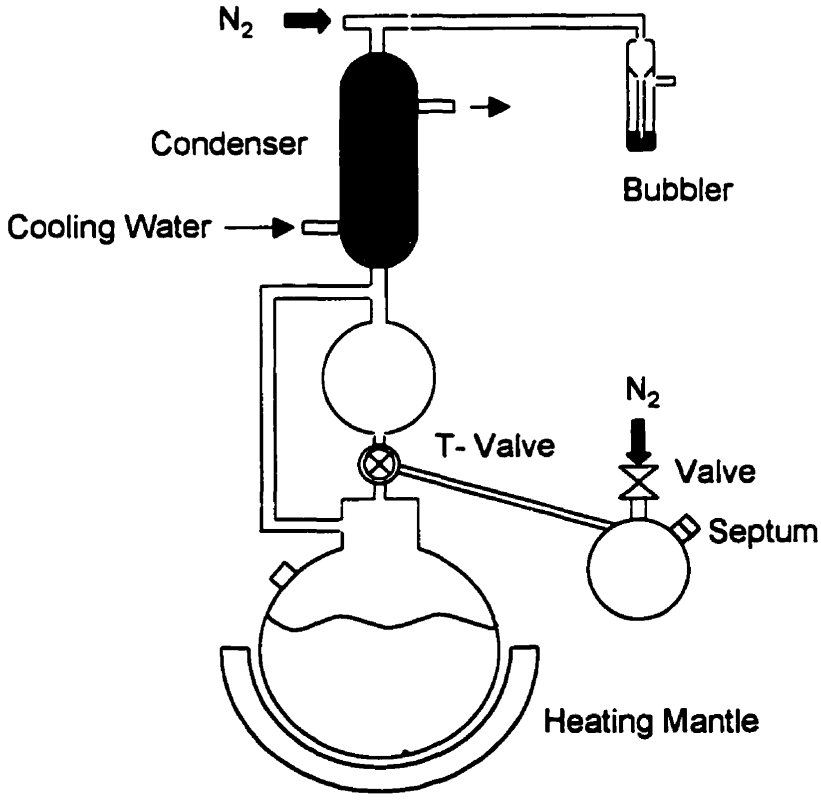

Figure 3.1 Toluene purification and distillation apparatus

3.1.2. Gases

Three different gases were used for the experiments. Nitrogen was used to provide inert atmosphere in the glove box, pipe lines, solvent purification apparatus, and polymerization

reactor system. Ethylene was the monomer used for the polymerization experiments. Ethylene and nitrogen were purified by passing through molecular sieves (type 4A for nitrogen and 5A calcium alumino-silicate for ethylene) and de-oxygen beds (copper(II) oxide supported on alumina). Hydrogen is a typical chain transfer agent for olefin polymerization and used without further purification. A mixture of hydrogen and nitrogen (foaming gas) was used to regenerate the catalyst bed for the glove box. For pressure control, dual stage stainless steel regulators (CONCOA) were used. A CGA 580 fitting was used for the nitrogen gas cylinder and CGA 350 fittings were used for hydrogen and ethylene gas cylinders. Table 3.2 shows the gases used in the experiments.

Table 3.2 Gases used in experiments

Name	Formula	Grade	Supplier
Ethylene	C_2H_4	CP	PRAXAIR
Foaming Gas	7 % H_2 + 93 % N_2	Not analyzed	PRAXAIR
Hydrogen	H_2	UHP	PRAXAIR
Nitrogen	N_2	UHP	PRAXAIR

3.1.3. Catalysts and Supports

Rac-ethylenebis(indenyl)zirconium dichloride was synthesized in our laboratory (Huang, 1995), the CGCTi was donated from Dow Chemical as 10 wt.-% solution in isoparaffin, and the other catalysts were purchased from Aldrich. Catalysts were stored and handled in the glove box. Table 3.3 shows the catalysts used in the experiments.

Table 3.3 Polymerization catalysts

Name	Formula	Supplier
Bis(cyclopentadienyl)zirconium dichloride	Cp_2ZrCl_2	Aldrich
Bis(cyclopentadienyl)hafnium dichloride	Cp_2HfCl_2	Aldrich
Constrained Geometry Catalyst (CGCTi)	See Fig. 4.1	Dow Chemical
Rac-ethylenebis(indenyl)zirconium dichloride	$Et[Ind]_2ZrCl_2$	Laboratory
Rac-ethylenebis(indenyl)hafnium dichloride	$Et[Ind]_2HfCl_2$	Aldrich

Three catalyst supports were used (Table 3.4). Different treatments of these supports further differentiated their behavior toward ethylene polymerization.

Table 3.4 Catalyst supports

Name	Supplier
Silica gel, grade 62, 60-200 mesh, 150 Å	Aldrich
Silica 952, see Table 3.5 for details	Grace Davison
MAO supported on Silica (SMAO), Al 24.4 wt.-%	Witco (Customer P.O. # : 16610)

Detailed information on Silica 952 from GRACE Davison was provided by the supplier as shown in Table 3.5.

Table 3.5 Analysis of silica 952 from GRACE Davison

Chemical Composition	Formula	Weight %
Total Volatile at 1750 °F		7.90
Silica	SiO_2	99.74
Alumina	Al_2O_3	0.04
Sodium	Na_2O	0.07
Sulfate	SO_4	0.01
Iron	Fe_2O_3	0.01
Calcium	Ca	0.07
Magnesium	Mg	0.02
Physical Property		**Quantity**
Surface area		310 m^2/g
Pore volume		1.62 mL/g
Particle Size Distribution		
Mesh (U.S. Standard Sieves)		**Recovered**
60		0.0
100		0.9
T-325		8.9

3.2. SUPPORTED CATALYST PREPARATION

3.2.1. Silica Pretreatment

Calcination

Ca. 100 g of silica was calcinated at a time. First, silica was transferred to a quartz cylindrical flask equipped with a vent line and a dip tube and valves for each line. The cylinder was placed in a vertical furnace and the lines were attached to UPH nitrogen and vented to the fumehood. The temperature was slowly increased to 500 °C under nitrogen flow through the silica by the dip tube. Calcination lasted 5 hours and then the temperature was lowered slowly to room temperature under constant nitrogen flow. Finally, the valves were closed and nitrogen and vent lines were disconnected to move the cylinder into the glove box for transferring and storing of the calcinated silica.

MAO Pretreatment

Special glassware was used to support MAO onto silica. In the glove box, ca. 5 g of calcinated silica and a magnetic stirring bar were placed into the flask shown in Fig. 3.2. The flask was capped with a septum. The flask was brought out of the glove box and placed in a water bath. The valve and the septum provided airtight fitting to prevent contamination from the atmosphere. Through the septum, ca. 50 mL of purified toluene was transferred and the temperature of the bath was increased to 50 °C. While continuously stirring, 10 g of 10 % MAO solution in toluene was added to the system drop-wise through a transfer needle. After addition of MAO, the mixture was stirred for 3 hours, then cooled to room temperature. Using the fritted-glass filter, the solid part was separated from the solution. For this process, the apparatus was connected to a vacuum line with a solvent trap and the flask was slightly tilted so that the solution would be drained through the filter inside. Nitrogen was introduced to the flask by a transfer needle through the septum. The filtered solid was washed with 20 mL of purified toluene for 2 to 3 minutes with vigorous stirring and then filtered again. After repeating the washing and filtering cycle for 5 times, the MAO treated silica was dried by applying vacuum to the flask. The final product was recovered as free flowing powder and transferred to a storage bottle in the glove box.

For the case of SMAO, calcination or MAO pretreatment were not performed, i.e., SMAO was used without any further treatment.

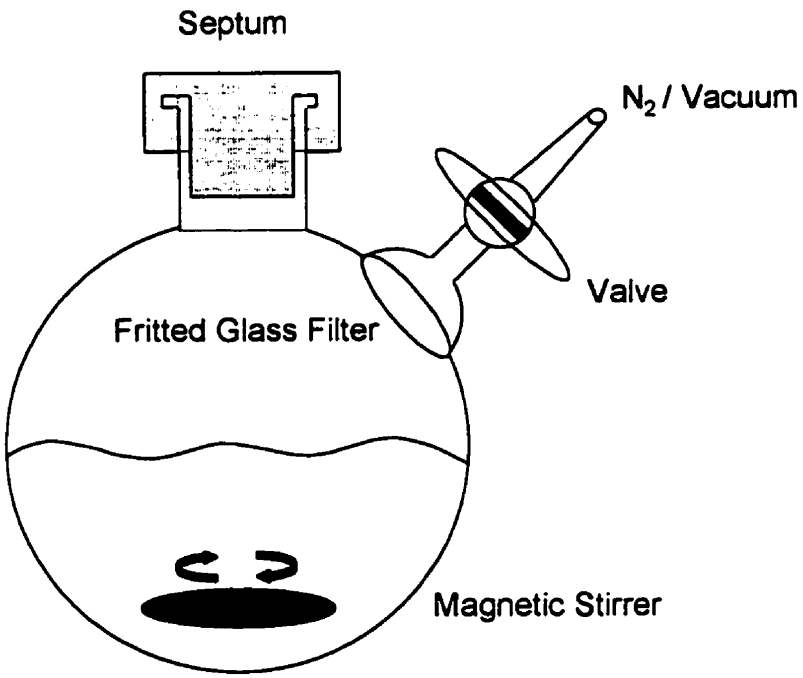

Figure 3.2 Glassware used for catalyst supporting

3.2.2. Catalyst Supporting

All the polymerizations in this thesis were conducted with supported metallocene catalysts. Silica from Aldrich was used for comparison purposes only. The main experiments were done with Silica 952 from GRACE Davison (Silica) and SMAO. 'Silica' refers to the calcinated Silica 952 from GRACE Davison from this point on unless mentioned otherwise. The supports used were silica without MAO pretreatment (Silica), MAO supported on silica from Witco (SMAO), and MAO pretreated Silica (MAO/Silica). For the metallocene supporting procedure, the same technique described in section 3.2.1 for the MAO pretreatment of silica was used. However, for the supporting of metallocenes, the amounts of support were between 0.5 to 1.5 g suspended in ca. 10 mL of toluene. Individual or mixtures of catalysts dissolved in

ca. 10 mL of toluene were transferred to the supporting reactor (Fig. 3.2) containing support suspended in toluene via a transfer needle. The recovered supported catalysts formed a free flowing powder. When supported, Cp_2HfCl_2 remained white but other catalysts turned to pale yellow or pink depending on the catalyst and support.

3.3. POLYMERIZATION

A semi-batch slurry reactor was used for the polymerizations. The Parr-mini autoclave reactor (300 mL, the headspace after addition of diluent is approximately 100 mL) used was equipped with a mass flow meter and a temperature control unit comprising a cooling coil and an electric heater (Fig. 3.3). The control was performed by a personal computer through analog to digital (A/D) and digital to analog (D/A) converters (Fig. 3.4). Two independent proportional - integral (PI) control loops were used to control the cold water flow in the cooling coil and the power input to the electric heater. Most polymerization temperatures, using this control technique, were maintained within ±0.2 °C of the set point. Details on PI control and parameter tuning are described in section 3.5. For MWD control, it is fundamental to have a precise control of polymerization temperature, since temperature oscillations during polymerization will broaden MWD significantly.

Before each polymerization, the autoclave reactor was heated up to 150 °C under vacuum and allowed to cool down under dry nitrogen flow to remove all moisture traces. Then, 145 mL of purified toluene (hexane and heptane used for comparison only) was transferred to the reactor by a transfer needle through a septum inlet under nitrogen pressure. Next, the temperature control was turned on and the reactor temperature was brought up to the set point. The cocatalyst (MAO) prepared in a serum bottle was transferred to the reactor using the same transfer method used for the solvent. The supported catalyst prepared in a separate serum bottle was mixed with ca. 10 mL of purified diluent and transferred to the reactor using another transfer needle. Throughout the experiment the mole ratios of Al/metal were kept close to 800. Hydrogen was injected in the reactor through a syringe or the built-in hydrogen injection port. Where diethyl zinc was used, it was mixed and injected together with

the cocatalyst. Polymerization was started by pressurizing the reactor with ethylene. Ethylene was supplied through the feed line on demand to keep the reactor pressure constant. Therefore, measuring ethylene feed flow rate through the on-line mass flow meter is equivalent to monitoring the polymerization rate. To minimize any mass or heat transfer limitations that might occur due to high polymer concentration in the reactor, polymerization was terminated when about 1 g of polymer was produced based on the ethylene mass flow. Most of the polymerizations were carried out from 20 minutes to 1 hour. To terminate the reaction, the monomer feed line was closed and the reactor was quickly depressurized by opening the outlet gas valve. The polymer slurry in the reactor was poured out into a beaker containing enough ethanol to wash and precipitate the polymer. Ca. 15 mL of acidic methanol was added to the mixture. The final product was washed with excess amount of ethanol, filtered, and dried in a vacuum oven overnight.

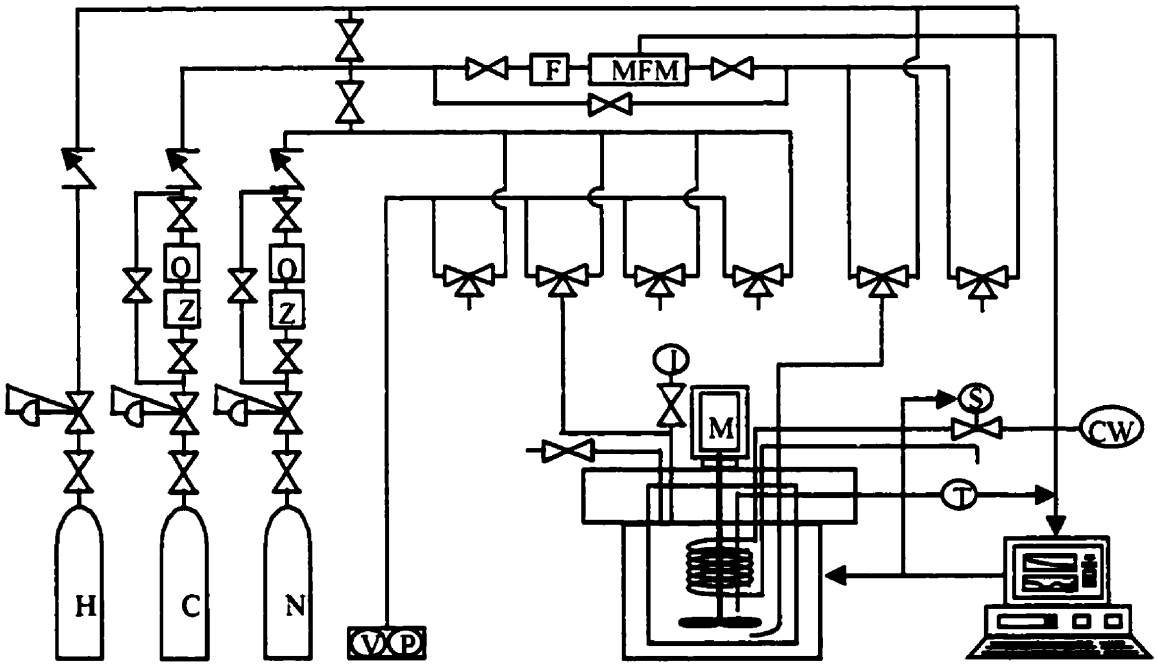

C	:	Ethylene	CW	:	Cooling Water
F	:	Inline Filter	H	:	Hydrogen
I	:	Injection Port	M	:	Motorized Stirrer Drive
MFM	:	Mass Flow Meter	N	:	Nitrogen
O	:	Oxygen Trap	S	:	Solenoid Valve
T	:	Thermocouple	VP	:	Vacuum Pump
Z	:	Moisture Trap			

Figure 3.3 Polymerization reactor system

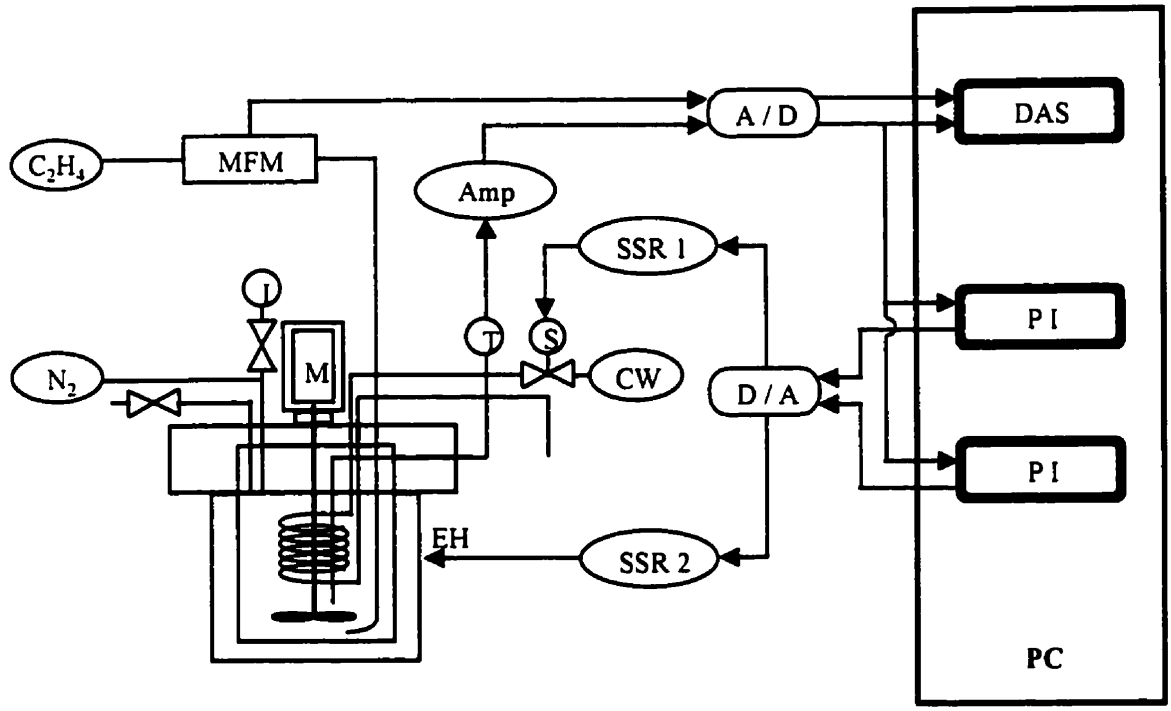

A/D : Analog to Digital Converter
D/A : Digital to Analog Converter
DAS : Data Acquisition System
EH : Electrical Heater
PI : Proportion Integral Control Unit
SSR : Solid State Relay
Other symbols are defined in Fig. 3.3

Figure 3.4 Temperature control of polymerization reactor

3.4. POLYMER CHARACTERIZATION

3.4.1. Crystallization Analysis Fractionation (CRYSTAF)

CRYSTAF is a new technique that allows measuring the distribution of chemical compositions in linear low density polyolefins (LLDPE). Between 0.010 and 0.015 g of polymer sample were placed in the crystallization vessels. 30 mL of TCB containing 0.005 wt.-% Irganox 1010 was introduced into the crystallization vessels by an automatic dispenser. With stirring at 150 rpm, the solution was heated up to 160 °C at a rate of 20 °C/min. The polymer solution was kept at 160 °C for 60 minutes with a stirring rate at 200 rpm to ensure complete dissolution. Then, the temperature was decreased to 95 °C at the rate of 20 °C/min and kept at 95 °C for 60 minutes for equilibration. During sampling, the stirring was reduced to 100

rpm and temporarily stopped when the solution was withdrawn through the filter. Initial sample concentration was measured at 95 °C after the equilibration. The crystallization rate was 0.1 °C/min from 95 to 65 °C and 0.2 °C/min from 65 to 30 °C. TCB was used as the solvent. A two channel infrared (IR) sensor was used to measure the concentration of the polymer solution during the crystallization. At 30 °C the final concentration of the polymer solution was measured. This measurement was combined with the initial one made at 95 °C and used to establish the baseline for the subsequent calculations.

After the analysis was finished the auto cleaning procedure was performed at 160 °C with stirring at 200 rpm. All the remaining solution was drained through the dip tubes in the reactors. Then 5 mL of TCB was transferred through the filter in the reactors and drained through the dip tubes again. This cycle was repeated with another 10 mL and 35 mL of TCB. Finally, the system was cooled down to room temperature and ready for the next analysis.

3.4.2. Gel Permeation Chromatography (GPC)

Molecular weight distributions of polyethylene were determined by high temperature gel permeation chromatography (Waters GPCV 150+) with universal calibration, using TCB as the eluent at 140 °C with flow rate of 1.0 mL/min. GPCV 150 + has three zones with different temperature settings. In the column compartment, banks of columns are placed at high temperature. The sample tray and auto sampler are located in the injection compartment. And finally, the high-pressure liquid chromatography pump is located in the pump compartment. The temperature in the column compartment and injection compartment was kept at 140 °C, but 60 °C was used for the pump compartment.

Preparation of Eluent

To prevent polymer degradation, 1.5 g of an anti-oxidant (Irganox 1010) was added to 4 liters of TCB. When the anti-oxidant was dissolved, the solution was contacted to activated silica to remove moisture, and then filtered through 10 μm membrane filters under vacuum. The final filtrate was transferred to the eluent reservoir and continuously stirred to prevent any

precipitation. To reduce chromatogram base line fluctuation, air was removed from the eluent by a degassing device (Shodex Degas, model KT-27, Showa Denko, Inc.).

GPC Columns

Three linear columns (Styragel HT 6E, Waters) were used for GPC analysis. The nominal molecular weight range for these columns is from 5,000 to 10,000,000 g/mole.

Universal Calibration

Polystyrene standards with narrow molecular weight distributions were used for establishing the universal calibration. Four standards per decade are generally required for the calibration over the molecular weight range, which is typically 10^3 to 10^6. Since the Styragel HT 6E columns are designed to cover molecular weight ranges from approximately 5,000 to 10 million, 19 polystyrene standards with molecular weights ranging between 2,400 and 4,200,000 were used for the calibration. Occasionally, analyses on broad standards were conducted to check the validity of the calibration and state of the columns.

Sample Preparation

Samples were prepared in 4 mL screw cap vials used in the auto-injection tray. Individual filtration of the polymer samples was not required. Instead, polymer solutions were injected through 45 μm in-line filters, which were replaced regularly.

The concentration of the samples were chosen to give the "optimum" output for the refractive index (RI) and viscosity detectors, in a reasonably low concentration which would not cause intermolecular interactions between polymer chains.

For narrow polystyrene standards, the following empirical equation suggested by Waters was used :

$$0.025 = [\eta] \cdot (Con.\%) \tag{3.1}$$

$$[\eta] = kM^{\alpha} \tag{3.2}$$

where, k = 0.00015, α = 0.7 for polystyrene, and Conc. % = [g/L]

For most of the regular polyethylene broad samples, ca. 1.5 mg of polymer was dissolved in 4 mL of TCB in a GPC vial. All the vials prepared in this way were left in the GPC injection compartment for 5 to 25 hours before injection to ensure proper polymer dissolution. 300 μL of the sample solution was injected for analysis.

3.4.3. FT-IR and FT-IR/LC Transform Analysis

For copolymer composition analysis, samples were first hot pressed at 350 °F to make thin circular films of about 1 cm in diameter. To make uniform films, the samples were allowed to melt for about 1 minute then pressed at 400 psi for 10 seconds. The peak heights appearing at 720, 745, 968, 1150, 1368, and 1380 cm^{-1} were of primary interest.

LC Transform

To measure the comonomer content across different molecular weight regions, LC-transform analysis was conducted using Model 303 LC-Transform System from Lab Connections, Inc. A simple illustration is shown in Fig. 3.5. In this method, the eluent, which contains fractionated polymer from GPC, is continuously collected on a rotating disk for off-line FT-IR analysis. For proper precipitation of the samples on the disk, the flow rate of eluent in GPC was set to 0.5 mL/min. When LC-Transform is being used, the eluent flow was directed to a heated transfer line (140 °C) to be sprayed through an ultrasonic nebulizer on the germanium disk in a vacuum chamber. The nozzle was kept at 110 °C and the stage temperature was 135 °C. A timer was used to start rotating the disk after waiting a predetermined time interval from the injection of the sample in GPC. Samples were collected at a rotation speed of 10 degree/min. Comonomer contents of the samples coated on the reflective germanium disk are directly measured by FT-IR using a special accessory. The accessory consists of arrays of mirrors to direct the IR rays to go through the sample, be reflected by the disk, and then finally reach the sensor.

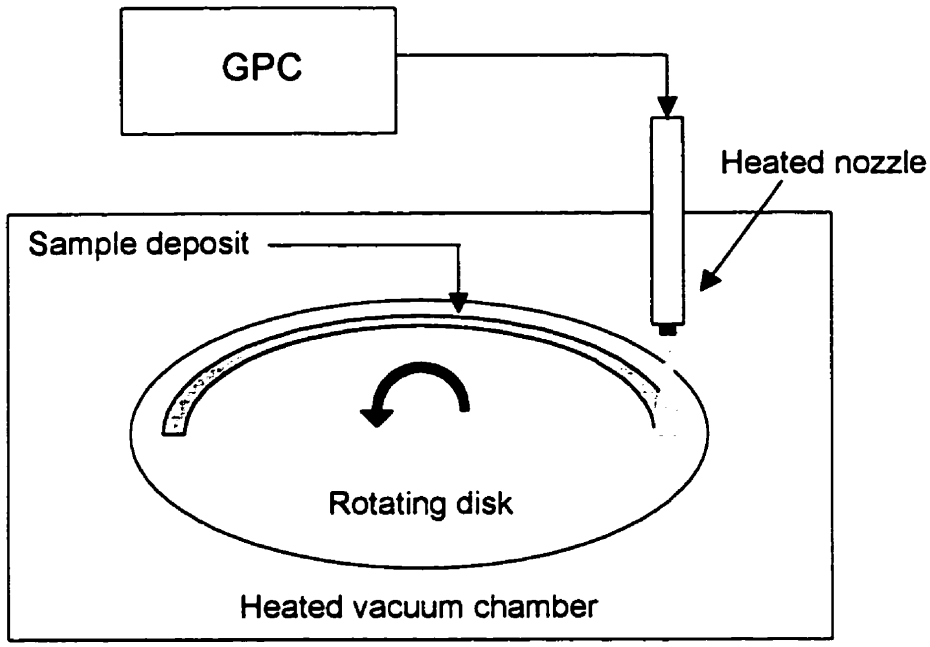

Figure 3.5 Sample collection on a rotating disk in LC-Transform

3.4.4. Differential Scanning Calorimetry (DSC)

DSC (TA Instruments) was calibrated with indium by setting its melting point to 156.61 °C. About 5 to 10 mg of sample was prepared in DSC pans and pelletized to be analyzed. The melting point was measured at the second melting cycle at the temperature ramp of 10 °C/min. for both heating and cooling. Between every cycle of the temperature ramp, the sample was allowed to equilibrate at isothermal conditions for 1 minute.

3.4.5. Nuclear Magnetic Resonance (NMR) Spectroscopy

A Bruker AC 300 NMR was used for the analyses. Samples were prepared in 10 mm NMR tubes at a concentration of ca. 10 wt.-% polymer in TCB. To prevent air bubbles forming during dissolution, polymer powder was first hot pressed at 350 °F to make a thin film, then cut into small strips and transferred to NMR tubes. TCB containing 0.005 % Irganox 1010

was added dropwise until the sample was almost covered with solvent. After heating in an oven for 20 – 30 minutes at 145 °C, the sample was ready for the analysis. For the analysis, the probe temperature was 125 °C, spinning was 15 rpm, and the proton decoupling was turned on. Some important parameters used include flip angle = 33 °, D1 = 3 sec, S2 = 8H, RD = 0, PW = 4 μs, DE = 75 μs, NS = 100, DS = 0, P9 = 95, D2 = 0.005 sec.

3.5. PROCESS CONTROL

To achieve reliable and reproducible polymerizations, it is essential to have good control over polymerization conditions such as temperature, monomer pressure, stirring, etc. Among these conditions, polymerization temperature and monomer pressure can significantly affect the physical properties of the produced polymers. Considering the high activity and high exothermicity of the reaction, temperature control is especially important. In our system, a dual stage pressure regulator maintains the monomer pressure constant. For temperature control, a cooling coil and an electrical heating jacket was used to maintain the polymerization temperature close to its set point. For temperature measurement in the polymerization reactor, an 8 channel 20 bit analog to digital converter was used, which was equipped with a type J thermocouple and an internal cold junction for temperature correction.

To have good temperature control, proper tuning of control parameters is very important. Due to the character of the polymerization system, there are several constraints associated with temperature control. For instance, a large temperature overshoot is not allowed, since it could deactivate the catalyst and increase the risk of solvent fire. Sluggish control can cause broadening of molecular weight or chemical composition distributions. However, too aggressive control will cause fluctuation of reactor head space pressure, which in turn, will cause difficulties in the reaction rate measurements through the mass flow meter.

When the control parameters were poorly tuned, the temperature was stable until the polymerization started. However, as soon as the highly exothermic polymerization started, the temperature became unstable as shown in Fig. 3.6.

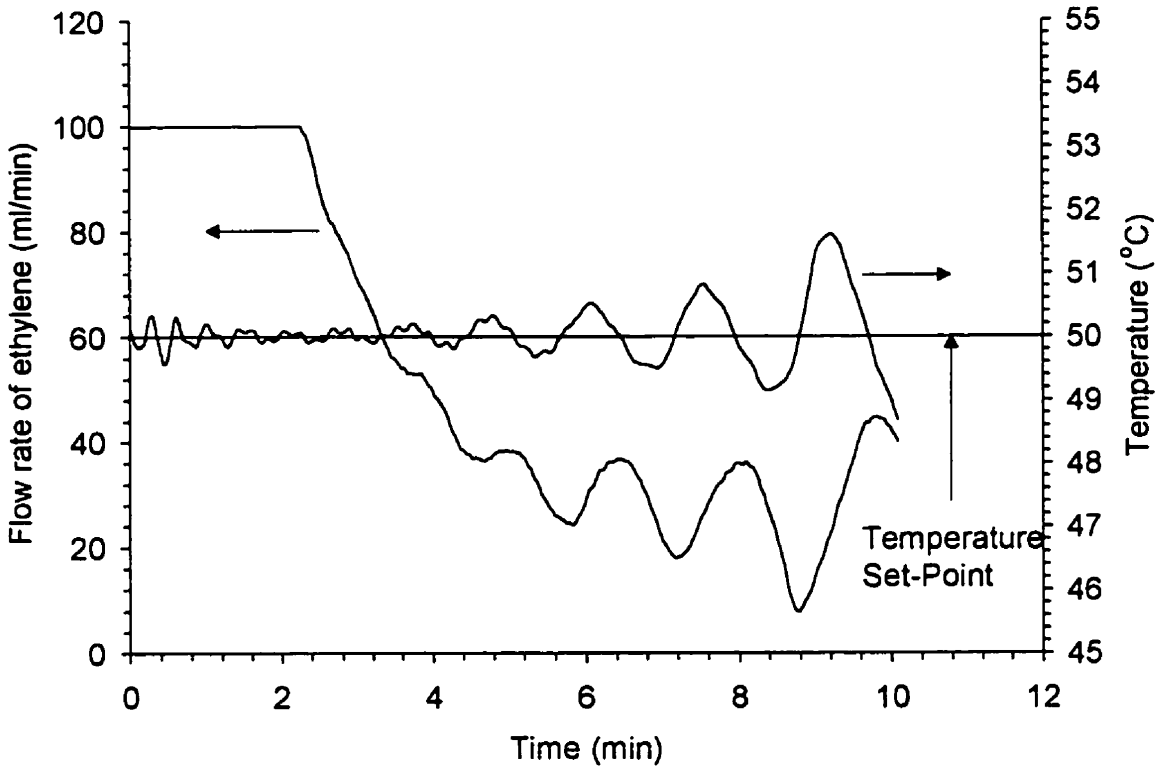

Figure 3.6 Unstable temperature control

Fig. 3.6 shows that charging the polymerization reactor with ethylene caused a small temperature fluctuation between 0 to 1 minute due to the temperature difference between the gas and reaction diluent. However, with the beginning of polymerization the temperature control becomes unstable. (The ethylene flow rate shown for the first 2 minutes is above the sensor maximum flow range; as the diluent approaches saturation with ethylene, the flow rate begins to stabilize at around 25 mL/min.) As the temperature control becomes unstable, the flow rate starts fluctuating due to the varying solubility of ethylene in the diluent caused by the temperature oscillations. It is interesting to notice that even though the amplitude of the temperature oscillation was less than 2 °C, the flow rate of ethylene could vary by more than 20 mL/min. This demonstrates the importance of good temperature control in accurately measuring polymerization rate through a mass flow meter.

For proper tuning of the control parameters, it is necessary to characterize the process. For this purpose, temperature step tests were performed at several polymerization conditions without injecting catalysts. Eq.(3.3) was used as the transfer function.

$$G_{process}(s) = \frac{\bar{y}_m(s)}{\bar{c}(s)} \approx \frac{K\bar{e}^{t_d s}}{\tau s+1} \tag{3.3}$$

where, $\bar{y}_m(s)$ = output function, $\bar{c}(s)$ = input function, K = process gain, τ = time constant, and t_d = time delay.

Fig. 3.7 shows the temperature response of the reaction medium in the reactor after heating was increased from 50 % to 60 % stepwise with constant cooling at 10 % of its full capacity. Interestingly, an inverse response was observed initially. From this test, the process gain K was measured as 0.68 and the time constant for heating, τ, was estimated as 12.5 min. The delay time (t_d) observed was 1.5 min.

Fig. 3.8 shows the response of the temperature subjected to step change in cooling from 10 % to 15 % at constant heating at 60 %. From this test, the process gain, time constant, and delay time for cooling were estimated as –0.70, 6.36, and 0.1~1 min, respectively.

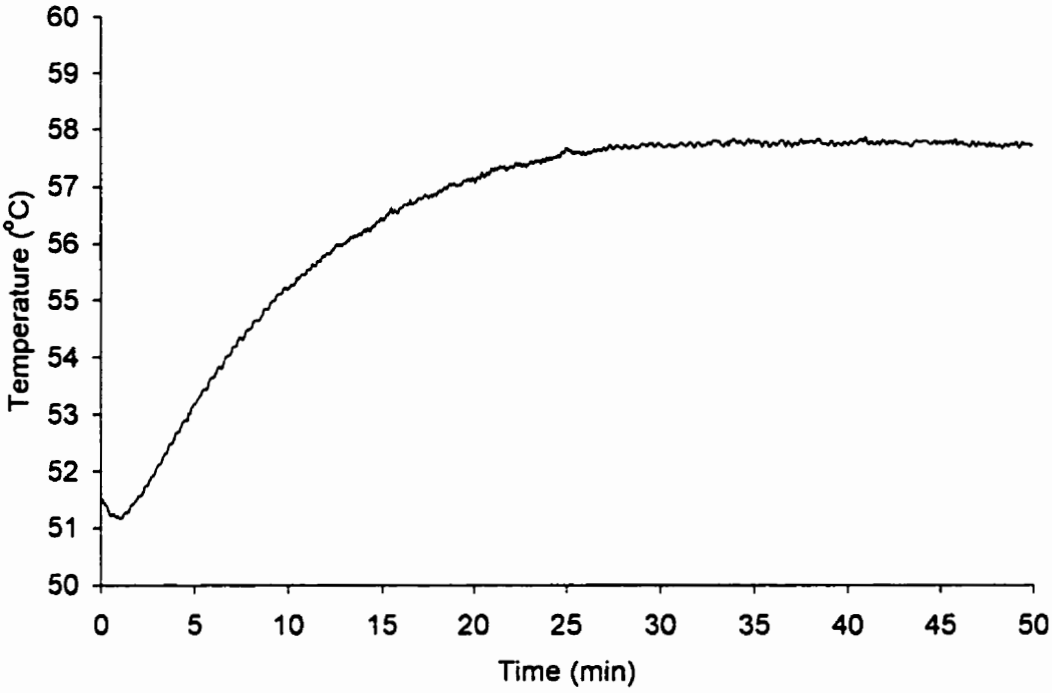

Figure 3.7 Step test: constant cooling at 10 %, step increase of heating from 50 % to 60 %

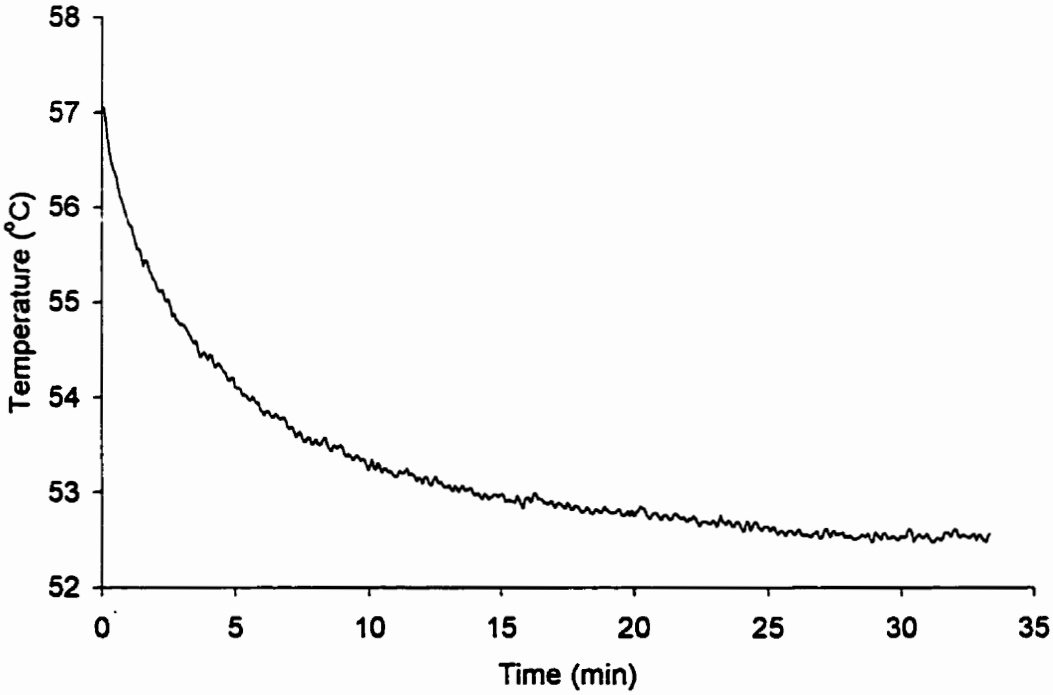

Figure 3.8 Step test: constant heating at 60 %, step increase of cooling from 10 % to 15 %

Using these process parameters (Table 3.6), control parameters for PI control were calculated using Cohen-Coon, integral of the time-weighted absolute error (ITAE), internal model control (IMC), and Dahlin's algorithms.

Table 3.6 Process parameters estimated by step test method

	K	τ	t_d
Heating	0.68	12.5	1.5
Cooling	- 0.70	6.36	0.1-1.0

Example of Cohen and Coon Method

The following example describes the estimation of control parameters based on Cohen-Coon controller design relations.

$$K_c = \frac{1}{K}\frac{\tau}{t_d}\left(0.9 + \frac{t_d}{12\tau}\right) \tag{3.4}$$

$$\tau_I = t_d \frac{30 + 3\frac{t_d}{\tau}}{9 + 20\frac{t_d}{\tau}} \tag{3.5}$$

where, K_c = control gain and τ_I = integral time constant.

Using the process parameters in Table 3.6 for Eq. 3.4 and 3.5, the control gain and integral time constant are calculated. For other methods, examples can be found in the book by Seborg *et al.* (1989). Table 3.7 summarizes the calculated control parameters based on the previously mentioned algorithms.

Fig. 3.9 describes the overall feed back temperature control model in a block diagram. First the set point (y_{sp}) and the actual measurement (y_m) will be compared to initiate proper control action toward the heater and cooling water valve. In this step, the PI control algorithm will determine the amount of power required for the heater and the flow rate of the cooling water. Since on/off type solenoid relays are used instead of proportional output devices, the

ratio of on and off within each control cycle was varied to give proportional output. For instance, to generate 80 % of heating output, the heater was turned on for 4 sec. and off for 1 sec. during its 5 sec. cycle time. By these control actions the process will respond according to the model characterized for the system toward moving closer to the set point.

Table 3.7 Summary of estimated control parameters based on different algorithms

Method		K_C	τ_I
Cohen-Coon	Heating	11.2	4.0
	Cooling (t_d = 0.1)	81.9	0.3
	Cooling (t_d = 1.0)	8.3	2.5
ITAE Load	Heating	10	4.4
	Cooling (t_d = 0.1)	70	0.6
	Cooling (t_d = 1.0)	7.5	2.7
IMC	Heating	6.5	13.5
	Cooling	4.6	6.4
Dahlin	Heating	0.73	12.5
	Cooling	0.71	6.4

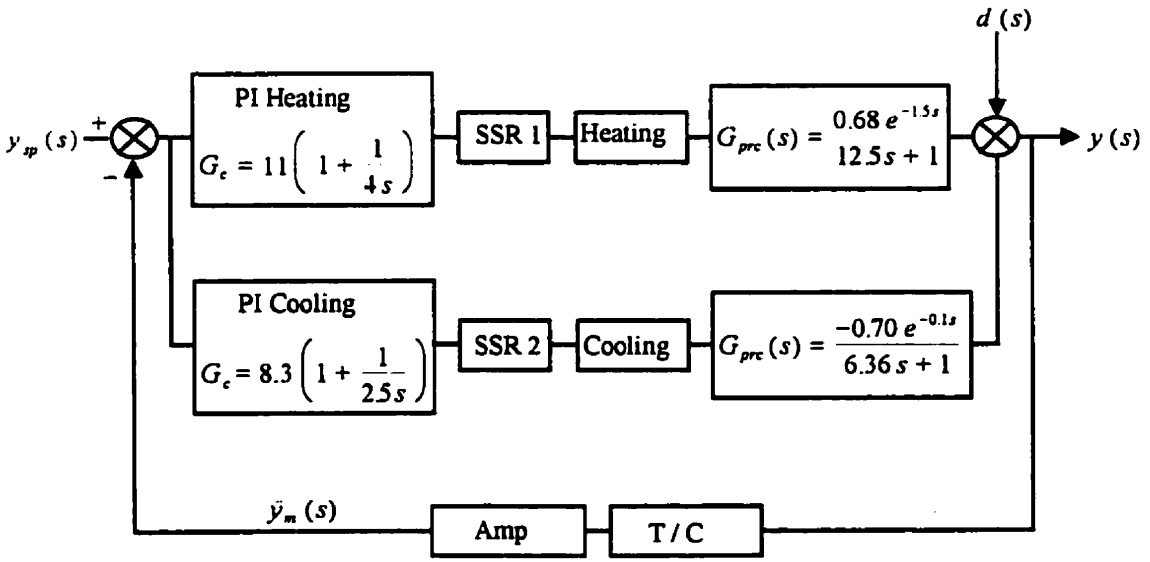

Figure 3.9 Block diagram for temperature control using Cohen-Coon

Fig. 3.10 compares the results from using different control parameters determined by each algorithm. It is shown that the Dahlin method has less high frequency oscillation, however, more overshoot and sluggish control. Cohen-Coon algorithm provided the lowest overshoot and the fastest stabilization. The response from IMC was somewhere in between Dahlin and Cohen -Coon algorithms. The response based on ITAE was similar to the response based on Cohen-Coon, therefore, it was omitted from the plot. When slightly modified parameters, estimated from Cohen-Coon method, were used for the temperature control during actual polymerizations, the temperature remained within ± 0.2 °C from the set point most of the time. Fig. 3.11 shows representative example of polymerization temperature control and monomer flow during an ethylene polymerization run.

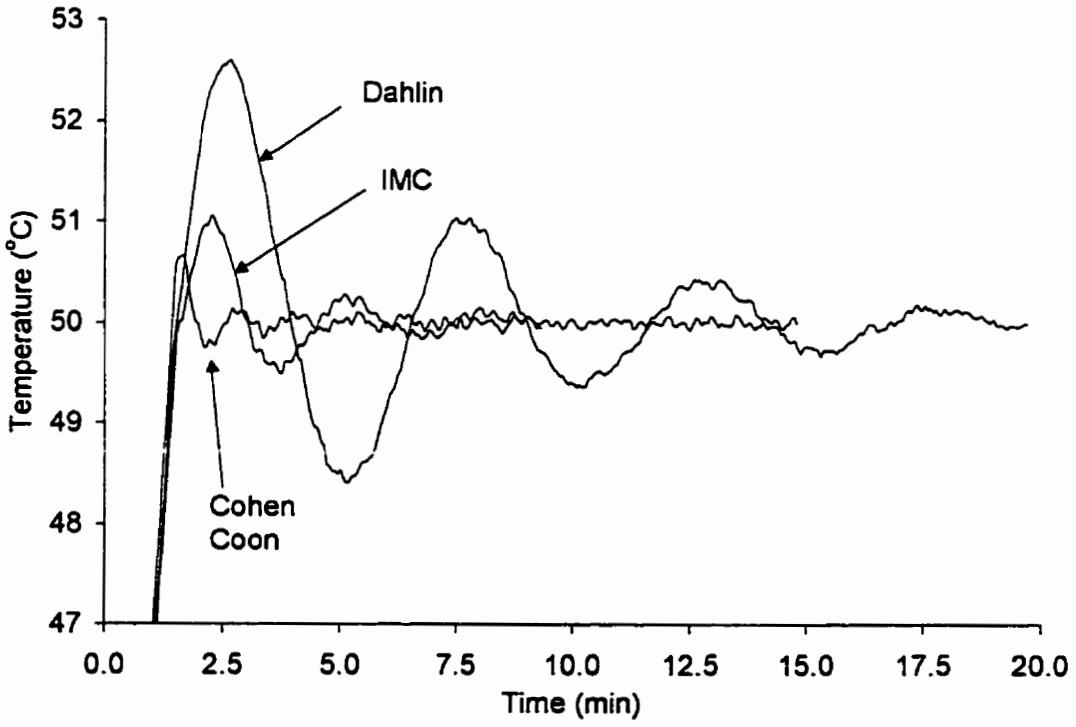

Figure 3.10 Comparison of different tuning methods on temperature control

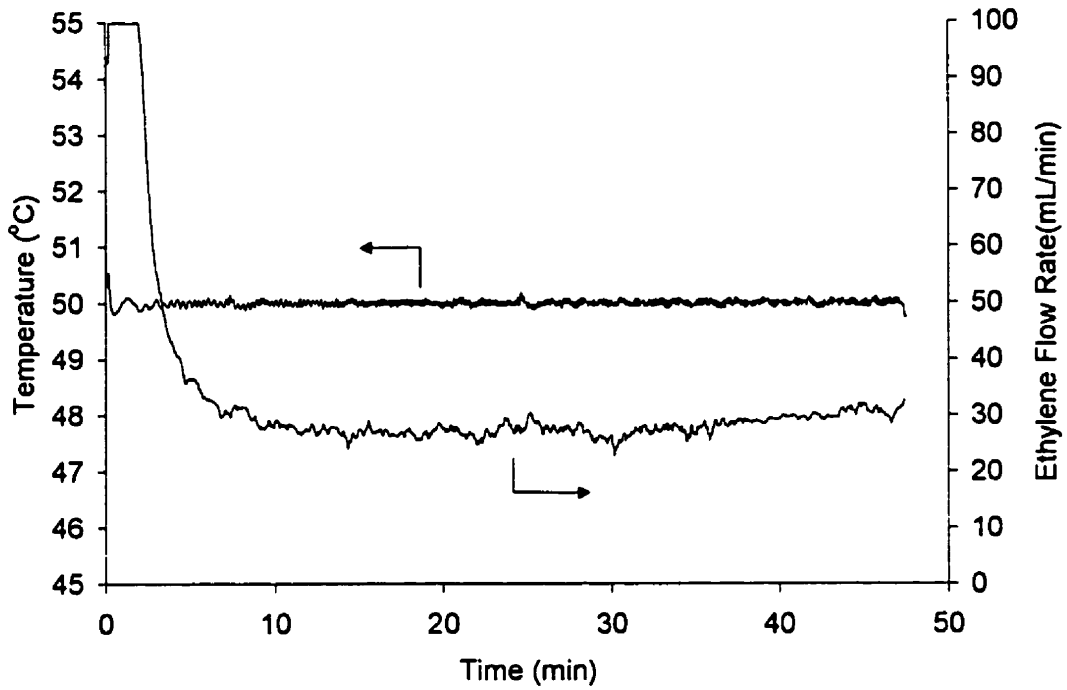

Figure 3.11 Polymerization temperature and ethylene flow rate measurements ($Et[Ind]_2ZrCl_2$, 50 °C, $P_{Ethylene}$ = 50 psi)

CHAPTER 4
HOMOPOLYMERIZATION

The primary purpose of the research described in this chapter is to propose an alternative way of controlling microstructure of polyolefins that does not involve the use of reactor cascade technology. Since reactor cascade technology involves at least two reactors operated at different polymerization conditions, the polymers produced at each reactor are not fully mixed at the microparticle level. Thus, for some applications, an additional mixing step is required to enhance homogeneity of the polymer (Scheirs *et al.*, 1996). Therefore, it will be more cost effective if one can produce the same kind of polymers in a single reactor.

The first step for controlling microstructure of polymer is the control of molecular weight distribution (MWD). To produce polymers with bimodal MWD in a single reactor, mixtures of metallocene catalysts supported onto a single support were investigated. For this purpose, three different catalysts were selected which produced polymers with different average molecular weights. For the continuation of the investigation for copolymers in the next chapters, different catalyst geometries were considered as well, which affect reactivity ratios in case of copolymerization. Each catalyst has varying sensitivities toward polymerization conditions such as monomer pressure in the reactor, temperature, and chain transfer agent concentration (Table 4.1 and Fig. 4.1).

Once correlations between polymerization conditions and molecular weights of polymers produced with each metallocene are established, MWD of polyethylene can be controlled by two different methods. In the first method, MWD can be controlled by combining different metallocenes at different ratios. For instance, according to Table 4.1, the combination of $Et[Ind]_2ZrCl_2$ and Cp_2HfCl_2 produces a catalyst that will synthesize polymer with low and high molecular weight chains, thus the MWD will be broad. On the other hand, the combination of $Et[Ind]_2ZrCl_2$/CGCTi or CGCTi/Cp_2HfCl_2 produces catalysts that will synthesize polymers with low to medium or medium to high chain lengths at a given polymerization condition, respectively.

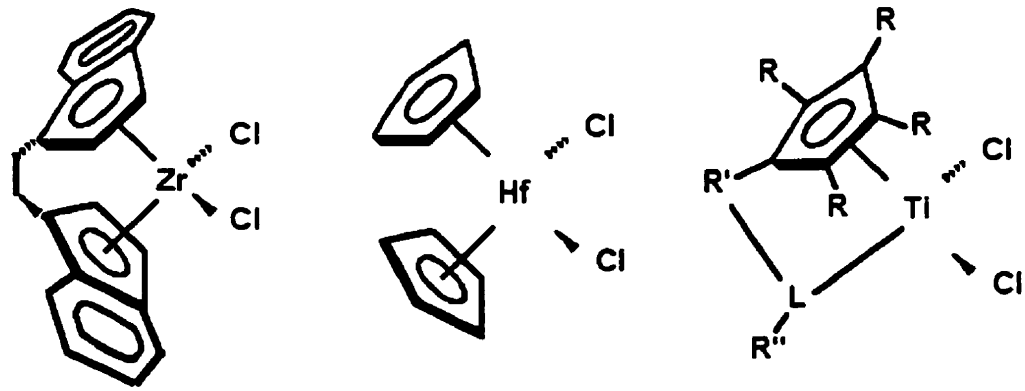

$Et[Ind]_2ZrCl_2$ Cp_2HfCl_2 CGCTi

Figure 4.1 Catalyst structures (CGCTi - constrained geometry catalyst with Ti center : R, R', R'' - alkyl group, L - bridge group)

Table 4.1 Catalysts behavior based on preliminary experimental results

Catalyst	M_n	Comonomer Incorporation	Sensitivity Toward Chain Transfer Agent
$Et[Ind]_2ZrCl_2$	Low	Low	Low
Cp_2HfCl_2	High	Medium	High
CGCTi	Medium	High	High

M_n : Number average molecular weight

The second way of controlling MWD is to take advantage of the different sensitivities of metallocene catalysts toward varying polymerization conditions. For a given combination of metallocene catalysts, MWD can be manipulated by varying polymerization conditions as long as each catalyst has a different response toward the change in the manipulated variable.

In this chapter, the effect of polymerization temperature, chain transfer agent concentration, and impurity on the polymerization of ethylene will be investigated. The feasibility of controlling MWD through the combination of catalysts and/or selecting different polymerization conditions for a given combined catalyst will be investigated. This chapter will

investigate the combined catalyst $Et[Ind]_2ZrCl_2$ / Cp_2HfCl_2 supported on Silica/MAO in the ratio of 0.36 mol/mol. This catalyst will be called the "combined catalyst".

4.1. CATAYST ACTIVITY AND POLYMERIZATION RATE PROFILE

The activities of each catalyst for ethylene homopolymerization at different polymerization conditions are reported in Appendix A. For supported metallocenes, the reproducibility of activities for each catalyst was poor. However, the produced polymers still had very reproducible MWDs regardless of the varying activity. Table 4.2 summarizes the average activities for each catalyst.

Table 4.2 Average (over polymerization time) activities of catalysts for ethylene homopolymerization [kg PE/(mol metal × atm ethylene × hr)]

Catalyst	40 °C	50 °C
$Et[Ind]_2ZrCl_2$	1,970	2,480
Cp_2HfCl_2	210	345
CGCTi	31	48

As can be predicted from a simple Arrhenius equation, the activity increases at higher polymerization temperatures for all catalysts. Polymerization rate results at different ethylene pressures indicate that the polymerization was 1st order with respect to ethylene pressure. However, in the case of $Et[Ind]_2ZrCl_2$ with hydrogen, the activity decreased with increasing hydrogen concentration as shown in Fig. 4.2. No significant trends of increasing or decreasing activities were observed in other catalysts under varying hydrogen concentrations.

Fig. 4.3 shows representative polymerization rate profiles for each catalyst. When ethylene is charged initially, the flow rate is out of the sensor maximum range, therefore, it appears as a straight line at the top of the curve. Soon, saturation of ethylene into the reaction diluent occurs and as a result the flow rate begins to decrease. For the case of $Et[Ind]_2ZrCl_2$, the activity was very high at these conditions, therefore the reaction had to be stopped shortly

after the start of polymerization to avoid mass transfer resistances. For Cp_2ZrCl_2 and CGCTi, the flow rates reach steady state approximately 10 minutes after the start of polymerization. Throughout the experiments, the observed polymerization rate profiles showed steady activity or slight deactivation.

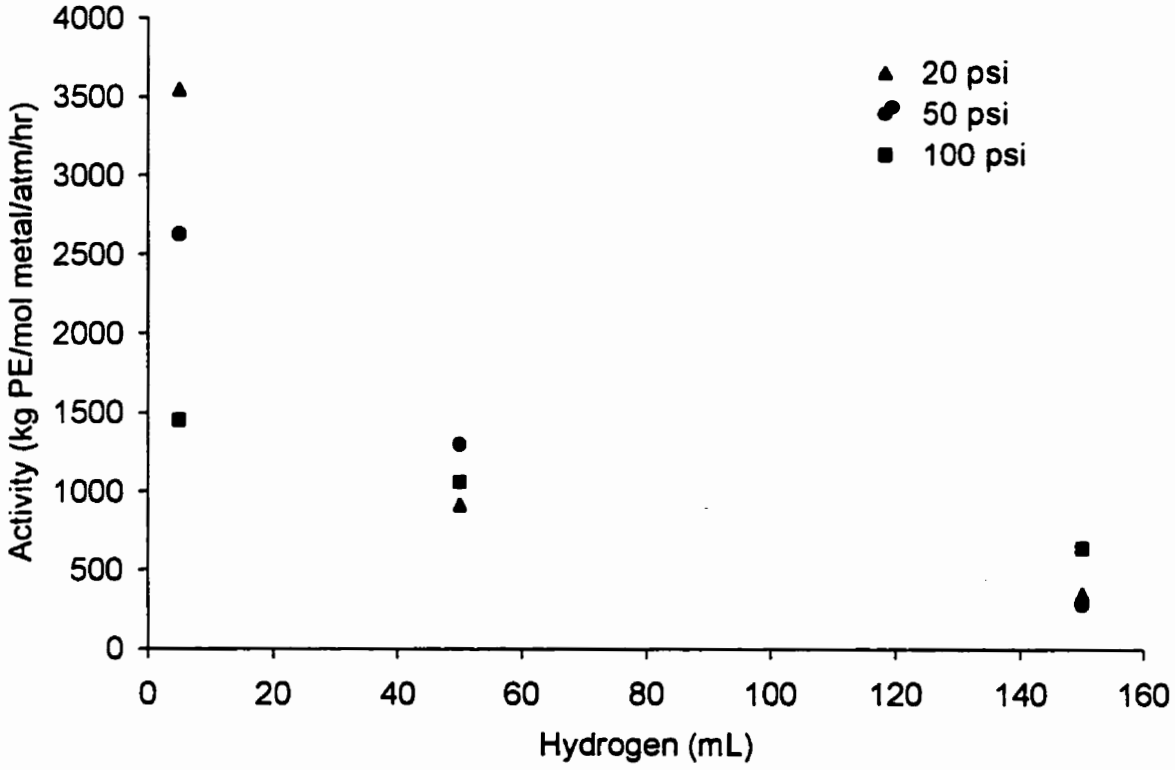

Figure 4.2 Effect of hydrogen partial pressure and ethylene pressures on catalyst activity for $Et[Ind]_2ZrCl_2$, 50 °C

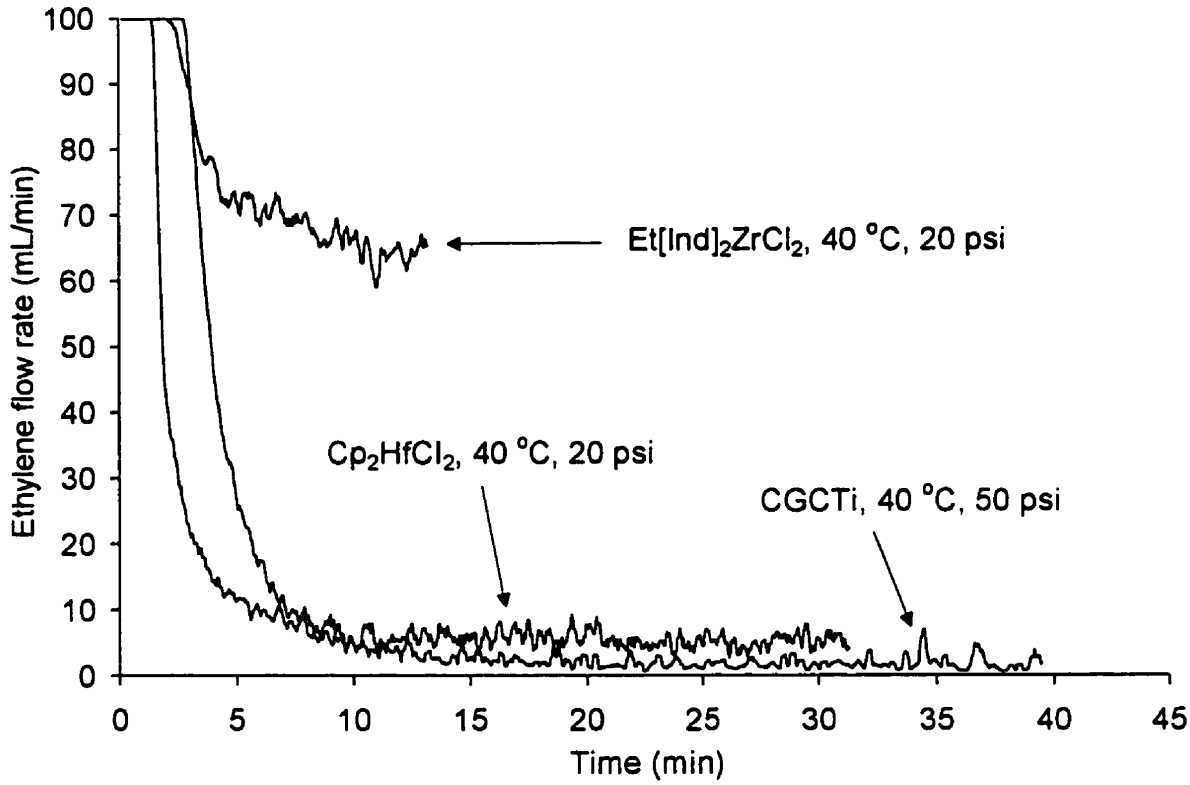

Figure 4.3 Polymerization reaction rates for each catalyst (measured as flow rate of ethylene to the polymerization reactor)

4.2. SUPERPOSITION OF MOLECULAR WEIGHT DISTRIBUTIONS

Deconvolution of Molecular Weight Distribution

The molecular weight distribution of polymers produced with combined catalysts is the superposition of the MWDs of polymer chains produced at each active catalyst site type. Metallocene catalysts have uniform site types that produce polymers with MWDs that follow closely Flory's most probable distribution. Although, Flory's distribution is defined for instantaneously produced polymer chains, it also applies for accumulated polymer chains if the reactor is operated at steady-state. Therefore, the MWD of polymer produced with a combined catalyst can be deconvoluted into two or more Flory's distributions.

The weight chain length distribution of polymer made with a single site catalyst is given by the equation:

$$W(n) = n \cdot \tau^2 \cdot e^{-\tau n} \tag{4.1}$$

where n is chain length and the parameter τ in Flory's distribution (the reciprocal of the number average degree of polymerization at steady state) can be expressed as follows

$$\tau = \frac{R_M}{R_p} + \frac{R_\beta}{R_p} + \frac{R_{CTA}}{R_p} + \frac{R_{MAO}}{R_p} = \frac{k_M}{k_p} + \frac{k_\beta}{k_p[M]} + \frac{k_{H_2}[H_2]}{k_p[M]} + \frac{k_{MAO}[MAO]}{k_p[M]} \tag{4.2}$$

where R_p, R_M, R_β, R_{CTA}, and R_{MAO} are the rates of propagation, transfer to monomer, β-hydride elimination, transfer to chain transfer agent, and transfer to MAO, respectively, and k_p, k_M, k_β, k_{CTA}, and k_{MAO} are their equivalent rate constants. [M], [H_2], and [MAO] are the concentrations of monomer, hydrogen, and MAO. Therefore, the overall MWD of a polymer made with two different metallocenes can be expressed as a superposition of two Flory's distributions :

$$W(n) = w_1 n\tau_1^2 \cdot e^{-\tau_1 \cdot n} + w_2 n\tau_2^2 \cdot e^{-\tau_2 \cdot n} \tag{4.3}$$

where $W(n)$ is the weight chain length distribution for polymer molecules with n monomer units, w_i is the weight fraction of polymer made on each catalyst site type, and τ_i is the overall ratio of chain termination rates to chain propagation rate for each site type.

Fig. 4.4 shows that for the combined catalyst ($Et[Ind]_2ZrCl_2/Cp_2HfCl_2$), the bimodal MWD is very well described by the superposition of two Flory's distributions, each with polydispersity index (PDI) of 2. The low and high molecular weight peaks in the bimodal MWD correspond to polymer chains produced on $Et[Ind]_2ZrCl_2$ and Cp_2HfCl_2 sites, respectively.

The higher molecular weight of polyethylene produced with Cp_2HfCl_2 maybe caused by the greater metal-carbon bond enthalpy for hafnium (Heiland and Kaminsky, 1992). This factor will also reduce the activity of Cp_2HfCl_2 due to slower rate of monomer insertion into the bond between the metal and the growing polymer chain, as was shown in Table 4.2. The

differences in activity of catalysts must be considered in the design of combined catalysts to produce polymers with proper ratio of high and low molecular weight fractions.

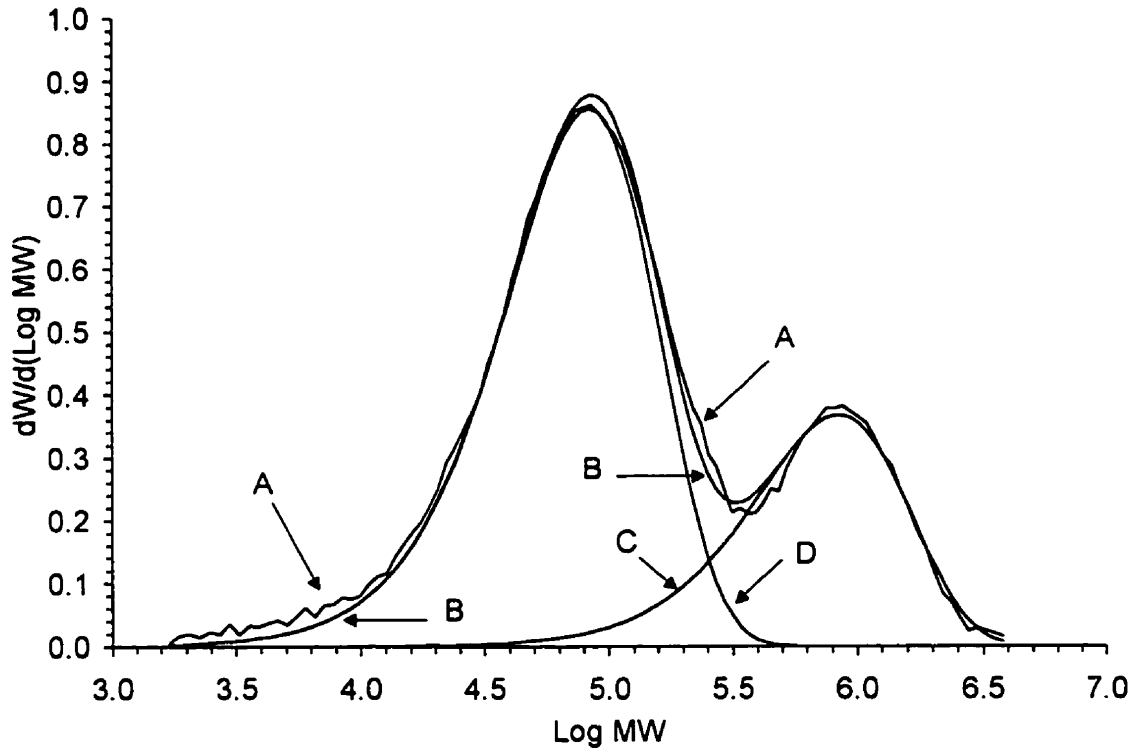

Figure 4.4 Fit of bimodal MWD with two Flory's distributions: (A) experimental distribution measured by GPC, 40 °C, $P_{Ethylene}$ = 120 psi, combined catalyst ($Et[Ind]_2ZrCl_2$ / Cp_2HfCl_2 = 0.36 mol/mol at initial feed for supporting); (B) superposition of (C) and (D); (C, D) Flory's distributions for polyethylene produced with Cp_2HfCl_2 and $Et[Ind]_2ZrCl_2$, respectively

$R^2 = 0.995$

$w_{Zr} = 0.70$, $w_{Hf} = 0.30$

95 % confidence intervals for τ :

$0.0006639 \leq \tau_{Zr} \leq 0.0006785$

$0.00006491 \leq \tau_{Hf} \leq 0.00006833$

4.3. EFFECT OF POLYMERIZATION TEMPERATURE

Fig 4.5 shows the effect of polymerization temperature on the MWD of polyethylene made with the combined catalyst. From the comparison of the peak areas, it is noticed that the relative amount of polyethylene produced on Cp_2HfCl_2 sites decreases as the polymerization temperature increases. This could be explained if $Et[Ind]_2ZrCl_2$ had higher activation energy than that of Cp_2HfCl_2. However, considering the results in Table 4.2, it is more likely that the observed changes are caused by faster deactivation of Cp_2HfCl_2 active sites at higher polymerization temperatures. It is clear, however, that the MWD of the polymer can be controlled by varying the polymerization temperature.

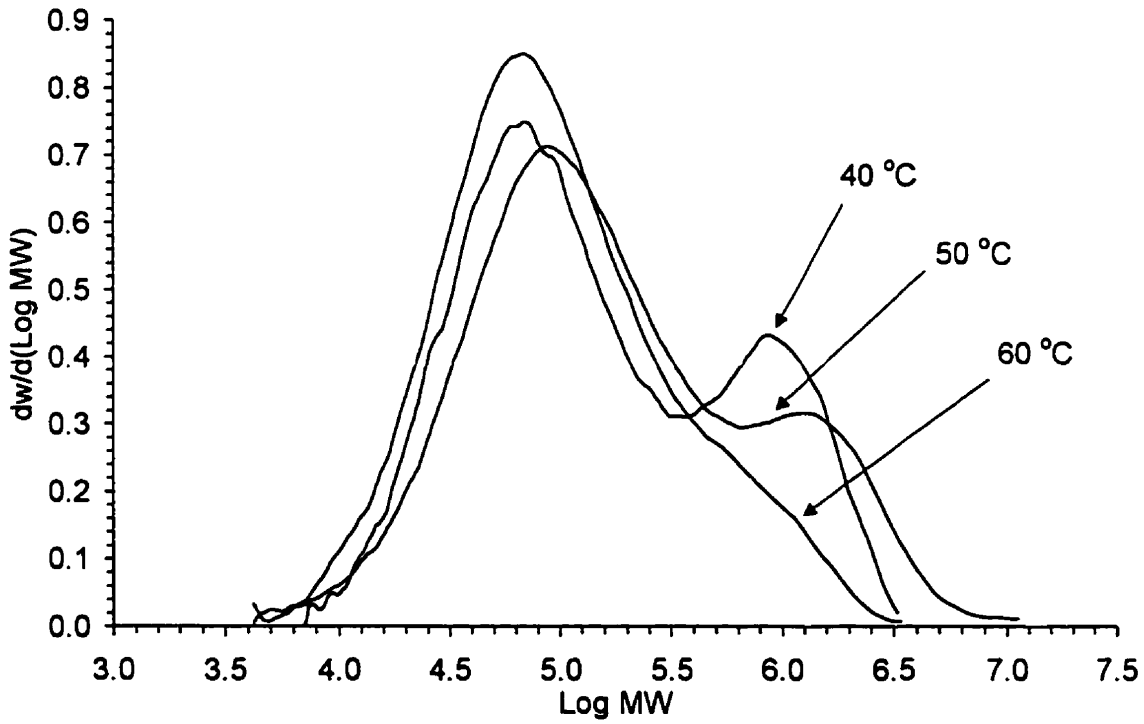

Figure 4.5 Effect of polymerization temperature on MWD of polyethylene (combined catalyst, $P_{Ethylene}$ = 50 psi)

4.4. EFFECT OF ETHYLENE PRESSURE

Figs. 4.6 and 4.7 show the effect of ethylene pressure (concentration) on MWD of polyethylene produced with the combined metallocene catalyst. Unlike the temperature effect, which affected the ratio of low and high molecular weight polymers more than anything else, changing monomer pressure will affect the separation of the two peaks in the bimodal MWD. In both Figs. 4.6 and 4.7, apparently the peaks corresponding to the MWD of polymer produced by $Et[Ind]_2ZrCl_2$ show decreasing molecular weights as the ethylene pressure increases. However, the MWD of the chains produced by Cp_2HfCl_2 sites stays either unaffected (50 °C) or slightly increases (40 °C) as the ethylene pressure increases.

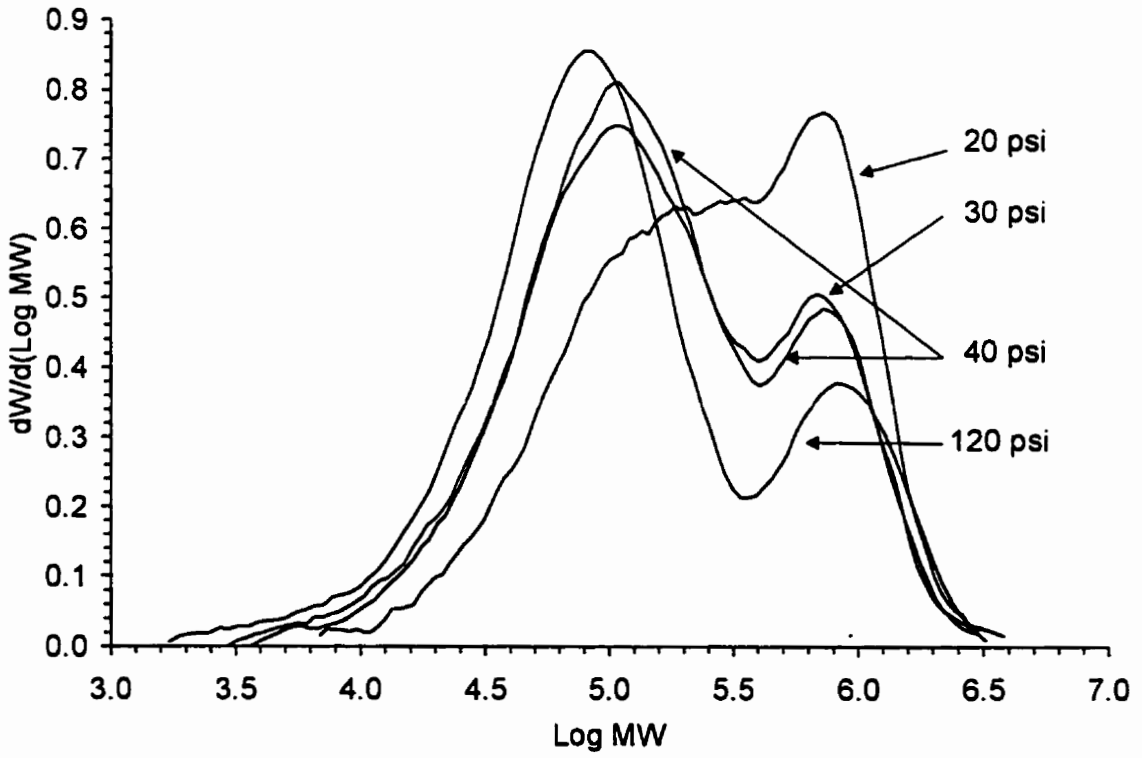

Figure 4.6 Effect of ethylene pressure on MWD of polyethylene during polymerization (combined catalyst, 40 °C)

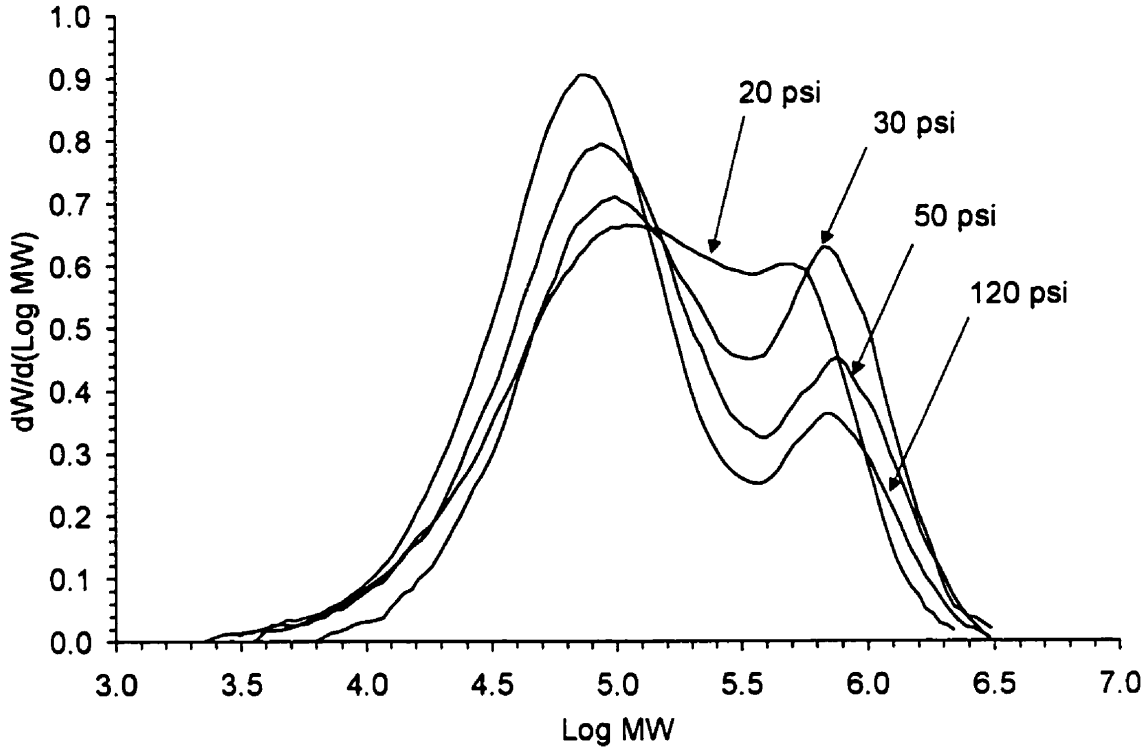

Figure 4.7 Effect of ethylene pressure on MWD of polyethylene during polymerization (combined catalyst, 50 °C)

The peak positions and relative areas in the bimodal MWD depend on the degree of overlapping of the individual peaks. Therefore, to more accurately check the actual trends of peak shifting and changes in relative peak areas, the MWD was deconvoluted into two Flory's distributions. By monitoring the increase or decrease of the τ's in Flory's distribution, the number average molecular weights for each site type can be calculated. Figs. 4.8 and 4.9 show the number average molecular weights estimated by deconvolution of MWD of polyethylenes produced at each site type as a function of ethylene pressure. Since increasing ethylene pressure leads to an increase in M_n of polymer made on Cp_2HfCl_2 but a decrease in M_n of polymer made on $Et[Ind]_2ZrCl_2$, the MWD of the combined polymer becomes increasingly bimodal at higher ethylene pressures.

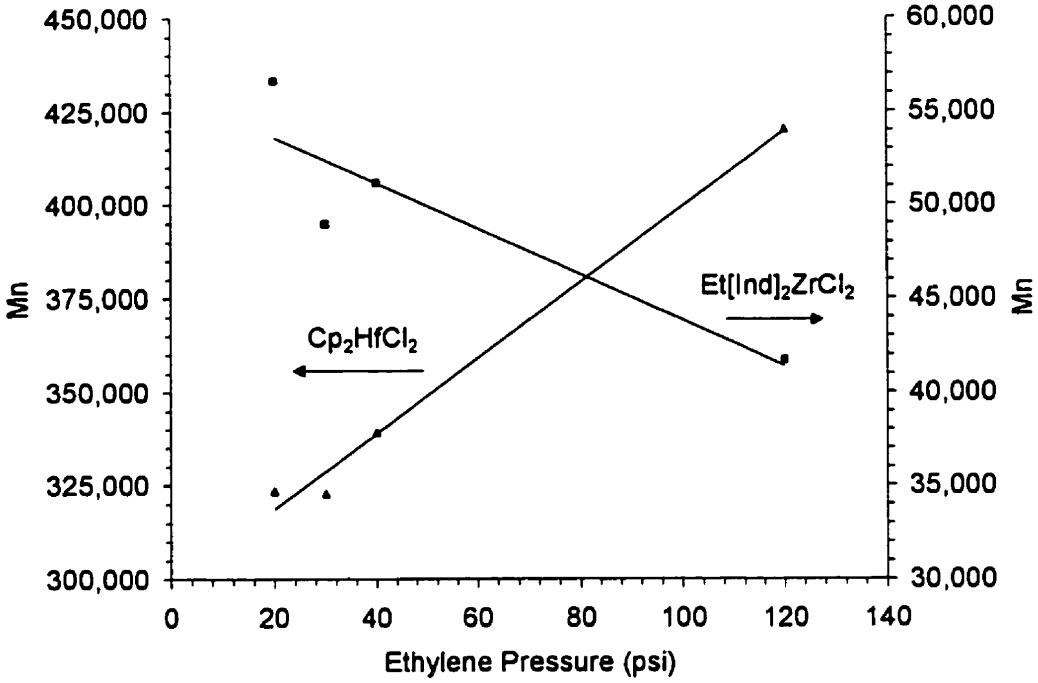

Figure 4.8 Number average molecular weight of polymer produced at each catalyst site estimated by MWD deconvolution (combined catalyst, 40 °C)

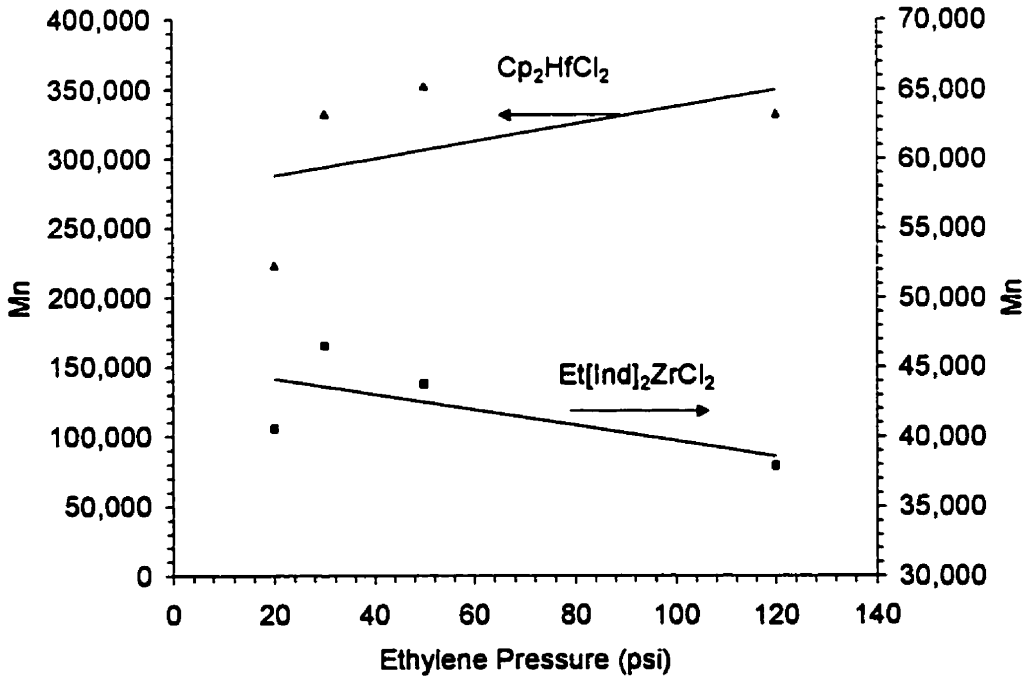

Figure 4.9 Number average molecular weight of polymer produced at each catalyst site estimated by MWD deconvolution (combined catalyst, 50 °C)

This effect is also confirmed from the PDI values obtained via GPC analysis, which is the measure of the breadth of MWD. Fig. 4.10 clearly shows that there is a linear relationship between the PDI of polyethylenes with bimodal MWD and ethylene pressure. One exception was observed for the polymer produced at the ethylene pressure of 20 psi, which had only a broad unimodal MWD. Table 4.3 summarizes the average molecular weights of the polymers shown in Fig. 4.10.

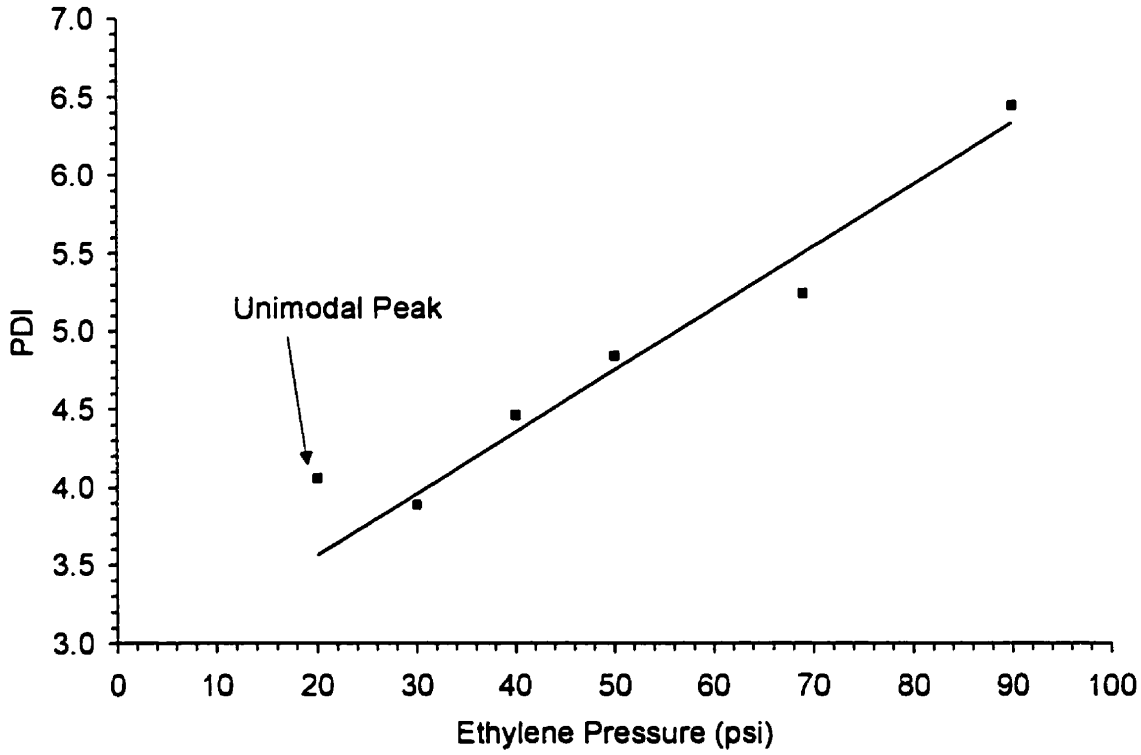

Figure 4.10 Effect of ethylene pressure on polydispersity index during polymerization (combined catalyst, 50 °C)

The monomer pressure dependency of MWD was further investigated from the molecular weight analysis of polyethylenes produced at different ethylene pressures with individually supported metallocene catalysts. According to Eq. (4.2), as the monomer pressure increases, τ will decrease and thus the average molecular weight will increase. For the case of polyethylene produced with Cp_2HfCl_2, based on the observations from the bimodal MWD's, it seems that the molecular weight increases slightly with increasing monomer pressure. When

hydrogen was added to the polymerization system as a chain transfer agent to reduce the molecular weight, it was clearly seen that as the monomer pressure increased, the molecular weight of the polymer produced by Cp_2HfCl_2 increased as shown in Fig. 4.11.

Table 4.3 Average molecular weights of polyethylene produced at different ethylene pressures (combined catalyst, 50 °C)

Pressure (psi)	M_n	M_w	PDI	Shape
20	67,500	274,100	4.06	Unimodal
30	94,100	366,100	3.89	Bimodal
40	63,700	283,600	4.45	Bimodal
50	63,600	308,200	4.84	Bimodal
70	74,400	389,900	5.24	Bimodal
90	93,400	601,500	6.44	Bimodal

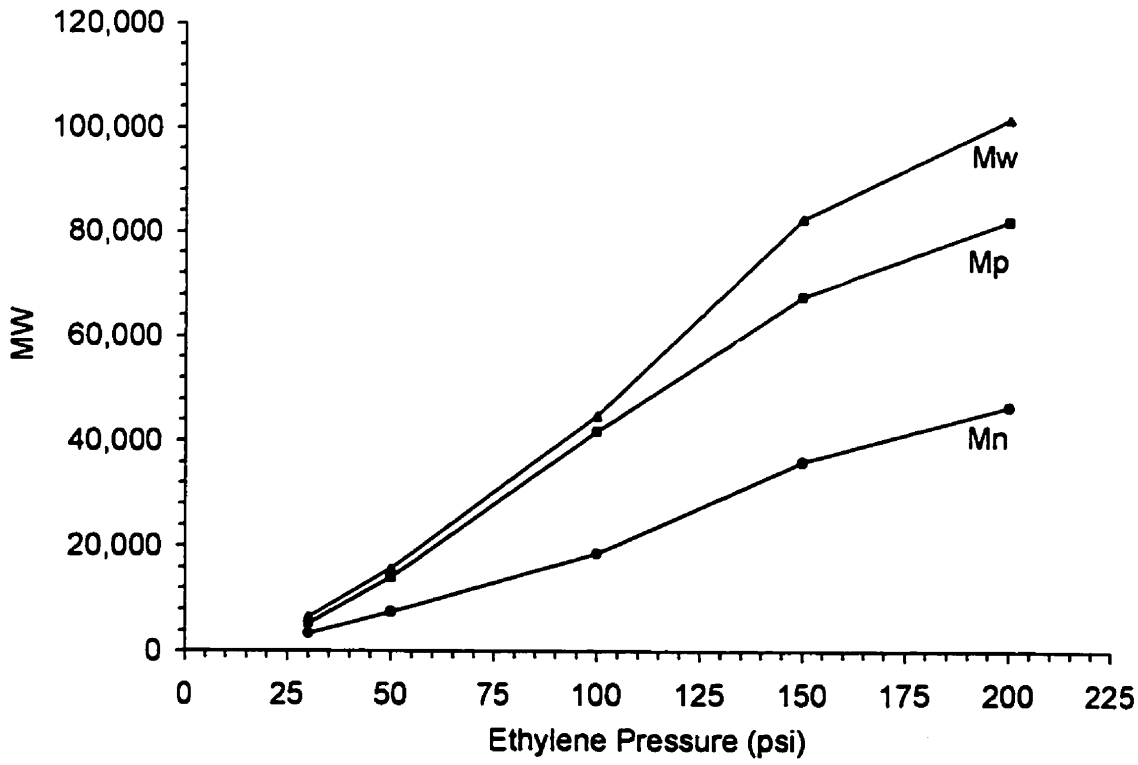

Figure 4.11 Effect of ethylene pressure on molecular weight of polyethylene made with Cp_2HfCl_2 (50 °C, hydrogen = 150 mL)

Fig. 4.12 shows the dependency of molecular weights of polymer produced with $Et[Ind]_2ZrCl_2$ on monomer pressure. In the absence of hydrogen pressure or at low hydrogen concentrations, the molecular weight of polyethylene produced with $Et[Ind]_2ZrCl_2$ decreases as ethylene pressure increases for ethylene pressures less than 100 psi. This result is quite unexpected. The fact that the peak molecular weight is apparently not affected by changes in ethylene pressure at higher pressures (> 100 psi) is another remarkable observation. Section 4.5 will propose some explanations for these observations.

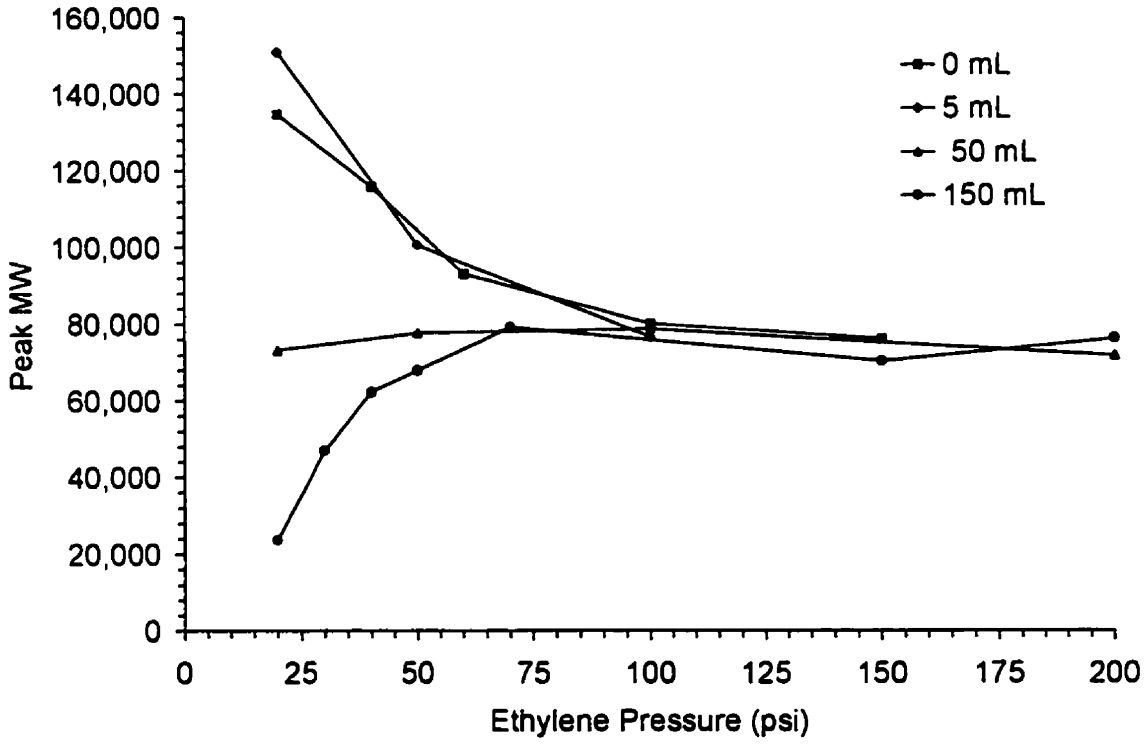

Figure 4.12 Effect of ethylene pressure and hydrogen concentration on peak molecular weight of polyethylene produced with $Et[Ind]_2ZrCl_2$ (50 °C)

4.5. MECHANISMS OF CHAIN TRANSFER

Fig. 4.13 shows that the molecular weight of polyethylene produced with Cp_2HfCl_2 decreases as the concentration of hydrogen increases. Therefore, it appears that the controlling chain transfer mechanism is the transfer to hydrogen (β-hydride elimination might also play a secondary role). Among these two chain termination mechanisms, chain transfer to hydrogen seems to have a more important role, because the molecular weight of polymers produced with Cp_2HfCl_2 decreases sharply even with a small amount of added hydrogen.

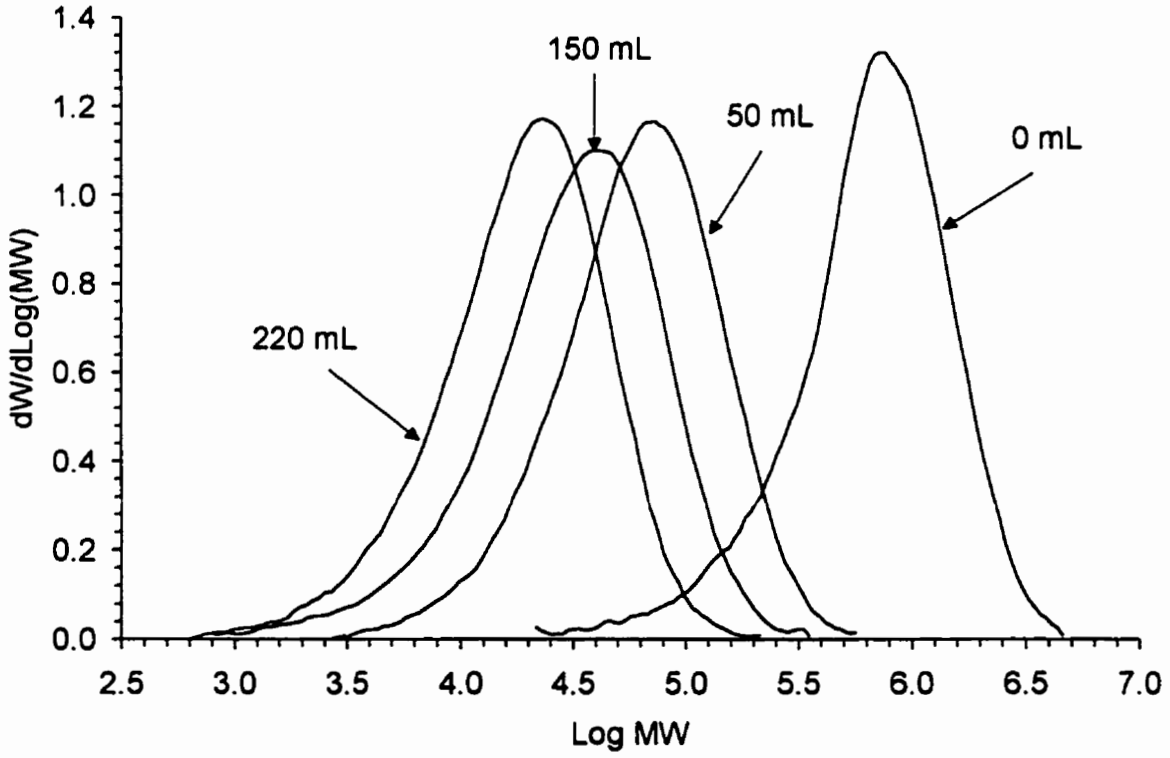

Figure 4.13 Effect of hydrogen concentration on polyethylene MWD (Cp_2HfCl_2, 50 °C, $P_{Ethylene}$ = 100 psi)

In the case of $Et[Ind]_2ZrCl_2$, it was shown previously in Fig. 4.12 that the position of the molecular weight peak of polyethylene produced by $Et[Ind]_2ZrCl_2$ is a function of both

ethylene pressure and hydrogen initial concentrations. The molecular weight of polymer produced at lower ethylene pressures (less than 100 psi) decreases with increasing hydrogen concentration. Based on Eq. (4.2), the observed trend indicates that at lower ethylene pressures, chain transfer to hydrogen plays a significant role. However, when higher ethylene pressures were used, the molecular weight of polyethylene produced with $Et[Ind]_2ZrCl_2$ became independent of ethylene pressure and hydrogen concentration, as shown in Fig. 4.14.

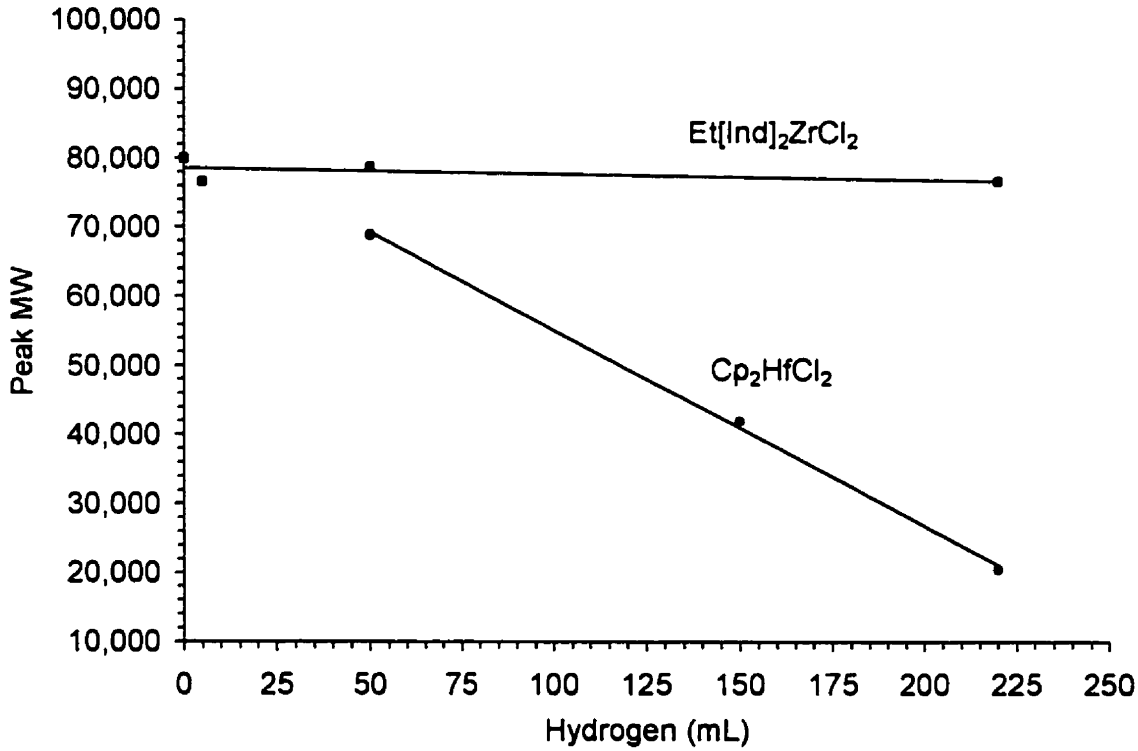

Figure 4.14 Effect of hydrogen concentration at 50 °C, $P_{Ethylene}$ = 100 psi

Therefore, for ethylene pressures higher than 100 psi, it appears that transfer to monomer becomes the dominating chain transfer mechanism for $Et[Ind]_2ZrCl_2$. This can be explained by noticing that, at low ethylene pressures and higher hydrogen concentration, transfer to hydrogen is the dominant process, i.e.:

$$\tau \cong \frac{k_{H_2}[H_2]}{k_p[M]} >> \frac{k_M}{k_p} + \frac{k_\beta}{k_p[M]} + \frac{k_{MAO}[MAO]}{k_p[M]} \qquad (4.4)$$

For increasing monomer pressures (i.e., increasing $k_p[M]$ values in the denominator) one might assume that

$$\tau \cong \frac{k_M}{k_p} >> \frac{k_\beta}{k_p[M]} + \frac{k_{H_2}[H_2]}{k_p[M]} + \frac{k_{MAO}[MAO]}{k_p[M]} \tag{4.5}$$

However, the decrease in the molecular weight of polyethylene with increasing ethylene pressure up to about 100 psi for low hydrogen concentrations has yet to be explained. One might speculate that gaseous impurities that act as chain transfer agents introduced with the ethylene feed may be partially responsible for this phenomenon.

4.6. MWD CONTROL BY VARYING HYDROGEN CONCENTRATION

The observed differences in polymer chain transfer mechanisms involved with these two catalysts at higher ethylene pressure can provide an effective way of controlling MWD. For ethylene pressures higher than 100 psi, hydrogen can be used to control the MWD of polyethylene produced with Cp_2HfCl_2 without significantly affecting the MWD of polyethylene produced with $Et[Ind]_2ZrCl_2$. Fig. 4.15 demonstrates how the overall MWD of polyethylene made with the combined catalyst can be controlled by simply varying hydrogen concentration. As predicted, the MWD of polymer produced by $Et[Ind]_2ZrCl_2$ does not change significantly with hydrogen concentration. However, the molecular weight of polyethylene produced by Cp_2HfCl_2 decreases significantly with addition of hydrogen. As shown in Fig.4.15, regardless of the presence of the hydrogen, the MWD of polymer produced by the combined catalyst represents the superposition of the MWD of the individually produced polymers. Table 4.4 summarizes the molecular weights of polymers shown in Fig 4.15. The molecular weight averages for each metallocene were obtained by deconvolution into Flory's distributions.

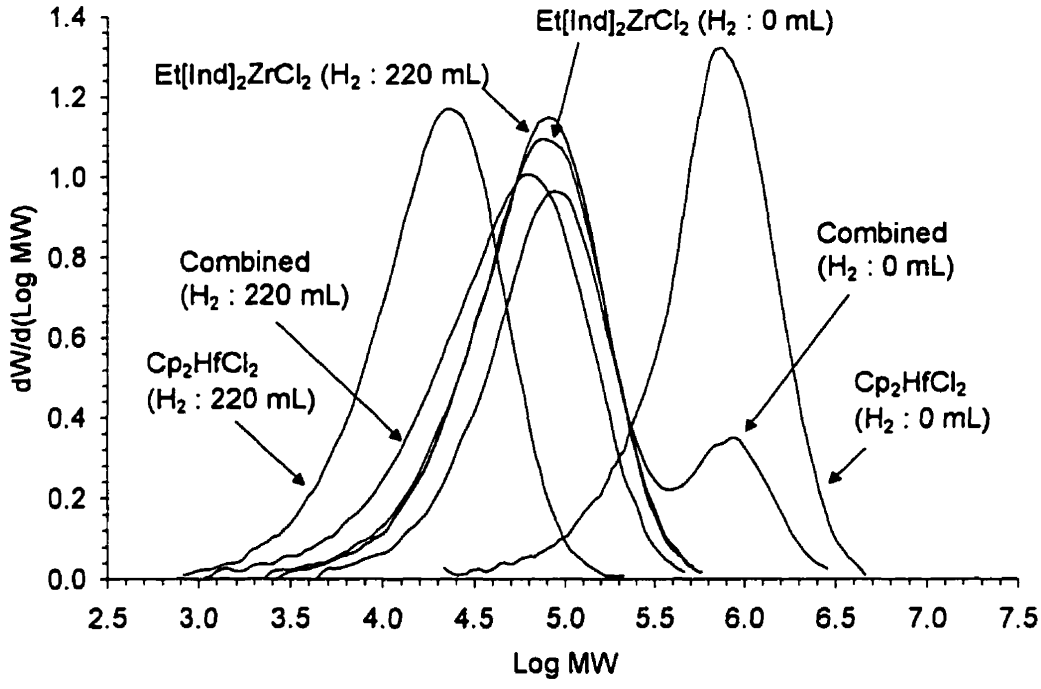

Figure 4.15 Effect of hydrogen concentration on MWD of polyethylene made with combined catalyst (50 °C, $P_{Ethylene}$ = 100 psi)

Table 4.4 Average molecular weights of polymer produced by single and combined supported metallocenes (50 °C, $P_{Ethylene}$ = 100 psi, Al/metal ≈ 800)

Catalyst	No Hydrogen			
	M_n[a]	M_p[b]	M_w[c]	PDI[d]
Cp_2HfCl_2	425,500	754,600	852,600	2.00
$Et[Ind]_2ZrCl_2$	40,000	80,000	89,600	2.24
Combined(Hf/Zr)	64,000	84,900	264,400	4.13
	With 220 mL of Hydrogen			
Cp_2HfCl_2	12,600	20,500	25,800	2.05
$Et[Ind]_2ZrCl_2$	43,200	76,500	90,700	2.10
Combined	24,900	61,100	69,100	2.78

[a] Number-average molecular weight

[b] Peak molecular weight

[c] Weight-average molecular weight

[d] Polydispersity index (M_w/M_n)

Fig. 4.16 demonstrates how the MWD of polyethylene made with the combined catalyst can be controlled by varying hydrogen pressure. The low molecular weight tail in Fig. 4.16, in the case of 150 mL and 280 mL of hydrogen injections, corresponds to the polymer produced by Cp_2HfCl_2 sites (note that fraction of the low MW tail is outside the calibration range). The result is remarkable considering the fact that in the absence of hydrogen Cp_2HfCl_2 produces polyethylene with much higher molecular weight than that produced by $Et[Ind]_2ZrCl_2$.

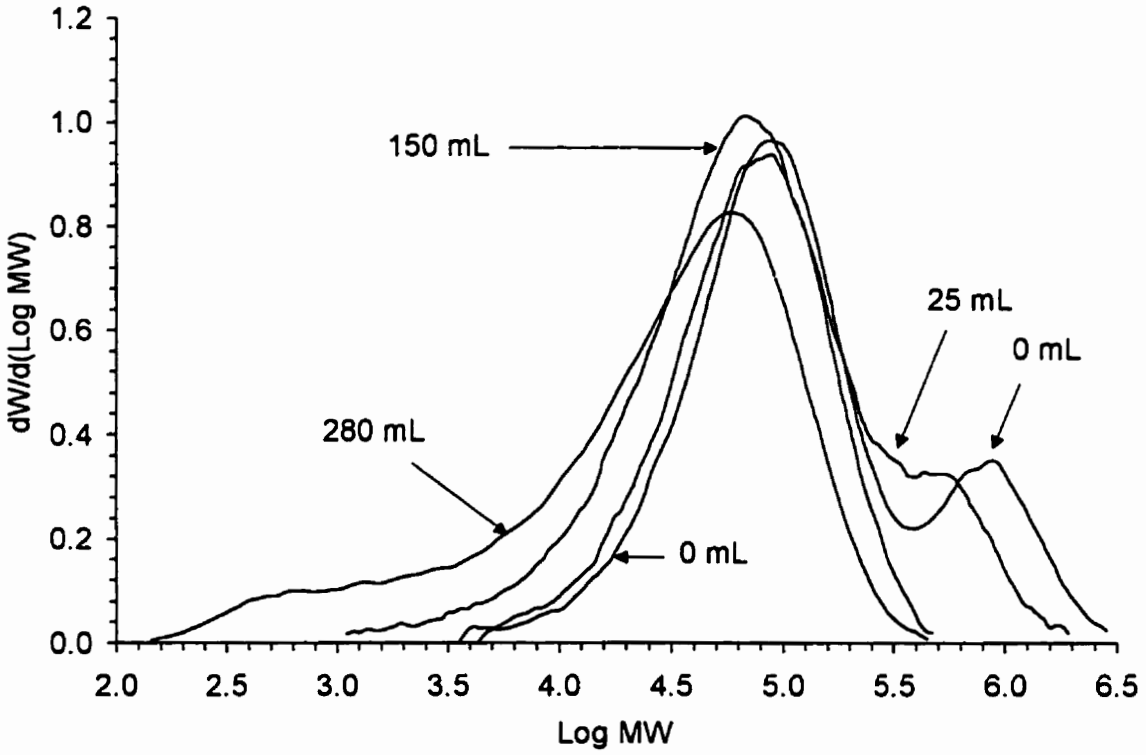

Figure 4.16 Effect of hydrogen concentration on MWD of polyethylene made with combined catalyst (50° C, $P_{Ethylene}$ = 100 psi)

Fig. 4.17 shows how the value of the number average molecular weights of the chains produced on each metallocene vary as a function of hydrogen pressure. Table 4.5 summarizes the molecular weight averages determined by GPC analysis. It is interesting to observe how PDI decreases as the two MWD's overlap at increasing hydrogen concentrations, and then

finally increases again as the peak corresponding to polymer produced on Cp_2HfCl_2, which used to have higher molecular weight, appears at the lower molecular weight region.

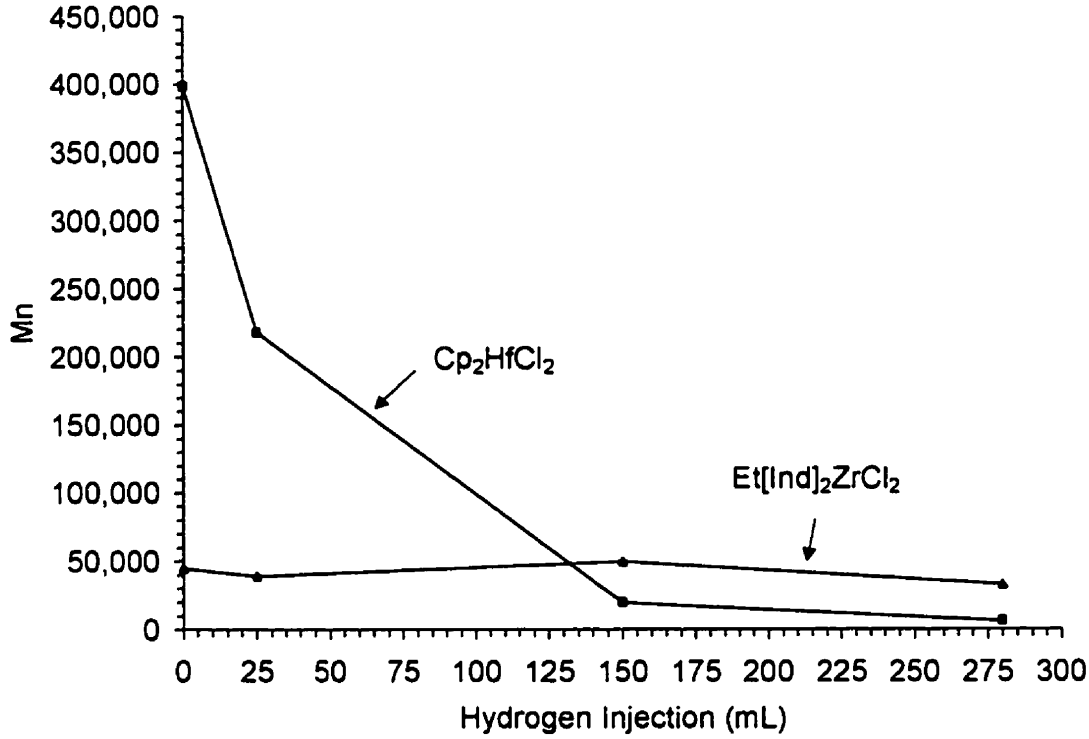

Figure 4.17 Effect of hydrogen concentration on number average molecular weights obtained by deconvolution of MWD into two Flory's distributions (combined catalyst, 50 °C, $P_{Ethylene}$ = 100 psi)

Table 4.5 Effect of hydrogen concentration on average molecular weights of polymer produced by the combined catalyst (50 °C, $P_{Ethylene}$ = 100 psi)

Hydrogen (mL)	M_n	M_p	M_w	PDI
0	64,000	84,900	264,400	4.13
25	54,900	87,800	183,700	3.35
150	27,600	65,300	78,900	2.86
280	5,500	58,800	53,800	9.78

In Fig.4.18, when a lower ethylene pressure is used, the overall MWD of polyethylene made with the combined catalyst shifts to lower molecular weights as hydrogen concentration increases. This is due to the fact that, when low ethylene pressures are used, the molecular weights of the polymers produced by $Et[Ind]_2ZrCl_2$ are also determined by transfer to hydrogen, as shown previously in Fig. 4.12 and Eqs. (4.4) and (4.5). Therefore, by the selective variation of hydrogen and ethylene pressures, the MWD of polyethylene made with this combined metallocene catalyst can be effectively controlled.

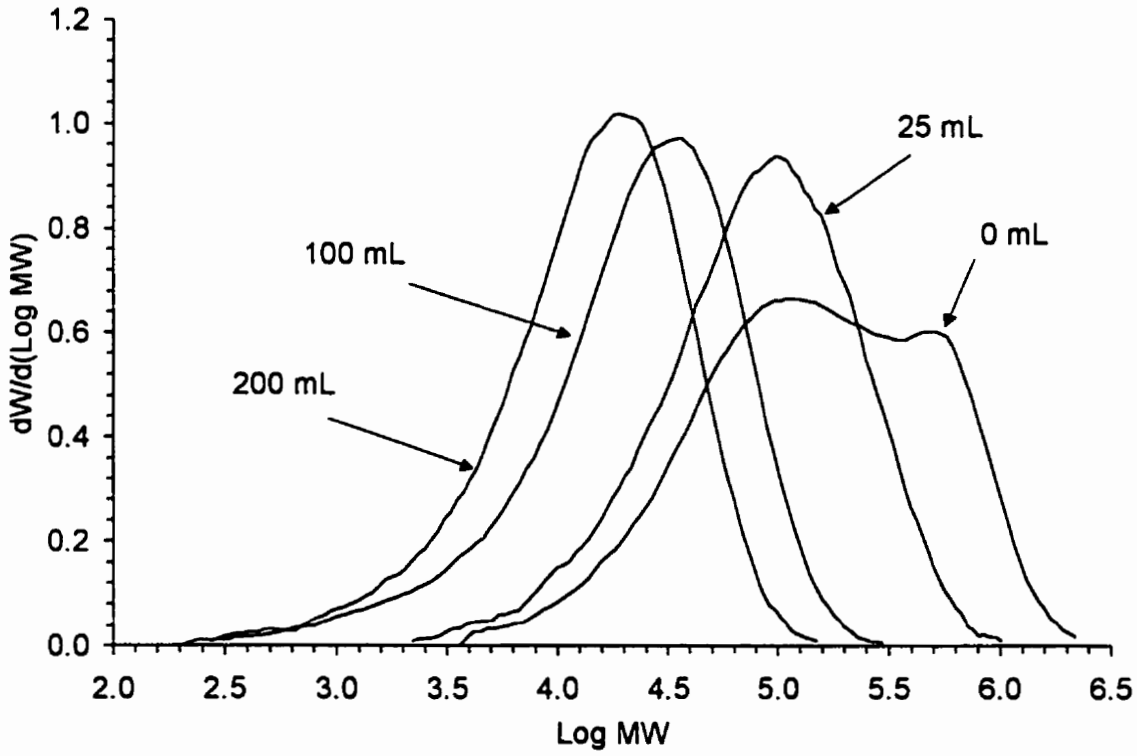

Figure 4.18 Effect of hydrogen concentration on MWD of polyethylene made with combined catalyst (50° C, $P_{Ethylene}$ = 20 psi)

4.7. EFFECT OF IMPURITIES

It was shown in Figs. 4.6 and 4.7 that the areas under the individual peaks, and thus, the amounts of polymer made by each site type, vary with ethylene pressure. It is commonly accepted that the polymerization rates in these systems are 1st order with respect to monomer concentration, i.e.

$$R_p = k_p[M][C^*] \tag{4.6}$$

where k_p is the polymerization propagation rate constant, and [M] and [C^*] are the concentrations of monomer and catalyst active sites, respectively. Since the polymerization rate is directly proportional to monomer and catalyst concentrations, the relative amounts of polyethylene made on each site type (w_1 and w_2 in Eq.4.3) should be independent of ethylene pressure. Figs. 4.6 and 4.7 seem to indicate that $Et[Ind]_2ZrCl_2$ and Cp_2HfCl_2 have different reaction orders with respect to ethylene concentration (or pressure). To explain this behavior, impurities that may be contained in the monomer feed were considered. Since the polymerizations take place in a semi-batch reactor, any gaseous catalyst poison that might be present in the ethylene feed will accumulate in the reactor at increasing rate for higher pressures. Figs. 4.6 and 4.7 seem to indicate that Cp_2HfCl_2 is preferentially poisoned by impurities that might be introduced by the ethylene feed. In order to test this hypothesis, experiments were conducted without the monomer purification apparatus and compared to the results obtained from normal polymerization procedures where ethylene is purified by passing through de-oxygen and de-humidification columns. Fig. 4.19 shows the effect of gaseous impurities contained in ethylene on the MWD of the produced polyethylene. Table 4.6 summarizes the relative amount of polyethylene produced on each catalyst site estimated by deconvolution into two Flory's distributions. When non-purified ethylene is used, the relative areas corresponding to polyethylene produced on Cp_2HfCl_2 sites decrease significantly as ethylene pressure increases from 150 psi (D) to 200 psi (C). However, when purified ethylene is used, the relative amount of polymer produced on Cp_2HfCl_2 sites is independent of ethylene pressure. Therefore, it is reasonable to say that the decrease in the area of the MWD peak corresponding to polymers produced on Cp_2HfCl_2 sites is due to the selective poisoning of these sites by impurities contained in the ethylene gas. One might speculate that, since these

impurities selectively deactivate Cp_2HfCl_2 sites, it is also possible (but perhaps not desirable) to control the shape of the MWD by injecting prescribed amount of impurities into the reactor during polymerization.

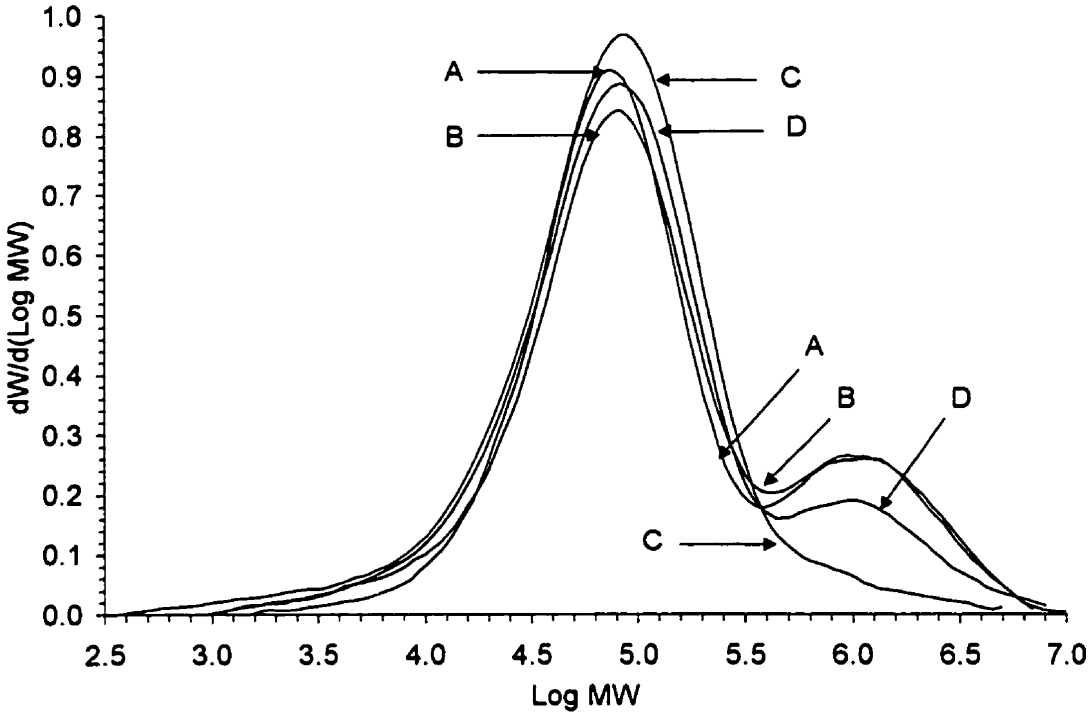

Figure 4.19 Effect of gaseous impurities on MWD of polyethylene (combined catalyst, 40 °C): (A) $P_{Ethylene}$ = 200 psi, purified; (B) $P_{Ethylene}$ = 150 psi, purified; (C) $P_{Ethylene}$ = 200 psi, non-purified; (D) $P_{Ethylene}$ = 150 psi, non-purified

Table 4.6 Effect of gaseous impurity and selective poisoning: relative amount of polyethylene produced on each site calculated on the basis of deconvolution of MWD by using two Flory's distributions

Ethylene	Pressure (psi)	$W_{Cp_2HfCl_2}$[a]	$W_{Et[Ind]_2ZrCl_2}$[b]
Non-Purified	150	19	81
	200	8	92
Purified	150	26	74
	200	25	75

[a] Weight Percent of Polyethylene Produced on the Cp_2HfCl_2 site

[b] Weight Percent of Polyethylene Produced on the $Et[Ind]_2ZrCl_2$ site

4.8. CONCLUSION

Control of MWD in ethylene polymerization was demonstrated using a bimetallic silica-supported metallocene catalyst. The catalyst produced by supporting two metallocenes onto a single support was able to produce polymers with bimodal or broad unimodal molecular weight distributions depending on polymerization conditions. Polymerization temperature, monomer pressure, selective poisoning of active sites, and injection of hydrogen as a chain transfer agent proved to be effective methods of controlling MWD. Polymers produced by the same bimetallic catalyst under different hydrogen pressures can have MWD's varying from unimodal to bimodal, with high or low molecular weight shoulders. Through our investigation, it was demonstrated that the combination of metallocene catalysts in a support can provide a direct way of customizing MWD of polyethylene which in turn dictates the physical properties of the polymer. The unusual behavior of ethylene polymerization using supported $Et[Ind]_2ZrCl_2$ at low ethylene pressures needs further explanation. However, the observed trend helps one to effectively control the MWD of polyethylene by selecting different monomer pressures.

CHAPTER 5
SUPPORT EFFECT

Metallocene catalysts are generally believed to have uniform site types even after being supported. In the previous chapter, it was shown that the homopolymers produced with single metallocene supported catalysts have narrow molecular weight distributions (MWD) with polydispersity indexes (PDI) close to two or slightly higher. These MWDs can be well represented by Flory's most probable distribution, indicating that there is only one active site type as long as MWDs are concerned.

However, some supporting techniques can also lead to polyolefins with broad MWDs, which has been associated with the formation of several active site types and/or mass transfer resistances during polymerization (Kim *et al.*, 1999). For the case of copolymers, besides MWD determination, it is necessary to measure the chemical composition distribution (CCD) to have a more complete understanding of active site types and polymer properties. Until recently, temperature rising elution fractionation (TREF) used to be the only method available to measure CCD of polyolefins. Although TREF provides a wealth of micro-structural information, its long analysis time (one sample takes about 60 hours for analysis) makes it difficult to be used in a more systematic way to investigate the CCD of polyolefins. Crystallization analysis fractionation (CRYSTAF) is a new technique to determine CCD of semi-crystalline polymers, which not only reduces the analysis time (12 hours per sample), but also allows one to run up to five samples simultaneously. Therefore, the effect of different catalyst active site types on the CCD of copolymers can be determined in a relatively short time.

In this chapter, the number of active site types of supported metallocenes is examined through the analysis of the CCD and MWD of copolymers made with these catalysts. It will be shown that even for polyolefins that have narrow MWD, CCD can be very broad or multimodal, indicating the presence of more than one catalyst active site types during polymerization.

5.1. SUPPORT TYPES AND SUPPORTED CATALYST PREPARATION

Calcinated Silica 952 from Davison (**Silica**), MAO supported on silica from Witco (**SMAO**), and MAO-pretreated silica 952 (**MAO/Silica**) were used as catalyst supports. The aluminum content for MAO treated silica is approximately 7 wt.-% (Santos *et al.*, 1977) and Al in SMAO is 24.4 wt.-%. Bridged or non-bridged zirconium or hafnium catalysts were individually supported onto these three supports. MAO pretreatment of silica and impregnation of the catalysts on the support were conducted under high purity nitrogen atmosphere in a specially designed flask equipped with internal sintered glass filter. Ca. 0.5 g of support was first suspended in ca. 10 mL of toluene at 50 °C with vigorous stirring. MAO (for silica pretreatment) or catalyst dissolved in 10 mL of toluene was added slowly to the suspended support mixture (over a period of 15 min.) and stirred for 1 hr. Finally the supported catalyst was filtered through the internal glass filter, washed several times, and dried under vacuum. The supported catalyst was recovered as free flowing powder and stored in a glove box (Nexus, Vacuum/Atmospheres Co.) under dry nitrogen.

5.2. CATALYST ACTIVITIES

The activities of each supported catalyst are presented in Tables 5.1 and 5.2. All the polymerizations took place at $P_{Ethylene}$ = 100 psi with 5 mL of 1-hexene as the comonomer. All the investigated supported catalysts showed fairly good activities for ethylene/1-hexene copolymerizations. Two different kinds of chain transfer agents were used. One is $(C_2H_5)_2Zn$ and the other is hydrogen. The size of hydrogen molecules is substantially smaller than the size of $(C_2H_5)_2Zn$.

Table 5.1 Activity for supported hafnium catalysts [kg polymer/(mol metal·atm·hr)]

Catalyst	No CTA	$(C_2H_5)_2Zn$ 0.1 g	$(C_2H_5)_2Zn$ 0.5 g	H_2 25 mL
Cp_2HfCl_2/SMAO	620	440	410	340
Cp_2HfCl_2/Silica	1220	1540	1660	1420
Cp_2HfCl_2/MAO/Silica	---	240	130	---
Et[Ind]$_2HfCl_2$/SMAO	310	160	250	150
Et[Ind]$_2HfCl_2$/Silica	1420	540	120	150

CTA: Chain Transfer Agent

Table 5.2 Activity for supported zirconium catalysts [kg polymer/(mol metal·atm·hr)]

Catalyst	No CTA	$(C_2H_5)_2Zn$ 0.1 g	H_2 25 mL
Cp_2ZrCl_2/SMAO	1100	1210	1680
Cp_2ZrCl_2/Silica	2740	2030	3120
Et[Ind]$_2ZrCl_2$/SMAO	2200	2720	1620
Et[Ind]$_2ZrCl_2$/Silica	1460	860	1710

5.3. MOLECULAR WEIGHT DISTRIBUTION

Tables 5.3 and 5.4 show molecular weight averages and PDIs of polymers made with the different supported catalysts. It seems that non-bridged catalysts tend to produce polymers with higher molecular weight when supported onto **SMAO**. The PDIs indicate slightly broad MWDs for single site catalyst (for Flory's distribution, PDI equals to two). However, all the MWDs determined by GPC analysis showed a narrow single unimodal distributions and there was no apparent indication of multiplicity in the types of the active sites for the catalysts investigated.

Table 5.3 Weight average molecular weights and PDI for hafnium catalysts

Catalyst	No CTA		$(C_2H_5)_2Zn$ 0.1 g		$(C_2H_5)_2Zn$ 0.5 g		H_2 25 mL	
	M_w	PDI	M_w	PDI	M_w	PDI	M_w	PDI
1/SMAO	470,600	2.2	181,000	2.8	42,400	2.6	33,700	2.5
1/Silica	299,600	2.2	142,400	2.3	30,600	2.5	51,500	2.2
1/MAO/Silica	286,500	3.0	119,700	2.5	45,700	2.6	94,200	2.4
2/SMAO	336,900	3.1	68,600	2.7	32,800	2.3	38,000	2.5
2/Silica	243,400	1.6	47,300	2.7	11,900	2.5	59,700	2.7

1 : Cp_2HfCl_2

2 : $Et[Ind]_2HfCl_2$

Table 5.4 Weight average molecular weights and PDI for zirconium catalysts

Catalyst	No CTA		$(C_2H_5)_2Zn$ 0.1 g		H_2 25 mL	
	M_w	PDI	M_w	PDI	M_w	PDI
3/SMAO	437,600	1.9	75,200	2.7	34,300	2.5
3/Silica	176,600	2.2	67,800	2.4	29,200	2.1
4/SMAO	126,000	2.3	26,700	2.7	31,200	2.2
4/Silica	126,900	3.3	34,100	2.8	30,800	2.6

3 : Cp_2ZrCl_2

4 : $Et[Ind]_2ZrCl_2$

5.4. CHEMICAL COMPOSITION DISTRIBUTION

5.4.1. Hafnocenes

Fig. 5.1 shows the CRYSTAF profile of an ethylene/1-hexene copolymer produced by Cp_2HfCl_2 supported on MAO-pretreated silica. Although the CCD is bimodal, the MWD of the sample is unimodal and narrow. The polymers corresponding to each peak were

fractionated with a modified CRYSTAF setup and the MWDs of each fraction were measured by GPC. As indicated in Fig. 5.1, the molecular weight averages of each fraction are very similar.

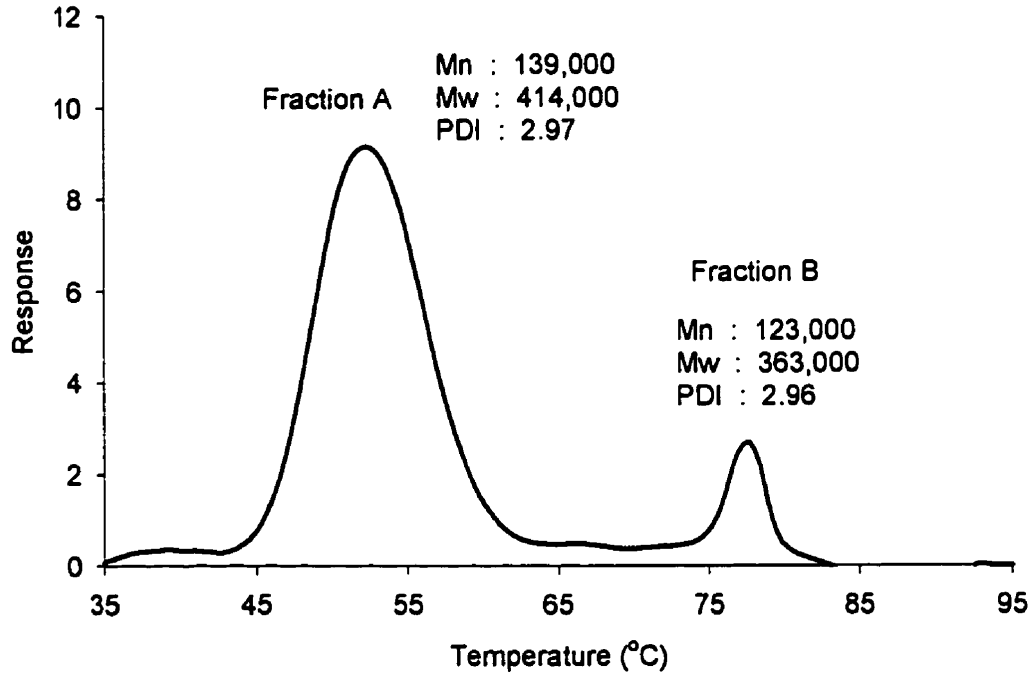

Figure 5.1 CRYSTAF profile of poly(ethylene-co-1-hexene) produced with Cp_2HfCl_2/MAO/Silica and average molecular weights of the fractions, 40 °C, $P_{Ethylene}$ = 50 psi, 1-hexene = 2.5 mL

Fig. 5.2 shows the CCDs of polymers produced with Cp_2HfCl_2 on different supports. The polymer produced with Cp_2HfCl_2 supported on **Silica** (with no MAO pretreatment) has only a single low-crystallinity peak. On the other hand, Cp_2HfCl_2 supported on **SMAO** and MAO-pretreated SiO_2 (**MAO/Silica**) produced ethylene/1-hexene copolymers having bimodal CCDs. This figure illustrates how support treatment can significantly affect CCD of ethylene/1-hexene copolymers made with a single supported metallocene.

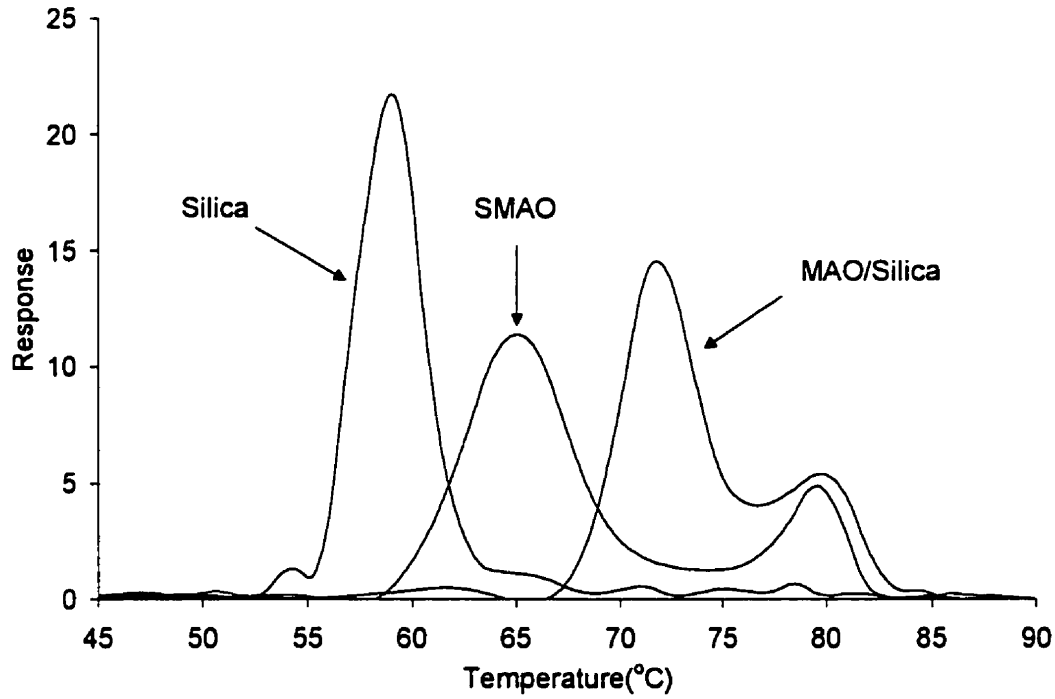

Figure 5.2 CRYSTAF profiles of poly(ethylene-co-1-hexene) produced with Cp_2HfCl_2 without use of CTA, 50 °C, $P_{Ethylene}$ = 100 psi, 1-hexene = 5 mL

Fig. 5.3 compares the CCDs of copolymers made with different supported Cp_2HfCl_2 catalysts in presence of a chain transfer agent, $(C_2H_5)_2Zn$. Very low molecular weight polymer chains are likely responsible for the low crystallinity tails observed in Fig. 5.3. (see Table 5.3 for molecular weight averages). The trends are similar to the ones shown in Fig. 5.2, but in this case, the peaks overlap significantly more. It can be speculated that there might be two distinctive active site types for catalysts supported on **MAO/Silica** and **SMAO** due to the presence of isolated OH and OH-MAO groups on the surface of the support. For non-treated silica (**Silica**), mostly isolated OH groups are present, thus leading to a single site type as shown in Fig. 5.2. Therefore, the peak appearing at the crystallization temperature of about 60 - 70 °C in Fig. 5.3 might correspond to polymer produced at silica-metallocene sites. Consequently, the peak appearing at about 80 °C in Fig. 5.3 corresponds to polymer produced at silica-MAO-metallocene sites. Notice that **SMAO** has an Al content of 24.4 wt.-% versus the estimated 7 wt.-% or less for **MAO/Silica**. In agreement with this, the 80 °C centered peak of polymer made with **SMAO** is significantly more apparent than the one for

MAO/Silica. The appearance of the small higher crystalline peak for polymers made with **Silica** may be caused by in situ formation of MAO-OH sites from the injected cocatalyst and reattachment of leached catalyst from the support to this MAO-OH site. It is also interesting to notice that copolymers with these microstructures (i.e., broad CCD and relatively narrow MWD) would be well suited for application requiring high environmental stress cracking resistance, since the tie molecules would have molecular weights comparable to the crystalline matrix.

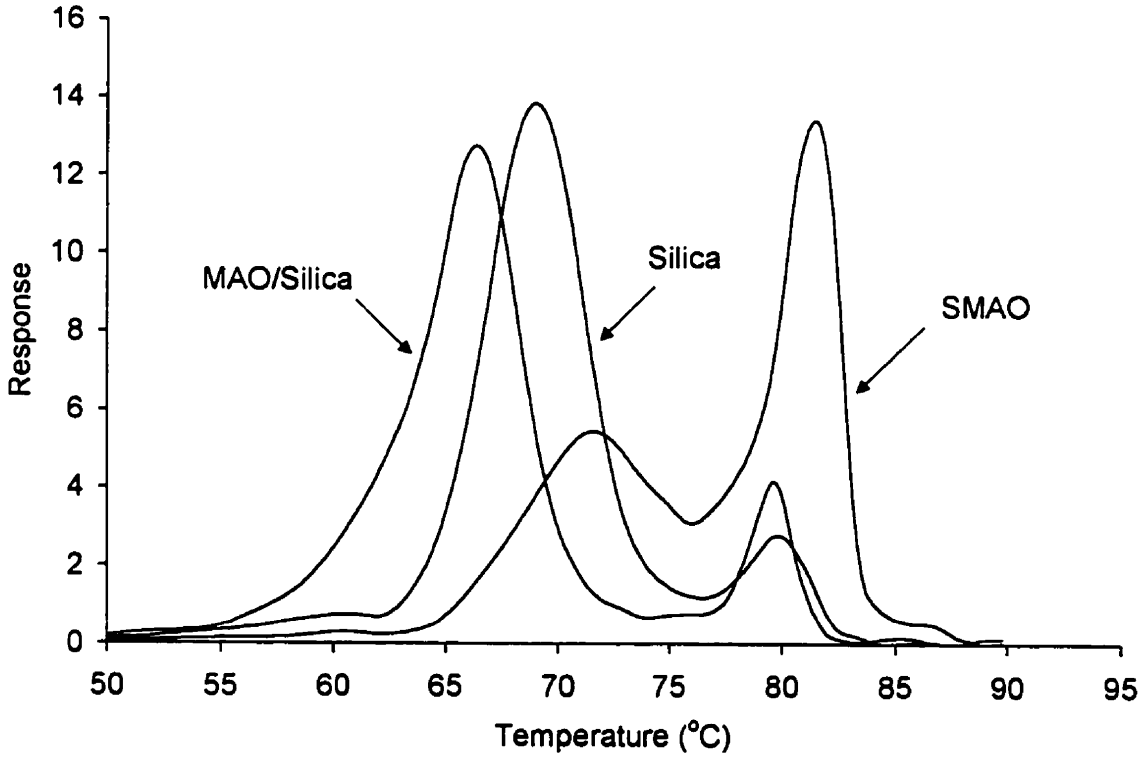

Figure 5.3 CRYSTAF profiles of poly(ethylene-co-1-hexene) produced with Cp_2HfCl_2 with 0.1 g of $(C_2H_5)_2Zn$, 50 °C, $P_{Ethylene}$ = 100 psi, 1-hexene = 5 mL

Fig. 5.4 shows the CRYSTAF profiles when the amount of $(C_2H_5)_2Zn$ is increased from 0.1 to 0.5 g. The same trends shown in Figs. 5.3 and 5.4 are again observed : a higher crystallinity peak centered at around 80 °C associated with silica-MAO-metallocene sites and a lower crystallinity peak centered around 70 °C associated with silica-metallocene sites. Lower crystallinity tails are also observed but they are likely associated with the lower

molecular weight chains made when 0.5 g of $(C_2H_5)_2Zn$ is used (see Table 5.3). Although CRYSTAF fractionation is mainly controlled by short chain branching, very short polymer chains will have increased solubility in TCB and appear as a low crystallinity tail.

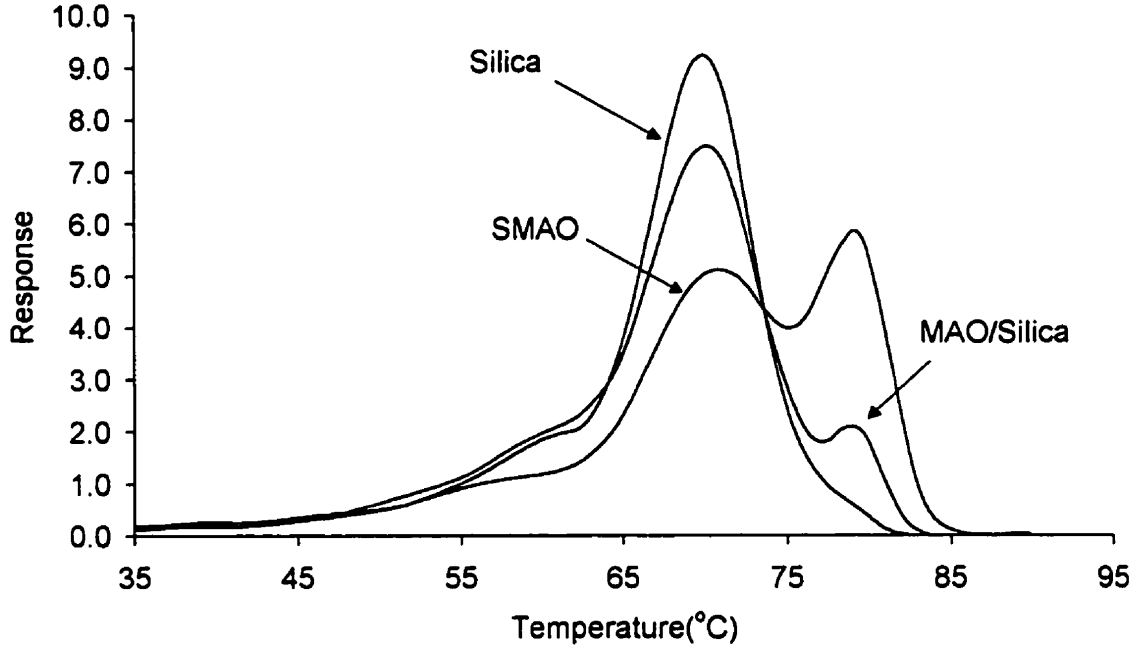

Figure 5.4 CRYSTAF profiles of poly(ethylene-co-1-hexene) produced with Cp_2HfCl_2 with 0.5 g of $(C_2H_5)_2Zn$, 50 °C, $P_{Ethylene}$ = 100 psi, 1-hexene = 5 mL

Fig. 5.5 shows the CCD of polymers produced with Cp_2HfCl_2 in the presence of 25 mL of hydrogen. Similar trends are observed, but peak overlapping is less clear than in the case of polymers made with 0.1 g of $(C_2H_5)_2Zn$. Compared to Fig. 5.3, the lower crystalline peaks of polymer produced with **Silica** and **MAO/Silica** appear at reversed positions. The appearance of low crystalline shoulder is less significant compared to the 0.5 g $(C_2H_5)_2Zn$ case.

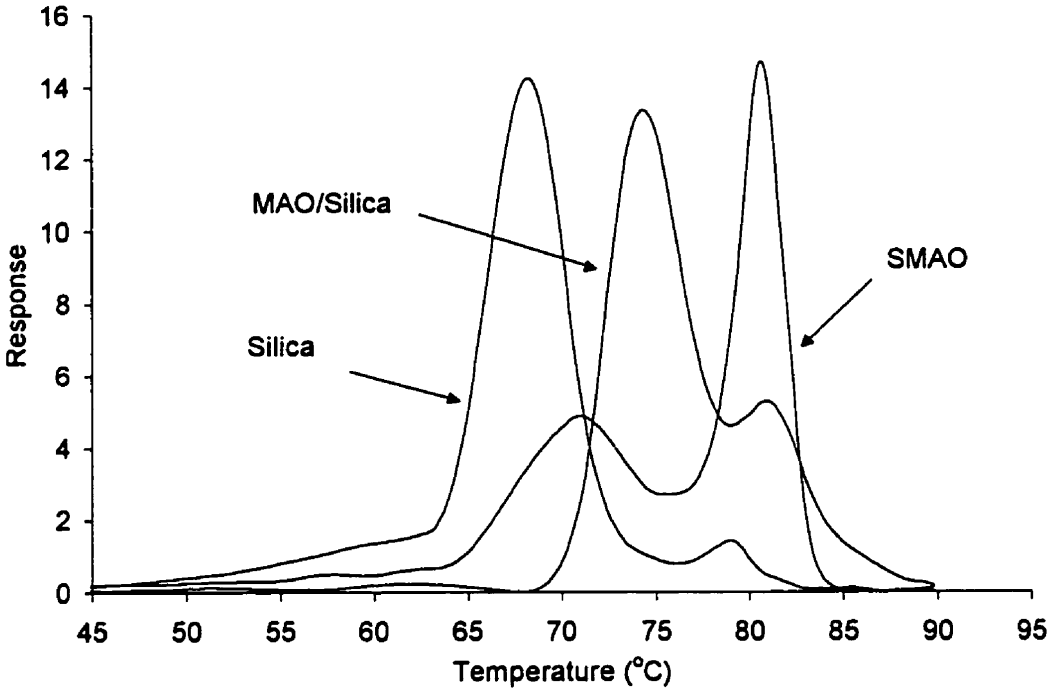

Figure 5.5 CRYSTAF profiles of poly(ethylene-co-1-hexene) produced with Cp_2HfCl_2 with 25 mL of H_2, 50 °C, $P_{Ethylene}$ = 100 psi, 1-hexene = 5 mL

Figs. 5.6 to 5.9 show that for the $Et[Ind]_2HfCl_2$ system, the effect of support on CCD is less apparent. All the polymers have narrow and uniform distributions. One exception is the polymer produced with $Et[Ind]_2ZrCl_2$ supported on Silica, which seems to have a little broader CCD than the others and apparently more comonomer content compared to the polymer produced with the same catalyst supported on **SMAO**. This might have been caused by some experimental error during polymerization. For all the other systems, the polymers produced with $Et[Ind]_2ZrCl_2$ supported on **SMAO** have slightly higher comonomer content. Judging from the change in the location of the CRYSTAF peak when a chain transfer agent was used, the comonomer content of the produced polymer seemed to increase slightly. Considering the fact that crystallization temperatures are still high, this does not seem to be caused by lower molecular weight fractions of the samples. It is not clear why the chain transfer agent would increase comonomer incorporation during polymerization.

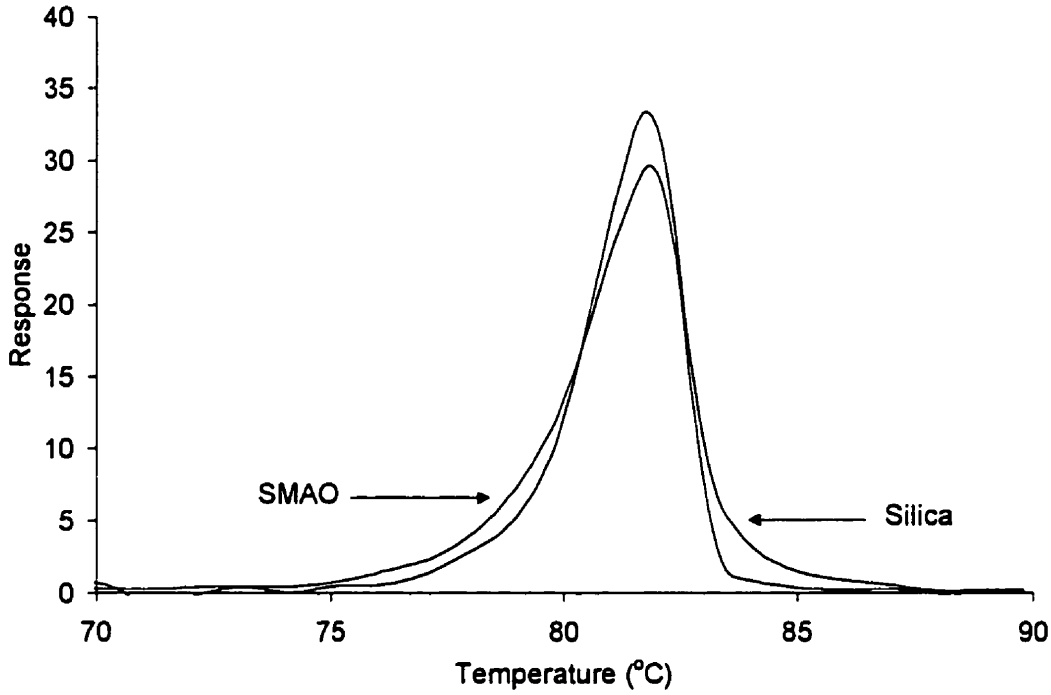

Figure 5.6 CRYSTAF profiles of poly(ethylene-co-1-hexene) produced with $Et[Ind]_2HfCl_2$ without use of CTA, 50 °C, $P_{Ethylene}$ = 100 psi, 1-hexene = 5 mL

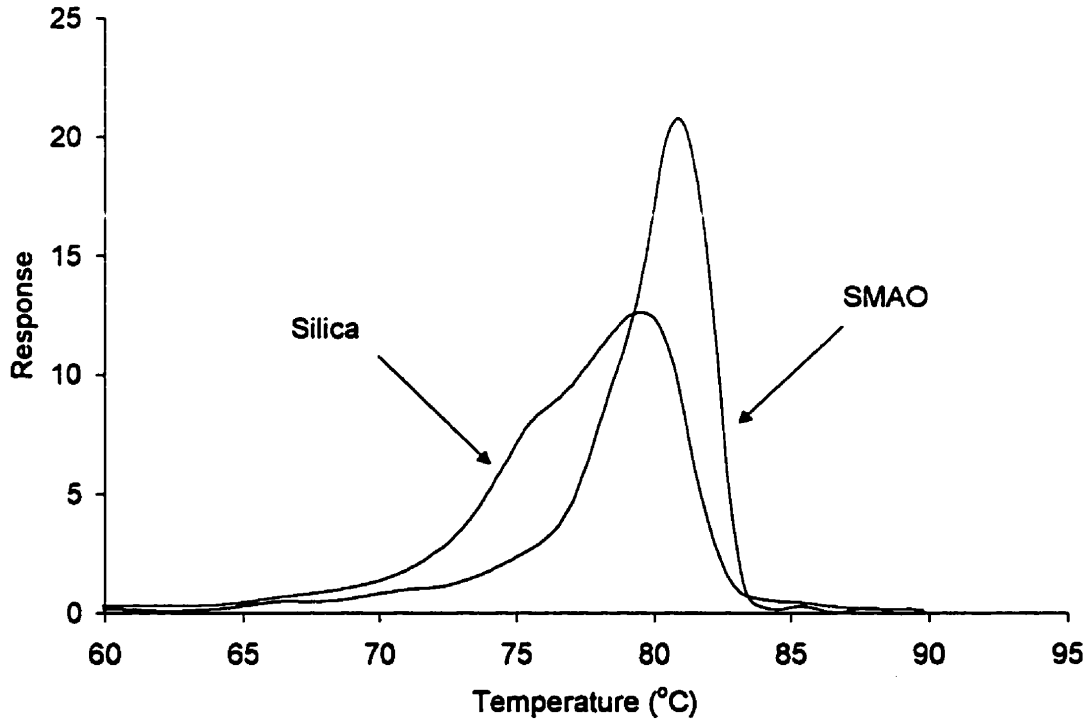

Figure 5.7 CRYSTAF profiles of poly(ethylene-co-1-hexene) produced with $Et[Ind]_2HfCl_2$ with 0.1 g of $(C_2H_5)_2Zn$, 50 °C, $P_{Ethylene}$ = 100 psi, 1-hexene = 5 mL

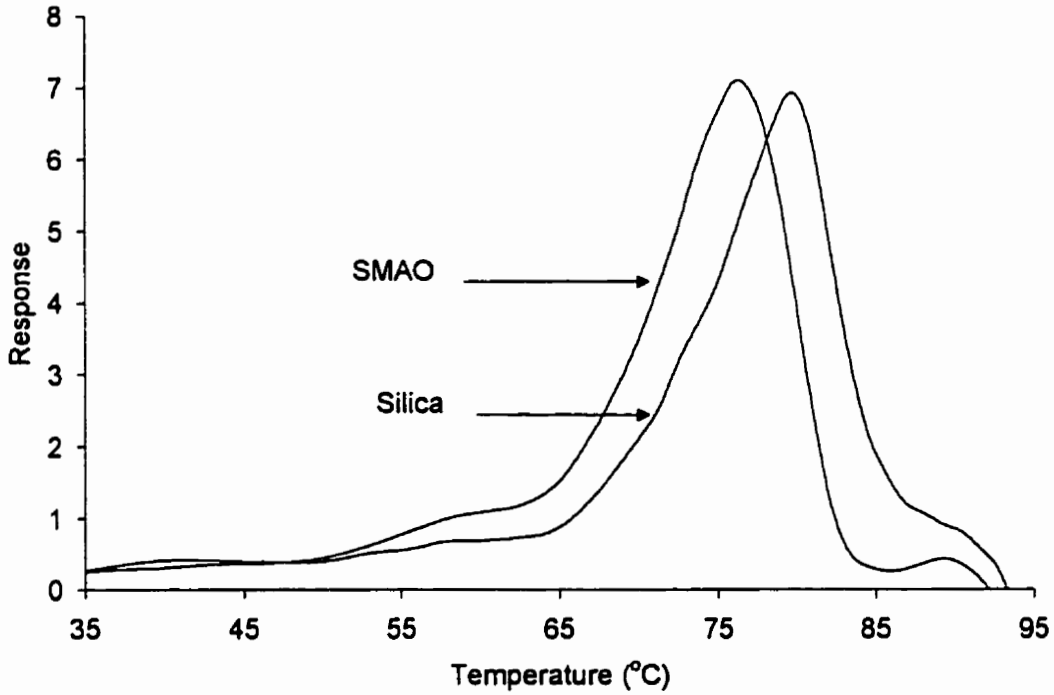

Figure 5.8 CRYSTAF profiles of poly(ethylene-co-1-hexene) produced with $Et[Ind]_2HfCl_2$ with 0.5 g of $(C_2H_5)_2Zn$, 50 °C, $P_{Ethylene}$ = 100 psi, 1-hexene = 5 mL

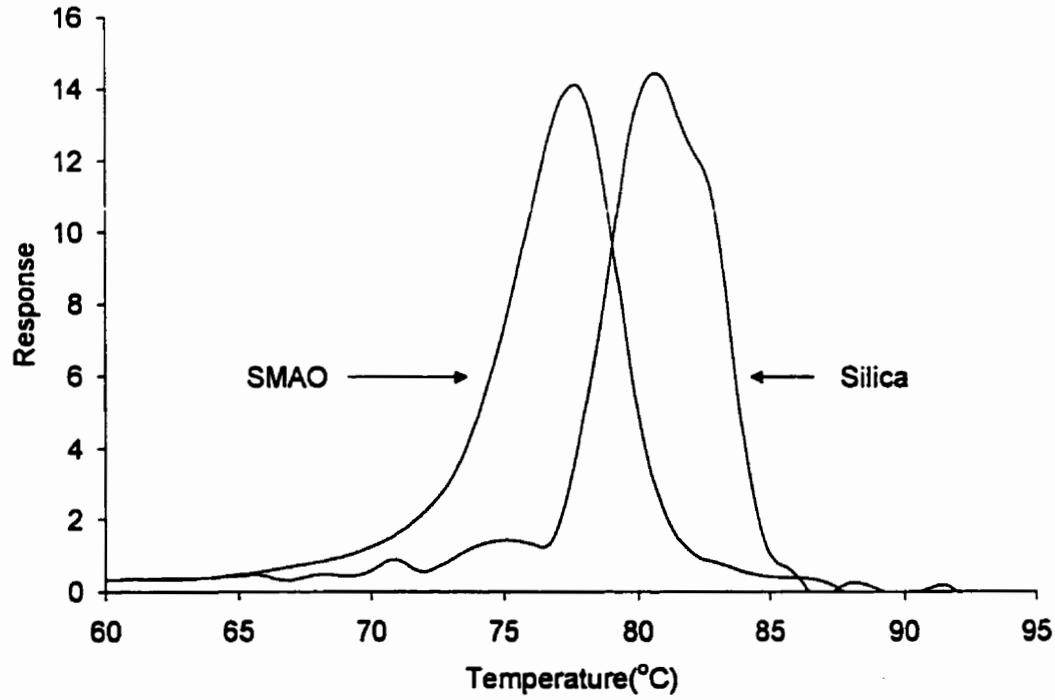

Figure 5.9 CRYSTAF profiles of poly(ethylene-co-1-hexene) produced with $Et[Ind]_2HfCl_2$ with 25 mL of H_2, 50 °C, $P_{Ethylene}$ = 100 psi, 1-hexene = 5 mL

5.4.2. Zirconocenes

For the case of Cp_2ZrCl_2, only narrow and unimodal CCDs were obtained. As shown in Figs. 5.10 to 5.12, for the polymers produced with Cp_2ZrCl_2/SMAO, the crystallization peak appeared at lower temperature regions compared to the polymers produced with Cp_2ZrCl_2/Silica, regardless the use of chain transfer agents. It seems that silica-MAO-metallocene and silica-metallocene sites differ slightly in their ability to incorporate comonomer into the growing polymer chain, but not enough to form bimodal CCDs.

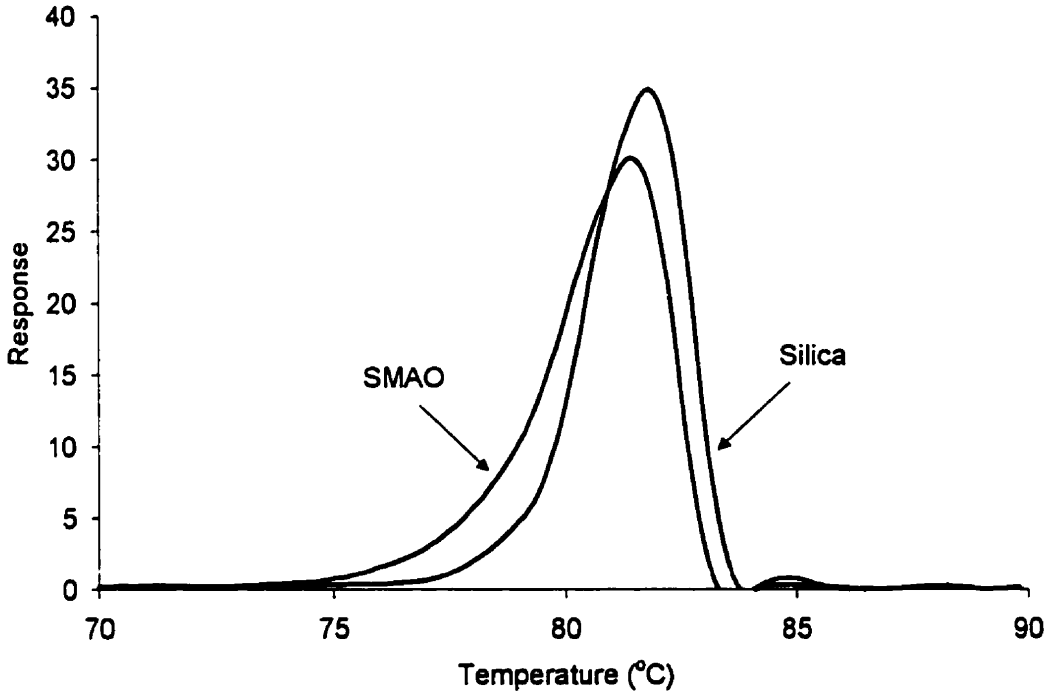

Figure 5.10 CRYSTAF profiles of poly(ethylene-co-1-hexene) produced with Cp_2ZrCl_2 without use of CTA, 50 °C, $P_{Ethylene}$ = 100 psi, 1-hexene = 5 mL

When hydrogen was used as the chain transfer agent, the crystallization peak temperature of the polymers produced with Cp_2ZrCl_2 supported either on **SMAO** or **Silica**, decreased approximately by 2 °C compared with the case of no chain transfer agent or diethyl zinc as the chain transfer agent. Slight tailing was also observed when hydrogen was used.

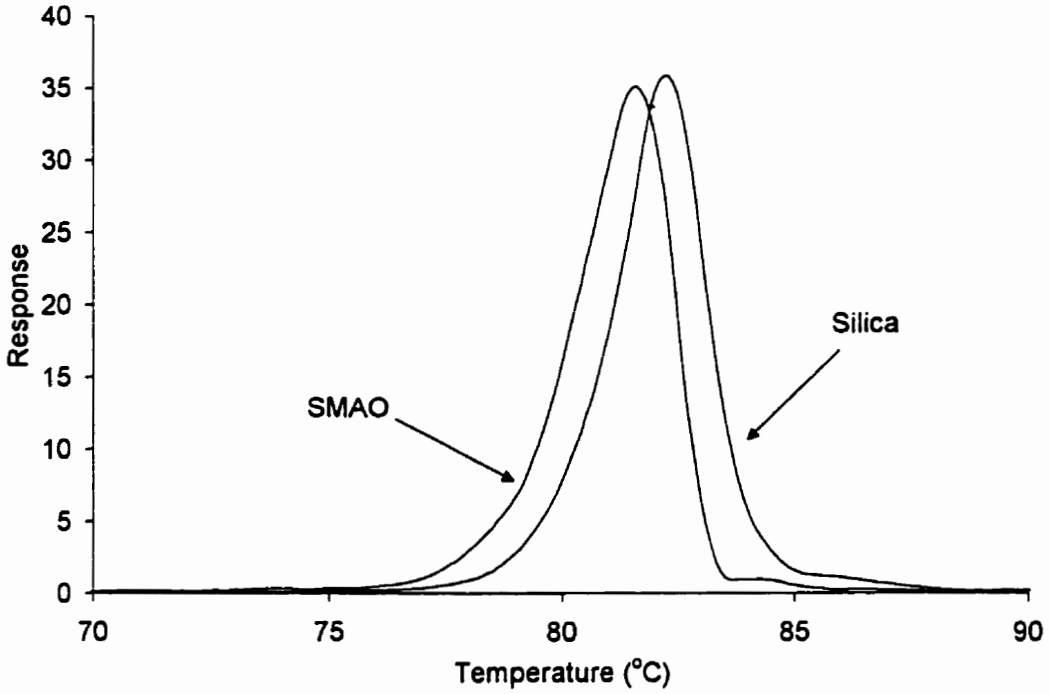

Figure 5.11 CRYSTAF profiles of poly(ethylene-co-1-hexene) produced with Cp_2ZrCl_2 with 0.1 g of $(C_2H_5)_2Zn$, 50 °C, $P_{Ethylene}$ = 100 psi, 1-hexene = 5 mL

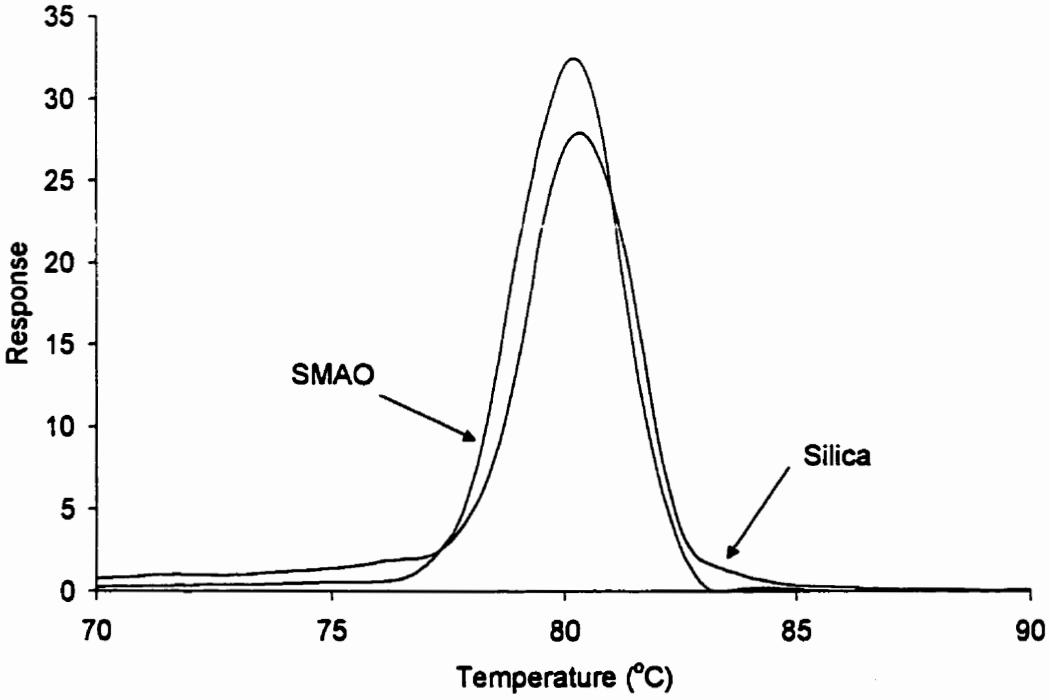

Figure 5.12 CRYSTAF profiles of poly(ethylene-co-1-hexene) produced with Cp_2ZrCl_2 with 25 mL of H_2, 50 °C, $P_{Ethylene}$ = 100 psi, 1-hexene = 5 mL

Figs. 5.13 to 5.15 show the CCDs of polymer produced with $Et[Ind]_2ZrCl_2$ supported on either **SMAO** or **Silica** for different polymerization conditions. For the case of $Et[Ind]_2ZrCl_2$, the CCD of polymer produced with the catalyst supported on **Silica** was always broader than that of polymer produced with the same catalyst supported on **SMAO**. The CCDs of polymer made with both catalysts are unimodal.

In terms of peak positions, the polymers produced with $Et[Ind]_2ZrCl_2$/SMAO have lower crystallization temperatures regardless of the presence of chain transfer agents. Therefore, it seems that zirconocenes supported on **SMAO** tend to incorporate more comonomer into the growing polymer chains.

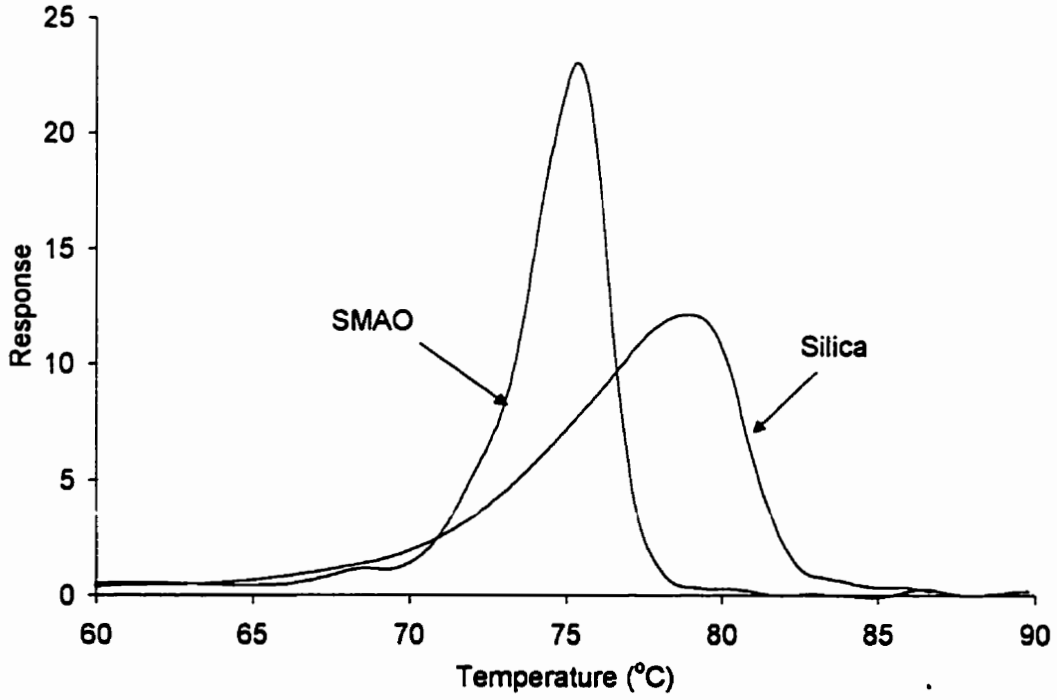

Figure 5.13 CRYSTAF profiles of poly(ethylene-co-1-hexene) produced with $Et[Ind]_2ZrCl_2$ without use of CTA, 50 °C, $P_{Ethylene}$ = 100 psi, 1-hexene = 5 mL

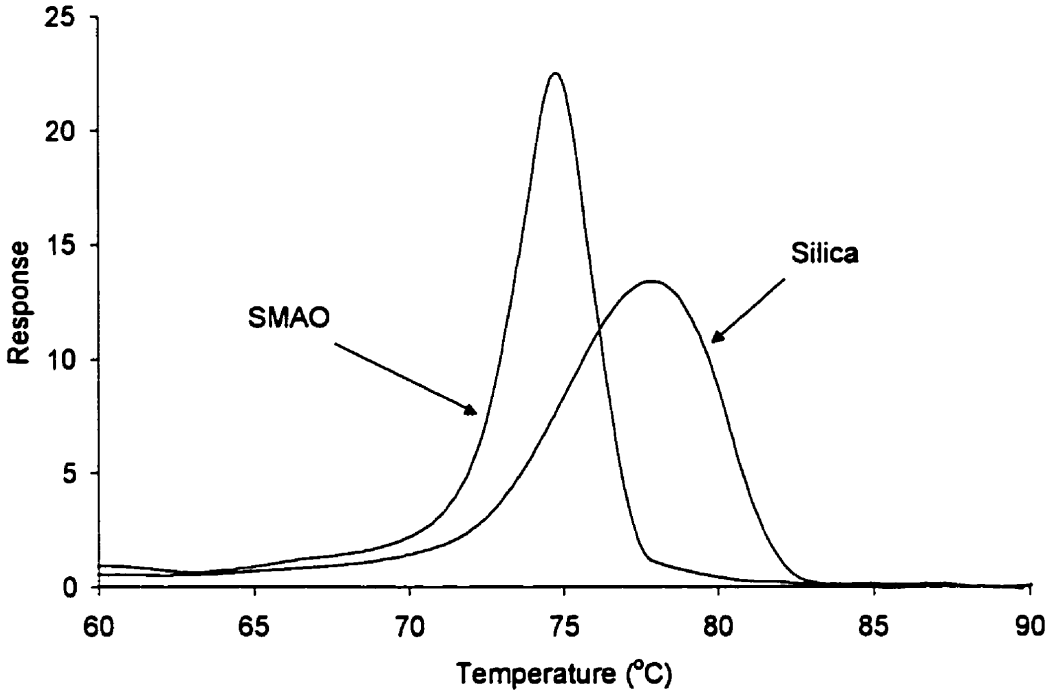

Figure 5.14 CRYSTAF profiles of poly(ethylene-co-1-hexene) produced with $Et[Ind]_2ZrCl_2$ with 0.1 g of $(C_2H_5)_2Zn$, 50 °C, $P_{Ethylene}$ = 100 psi, 1-hexene = 5 mL

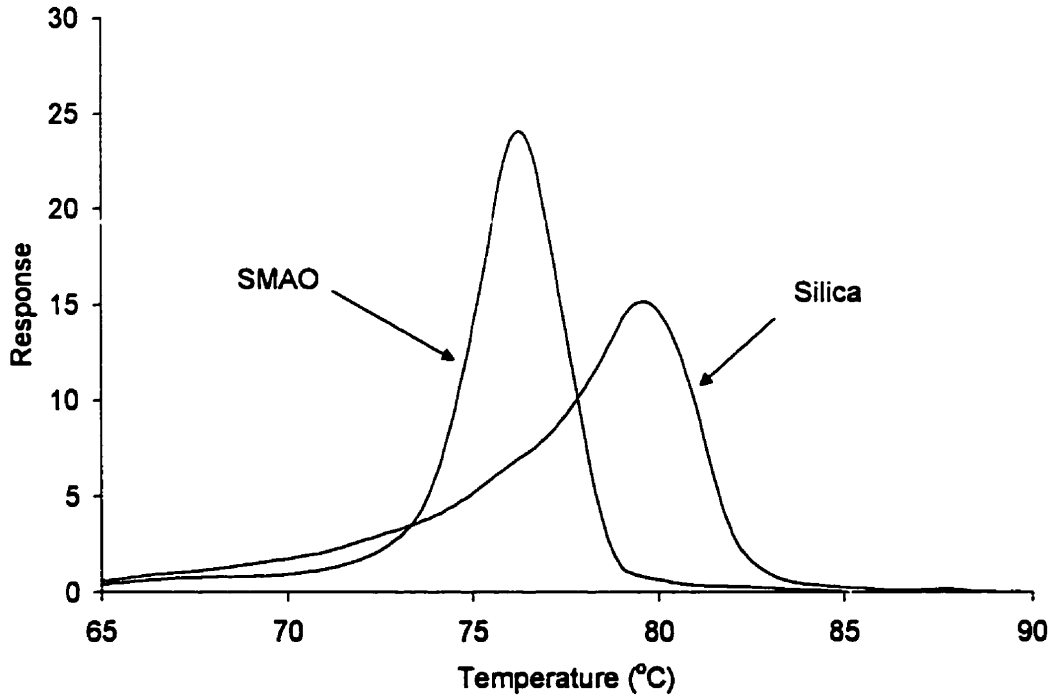

Figure 5.15 CRYSTAF profiles of poly(ethylene-co-1-hexene) produced with $Et[Ind]_2ZrCl_2$ with 25 mL of H_2, 50 °C, $P_{Ethylene}$ = 100 psi, 1-hexene = 5 mL

5.5. CONCLUSION

The chemical composition distribution of ethylene/1-hexene copolymers made with supported metallocene catalysts can be significantly altered by the way the support is treated. Interestingly, these support treatments do not influence the breadth of molecular weight distribution in a marked way.

For the four catalysts tested, Cp_2HfCl_2 was the most sensitive to support treatment. Unimodal (mainly) CCD was obtained for the polymers produced with Cp_2HfCl_2 when **Silica** was used, while bimodal CCDs resulted when either **MAO/Silica** or **SMAO** were used as supports. This has been tentatively linked to the presence of OH and OH-MAO supporting sites on the surface of these catalysts.

For zirconocene catalysts, polymers produced with catalysts supported on **SMAO** had lower crystallization temperatures than those of polymers produced with the same catalyst supported on **Silica**, indicating more comonomer content in the polymer chain. In terms of the broadness of CCDs, all zirconocene catalysts produced polymers with unimodal CCDs regardless of the support type or the presence of chain transfer agents. However, the CCDs of polymers produced with $Et[Ind]_2ZrCl_2$/Silica were significantly broader than those of other copolymers produced with zirconocene catalysts.

CHAPTER 6
COPOLYMERIZATION

Conventional linear low-density polyethylenes (LLDPE) made with Ziegler-Natta catalysts have broad and multimodal chemical composition distributions (CCD), in contrast to the narrow CCDs of high-pressure low-density polyethylenes (HP-LDPE). For the conventional copolymers produced with Ziegler-Natta catalysts, the amount of short chain branches (SCB) decreases with increasing molecular weight. (Hosoda, 1988, Defoor *et al.*, 1992). Higher contents of comonomer in shorter chains limit the application of these products, especially in areas such as food packaging and medical applications, because the amorphous short chains can easily diffuse into the surrounding environment. Therefore, it is important to be able to control CCD simultaneously with MWD.

Although in some cases the CCDs of copolymers produced with metallocene catalysts are also broad, in general they are much narrower than the ones made with conventional Ziegler-Natta catalysts. Therefore, by proper combination of metallocene catalysts, CCD of polyolefins can be effectively controlled.

A good example, which illustrates the importance of simultaneous control of CCD and MWD, is found in PE100 polyethylene resins. PE100 resins are used mainly in pipe applications and they are characterized by exceptionally high environmental stress-crack resistance, good resistance to rapid crack propagation, and very high creep resistance. The high environmental stress-crack resistance is believed to be the result of the presence of tie-molecules. Tie molecules are polymer chains that link two or more crystalline lamellae through the amorphous phase. Ideally, tie molecules should be long molecules containing crystallizable and non-crystallizable sections. For copolymers of ethylene and α-olefins, the crystallizable sections are long sequences of ethylene monomer units, while the non-crystallizable sequences contain the α-olefin comonomer units or short chain branches. It is envisioned that the crystallizable sections of the tie molecules belong to different adjacent lamellae, while the non-crystallizable sections are located in the amorphous phase. In this way, the molecules can be

considered to act as a binder among different lamellae, with binding strength proportional to valence forces. Therefore, the tie molecules will enhance resistance to applied stresses by establishing links between crystalline blocks.

The key criterion to increase the concentration of tie molecules or to produce copolymers that would meet the physical specifications of PE100 is to produce copolymers with bimodal MWD with higher comonomer content in the high molecular weight region. Since it is very difficult to achieve a truly homogeneous bimodal blend solely by mechanical blending of two different resins, reactor cascade technologies are used to produce PE100 resins. In the first reactor, polymerization is conducted in the presence of comonomer but without hydrogen to produce high molecular weight copolymer. The copolymer is continuously transferred to the second reactor where ethylene is polymerized in the presence of hydrogen and without addition of comonomer to produce lower molecular weight homopolymer chains (Scheirs *et al.*, 1996). If a single catalyst could produce PE100-type copolymers in a single reactor, the polymerization process would be significantly simplified.

In Chapters 4 and 5, MWD control in homopolymerization and the effect of support treatment on CCD of copolymers produced with supported metallocene catalysts were investigated. In this chapter, the research is extended to ethylene/1-hexene copolymerization to investigate ways of controlling the MWD and CCD of copolymer chains. Finally, three-dimensional MWD-CCD cross fractionation plots are generated through Monte-Carlo simulations to illustrate some important issues involved in the characterization of these copolymers.

6.1. PRELIMINARY EXPERIMENTAL RESULTS

All polymerizations described in Chapter 6 involve metallocenes supported on Silica/MAO. Every polymerization used 1-hexene as the comonomer. No other types of supports or comonomers were used.

6.1.1. Correlation Between Average Molecular Weight and CRYSTAF Measurements

When copolymer chains are reasonably long, CCDs measured by CRYSTAF should be determined only by the distributions of short chain branching and not by the molecular weights of the samples. Fig. 6.1 shows the relationship between the peak crystallization temperature measured with CRYSTAF versus number average molecular weight of poly(ethylene-co-1-hexene) samples produced with $Et[Ind]_2ZrCl_2$ at various polymerization conditions. No apparent correlation between peak crystallization temperature and number average molecular weight of the samples is observed.

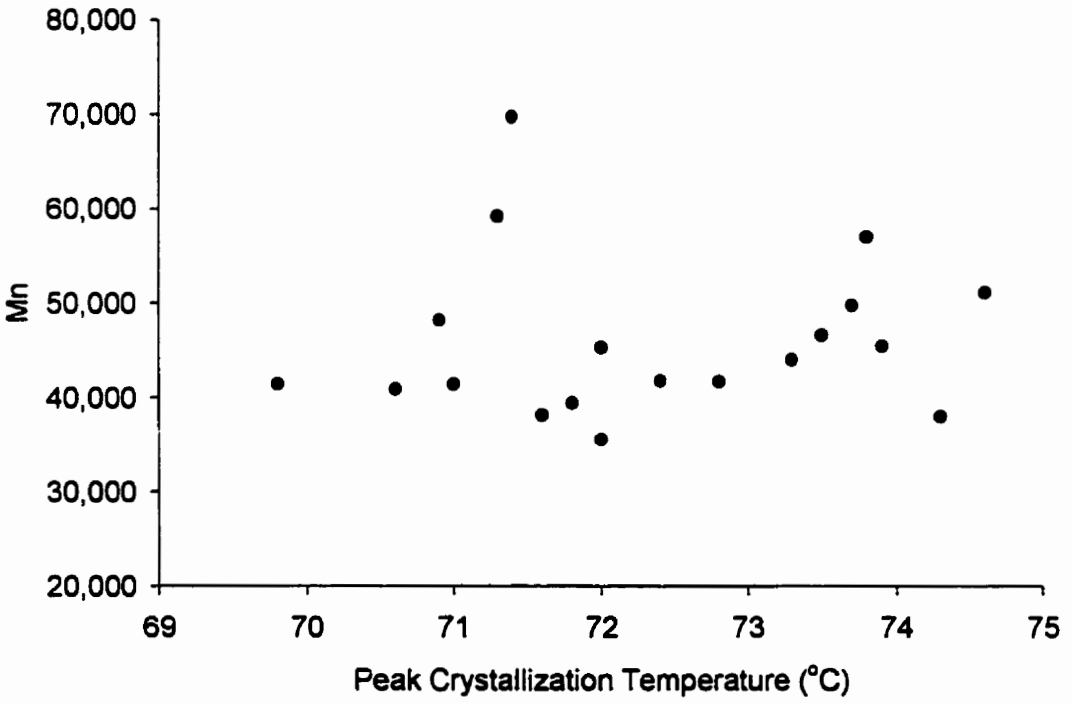

Figure 6.1 Peak crystallization temperature measured by CRYSTAF vs. number average molecular weight for poly(ethylene-co-1-hexene) samples

6.1.2. Average Molecular Weights Measured by GPC

Weight average molecular weights (M_w) and polydispersity indexes of the produced copolymers are presented in Appendix C. Figs. 6.2 through 6.9 show how M_w of copolymers produced with each supported catalyst varies with hydrogen concentration for several polymerization conditions. Throughout the experiments, the amount of 1-hexene and hydrogen concentration increments was varied proportionally to ethylene pressure.

Fig. 6.2 shows the M_w of copolymers produced with each supported catalyst at 40 °C under ethylene partial pressure of 20 psi, 1 mL of 1-hexene, and with various concentrations of hydrogen. The M_w of copolymers produced with $Et[Ind]_2ZrCl_2$ decreases very slightly with increasing hydrogen concentration in the polymerization reactor. However, for the copolymers produced with Cp_2HfCl_2 or CGCTi, M_ws decrease rapidly with the introduction of hydrogen and then start to decrease slowly as the concentration of hydrogen increases. At 40 °C and ethylene pressure of 20 psi, the M_ws of copolymers produced with CGCTi are always higher than those of copolymers produced with Cp_2HfCl_2. The M_w of copolymers produced with $Et[Ind]_2ZrCl_2$ was the lowest in absence of hydrogen, but the highest when higher hydrogen concentrations were used due to the rapid decrease in M_ws of copolymers produced with the other catalysts.

Fig. 6.3 shows M_ws of copolymers produced at 50 °C with the same ethylene pressure and hydrogen concentrations shown in Fig. 6.2. Compared to polymerization at 40 °C, the copolymers produced with $Et[Ind]_2ZrCl_2$ have similar M_ws. Copolymers produced with Cp_2HfCl_2 without hydrogen at 50 °C have higher M_ws than the ones made at 40 °C. When hydrogen is introduced, the M_ws of copolymers produced at 40 and 50 °C decrease to under 100,000 g/mole.

Interestingly, copolymers produced with CGCTi have higher M_ws at higher polymerization temperatures except for the case when no hydrogen was used. Also, M_ws decrease slower with hydrogen addition and thus the M_ws always stay above the M_ws of copolymers produced with $Et[Ind]_2ZrCl_2$.

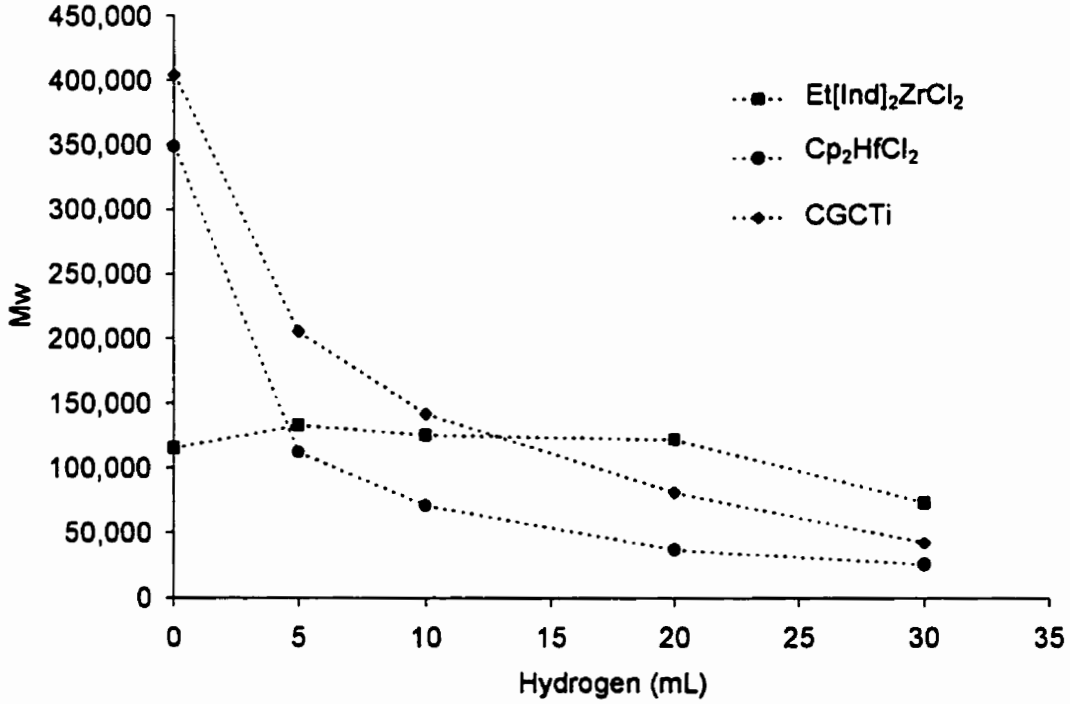

Figure 6.2 Weight average molecular weights of poly(ethylene-co-1-hexene): 40 °C, $P_{Ethylene}$ = 20 psi, 1-hexene = 1 mL

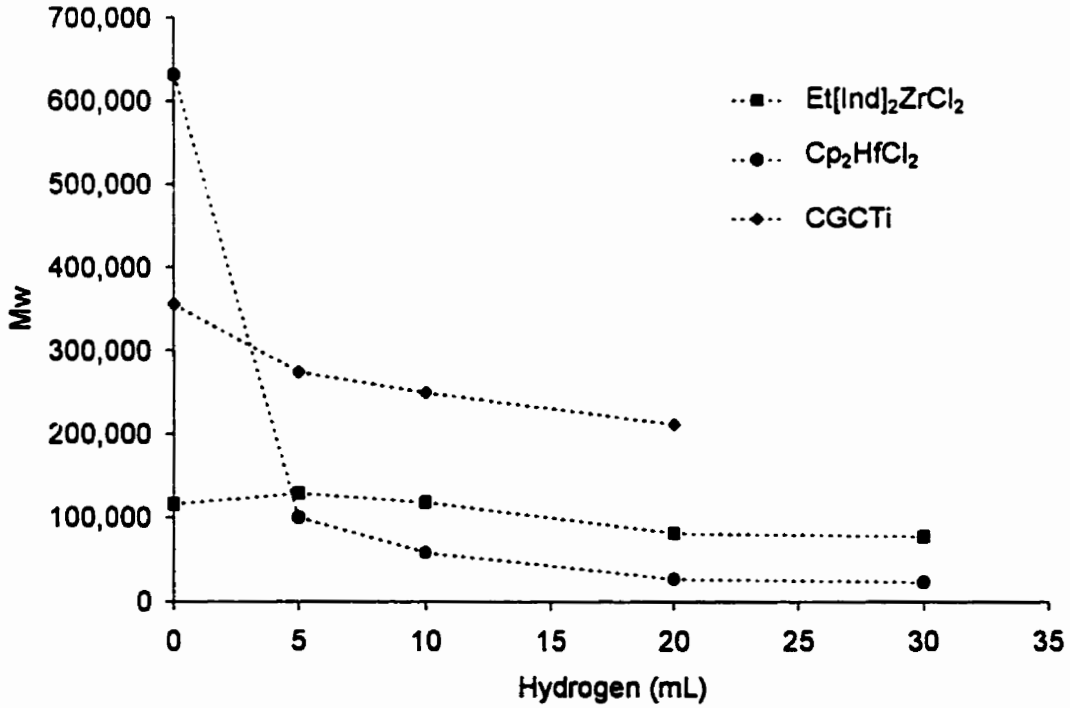

Figure 6.3 Weight average molecular weights of poly(ethylene-co-1-hexene): 50 °C, $P_{Ethylene}$ = 20 psi, 1-hexene = 1 mL

Figs. 6.4 and 6.5 show M_ws of copolymers produced at ethylene pressure of 50 psi, with 2.5 mL of 1-hexene and polymerization temperatures of 40 and 50 °C, respectively. Similar trends are observed. Again the copolymers produced with $Et[Ind]_2ZrCl_2$ show similar M_ws regardless of the concentration of hydrogen. The M_ws of copolymers produced with Cp_2HfCl_2 are the most sensitive to hydrogen concentrations. M_ws of copolymers produced with CGCTi are significantly higher when the higher polymerization temperature is used under the presence of hydrogen, but in the absence of hydrogen, M_ws are similar for both temperatures. The inversion of the average molecular weight (i.e., when the ratio of M_ws produced on each catalyst becomes unity) occurs at lower hydrogen concentration (ca. 5mL) for copolymers produced with Cp_2HfCl_2 and CGCTi. For copolymers produced with Cp_2HfCl_2 and $Et[Ind]_2ZrCl_2$, the inversion occurs at higher hydrogen concentration (ca. 20 mL). No M_w inversion occurs for the copolymers produced with $Et[Ind]_2ZrCl_2$ and CGCTi.

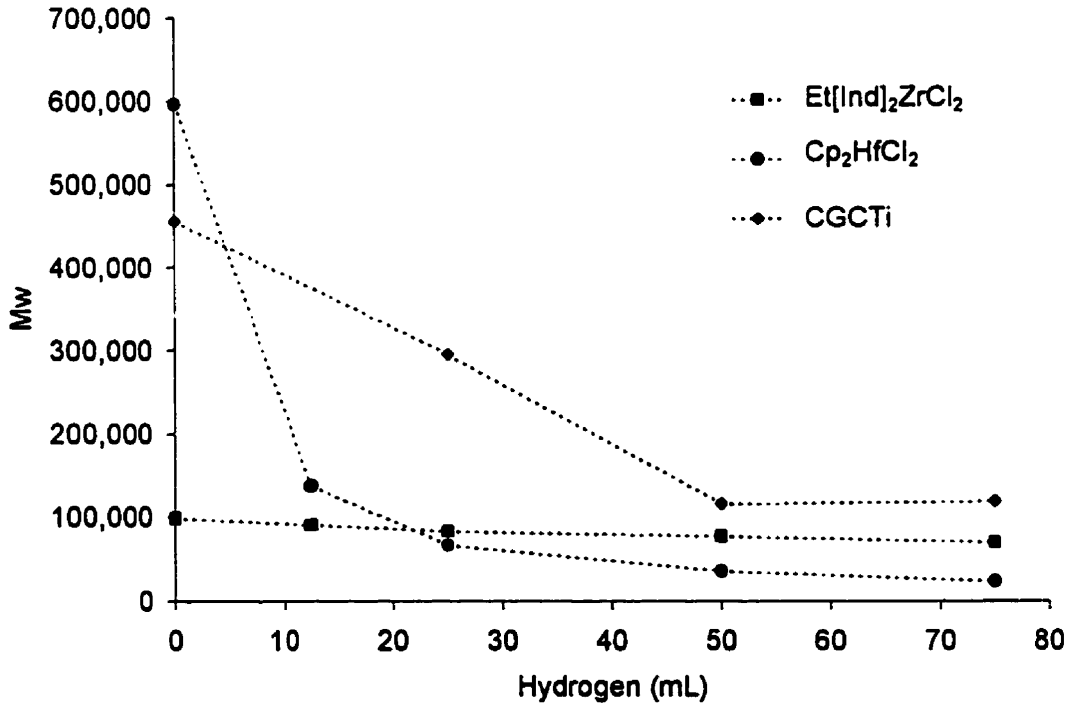

Figure 6.4 Weight average molecular weights of poly(ethylene-co-1-hexene): 40 °C, $P_{Ethylene}$ = 50 psi, 1-hexene = 2.5 mL

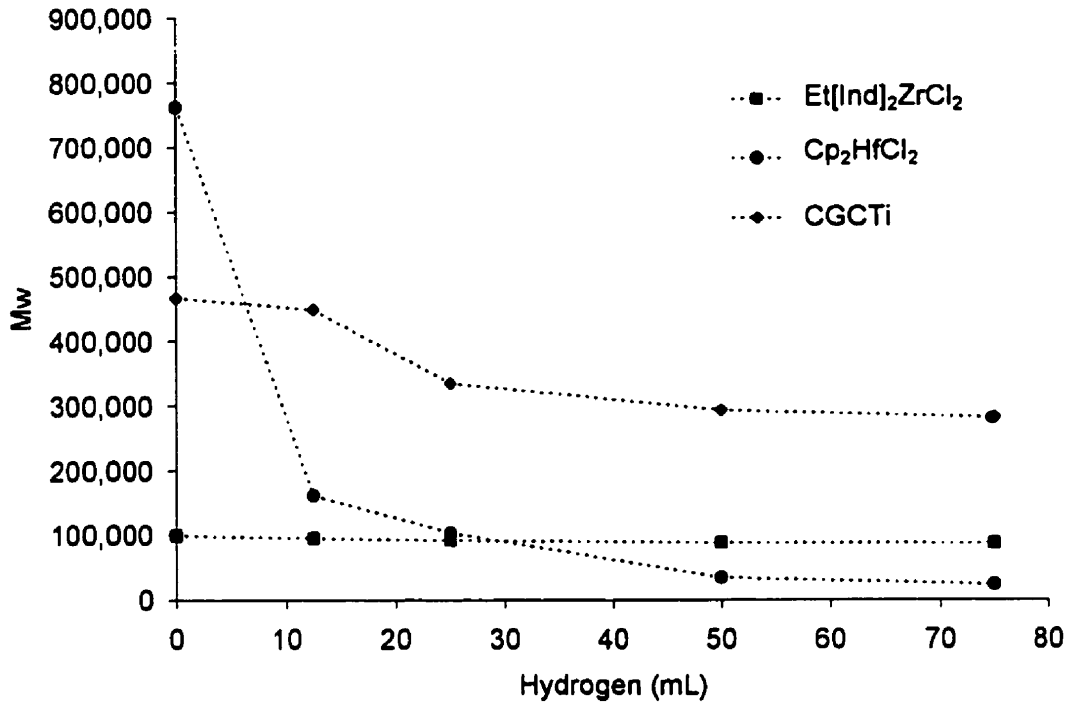

Figure 6.5 Weight average molecular weights of poly(ethylene-co-1-hexene): 50 °C, $P_{Ethylene}$ = 50 psi, 1-hexene = 2.5 mL

Figs. 6.6 and 6.7 show M_ws of copolymers produced at ethylene pressure of 100 psi with 5 mL of 1-hexene and polymerization temperatures of 40 and 50 °C, respectively. Copolymers produced with CGCTi at 40 °C always have the highest M_ws for all hydrogen concentrations. However, at 50 °C, copolymers produced with Cp_2HfCl_2 without hydrogen have higher M_ws than the ones produced with CGCTi. Unlike the previous cases, when ethylene pressure is 100 psi, M_ws of copolymers produced with CGCTi at 50 °C are lower then the ones made at 40 °C. Again, apparently the average molecular weights of copolymers produced with $Et[Ind]_2ZrCl_2$ are independent of hydrogen concentration.

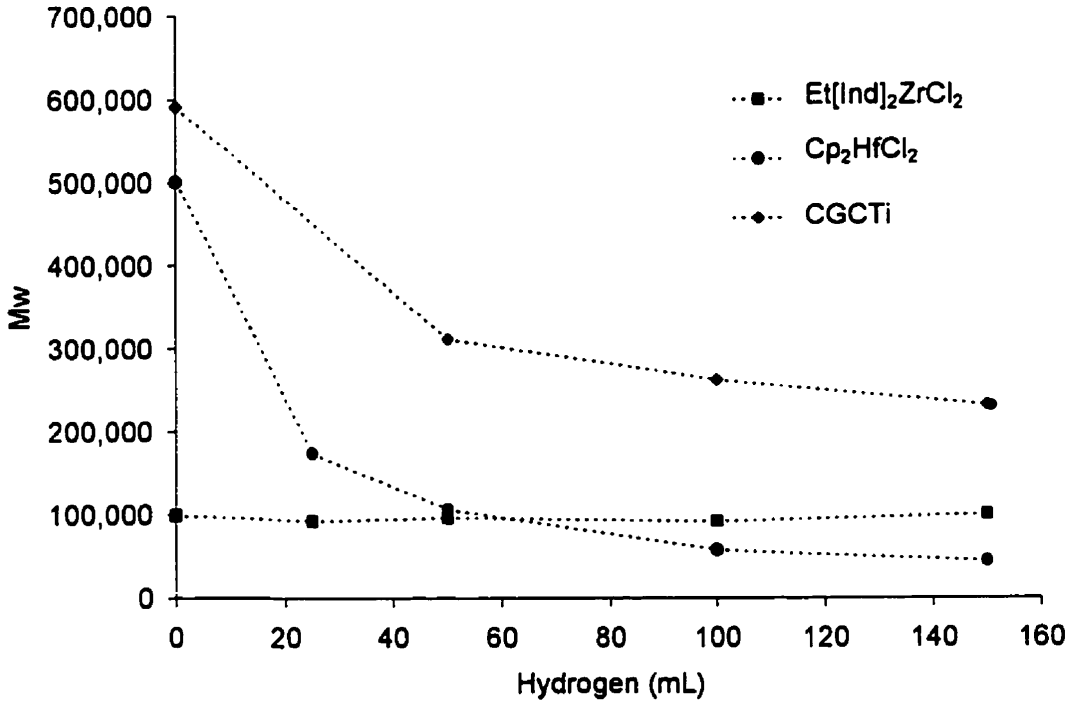

Figure 6.6 Weight average molecular weights of poly(ethylene-co-1-hexene): 40 °C, $P_{Ethylene}$ = 100 psi, 1-hexene = 5 mL

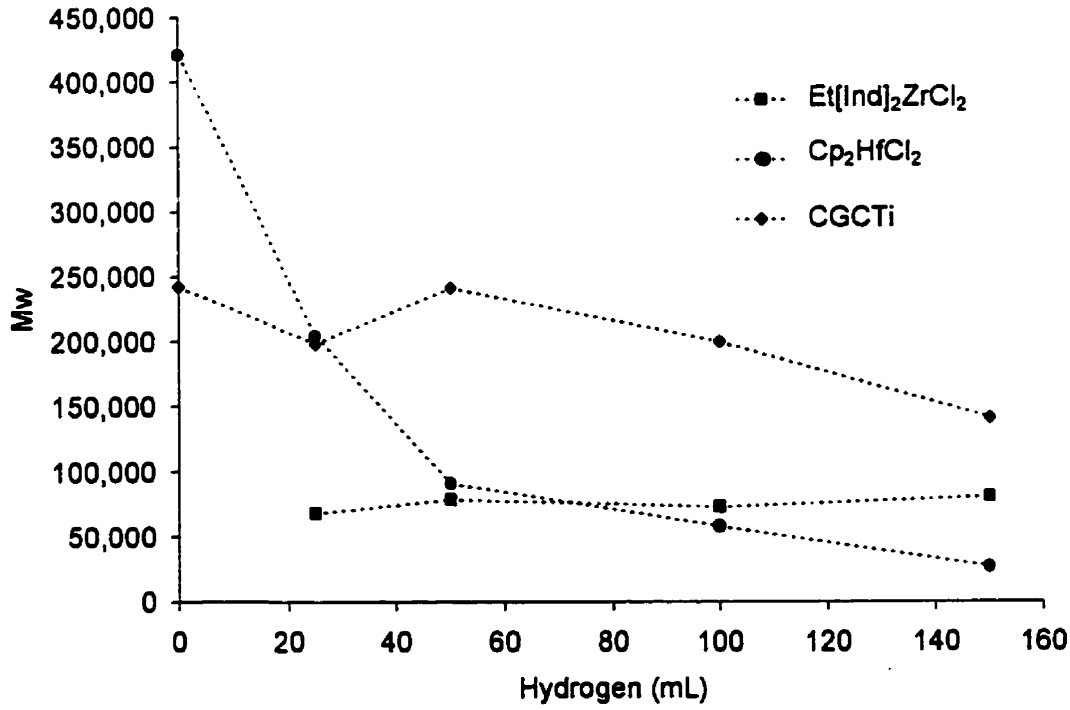

Figure 6.7 Weight average molecular weights of poly(ethylene-co-1-hexene): 50 °C, $P_{Ethylene}$ = 100 psi, 1-hexene = 5 mL

Figs. 6.8 and 6.9 show M_ws of copolymers produced at ethylene pressure of 150 psi, 7.5 mL of 1-hexene and polymerization temperatures of 40 and 50 °C, respectively.

For all polymerizations including the case with ethylene pressure of 150 psi, M_ws of copolymers produced with $Et[Ind]_2ZrCl_2$ are nearly independent of hydrogen concentration and polymerization temperature, especially for ethylene pressures over 50 psi. This trend was also observed for ethylene homopolymerization with $Et[Ind]_2ZrCl_2$, as discussed in Chapter 4. Also, it seems that for copolymers produced with CGCTi, M_ws are higher for higher polymerization temperatures when ethylene pressures are low (20 and 50 psi). However, higher M_ws are observed at lower polymerization temperatures when ethylene pressures are higher than 100 psi. For the case of copolymers produced with Cp_2HfCl_2, this effect is not obvious. For every polymerization condition, M_ws of copolymers produced with Cp_2HfCl_2 and CGCTi show strong dependency on hydrogen concentration, i.e., M_ws decrease rapidly with the introduction of hydrogen.

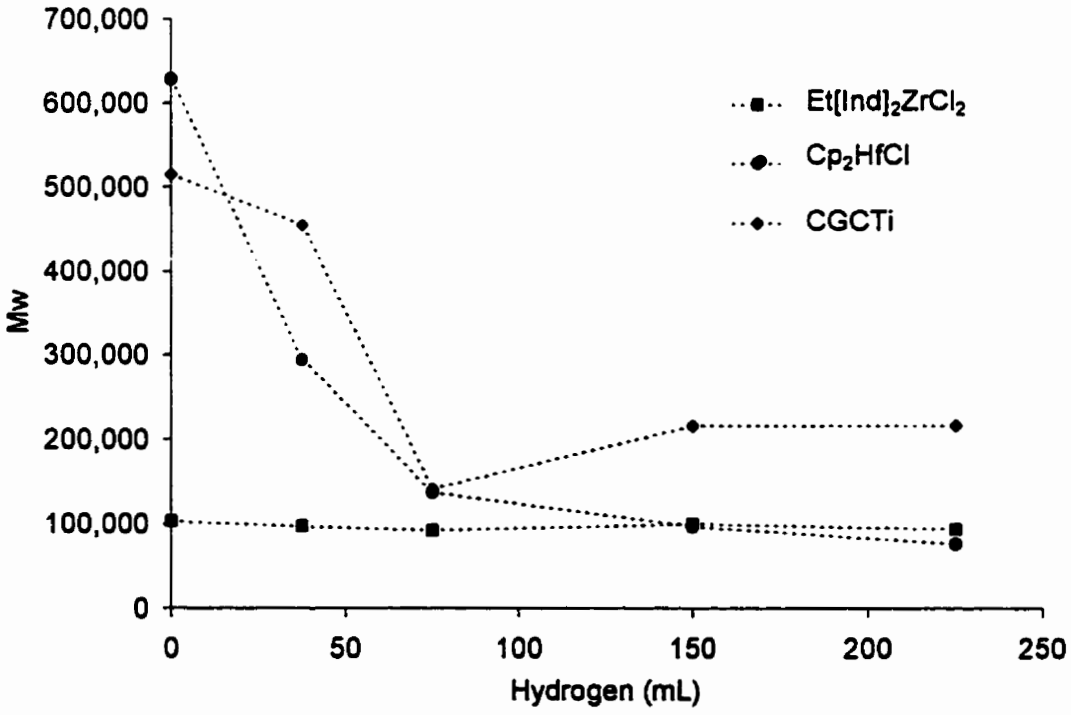

Figure 6.8 Weight average molecular weights of poly(ethylene-co-1-hexene): 40 °C, $P_{Ethylene}$ = 150 psi, 1-hexene = 7.5 mL

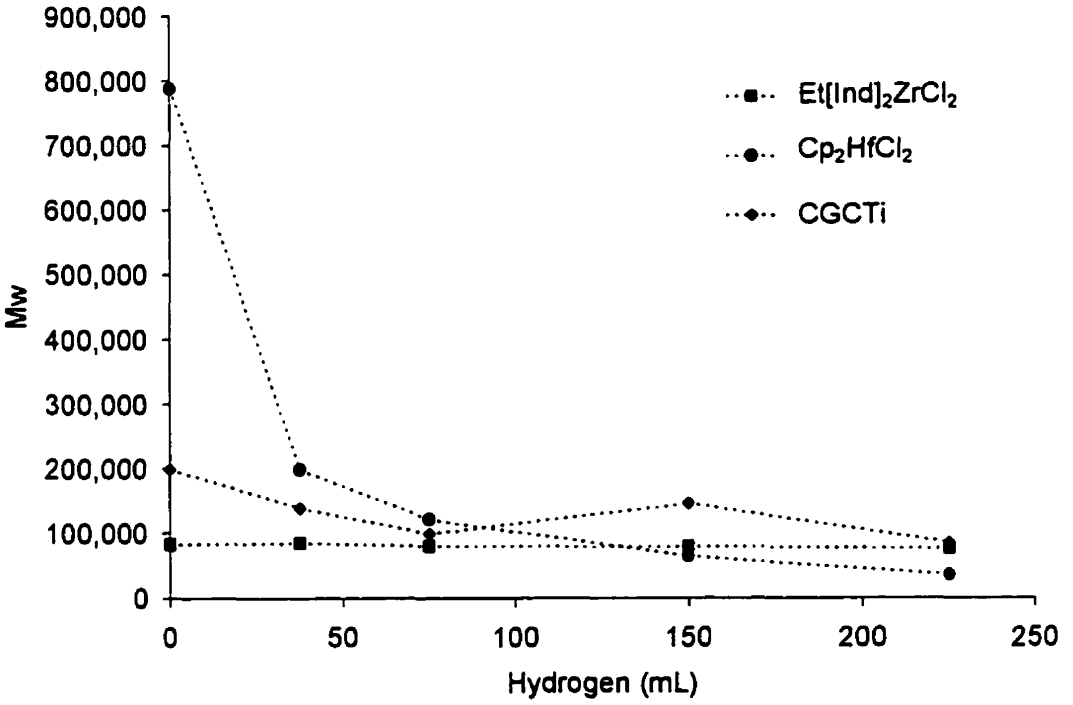

Figure 6.9 Weight average molecular weights of poly(ethylene-co-1-hexene): 50 °C, $P_{Ethylene}$ = 150 psi, 1-hexene = 7.5 mL

6.2. FACTORS INFLUENCING THE CONTROL OF MWD AND CCD

Out of many other factors, the accessibility of the comonomer to the active metal centers depends on the 'openness' of the metallic site and increases as $Et[Ind]_2ZrCl_2$ < Cp_2HfCl_2 < CGCTi among the catalysts used in this experiments (Fig. 4.1). Fig. 6.10 shows the CCD of poly(ethylene-co-1-hexene) measured by CRYSTAF produced with combined $Et[Ind]_2ZrCl_2$/CGCTi system at 40 and 50 °C. CCD peaks of copolymers produced with $Et[Ind]_2ZrCl_2$ at similar polymerization conditions appear at around 70 to 80 °C. Therefore, the peaks appearing between 70 to 85 °C correspond to the copolymer chains produced on $Et[Ind]_2ZrCl_2$ sites. Copolymers produced with CGCTi usually have very broad CCD and appear at lower crystallization temperatures. A significant portion of the copolymer is soluble in TCB at 30 °C. Therefore, it is reasonable to assign the peaks appearing at temperatures lower than 65 °C, including the soluble fractions, to the copolymer produced at CGCTi sites.

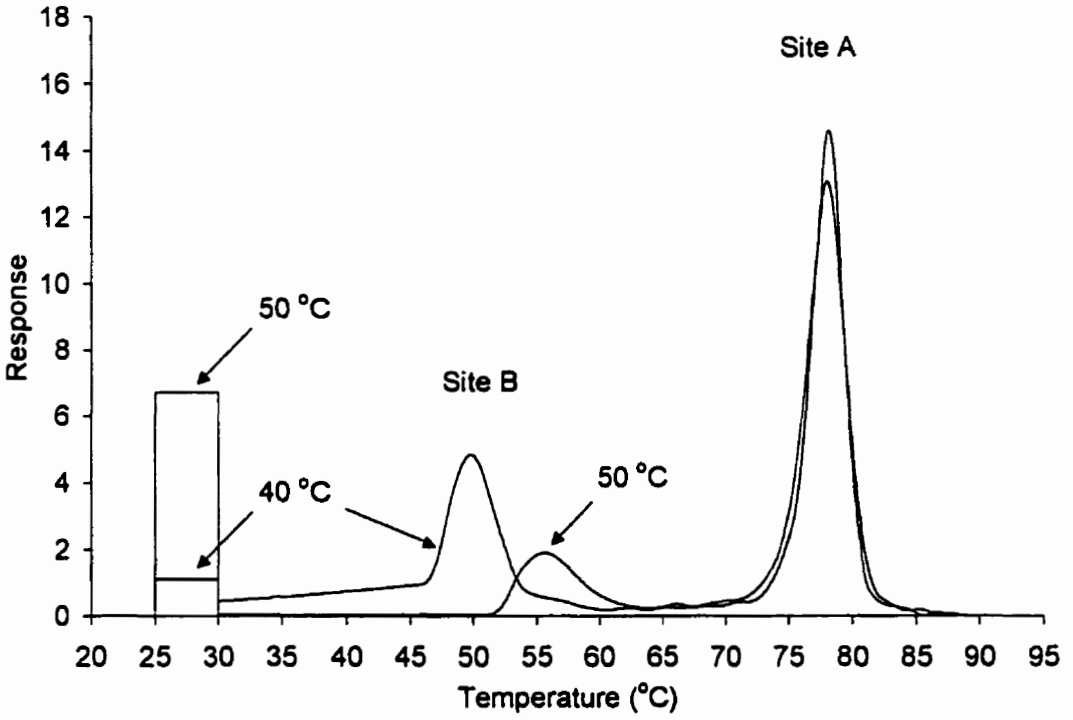

Figure 6.10 CCD of poly(ethylene-co-1-hexene) produced with a bimetallic supported catalyst (A: $Et[Ind]_2ZrCl_2$, B: CGCTi) at different polymerization temperatures, $P_{Ethylene}$ = 100 psi, 1-hexene = 5 mL

Fig. 6.11 shows the MWD of the samples shown in Fig. 6.10. Since CGCTi produces copolymers with higher molecular weights than $Et[Ind]_2ZrCl_2$ at ethylene pressure of 100 psi, the peak appearing at higher molecular weight corresponds to the copolymer chains produced at CGCTi sites. Therefore, the peak that appears at lower molecular weights corresponds to copolymers produced with $Et[Ind]_2ZrCl_2$. When the lower polymerization temperature was used (40 °C), the MWD shifts to higher molecular weight values. The peak corresponding to copolymer produced with CGCTi shifts more than the one assigned to copolymers produced with $Et[Ind]_2ZrCl_2$. This result agrees with the previous observations discussed in Section 6.1.2 (Figs. 6.6 and 6.7).

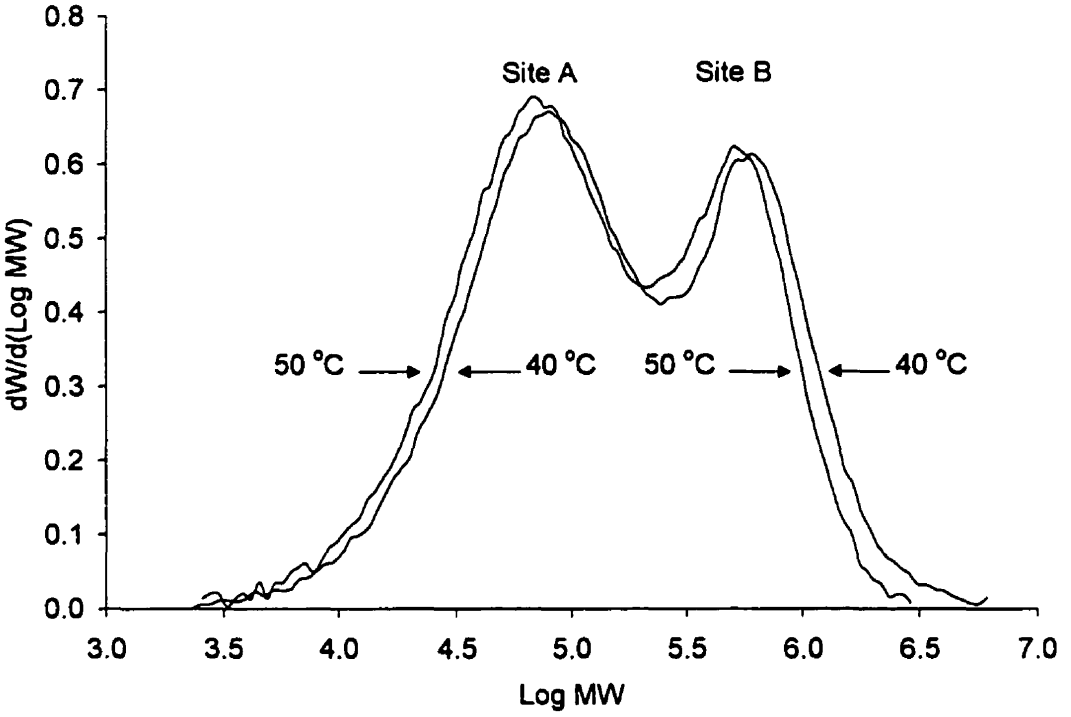

Figure 6.11 MWD of poly(ethylene-co-1-hexene) produced with a bimetallic supported catalyst (A: $Et[Ind]_2ZrCl_2$, B: CGCTi) at different copolymerization temperatures, $P_{Ethylene}$ = 100 psi, 1-hexene = 5 mL

From these results, it seems that the combined $Et[Ind]_2ZrCl_2$/CGCTi is able to produce copolymers with bimodal CCD and MWD, with higher comonomer content in the higher molecular weight chains. To verify that the higher molecular weight chains had higher comonomer fraction, the sample produced at 40 °C was analyzed with a LC-transform. First the LC-transform instrument was connected to the GPC so that the copolymer fractions could be collected according to molecular weight onto a rotating disk. The fractions deposited on the disk were analyzed with FT-IR to determine the comonomer content. The ratios of peak heights from two absorption bands, A_{1380} and A_{720}, were used to estimate the mol.-% of 1-hexene using a calibration curve found in the literature (Nowlin *et al.*, 1988). The accuracy of FT-IR measurements decreases when the high and low molecular weight end fractions are analyzed because they form very thin deposits. Nonetheless, Fig. 6.12 indisputably shows that the comonomer fraction in the copolymer increases with increasing molecular weight.

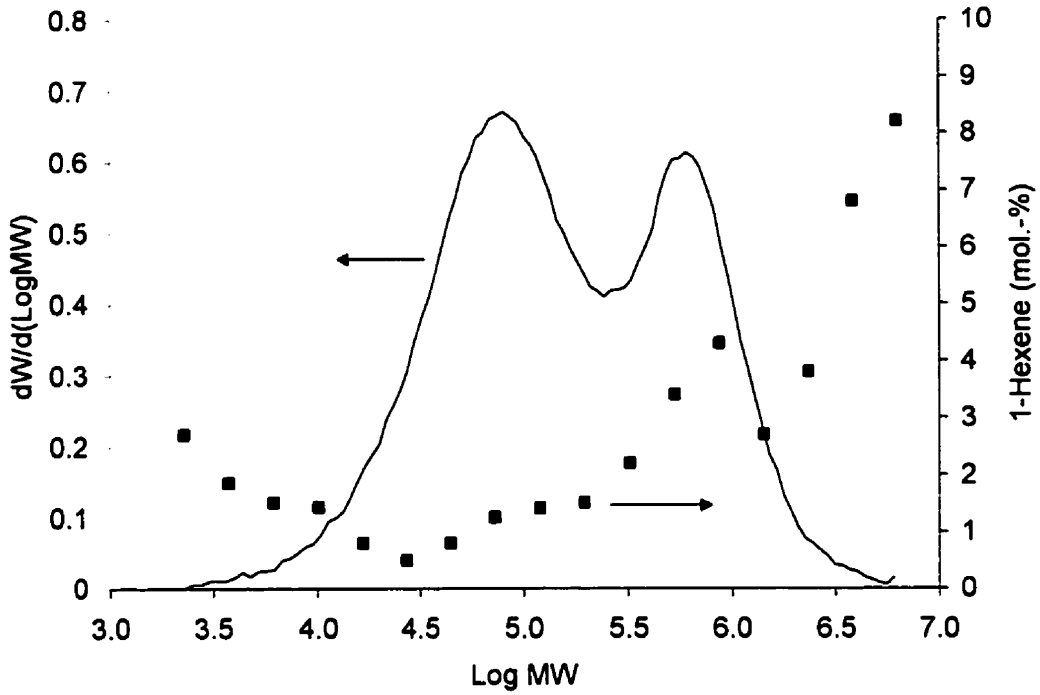

Figure 6.12 LC-Transform results of poly(ethylene-co-1-hexene) produced with a bimetallic supported catalyst (Et[Ind]$_2$ZrCl$_2$ / CGCTi), 40 °C, $P_{Ethylene}$ = 100 psi, 1-hexene = 5 mL

Figs. 6.13 to 6.18 show other possible combinations of CCD-MWDs of poly(ethylene-co-1-hexene) produced with combined Et[Ind]$_2$ZrCl$_2$/Cp$_2$HfCl$_2$ at various polymerization conditions.

Figs. 6.13 and 6.14 show CCD and MWD of copolymers produced at 40 °C, with 1 mL of 1-hexene, 30 mL of hydrogen, and ethylene pressure of 20 psi. The CCD of copolymer produced with Et[Ind]$_2$ZrCl$_2$ is sharp and narrow, but the CCD of copolymer produced with Cp$_2$HfCl$_2$ is very broad and encircles the narrow peak by Et[Ind]$_2$ZrCl$_2$. It is interesting to notice that these large differences cannot be detected by conventional average composition analysis by NMR. The copolymer produced with the combined catalyst show slightly broader CCD than that of copolymer produced with Et[Ind]$_2$ZrCl$_2$. The amount of copolymer produced at Cp$_2$HfCl$_2$ sites is much smaller than that produced at the other catalyst site. This is confirmed by the MWD of this copolymer as shown in Fig. 6.14. The MWD of copolymer produced with the combined catalyst closely resembles the MWD of copolymer produced with Et[Ind]$_2$ZrCl$_2$ alone. It seems that there was selective poisoning of Cp$_2$HfCl$_2$ sites, which is

more sensitive to impurities than $Et[Ind]_2ZrCl_2$. Therefore, most chains were produced at the $Et[Ind]_2ZrCl_2$ sites. However, this was not caused by an improper mixing ratio of $Et[Ind]_2ZrCl_2$ and Cp_2HfCl_2 catalysts during the preparation of the combined supported catalyst, as the next figures demonstrate that the presence of polymer chains produced on each site is clear.

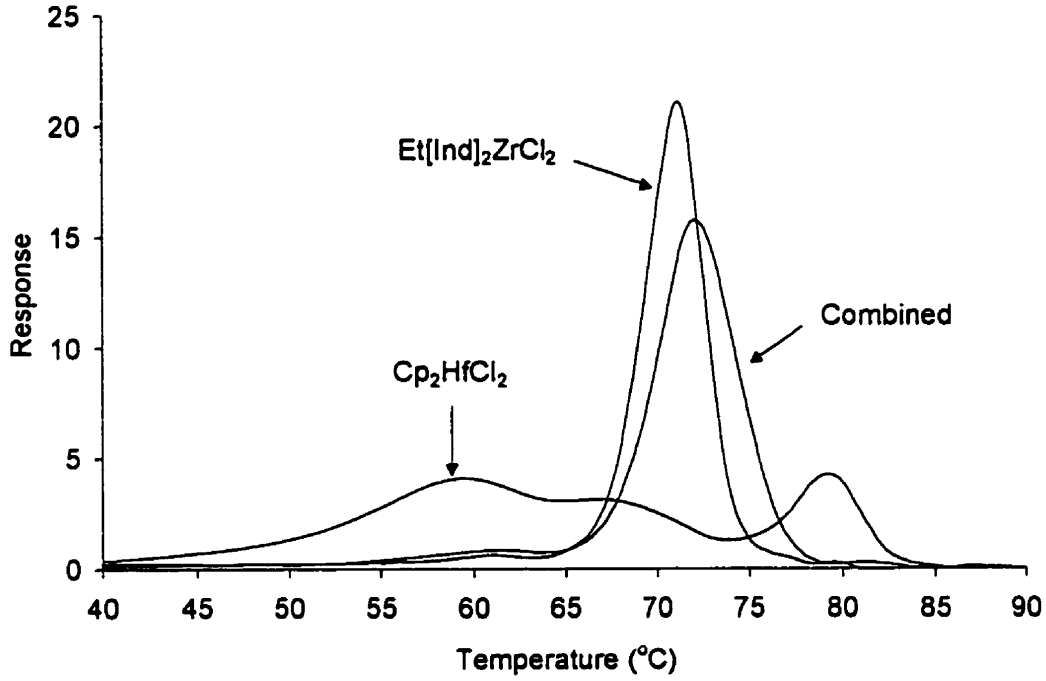

Figure 6.13 CRYSTAF results of poly(ethylene-co-1-hexene) produced with a bimetallic supported catalyst ($Et[Ind]_2ZrCl_2$ / Cp_2HfCl_2), 40 °C, $P_{Ethylene}$ = 20 psi, 1-hexene = 1 mL, H_2 = 30 mL

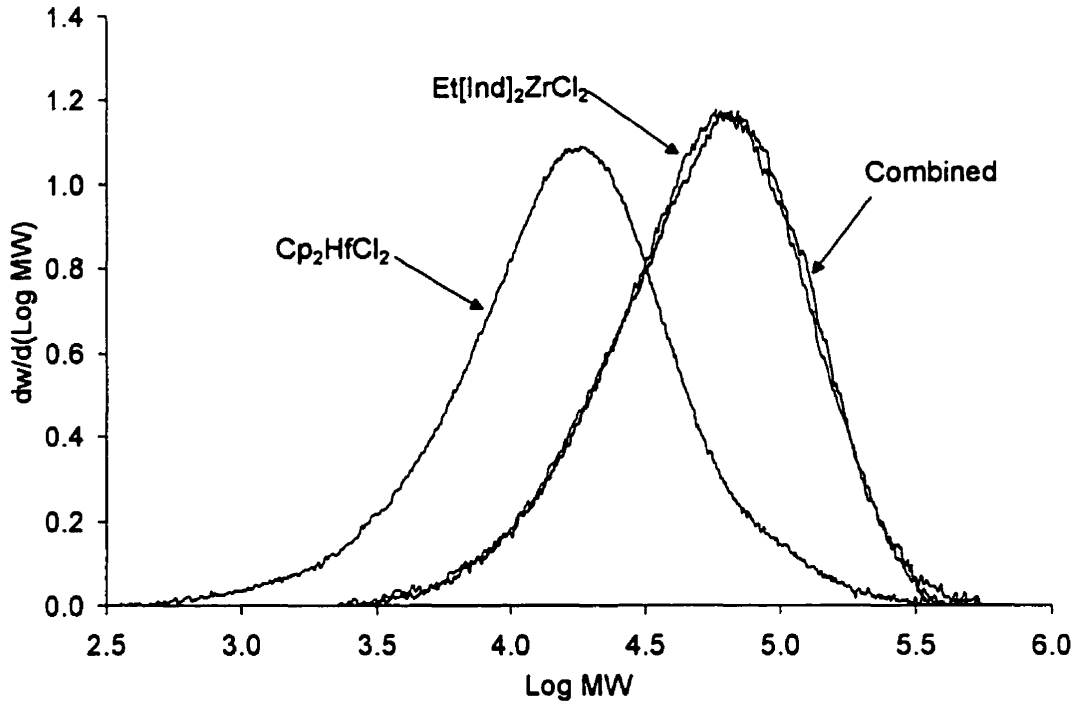

Figure 6.14 GPC results of poly(ethylene-co-1-hexene) shown in Fig. 6.13

Figs. 6.15 and 6.16 show the CCD and MWD of copolymers produced at 40 °C, with 2.5 mL of 1-hexene, and ethylene pressure of 50 psi. Fig. 6.15 shows that the CCD of copolymer produced with the combined catalyst is broader than the CCD of copolymer produced with $Et[Ind]_2ZrCl_2$, and has a low crystalline shoulder. However, the CCD of copolymer produced with the combined catalyst does not represent true superposition of each individual CCD. It seems that there is some bimolecular interaction between the different active sites, which causes the shifting of CCD of the copolymer produced with Cp_2HfCl_2 toward a higher crystalline region. This could also have been caused by small differences in the supporting procedure when Cp_2HfCl_2 was supported alone.

However, the MWD shows better superposition of individual distributions as shown in Fig. 6.16. From these CCD and MWD, the copolymer produced with the combined $Et[Ind]_2ZrCl_2$ / Cp_2HfCl_2 catalyst at 40 °C with 2.5 mL of 1-hexene at an ethylene pressure of 50 psi has bimodal MWD but unimodal CCD, with more comonomer incorporated at higher molecular weights.

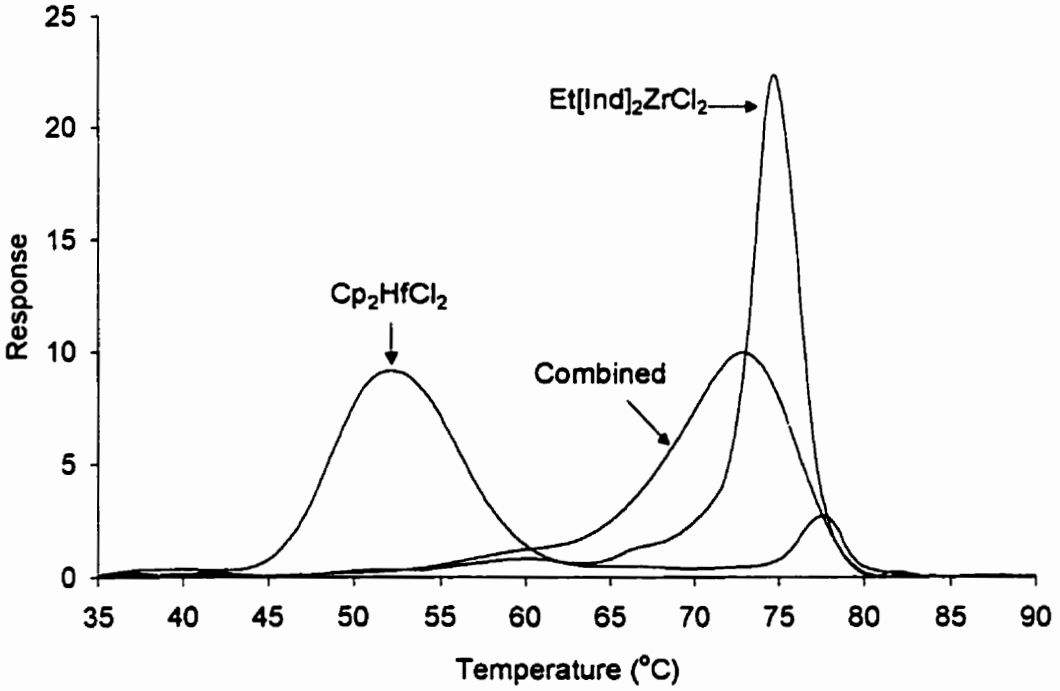

Figure 6.15 CRYSTAF results of poly(ethylene-co-1-hexene) produced with a bimetallic supported catalyst ($Et[Ind]_2ZrCl_2$ / Cp_2HfCl_2), 40 °C, $P_{Ethylene}$ = 50 psi, 1-hexene = 2.5 mL

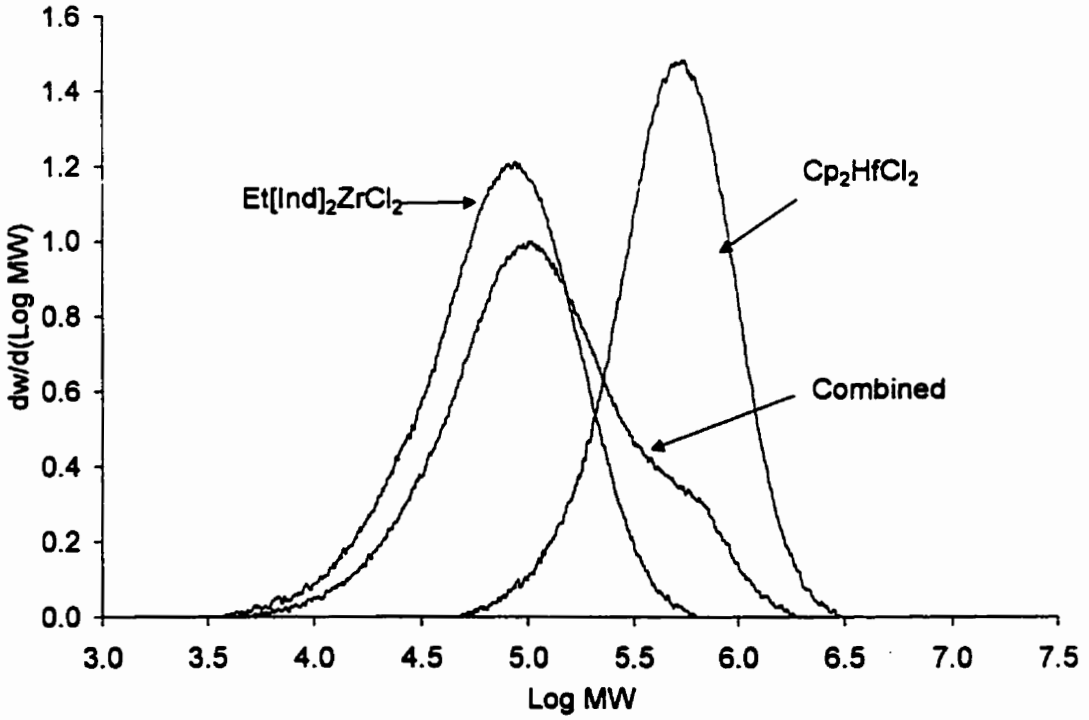

Figure 6.16 GPC results of poly(ethylene-co-1-hexene) shown in 6.15

Figs. 6.17 and 6.18 show the CCD and MWD of copolymers produced at 40 °C, with 5 mL of 1-hexene and ethylene pressure of 100 psi. The combined catalyst produces copolymers with broad CCD and MWD but both of them are unimodal. The copolymers produced with Cp_2HfCl_2 have bimodal CCD which encloses the CCD of copolymers produced with $Et[Ind]_2ZrCl_2$. Therefore, the microstructures of copolymers produced with the combined catalyst do not differ from each other significantly. The comonomer is still incorporated more in higher molecular weight chains, however, segregation of copolymer chains due to significant differences in chemical composition is less likely to occur as compared to the distributions shown in Figs. 6.10 and 6.11.

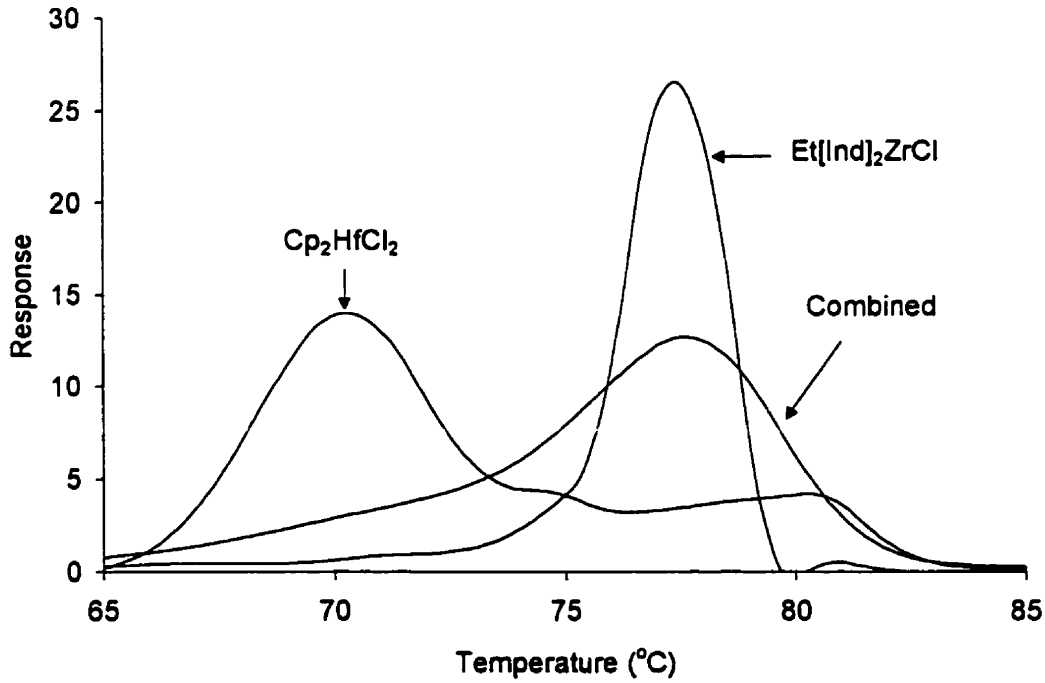

Figure 6.17 CRYSTAF results of poly(ethylene-co-1-hexene) produced with a bimetallic supported catalyst ($Et[Ind]_2ZrCl_2$ / Cp_2HfCl_2), 40 °C, $P_{Ethylene}$ = 100 psi, 1-hexene = 5 mL

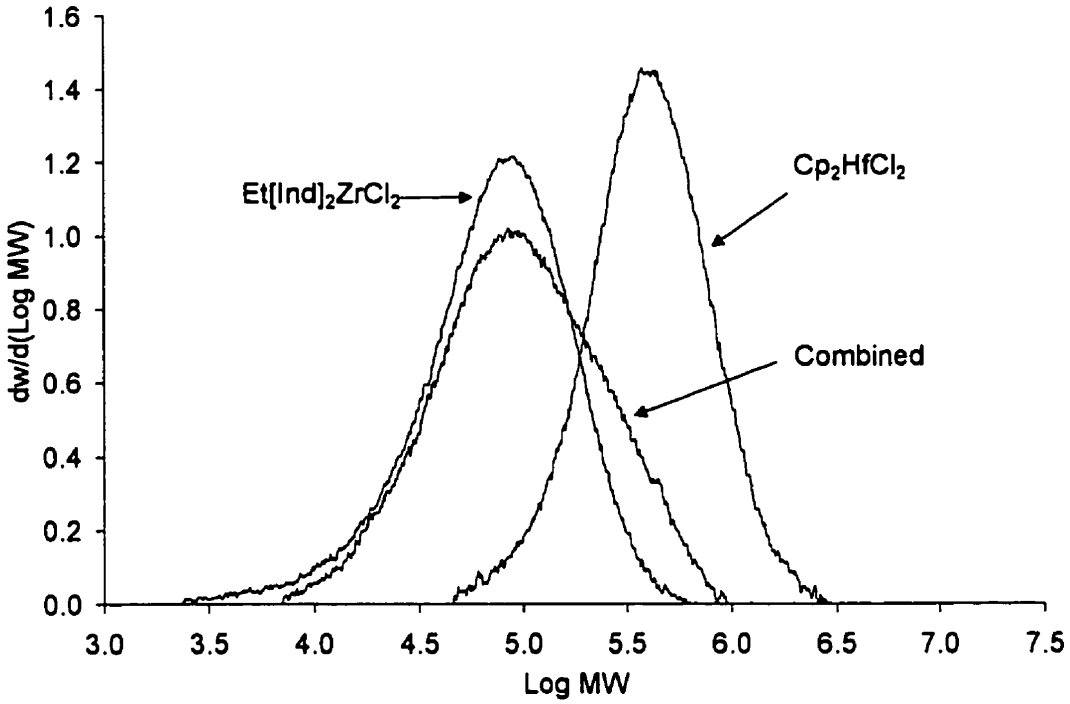

Figure 6.18 GPC results of poly(ethylene-co-1-hexene) shown in Fig. 6.17

More examples of CCD and MWD control at different polymerization conditions can be found in Appendix D.

Effect of Hydrogen

As discussed in Chapter 5, copolymers produced with Cp_2HfCl_2 supported on MAO/Silica show bimodal CCDs. In some cases where hydrogen was used, even trimodal CCDs were observed. Therefore, the effect of hydrogen on CCD of copolymers produced with Cp_2HfCl_2 was further examined. Figs. 6.19 to 6.23 show the effect of hydrogen on CCD of copolymers produced with Cp_2HfCl_2.

The positions of peaks appearing around 80 °C, which correspond to high crystalline copolymers, do not seem to be affected by hydrogen significantly. However, the low crystalline peak splits in two with increasing hydrogen concentration. As hydrogen concentration increases, a very low crystallinity peak moves to lower crystallinity regions, making the CCD trimodal.

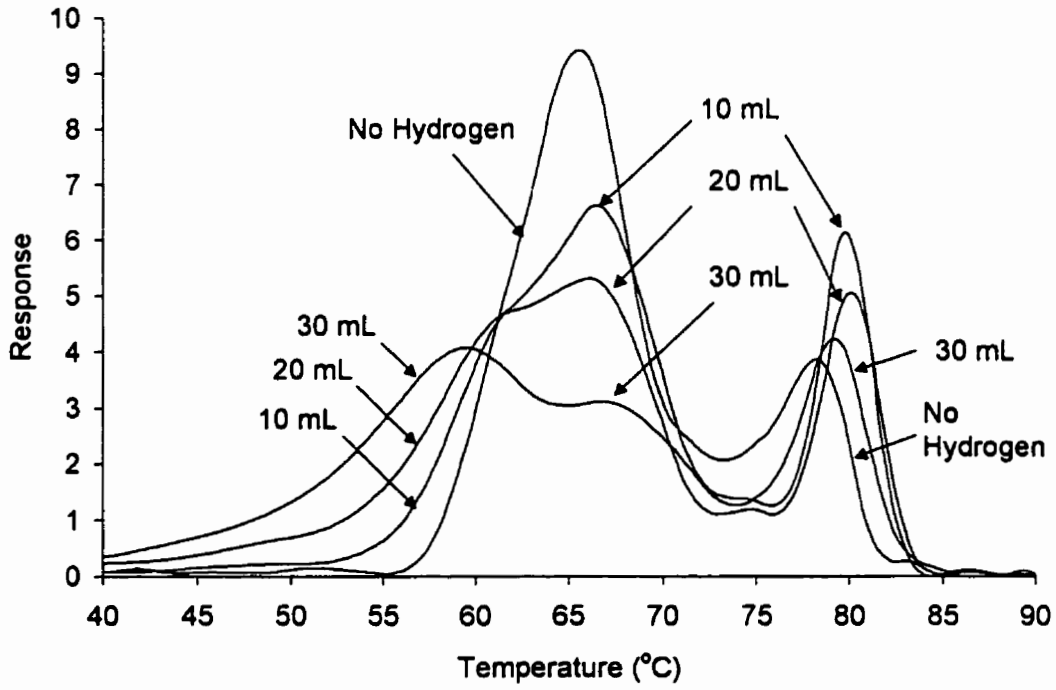

Figure 6.19 Effect of hydrogen concentration on CCD of poly(ethylene-co-1-hexene) produced with Cp_2HfCl_2 : 40 °C, $P_{Ethylene}$ = 20 psi, 1-hexene = 1 mL

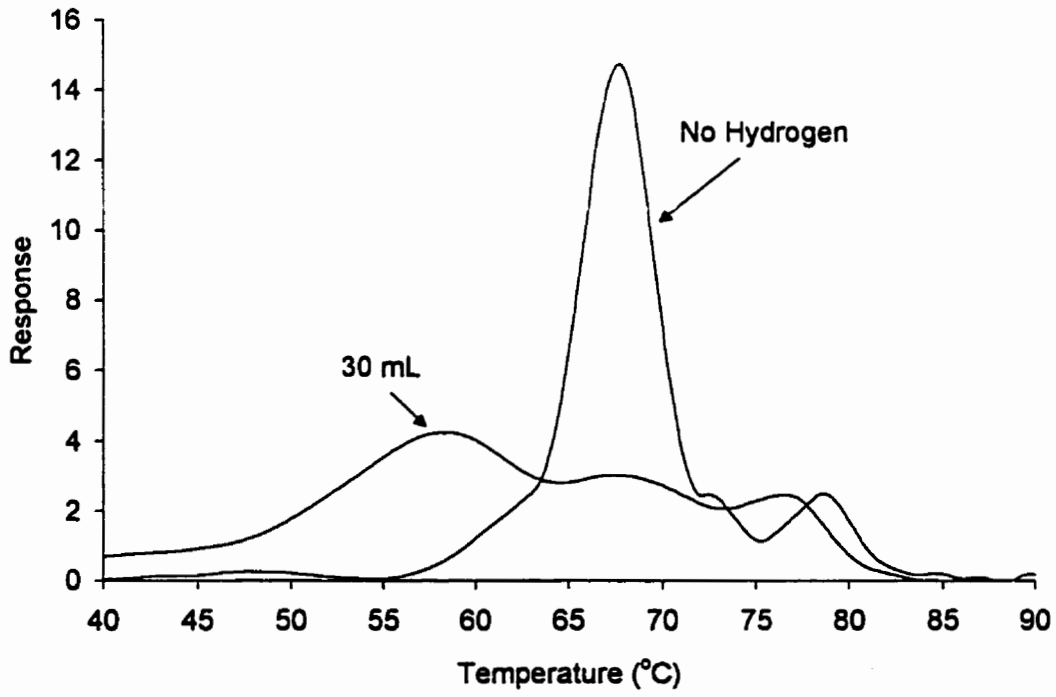

Figure 6.20 Effect of hydrogen concentration on CCD of poly(ethylene-co-1-hexene) produced with Cp_2HfCl_2, 50 °C, $P_{Ethylene}$ = 20 psi, 1-hexene = 1 mL

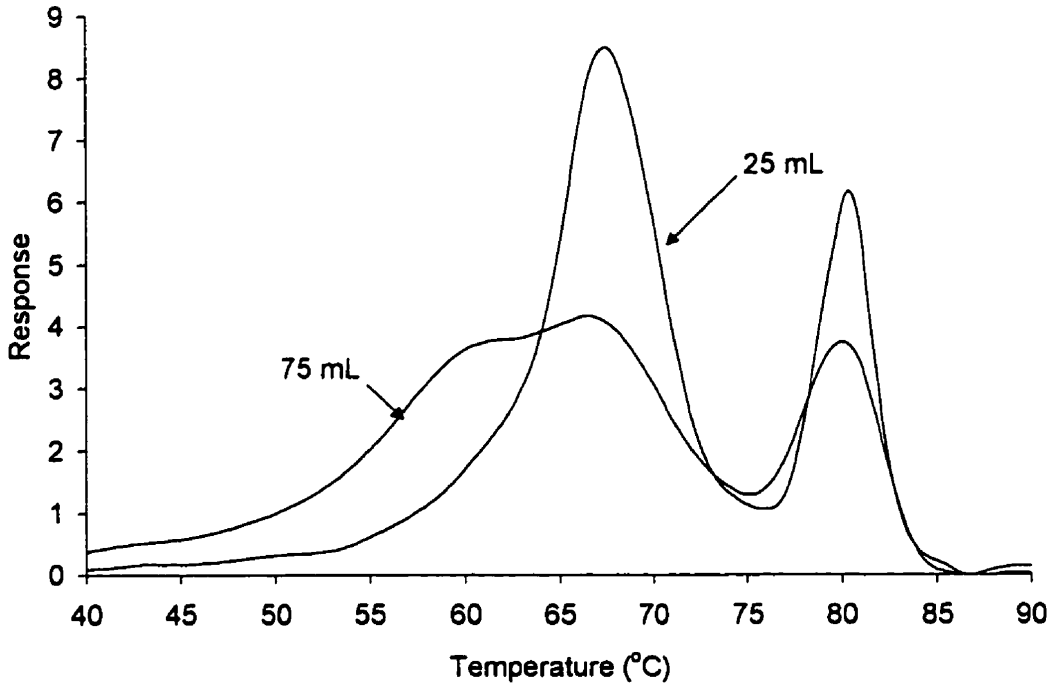

Figure 6.21 Effect of hydrogen concentration on CCD of poly(ethylene-co-1-hexene) produced with Cp_2HfCl_2, 40 °C, $P_{Ethylene}$ = 50 psi, 1-hexene = 2.5 mL

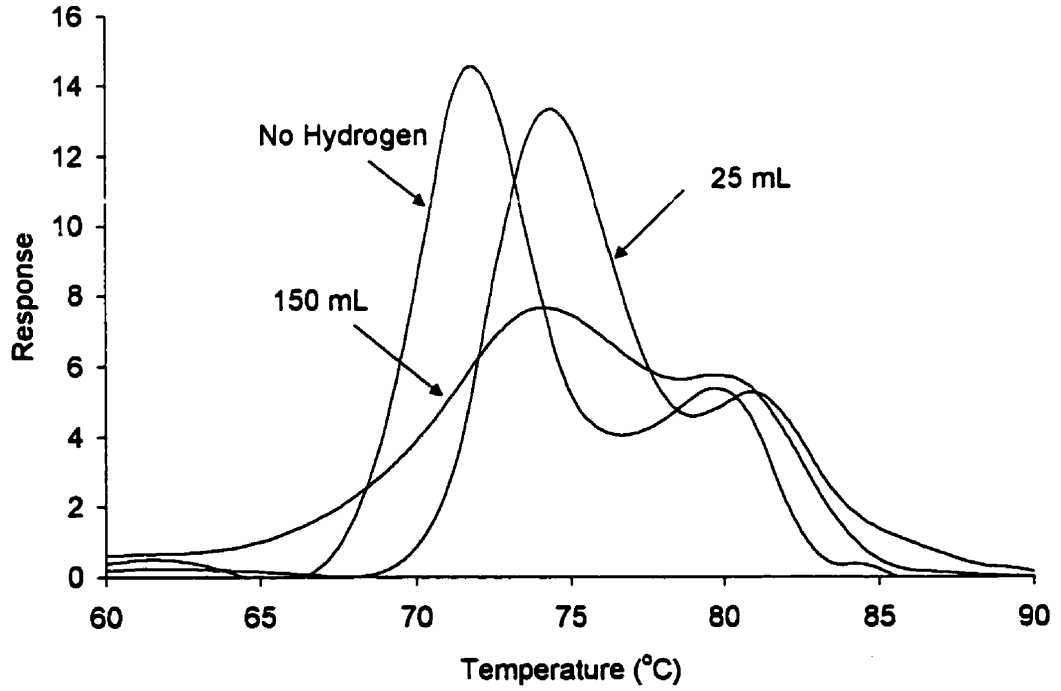

Figure 6.22 Effect of hydrogen concentration on CCD of poly(ethylene-co-1-hexene) produced with Cp_2HfCl_2, 50 °C, $P_{Ethylene}$ = 100 psi, 1-hexene = 5 mL

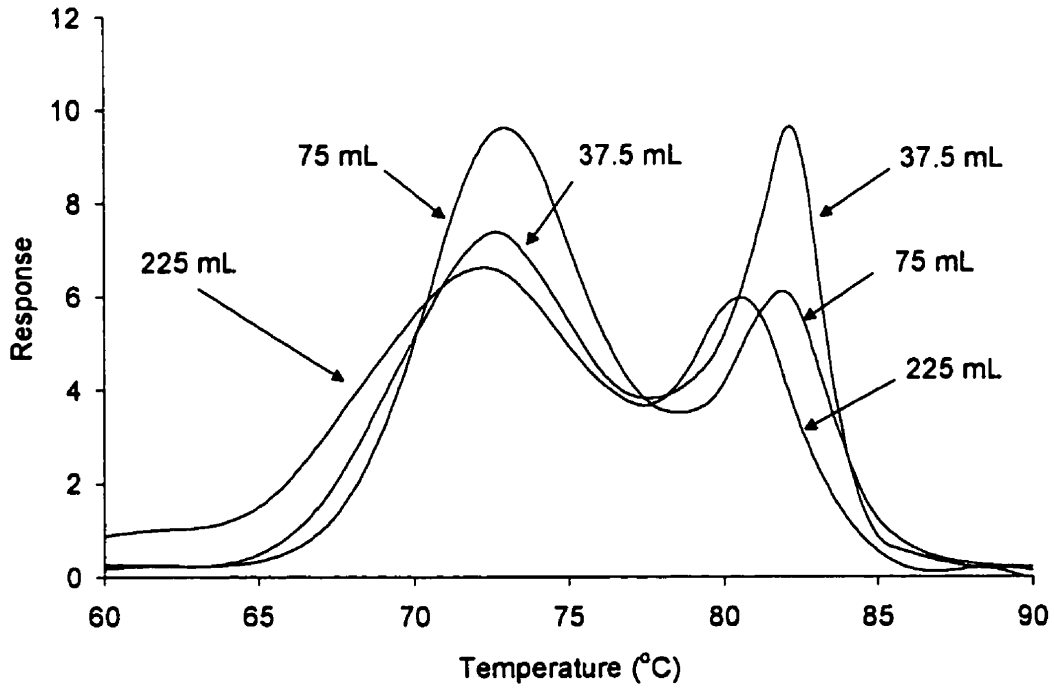

Figure 6.23 Effect of hydrogen concentration on CCD of poly(ethylene-co-1-hexene) produced with Cp_2HfCl_2, 40 °C, $P_{Ethylene}$ = 150 psi, 1-hexene = 7.5 mL

The effect of hydrogen on the CCD of copolymers produced with $Et[Ind]_2ZrCl_2$ is also of great interest. Fig. 6.24 shows CCD changes after injection of hydrogen for copolymers produced under ethylene pressures of 20 and 150 psi. In both cases, when hydrogen was used, the CCD peak appears at a significantly lower crystallinity temperature region and the distribution becomes broader. Although hydrogen does not significantly alter the molecular weights of copolymers produced with $Et[Ind]_2ZrCl_2$ as shown in Figs. 6.2 and 6.8, it appears that it enhances the ability of $Et[Ind]_2ZrCl_2$ to incorporate comonomer into the growing copolymer chains.

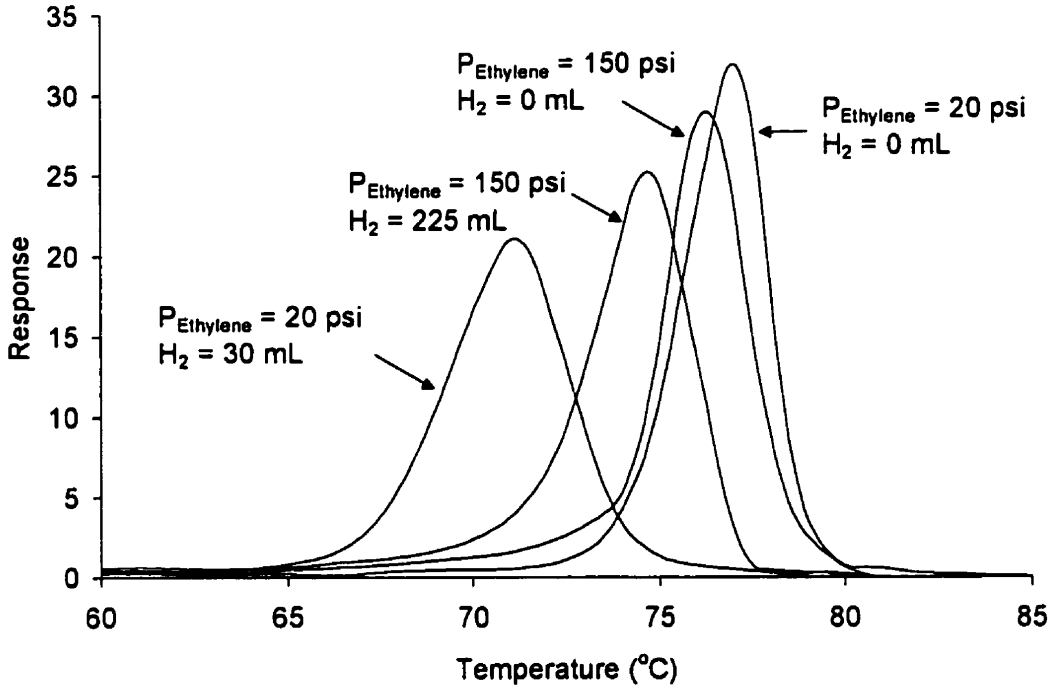

Figure 6.24 Effect of hydrogen concentration on CCD of poly(ethylene-co-1-hexene) produced with $Et[Ind]_2ZrCl_2$: 40 °C, 1-hexene = 1 and 7.5 mL for 20 and 150 psi, respectively

6.3. INFLUENCE OF POLYMER MICROSTRUCTURE ON ESCR

One of the main reasons for customizing CCD and MWD of polyolefins is to improve their physical properties such as environmental stress-crack resistance (ESCR). In this section, three industrial ethylene / 1-hexene copolymer samples with known ESCR were analyzed by CRYSTAF and GPC to shed light on the structure-property relationships and determine the range of chemical composition and molecular weight of copolymer chains, which will act as efficient tie-molecules. This information can be useful in designing copolymers with enhanced properties. The samples are named A, B, and C for confidentiality reasons and their ESCR values and molecular weights are listed in Table 6.1. Sample C was produced by reactor

cascade technology. One homopolymer sample was used as a reference for CCD measurements.

Table 6.1 Average properties of industrial poly(ethylene-co-1-hexene) samples

Sample	ESCR (hr)	M_w	PDI
Homopolymer	11	130,000	5.0
A	35	126,400	6.2
B	133	73,350	8.9
C	904	155,300	12.6

Fig. 6.25 reveals that sample C, which has extraordinarily high ESCR, has a high molecular weight tail and the broadest MWD. Samples A and B have similar MWDs except that the molecular weight of sample A is a little higher than that of sample B. However, the ESCR is almost 4 times higher for Sample B. Fig. 6.26 shows the CCD of each copolymer measured with CRYSTAF. All the samples are high density copolymers and have narrow CCDs. However, the CCDs do not show any distinct trend leading to a correlation with ESCR. In the case of CCD, the distributions of sample A and B are significantly different. Since a single set of MWD and CCD for each sample cannot lead to a distinct ESCR correlation, the samples were fractionated by preparative CRYSTAF (PolymerChar, Valencia, Spain) into four different fractions to be further analyzed.

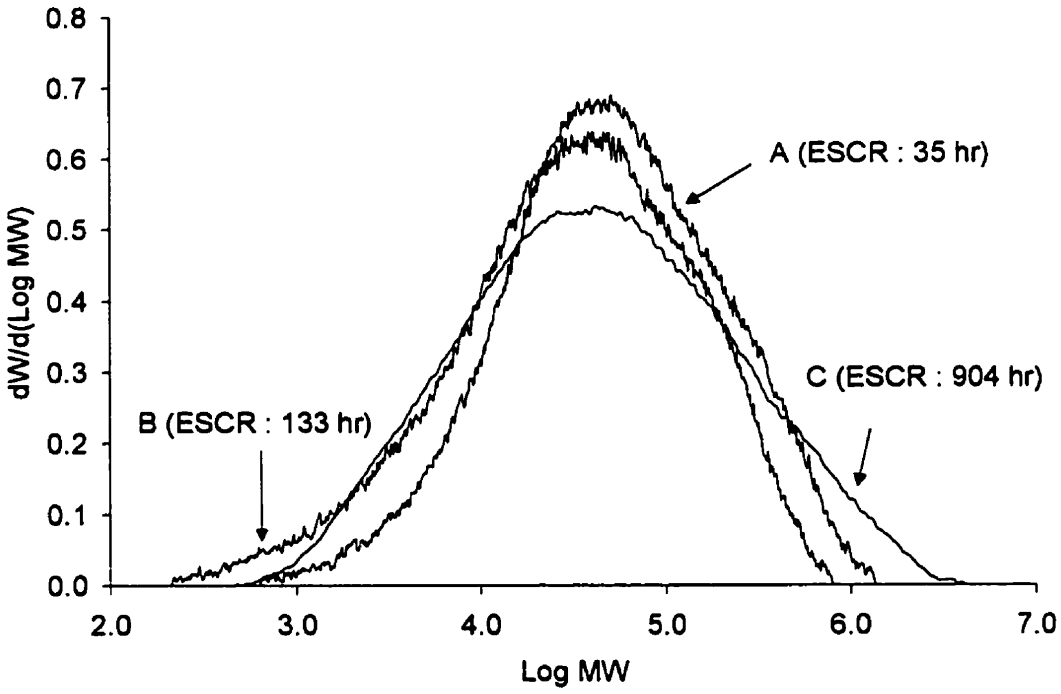

Figure 6.25 Overall MWD of each sample measured with GPC

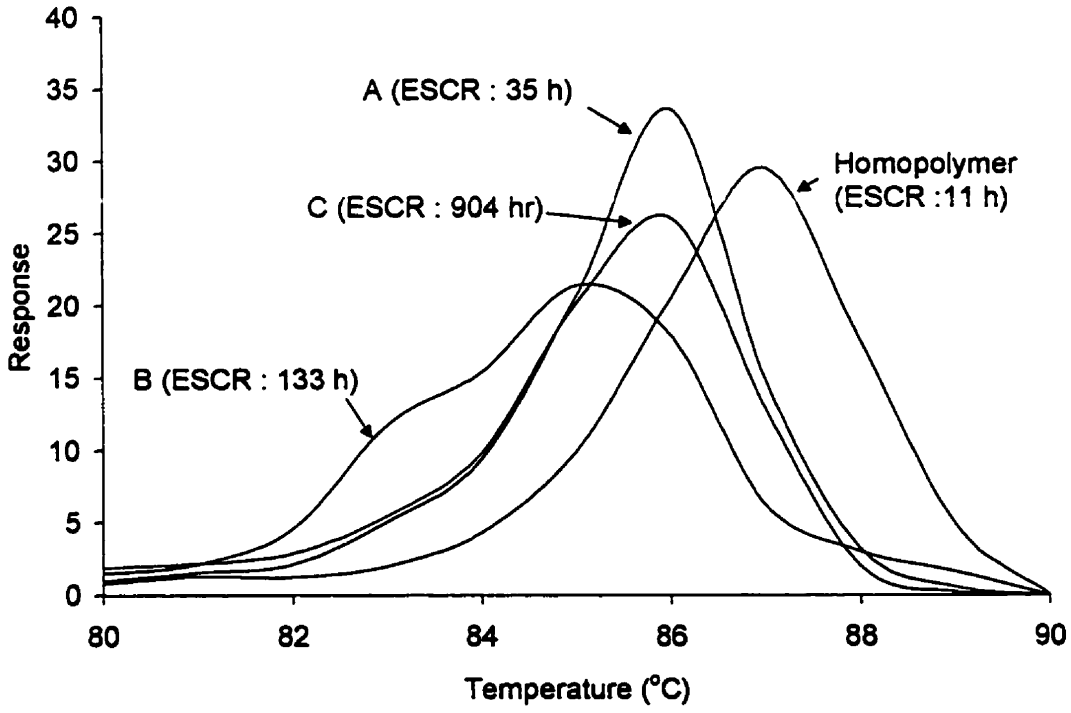

Figure 6.26 Overall CCD of each sample measured with CRYSTAF

The first fraction corresponds to polymers crystallizing in TCB below 75 °C. The second fraction was collected between 75 and 80 °C. The third fraction crystallized between 80 and 85 °C, and finally polymers crystallizing above 85 °C were collected as the fourth fraction.

Fig. 6.27 shows the ^{13}C-NMR results of each fraction for sample C. Fractions collected at lower crystallization temperatures have higher comonomer content and a variety of ethylene / 1-hexene sequences, which proves that the fractionation was properly performed based on comonomer content. Fraction 4 was almost pure homopolymer, and did not show any comonomer peaks in the ^{13}C NMR spectrum. Since we know that tie-molecules require some short chain branching, fraction 4 was not considered for further analysis. Peak assignments for ^{13}C-NMR analysis of ethylene/1-hexene copolymers are listed in Appendix E. The peak that at around 32 ppm in Fig. 6.27 corresponds to the saturated chain ends. The notation E and H represents ethylene and 1-hexene unit, respectively.

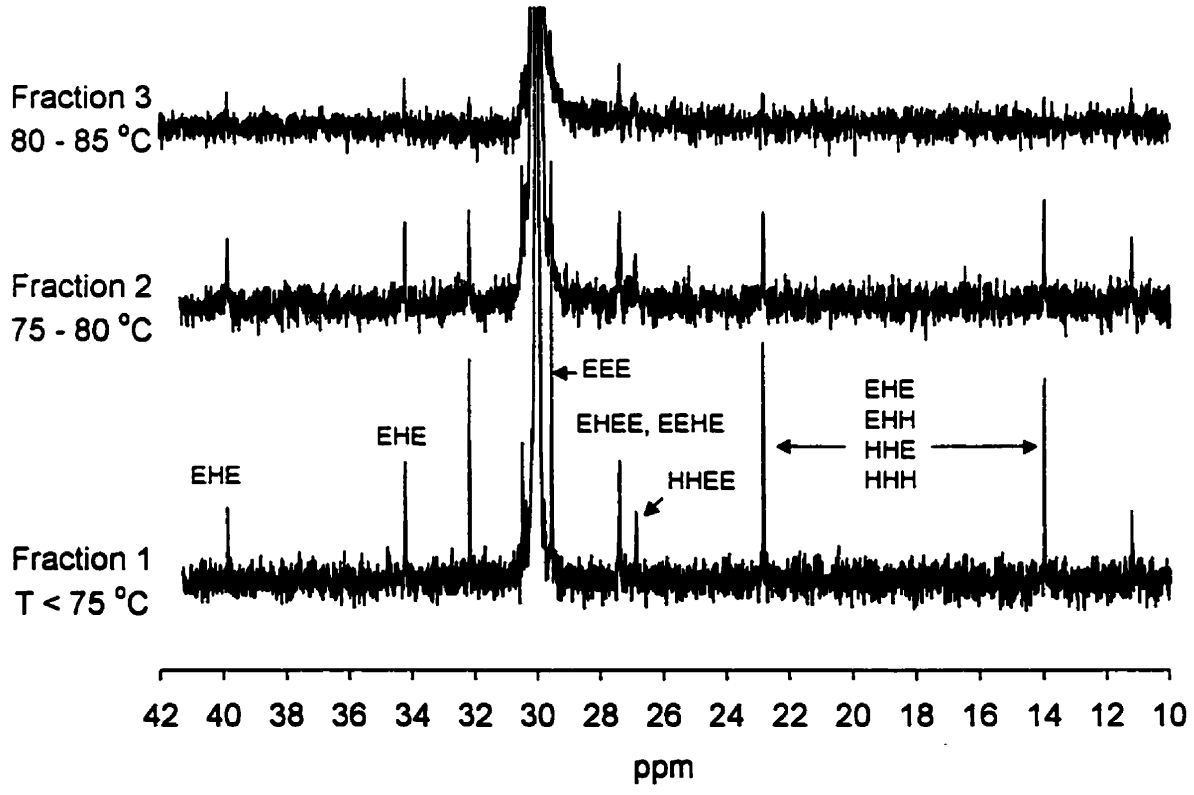

Figure 6.27 ^{13}C-NMR spectrum of fractions of sample C

Figs. 6.28 to 6.30 show the MWD of the fractions for each sample measured by GPC. For each sample, Fraction 1 has very low molecular weight except for sample C. For fraction 1, perhaps the comonomer content is too high to generate effective tie-molecules, since tie-molecules need to crystallize. Therefore, the first fractions were disregarded as possible candidates as tie-molecules. In Figs. 6.28 to 6.30, except for sample C, samples A and B show the typical chemical composition-molecular weight relation of copolymers produced with conventional Ziegler-Natta catalysts, i.e., more comonomers are concentrated in the lower molecular weight chains of the copolymer. On the other hand, the fractions of sample C have bimodal MWD with a high molecular weight component. Therefore, the higher molecular weight chains present in the fractions of sample C may act as better tie-molecules, which would explain its improved ESCR as compared to the other samples.

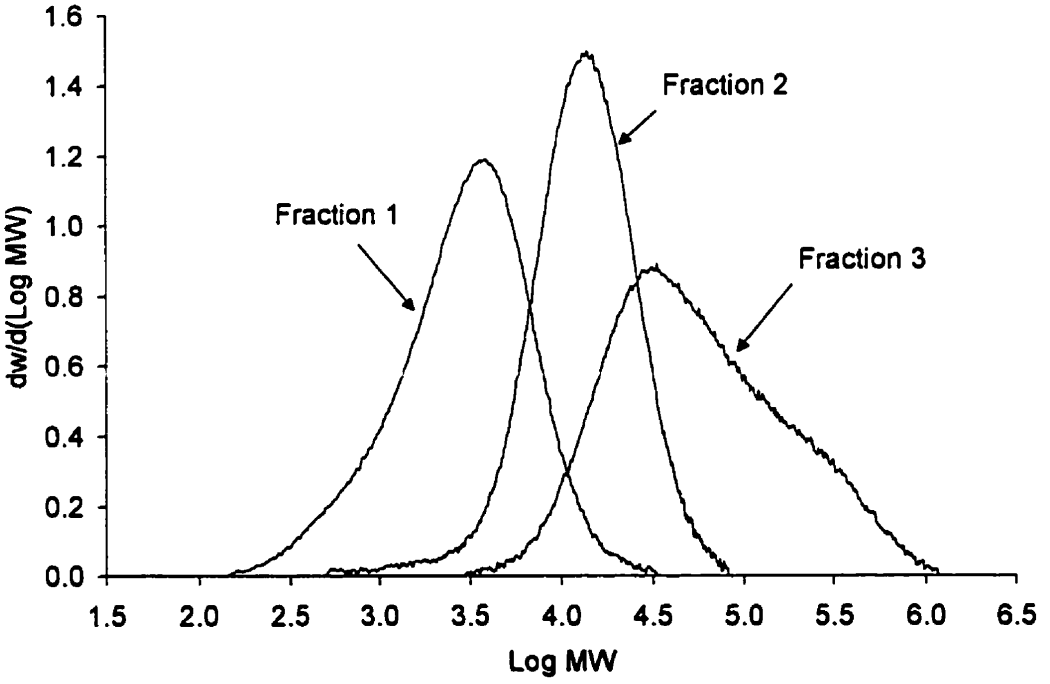

Figure 6.28 GPC measurements of CRYSTAF fractions from sample A

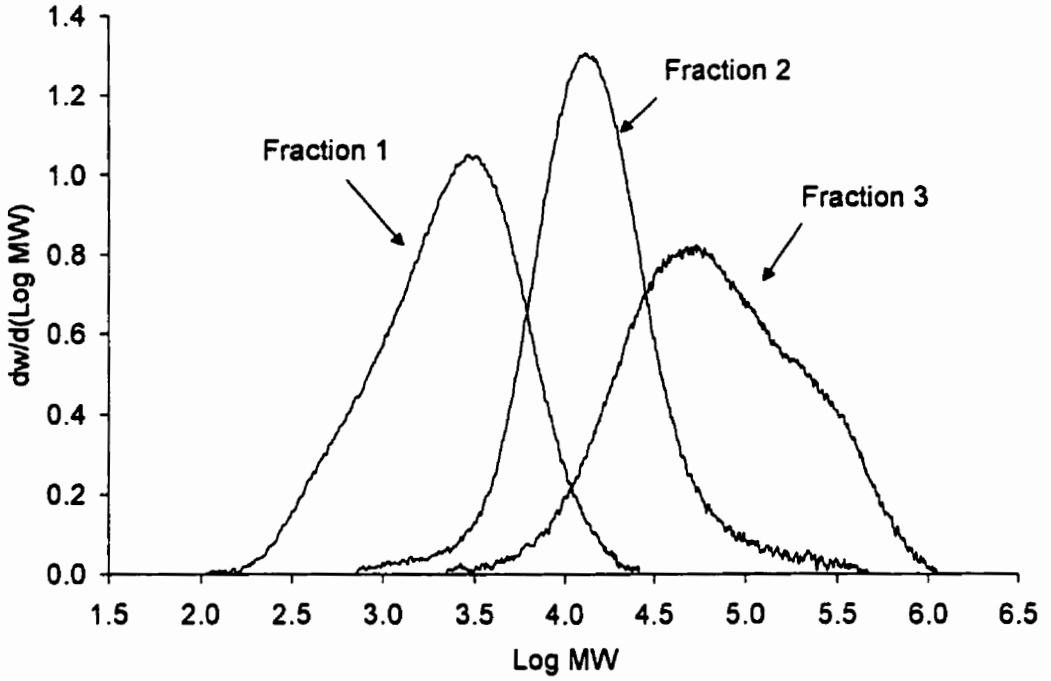

Figure 6.29 GPC measurements of CRSYTAF fractions from sample B

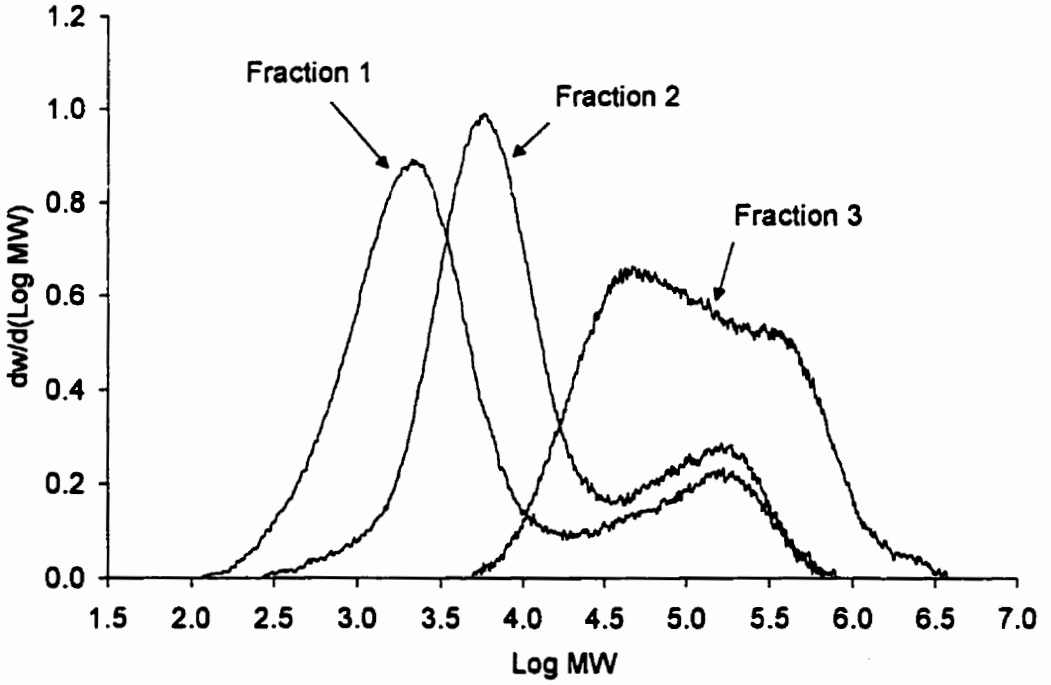

Figure 6.30 GPC measurements of CRSYTAF fractions from sample C

Figs. 6.31 and 6.32 compare the MWDs of fractions 2 and 3. One might assume that the longer copolymer chains would form better tie-molecules. Based on the unique ESCR performance of sample C, one might speculate that this would correspond to chains with Log MW > 4.75. The range of molecular weights that satisfies this constraint is indicated with a box in Figs. 6.31 and 6.32. As shown in Fig. 6.31, the weight fractions of copolymers in the shaded area increase significantly from sample A to C. Sample A, which has the lowest ESCR value, has the smallest fraction of copolymer chains in this region. Sample C, which has the highest ESCR value, has the largest fraction of copolymer chains in this region. It is interesting to note that there is still low molecular weight copolymers in the second fraction of sample C. Since sample C was produced with a reactor cascade technology, this peak is likely formed when unconverted comonomer from the first reactor was copolymerized in the second reactor in the presence of hydrogen.

Similar trends are observed for the fractions shown in Fig. 6.32.

Although the selection of crystallization temperatures and molecular weights is somewhat arbitrary, the correlation between MWD-CCD and tie-molecule concentration on ESCR values supports the results shown in this chapter, i.e., supported bimetallic catalysts can produce polymers having controlled MWD-CCD for maximizing ESCR in a single reactor.

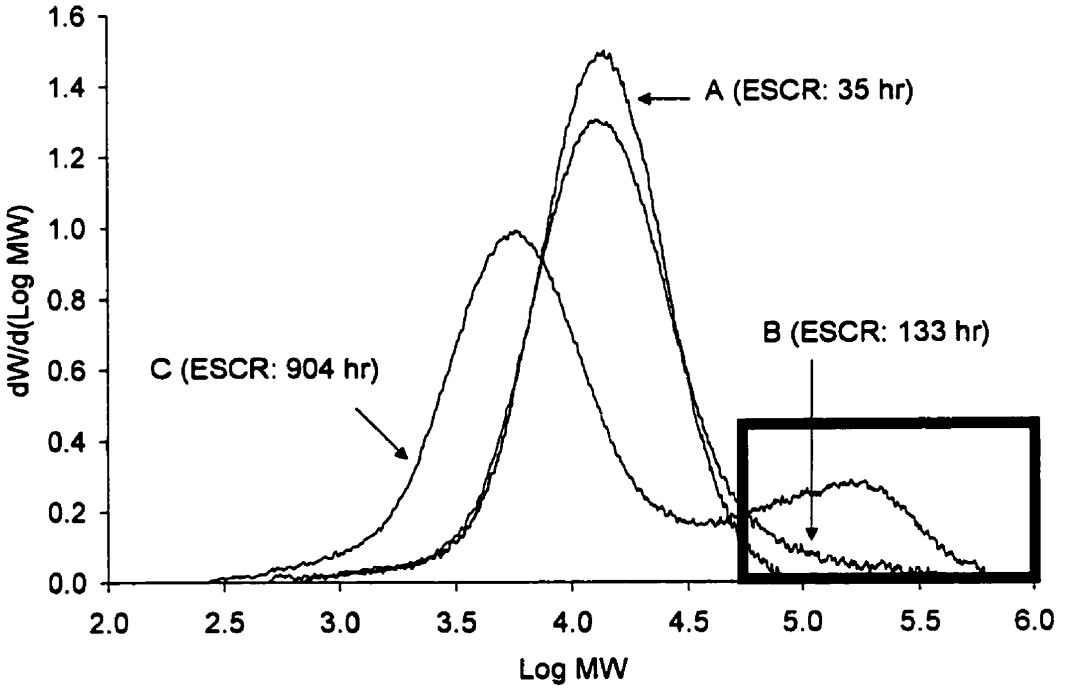

Figure 6.31 Comparison of MWD of the second fractions (75 - 80 °C)

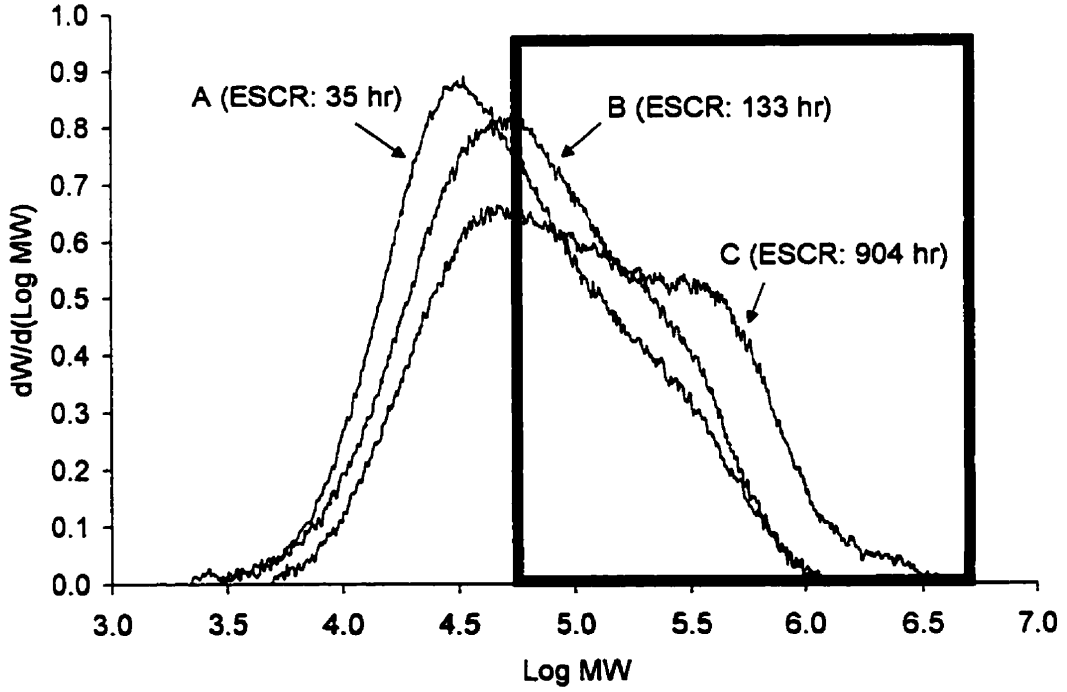

Figure 6.32 Comparison of MWD of the third fractions (80 - 85 °C)

6.4. MONTE-CARLO SIMULATION

If one can estimate approximate trends of chemical composition and molecular weight distributions of copolymers produced with combined catalysts based on the characteristics of individual catalysts at specific polymerization conditions, it will be easier to select catalysts and polymerization conditions to customize the microstructure of the product. As discussed previously, Flory's distribution can be used to generate instantaneous distributions of molecular weights. For comonomer composition distribution, Stockmayer's bivariate distribution can be used (Soares and Hamielec, 1995c).

In this section, a simple Monte-Carlo simulation was used to randomly generate copolymer chains with desired average chain length and average comonomer composition. Monte-Carlo simulation is based on random propagation of a process with given probability and can be quite time consuming. However, with the rapid progress in processing speed of computers, this approach can be used more easily. To get reasonable distributions of molecular weight and chemical composition, 200,000 copolymer chains were generated and each chain was analyzed for chain length, comonomer content, and maximum length of ethylene sequences in the chain.

Fig. 6.33 shows a three dimensional bivariate molecular weight and chemical composition distribution of ethylene/1-hexene copolymer generated by Monte-Carlo simulation, with the chain propagation probability of 0.9995 (i.e., M_n = 56,000) and average comonomer content of 2 %. The vertical height of the peak is determined by the weight fraction of the copolymer. Fig. 6.34 shows the contour map of the same distributions. From both plots it is clear that higher molecular weight chains have narrower CCDs. This is simply due to the statistical nature of copolymerization. The experimental confirmation of this phenomenon can be found in Fig. 6.24, where copolymers produced with hydrogen (lower molecular weight) have broader CCD than the ones produced without hydrogen.

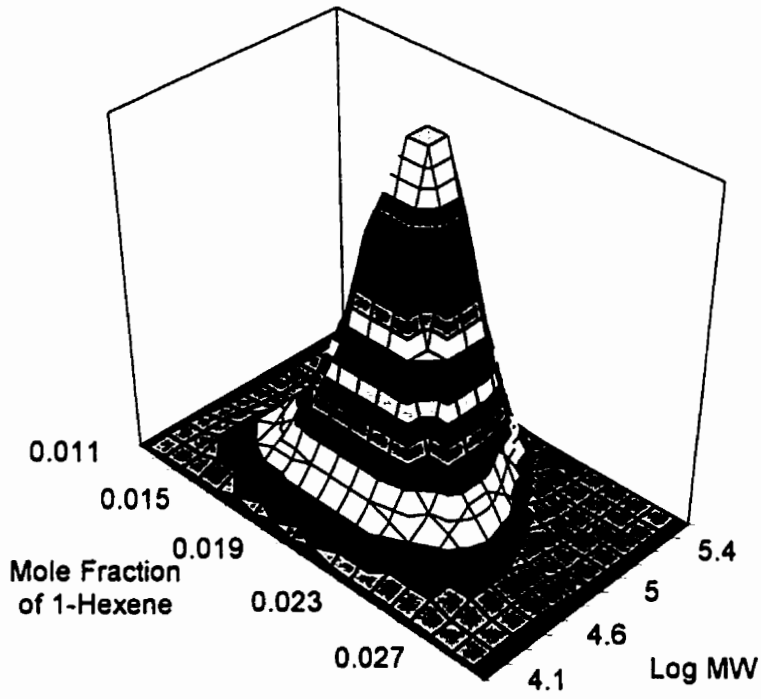

Figure 6.33 3D-view of the bivariate distribution of molecular weight and chemical composition obtained via Monte-Carlo simulation (probability of chain propagation = 0.9995, comonomer fraction = 0.02)

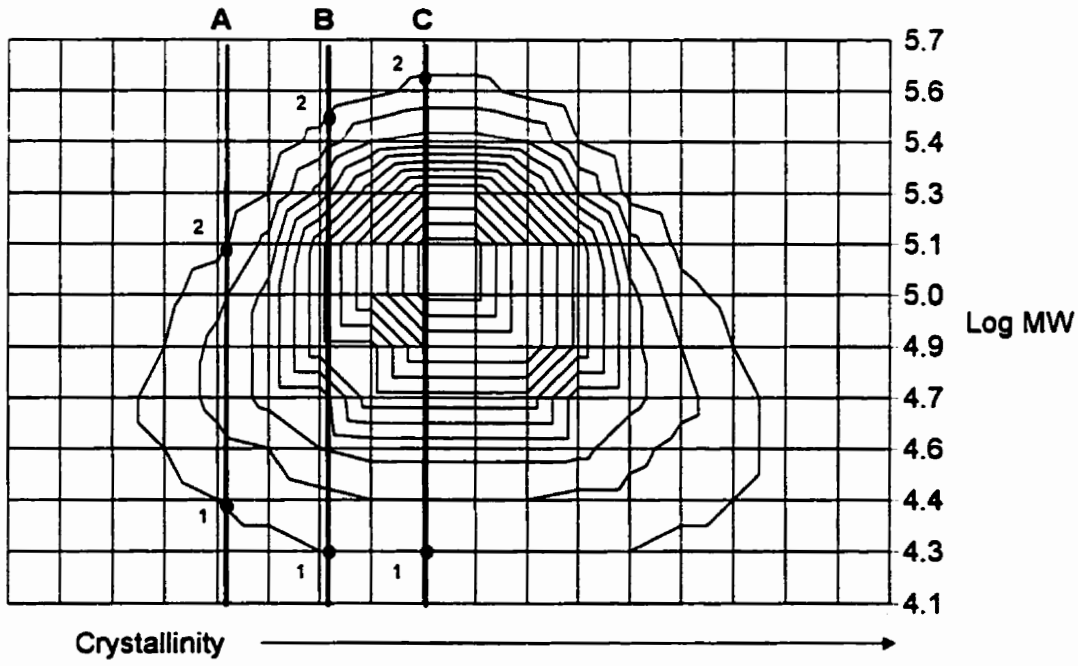

Figure 6.34 Contour map of the distributions shown in Fig. 6.33

In Fig. 6.34, since the direct conversion of comonomer content to crystallization temperature of copolymer is not available, the x-axis only indicates the direction of increasing crystallinity. For a detailed study of this relation, see Beigzadeh *et al.* (1998)

Figs. 6.35 and 6.36 show the side views of the distribution shown in Fig. 6.33 and they represent the overall CCD and overall MWD, respectively.

At this point it is clear that the Monte-Carlo simulation can illustrate these distributions clearly and the generated 200,000 chains are enough to provide meaningful results.

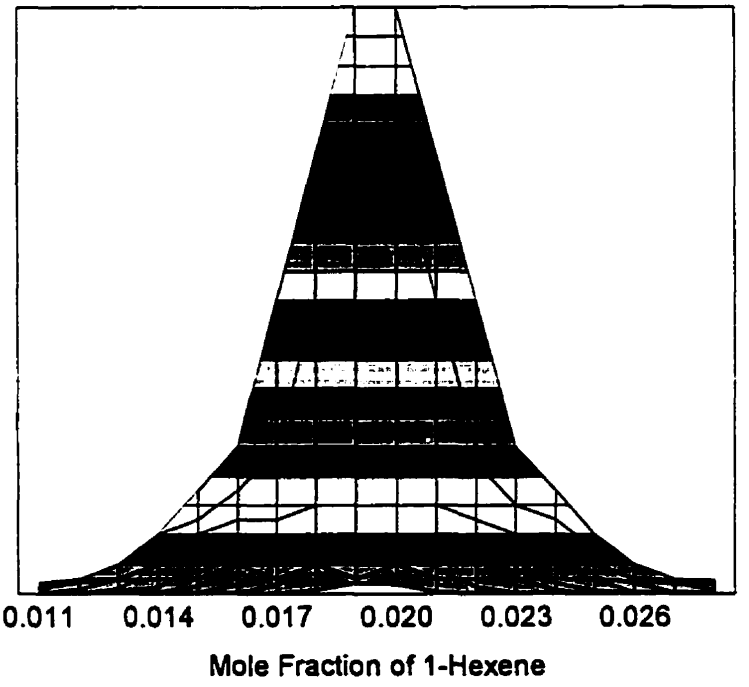

Figure 6.35 Side-view of Fig. 6.33 : CCD

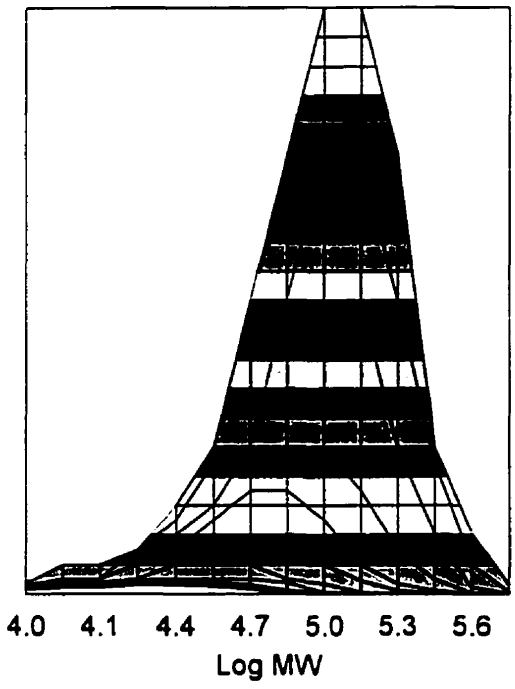

Figure 6.36 Side-view of Fig. 6.33 : MWD

Other piece of information analyzed for each chain is the maximum length of ethylene sequences per chain. When the comonomers are not equally distributed in the copolymer chains, the crystallinity of a copolymer chain will depend on the length of crystallizable sections and not on the total comonomer content in the chain. Fig. 6.37 shows three different copolymer chains with the same molecular weight and chemical composition. However, the maximum ethylene sequence length increases as A < B < C. Therefore, if the chains are analyzed by CRYSTAF, sample C will have the highest crystallization temperature and A the lowest.

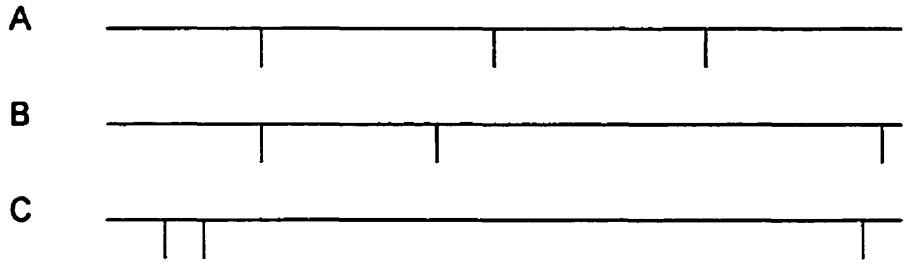

Figure 6.37 Copolymer chains with same molecular weight and comonomer content but different crystallinities

Fig. 6.38 shows the contour map of molecular weight vs. crystallinity of copolymer chains based on maximum ethylene sequence length from the same Monte-Carlo simulation results used in Figs. 6.33 and 6.34. If this copolymer was analyzed with CRYSTAF, this figure would provide more accurate representation than Fig. 6.34 that was based on the comonomer content in the chain. However, when copolymer chains are very long, the maximum sequence of ethylene is statistically dependent on comonomer content. Therefore, both approaches will produce similar results. On the other hand, as shown in Fig. 6.38, crystallinity and molecular weight are correlated when the molecular weights are low. If the copolymer is fractionated based on crystallinity as **A**, **B**, and **C** in Fig. 6.38, the MWD of the fractions (distribution between points 1 and 2) will be shifted toward higher molecular weight regions, and the molecular weights of points 1 and 2 will always increase. This trend was observed in our fractionated samples as shown in Figs. 6.28 to 6.30 (assuming that the catalysts used to produce the polymers have relatively uniform active site types). However, if the CCD measurement by CRYSTAF was based on the contour map shown in Fig. 6.34 and MWDs of different crystalline fractions (**A**, **B**, and **C**) were compared, the points 1 and 2 of fraction **C** will enclose the points in fraction **B** which has lower crystallinity. Similarly, the points 1 and 2 in fraction **B** will enclose the points 1 and 2 in fraction **A**. Therefore, MWDs of higher crystalline polymers would not always appear at higher molecular weight regions. Instead, the MWD of polymers with medium crystallinity will encircle the MWDs of polymers with low and high crystallinities.

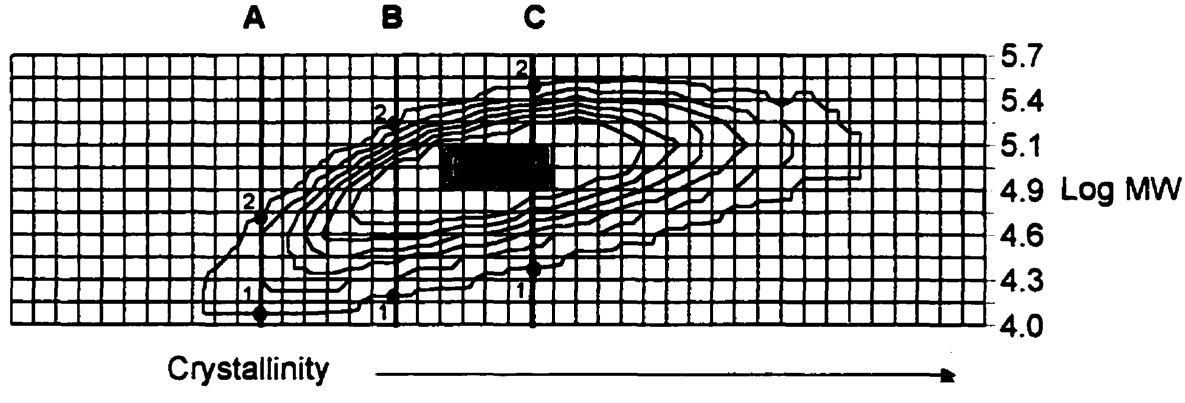

Figure 6.38 Contour map of sample in Fig. 6.33 based on maximum ethylene sequences per chain

Fig. 6.39 shows another contour map of a copolymer based on the maximum ethylene sequence. Compared to the previous case, the copolymer has the same average chain length but higher comonomer content. Compared to Fig. 6.38, the correlation between crystallinity and molecular weight became clearer even in higher molecular weight regions.

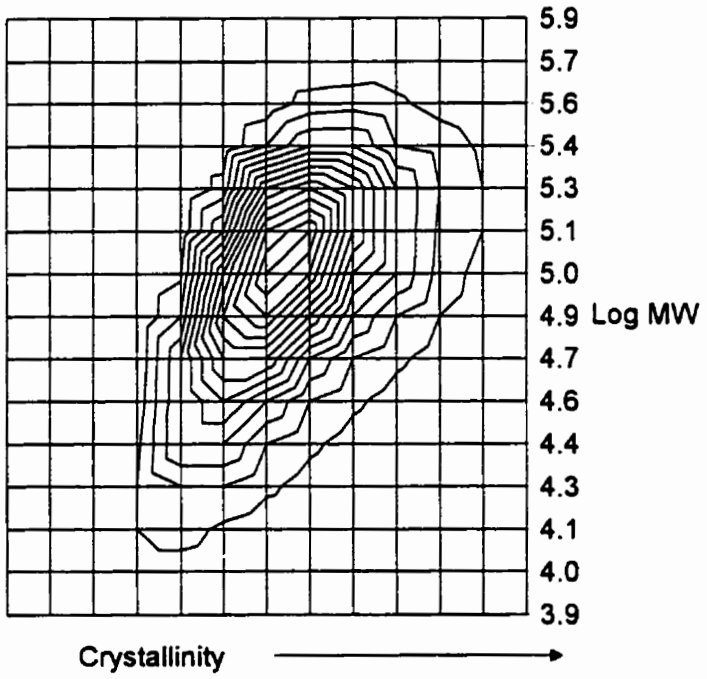

Figure 6.39 Contour map of copolymer chains generated by Monte-Carlo simulation based on maximum ethylene sequence (probability of chain propagation = 0.9995, comonomer fraction = 0.08)

However, when much longer copolymer chains are considered (M_n = 400,000), even if the average comonomer contents were to double, the correlation between crystallinity and molecular weight would become less significant as shown in Fig. 6.40.

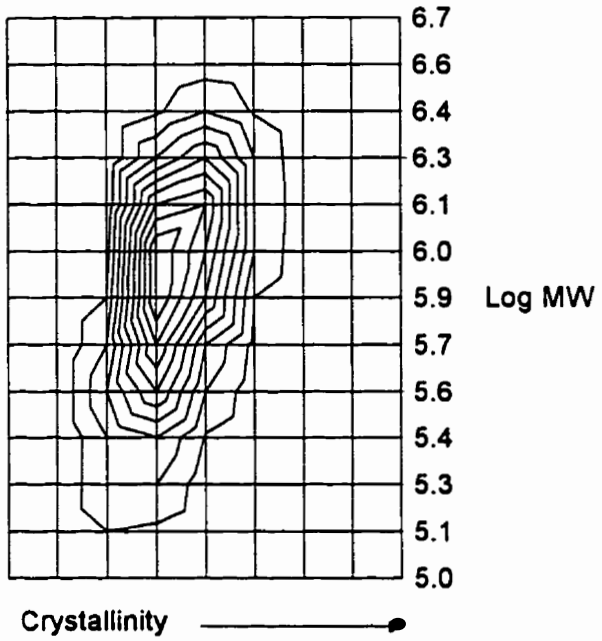

Figure 6.40 Contour map of copolymer chains generated by Monte-Carlo simulation based on maximum ethylene sequence (probability of chain propagation = 0.99993, comonomer fraction = 0.16)

The same type of simulation was conducted for copolymers made with mixed catalyst systems. Two sets of probabilities were used for the average chain lengths and comonomer contents for copolymers produced on each different catalyst site. Fig. 6.41 presents the simulation results for a copolymer produced with a combined catalyst. For the x-axis, the maximum ethylene sequence length was used instead of crystallinity or comonomer content. As can be seen in Figs. 6.41 and 6.42, when the ability of incorporating comonomer differs by two times, the CCD is clearly bimodal. However, in terms of molecular weight, this copolymer will still show a narrow unimodal distribution.

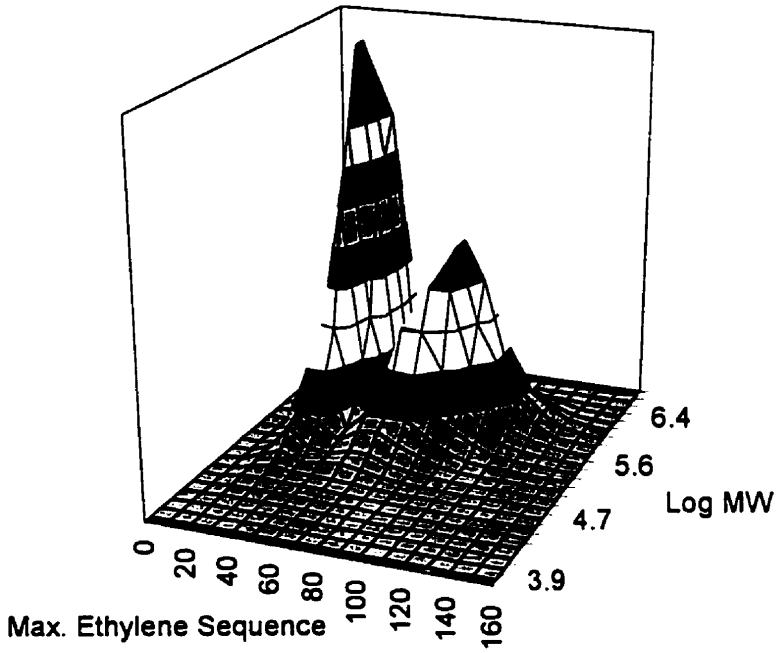

Figure 6.41 3D-view of Monte-Carlo simulation result for a combined catalyst : A (probability of chain propagation = 0.99993, comonomer fraction = 0.08), B (probability of chain propagation = 0.99993, comonomer fraction = 0.16), (A : B = 1 : 1, mole/mole)

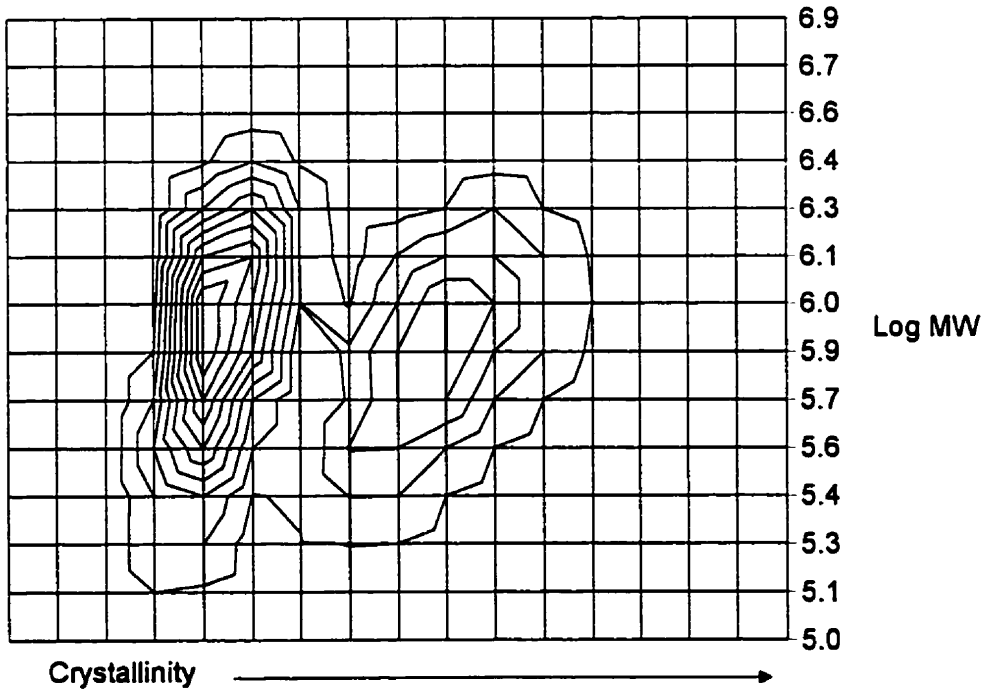

Figure 6.42 Contour map of sample in Fig. 6.41 based on maximum ethylene sequence length

Fig. 6.43 shows another simulation example of a copolymer produced with a combined catalyst. In this simulation, the molecular weight and comonomer content of polymer made on each site type are significantly different and adjusted in a way that the produced copolymers have the kind of distribution which favors formation of tie molecules. In Fig. 6.43, the higher molecular weight peak can generate the tie molecules, as long as the comonomer content is not too high, otherwise the ethylene sequences might not be long enough to crystallize efficiently.

Figs. 6.43 and 6.44 show that the maximum ethylene sequence of the peak that has the lower molecular weight average is strongly correlated with molecular weight. If CRYSTAF analysis was conducted for this sample, this bimodality might not be so obvious because the low molecular weight fraction of copolymer chains, having a lower comonomer content, would superimpose partially with the population made on the other catalyst site.

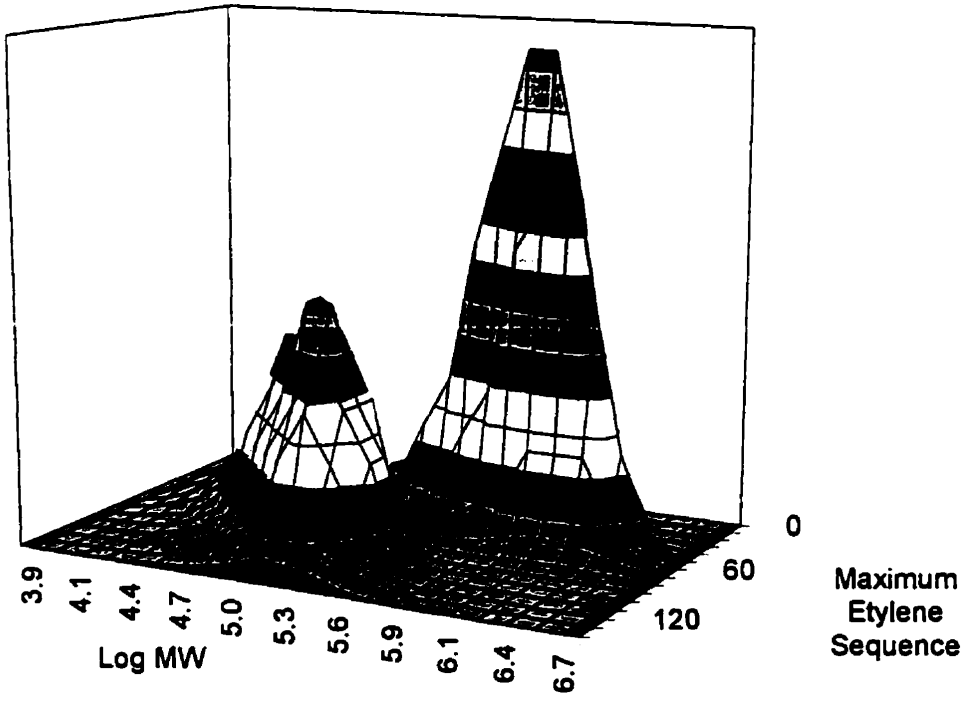

Figure 6.43 3D-view of Monte-Carlo simulation result for a combined catalyst : A (probability of chain propagation = 0.9995, comonomer fraction = 0.06), B (probability of chain propagation =0.99993, comonomer fraction = 0.16), (A : B = 10 : 1, mole/mole)

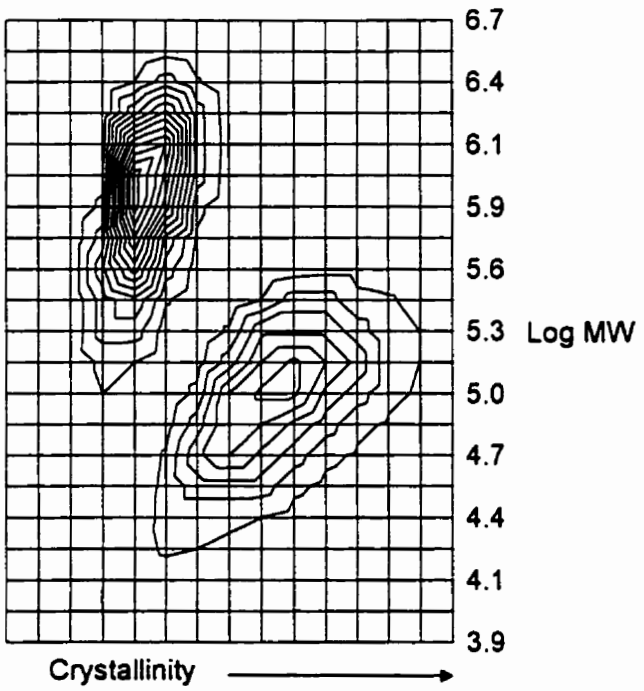

Figure 6.44 Contour map of sample in Fig. 6.43 based on maximum ethylene sequence length

6.5. CONCLUSION

MWD and CCD of ethylene and 1-hexene copolymers made with bimetallic supported metallocene catalysts can be efficiently controlled. The CCDs of copolymers produced with combined metallocenes follow similar trends as copolymers produced with individually supported catalyst.

Samples fractionated by preparative CRYSTAF showed that ESCR is related to the molecular weight of copolymer chains with intermediate crystallinity (tie molecules) as measured by solubility in TCB from 75 – 85 °C.

Monte-Carlo simulation can be used for the interpretation of copolymer microstructure and for modeling MWD-CCD cross fractionation analysis.

CHAPTER 7
MATHEMATICAL MODELING

Ziegler-Natta catalysts have been used most widely for olefin polymerizations because of their broad range of applications whether in homogeneous or heterogeneous forms. Heterogeneous Ziegler-Natta catalysts produce polymers with broad molecular weight and chemical composition distributions.

There have been numerous studies to investigate the cause of this broadening. Two main approaches were generally taken to explain the observed phenomena. One is the chemical kinetic approach and the other is the mass- and heat-transfer limitation approach. In the chemical kinetic approach, it is assumed that there are more than one distinctive type of catalyst active site producing polymer chains with different average chain properties. Therefore, the overall MWD is a superposition of individual MWDs for each site type and the polydispersity indexes are larger than the theoretical value of two for a single site catalyst.

In the mass- and heat-transfer approach, the broadening of the MWD is related to intraparticle and interparticle monomer concentration and temperature gradients caused by mass and heat transfer resistances during the polymerization. If there is any radial heterogeneity in monomer concentration or temperature across the growing polymer particle, the polymerization kinetics at each region would be different. Therefore the overall MWD will become broader compared to the case when there are no mass- or heat-transfer resistances.

In this chapter, MWD and CCD of polyolefins were represented with a modified multigrain model. The model considers multiple active site types, homo- and copolymerization, mass-transfer resistance between the catalyst surface and bulk slurry phase, and macro/microparticle diffusion effects. Depending on the radial positions of the growing polymer particle (macroparticle), different concentrations of monomer and thus different catalyst fragment (microparticle) growth rates will be observed. Temperature was assumed to be constant in the polymer particle, because estimated temperature gradients within polymer particles revealed to be insignificant.

The purpose of the simulations presented in this chapter is to determine the most probable factors causing the broadening of molecular weight and chemical composition distributions. Toward the end of this chapter, the effect of residence time distribution on MWD of polymers produced with bimetallic metallocenes is briefly examined.

7.1. POLYMERIZATION MODEL

To mathematically describe the sub-particle phenomena taking place in these polymerization systems, the physical particle formation and growth mechanisms needs to be defined first. In the Multigrain model, the original catalyst particles are fragmented at the very beginning of the polymerization and polymer grows around each fragment, thus forming an expanding polymer/catalyst particle.

7.1.1. Particle Fragmentation

Initially the catalyst particle is filled with inert gas, which is present in the glove box during catalyst preparation and storage. When the solid catalyst particles are introduced in the reaction medium, they will be filled with diluent first. As the monomer pressurization starts, the concentration of the monomer in the diluent will increase, and the monomer will diffuse to the catalyst particles. Depending on the pore structure and volume, monomer diffusion inside the particles will show different profiles. As the monomer reacts with catalyst, polymer chains will start growing and soon the solid catalyst particles will start to fragment.

Estenoz and Chiovetta (1996) modeled this initial fragmentation process based on polymer accumulation within the support-catalyzed polymer particle. According to them, the monomer will diffuse into the solid particles and reach the active sites via the access channels determined by the porous structure of the particles. These channels are the wider pores connected to the exterior bulk phase through a fluid continuum. Polymer is formed on the

active sites that are more easily available to the monomer (located on the walls of the access channels). Polymer accumulation in the narrowest zones of the pores creates obstructions to inward flow of monomer. This restriction hinders the diffusion of monomer towards less accessible active sites located on the surface of smaller and inner pores. As a consequence of this process, polymer accumulates mainly on the exterior surfaces of the particles and on the walls of the accessible pore channels. However, as polymerization continues, the produced polymer will generate hydraulic forces that cause the rupture of the catalyst particles, generating fragments that are kept together through polymer-chain linkages. The smaller pores in the interior of the fragments will soon be filled with polymer generating tensions that will lead to further fragmentation as shown Fig. 7.1. One important result of the catalyst fragmentation is that it allows previously blocked pores to become accessible to monomer and thus available for polymerization. The surfaces of these fragments contain active catalyst sites, and polymer will be produced around these fragmented microparticles. However, as polymerization continues, mass transfer resistances in the microparticle might become increasingly significant and, as a result, monomer concentration gradients might occur. Therefore, across the growing polymer particle (macroparticle) different polymerization rates, different average molecular weights, and different microparticle sizes might be expected.

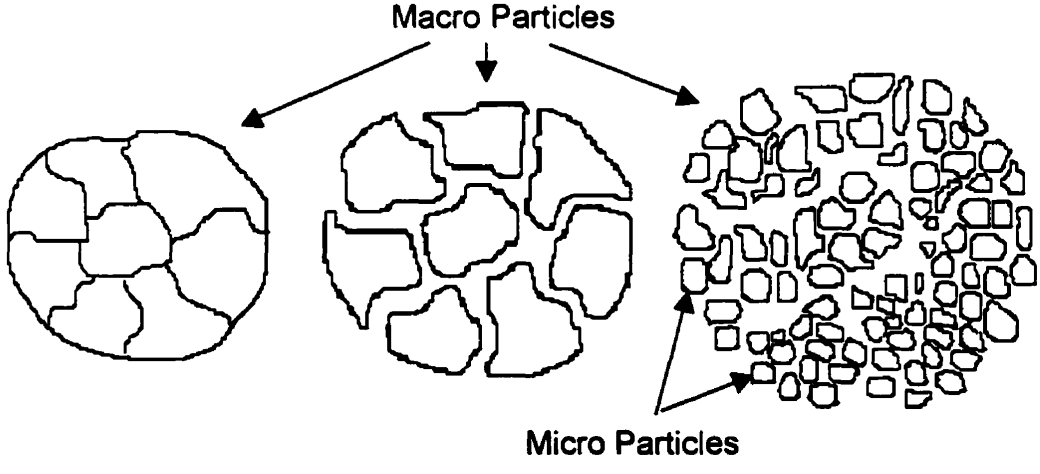

Figure 7.1 Schematic representation of fragmentation process during polymerization with heterogeneous Ziegler-Natta catalysts

The fragmented particles (microparticles) will grow at different rates depending on monomer concentration at their radial location. Initially, the microparticles located in the outer regions of the macroparticle will grow faster due to the monomer concentration gradient shown in Fig.7.2. However, after sufficient polymerization time, the monomer concentration gradient in the macroparticles becomes smaller. Then, the inner microparticles start to grow faster than the outer microparticles, because the inner microparticles have thinner polymer layers around the solid core, thus less monomer diffusion resistances. Therefore, after a certain polymerization time, the microparticle sizes at different radial positions will become similar and the microstructure of the polymer chains within the microparticles will not vary significantly as a function of radial position in the macroparticle.

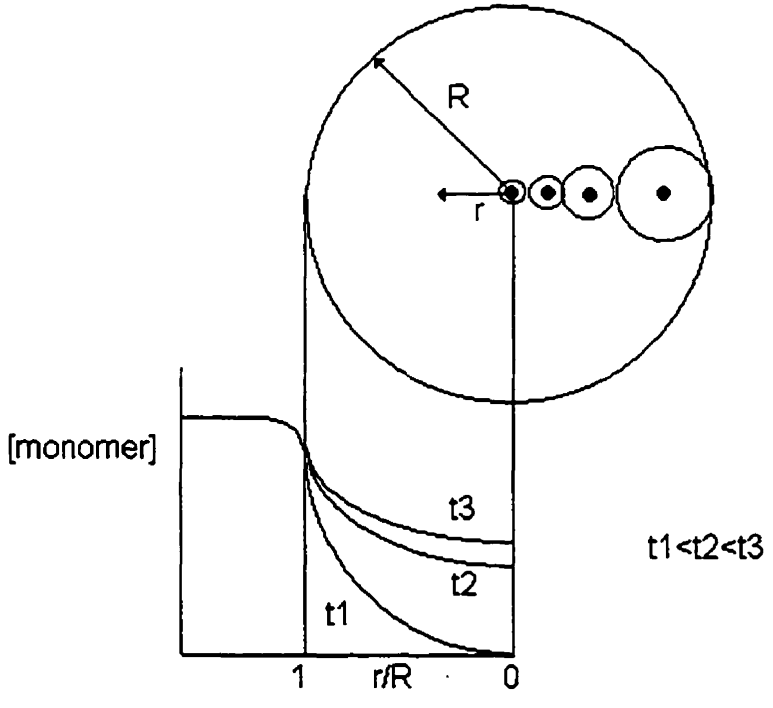

Figure 7.2 Schematic representation of multigrain model, macroparticle and microparticles

7.2. MODEL DEVELOPMENT

In this chapter, a model was developed by dividing the Multigrain model into three different regions where distinct mechanisms are involved.

The first region is the surface of the solid core in the growing microparticle, where the actual polymerization takes place. Calculations of polymerization kinetics are only done in this level. The assumptions involved in the first level are:

(1) The active catalyst sites exists only on the surface of the fragments.

(2) The solid core does not go through any further fragmentation.

(3) Produced polymer has long chains; thus the long chain approximations are valid.

(4) There are no binary interactions between two adjacent catalyst active sites.

(5) At time zero, all catalyst sites are activated (No cocatalyst effect was considered).

The solid catalyst core will be covered by polymer layers, forming the microparticle, and as polymerization continues the polymer layer will grow thicker. Because of mass transfer limitation of monomers through this polymer layer, the concentration of monomer at the surface of the solid core might become diffusion limited.

The second region models mass transfer across the growing microparticle to estimate the difference in monomer concentration between the surface of the solid core and outer boundary of microparticles. The governing diffusion coefficient within the microparticle is defined as D_S.

Finally, the third region is the growing macroparticle, which consists of a network of growing microparticles. In this level, the mass transfer between polymerization medium and polymer particle is considered in addition to its internal monomer concentration gradients. The monomer concentration gradient across the macroparticles is caused both by diffusion, with its diffusion coefficient D_L, and by different monomer consumption rates across the macroparticle during polymerization. The monomer consumption at each radial position is governed by the polymerization in the microparticles. Each level deals with different phenomena, therefore, different mathematical descriptions and numerical methods are used.

7.2.1. Level 1: Polymerization Kinetics

A copolymerization model is used to describe the mechanism in level 1. The steps involved in the kinetics of olefin polymerization are initiation, propagation, spontaneous chain transfer (β hydride elimination), and deactivation. For binary copolymerization, two different types of monomers and also polymer chains are considered according to the terminal model for copolymerization.

The basic homopolymerization kinetics steps with appropriate kinetic parameters are as follows :

Site Formation	:	C	+	*Cocatalyst*	⟶	C^*			
Initiation (k_i)	:	C^*	+	M	⟶	P_1			
Propagation (k_p)	:	P_r	+	M	⟶	P_{r+1}			
Spontaneous Chain Transfer (k_t)	:	P_r			⟶	C^*	+	D_r	
Deactivation (k_d)	:	P_r			⟶	C_d	+	D_r	
	:	C^*			⟶	C_d			

where,

C^*	:	active site
M	:	monomer
P_r	:	living polymer of chain length r
D_r	:	dead polymer of chain length r
C_d	:	deactivated active center

Initiation reaction takes place between an active catalyst site and a monomer, producing polymer of chain length 1. This chain will further react with monomers and grow by propagation reaction. The transfer reaction will terminate the chain growth producing a dead polymer chain and the original active catalyst site. For each chemical species, first order ordinary differential equations need to be solved.

The population balances for each chemical species are as follows :

Polymer of chain length 1 :

$$\frac{dP_1^i}{dt} = k_t^i C_\bullet^i M - k_p^i P_1^i M - (k_t^i + k_d^i) P_1^i \tag{7.1}$$

Number of active catalytic sites :

$$\frac{dC_\bullet^i}{dt} = k_t^i Y_0^i - (k_t^i M + k_d^i) C_\bullet^i \tag{7.2}$$

Moments of living polymer chains :

$$\frac{dY_0^i}{dt} = k_t^i C_\bullet^i M - (k_t^i + k_d^i) Y_0^i \tag{7.3}$$

$$\frac{dY_1^i}{dt} = k_t^i C_\bullet^i M - (k_t^i + k_d^i) Y_1^i + k_p^i M Y_0^i \tag{7.4}$$

$$\frac{dY_2^i}{dt} = k_t^i C_\bullet^i M - (k_t^i + k_d^i) Y_2^i + k_p^i M (2Y_1^i + Y_0^i) \tag{7.5}$$

Moments of dead polymer chains :

$$\frac{dX_0^i}{dt} = (k_t^i + k_d^i)(Y_0^i - P_1^i) \tag{7.6}$$

$$\frac{dX_1^i}{dt} = (k_t^i + k_d^i)(Y_1^i - P_1^i) \tag{7.7}$$

$$\frac{dX_2^i}{dt} = (k_t^i + k_d^i)(Y_2^i - P_1^i) \tag{7.8}$$

The cumulative molecular weights per site type can be calculated by :

$$M_n^i = m \frac{X_1^i + Y_1^i}{X_0^i + Y_0^i} \tag{7.9}$$

$$M_w^i = m \frac{X_2^i + Y_2^i}{X_1^i + Y_1^i} \tag{7.10}$$

where, m is the molecular weight of the monomer. The total cumulative molecular weight can be calculated by using the weight fractions of polymer produced on active site i, w_i.

$$w_i = \frac{Y_1^i}{\sum_{k=1}^{N} Y_1^k} \tag{7.11}$$

Using these weight fractions, the number average and weight average molecular weight can be expressed as :

$$M_n = \frac{1}{\sum_{k=1}^{N} \frac{w_k}{M_n^k}} \tag{7.12}$$

$$M_w = \sum_{k=1}^{N} w_k M_w^k \tag{7.13}$$

The polydispersity index is defined as :

$$\frac{M_w}{M_n} \tag{7.14}$$

For copolymers, pseudo kinetic constants (Hamielec and McGregor, 1983) can be defined for each catalytic site type to simplify the model as :

$$k_t = k_{t,A} f_A + k_{t,B} f_B \tag{7.15}$$

$$k_p = k_{p,AA}\Phi_A f_A + k_{p,AB}\Phi_A f_B + k_{p,BA}\Phi_B f_A + k_{p,BB}\Phi_B f_B \tag{7.16}$$

$$k_t = k_{t,A}\Phi_A + k_{t,B}\Phi_B \tag{7.17}$$

$$k_d = k_{d,A}\Phi_A + k_{d,B}\Phi_B \tag{7.18}$$

Using the pseudo kinetic constants, the concentration of each monomer bound to the polymer chain and the cumulative molecular weights can be expressed as :

$$\frac{dB_A}{dt} = k_{t,A} C_\bullet [A] + (k_{p,AA}\Phi_A + k_{p,BA}\Phi_B) Y_0 [A] \tag{7.19}$$

$$\frac{dB_B}{dt} = k_{t,B} C_\bullet [B] + (k_{p,BB}\Phi_B + k_{p,AB}\Phi_A) Y_0 [B] \tag{7.20}$$

$$M_n = (F_A m_A + F_B m_B) \frac{X_1 + Y_1}{X_0 + Y_0} \tag{7.21}$$

$$M_w = (F_A m_A + F_B m_B) \frac{X_2 + Y_2}{X_1 + Y_1} \tag{7.22}$$

where,

$$F_A = \frac{B_A}{B_A + B_B}, (F_B = 1 - F_A) \tag{7.23}$$

$$f_A = \frac{[A]}{[A]+[B]}, (f_B = 1 - f_A) \tag{7.24}$$

$$\Phi_A = \frac{k_{p,BA} f_A}{k_{p,AB} f_B + k_{p,BA} f_A}, (\Phi_B = 1 - \Phi_A) \tag{7.25}$$

7.2.2. Level 2: Microparticle

From the result of the level 1 modeling, the microparticle growth rate and radius can be estimated by simple mass and density relationships based on produced polymer at the surface of the solid catalyst core. In level 2 modeling, the concentration of monomer at the surface of the solid core is estimated, which in turn will be used with level 1 model to calculate chain growth. The monomer concentration at the catalyst surface depends on diffusivity of the polymer produced and which is expressed as :

$$\varepsilon_s \frac{\partial M}{\partial t} = \frac{1}{r^2} \frac{\partial}{\partial r} \left(D_S r^2 \frac{\partial M}{\partial r} \right) \quad , r_c \le r \le r_s \tag{7.26}$$

where, $M(r,t)$ is the monomer concentration in the microparticle, D_S diffusivity in the microparticles, r_c is the radius of solid core, r_s is the microparticle radius, and ε_s is the porosity of the microparticle.

The boundary and initial conditions are given by

$$r = r_c \quad : \quad 4\pi r_c^2 D_S \frac{\partial M}{\partial r} = \frac{4}{3} \pi r_c^3 R_{cs} \tag{7.27}$$

$$r = r_s \quad : \quad M = M_{eq} \quad , M_{eq}(M_l) \le M_l \tag{7.28}$$

$$t = 0 \quad : \quad M = M_{s0} \tag{7.29}$$

where, R_{cs} is the rate of polymerization at the catalyst particle surface expressed as :

$$R_{cs} = \sum_{i=1}^{N} k_p' C_*' M_c = k_p C_* M_c \tag{7.30}$$

The summation accounts for N types of active sites. M_c is the monomer concentration at the catalyst surface, which can be solved analytically under quasi steady-state assumption by substitution of the boundary conditions as follows :

$$M_c = \frac{M_{eq}(M_l)}{1 + \frac{k_p C_*}{3D_s} r_c^2 \frac{R_s - r_c}{R_s}} \tag{7.31}$$

In the same way the temperature profile can be expressed as :

$$\frac{dT}{dt} = \frac{k_e}{\rho_p C_p}\left(\frac{2}{r}\frac{\partial T}{\partial r} + \frac{\partial^2 T}{\partial r^2}\right) \tag{7.32}$$

Temperature profile can also be reduced to an analytic form using boundary conditions as :

$$T_{Cat} = T_{Macro} + \frac{\beta \frac{\alpha^2}{3}\left(\frac{\lambda - 1}{\lambda}\right)}{1 + \frac{\alpha^2}{3}\left(\frac{\lambda - 1}{\lambda}\right)} M_{Macro} \tag{7.33}$$

where,

$$\alpha = r_{cat}\sqrt{\frac{k_p C_*}{D'_{M_i}}} \tag{7.34}$$

$$\beta = \frac{(-\Delta H_p) D'_{M_i}}{k_e} \tag{7.35}$$

$$\lambda = \frac{r_{micro}}{r_{cat}} \tag{7.36}$$

7.2.3. Level 3: Macroparticle

In level 3, there are two different mechanisms involved that cause concentration gradients across the macroparticle: diffusion and monomer consumption by polymerization. To accommodate both, the growing macroparticle is divided into several regions (20 in this work) across the radial direction, forming shells with different thickness as shown in Fig.7.3.

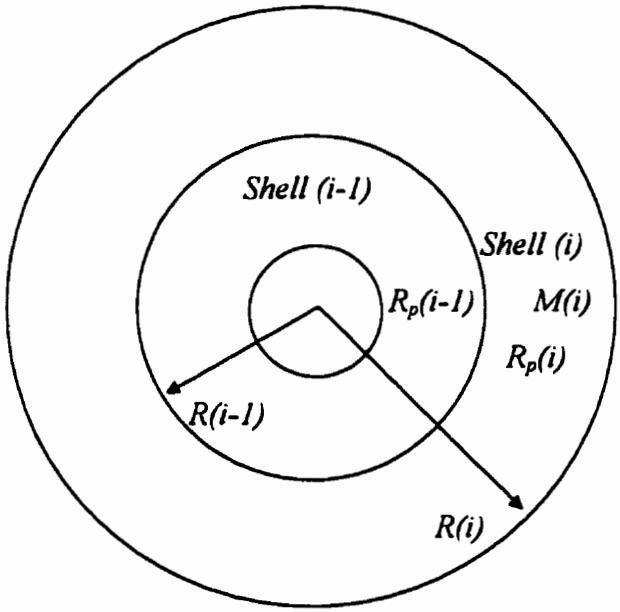

Figure 7.3 Schematic representation of macroparticle and its computational shells

The governing equation for the diffusion of monomer in the macroparticle is :

$$\varepsilon_l \frac{\partial M_l}{\partial t} = \frac{1}{r_l^2}\frac{\partial}{\partial r_l}\left(D_l r_l^2 \frac{\partial M_l}{\partial r_l}\right) - R_v \tag{7.37}$$

where ε_l is the porosity of the large macroparticle, $M_l(r_l,t)$ is the monomer concentration in the pores of the macroparticle, D_l is the pseudobinary macro-diffusion coefficient, and R_v is the reaction rate term. The polymerization rate is the total rate of consumption of monomer in an infinitesimal spherical shell at a given radius of the macroparticle.

The boundary and initial conditions are :

$$r_l = 0 \quad : \quad \frac{\partial M_l}{\partial r_l} = 0 \tag{7.38}$$

$$r_l = R_l \quad : \quad D_l \frac{\partial M_l}{\partial r_l} = k_s (M_b - M_l) \tag{7.39}$$

$$r_l = R_l \quad : \quad M_l = M_s \tag{7.40}$$

$$t = 0 \quad : \quad M_l = M_{l0} \tag{7.41}$$

Temperature profile across the macroparticle can be expressed as :

$$\frac{\partial T}{\partial t} = \frac{k_e}{\rho_p C_p}\left(\frac{2}{r}\frac{\partial T}{\partial r} + \frac{\partial^2 T}{\partial r^2}\right) - Q_p \tag{7.42}$$

The overall simulation procedure is described in the flow chart in Appendix F.

As was shown, level 1 model requires solving first order ordinary differential equations (ODE) and level 2 and 3 requires solving moving boundary partial differential equations (PDE). For ODE's, the LSODAR[†] subroutine was used and for the moving boundary PDE problem, a three point Lagrange interpolation method was used (Crank, 1990). In this technique, the partial differential equations can be expressed simply as:

$$f(x) = l_1(x) f(a_1) + l_2(x) f(a_2) + l_3(x) f(a_3) \tag{7.43}$$

where,

$$l_{i(x)} = \frac{p(x)}{(x - a_i) p'(a_i)} \tag{7.44}$$

$$p(x) = (x-a_0)(x-a_1)(x-a_2) \tag{7.45}$$

and $p'(a_i)$ is the derivative of $p(x)$ with respect to x, at $x = a_i$. Therefore, the second derivative and the first derivative of the function can be expressed as :

$$\frac{1}{2}\frac{d^2 f(x)}{dx^2} = \frac{f(a_0)}{(a_0 - a_1)(a_0 - a_2)} + \frac{f(a_1)}{(a_1 - a_0)(a_1 - a_2)} + \frac{f(a_2)}{(a_2 - a_0)(a_2 - a_1)} \tag{7.46}$$

and

$$\frac{df(x)}{dx} = l_0'(x) f(a_0) + l_1'(x) f(a_1) + l_2'(x) f(a_2) \tag{7.47}$$

[†] The May 7, 1982 version of LSODAR, Livermore Solver for Ordinary Differential Equations, with Automatic method switching for stiff and non-stiff problems, and with Root-finding. Linda R. Petzold and Alan C. Hindmarsh, Applied mathematics division 8331, Lawrence Livermore National Laboratory, Livermore, CA 94550120

where,

$$l_0' = \frac{(x-a_1)+(x-a_2)}{(a_0-a_1)(a_0-a_2)} \tag{7.48}$$

$$l_1' = \frac{(x-a_2)+(x-a_0)}{(a_1-a_0)(a_1-a_2)} \tag{7.49}$$

$$l_2' = \frac{(x-a_0)+(x-a_1)}{(a_2-a_0)(a_2-a_1)} \tag{7.50}$$

The macroparticle was divided in multiple thin layers for computational reasons. The radius of each shell depends on the volume of microparticles in the shell. The shell was defined in a way that each shell has the same number of microparticles, but due to diffusion resistances, will have different shell volumes. The growth rate of each shell will be different and the thickness of the shell changes during polymerization. Therefore, the boundaries of the shells are not fixed.

The advantage of using the Lagrange interpolation is that the interpolation positions (shell radius) do not have to be fixed or equally apart. From above expression, *f(x)* will be the monomer concentration at a radial position '*x*' and a_0 and a_2 will be the positions of previous and next shells, respectively. a_1 will be the radius where the monomer concentration is being calculated.

7.2.4. Modeling Parameters

Assuming that the catalyst has two different active site types and that interparticle mass transfer resistance is significant, simulations were performed using kinetic parameters presented in Table 7.1 and 7.2. Also, it was assumed that the catalyst was free of monomer initially. Basic kinetic parameter values were found in Bonini *et al.*(1995). Mass transfer coefficients were found in Sau and Gupta (1993).

Table 7.1 Kinetic parameters

	Site 1	Site 2	Units
Number of Active Site	$2.1 * 10^{-6}$	$9.0 * 10^{-7}$	mole
$k_{i,A}$	60	70	L/mol/sec
$k_{i,B}$	55	65	
$k_{p,AA}$	2000	2200	L/mol/sec
$k_{p,AB}$	200	210	
$k_{p,BA}$	300	320	
$k_{p,BB}$	660	725	
$k_{t,A}$	0.28	0.24	L/mol/sec
$k_{t,B}$	0.20	0.22	
$k_{d,A}$	0.0015	0.0016	L/mol/sec
$k_{d,B}$	0.0014	0.0013	
Particle Radius	0.005		cm
Number of Particles	10,000		

Table 7.2 Monomer information

	Monomer A	Monomer B	Units
Name	Ethylene	Propene	
Concentration	1.5	3.0	mol/L
Molecular Weight	28	42	g/mol
Mass transfer Coefficient	0.47	0.43	cm/s
Density	0.92	0.90	g/cm^3

For the effective diffusivity, values ranging from $D = 10^{-6}$ to 10^{-12} (cm^2/s) were used. Generally, the diffusivity in microparticles and macroparticles are not the same. Macroparticles have higher porosity than microparticles. Therefore, for macroparticles, at least five times higher diffusivities were used. The diffusivity of 10^{-12} cm^2/s was used to model the hypothetical cases where diffusion limitations were extremely high. This value is much smaller than usual literature diffusivity values used for modeling heterogeneous Ziegler-Natta

catalysts. However, the polymers produced with metallocene catalysts may exhibit higher diffusion limitations because polymers show different chain structures compared to that made with conventional Ziegler-Natta catalysts. For polypropylene, conventional Ziegler-Natta catalysts produces low crystalline polymers (atactic or low levels of isotactic polymers), but some metallocene catalysts produce highly isotactic polymers which has higher crystallinity. Therefore, using lower values of diffusivity seems to be a reasonable approach although the extent of how much lower the value can be is uncertain. Before the simulation of temperature gradient, a rough estimation of temperature difference in the polymer particles was performed based on Eq. 7.33. The temperature difference across polymer particle was insignificant even at the worst possible case. Therefore, the effect of temperature gradients is not considered in this chapter.

7.3. MODELING RESULTS

7.3.1. Effect of Diffusion on Monomer Concentration at Reaction Site

Figs. 7.4 to 7.8 show the monomer concentration at the catalyst surface of the microparticles. It is shown that there are radial monomer concentration gradients across the particles, and also that the monomer concentration in the particle increases as the inter-particle mass transfer (between bulk solution and polymer particle) continues to increase.

Fig. 7.4 shows the monomer concentration at the surface of the solid catalyst core, when the diffusivities for micro and macroparticles are relatively high. R_0 is the diameter of the macroparticle and R is the actual radial position in the macroparticle. Therefore, R/R_0 is the relative position moving from inside to outside of the particle, as R/R_0 varies from 0 to 1. Since the diffusivity in the microparticle is high, the concentration gradients are similar to the monomer concentration across the macroparticle. Due to the diffusion limitations and faster monomer consumption at the initial stage, it takes about 600 seconds for the outer shell reach the steady state monomer concentration, which is equal to the bulk monomer concentration in the reaction medium. However, the monomer concentration decreases as we move toward the

center of macroparticle due to continuous monomer polymerization in each shell. In this case, if the polymerization is terminated prematurely, i.e., less than 10 minutes, significant broadening in MWD and CCD could occur.

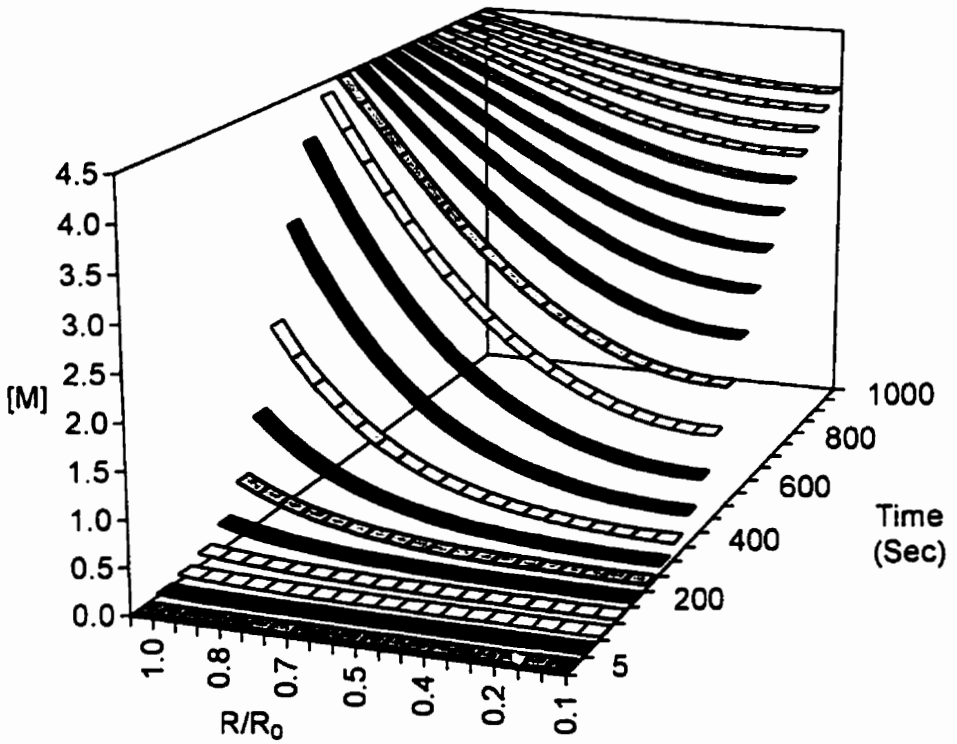

Figure 7.4 Monomer concentration across macroparticle : $D_S = 10^{-8}$, $D_L = 5 \cdot 10^{-8}$

Fig. 7.5 shows the monomer concentration at the surface of the solid catalyst core in microparticles, when the diffusivity for macroparticle is relatively high, but is low for microparticle. Since the concentration is governed by diffusion rather than polymerization, the concentration of monomer at the catalyst surface never reaches the bulk monomer concentration. However, compared to Fig. 7.4, the magnitude of concentration differences between inner and outer shells are smaller. Interestingly, although more serious diffusion limitation is applied to the system described in Fig. 7.5 compared the one in Fig. 7.4, narrower MWD and CCD are expected for the polymers produced in the same time span, due to smaller monomer concentration differences across the particle. However, reaction rate and molecular weights of polymers will decrease significantly.

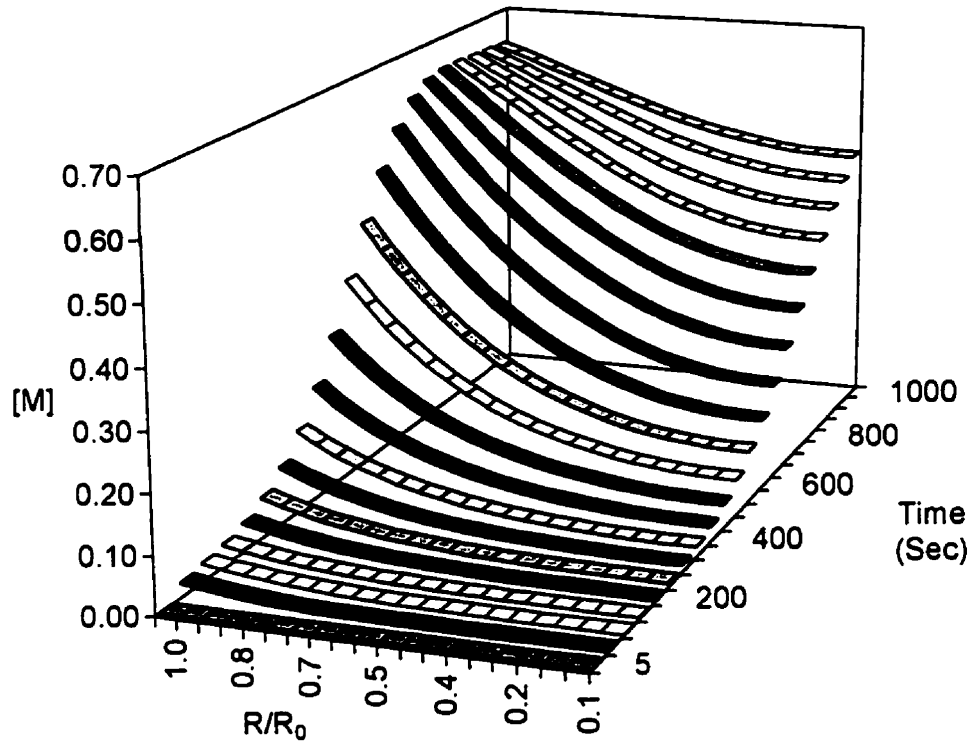

Figure 7.5 Monomer concentration across macroparticle : $D_S = 10^{-10}$, $D_L = 5 * 10^{-8}$

Fig. 7.6 shows the very initial monomer concentration distribution across the macroparticle for the system shown in Fig. 7.5. A very rapid increase in monomer concentration is observed from the outer shells at this stage, because the diffusion limitation in the microparticles is not significant yet. As the polymer layer at the microparticle builds up, the mass transfer resistance will start to take effect and finally, the concentration will be stabilized at a lower concentration than the bulk concentration, which is determined by the mass balance between the diffusion and monomer consumption by polymerization.

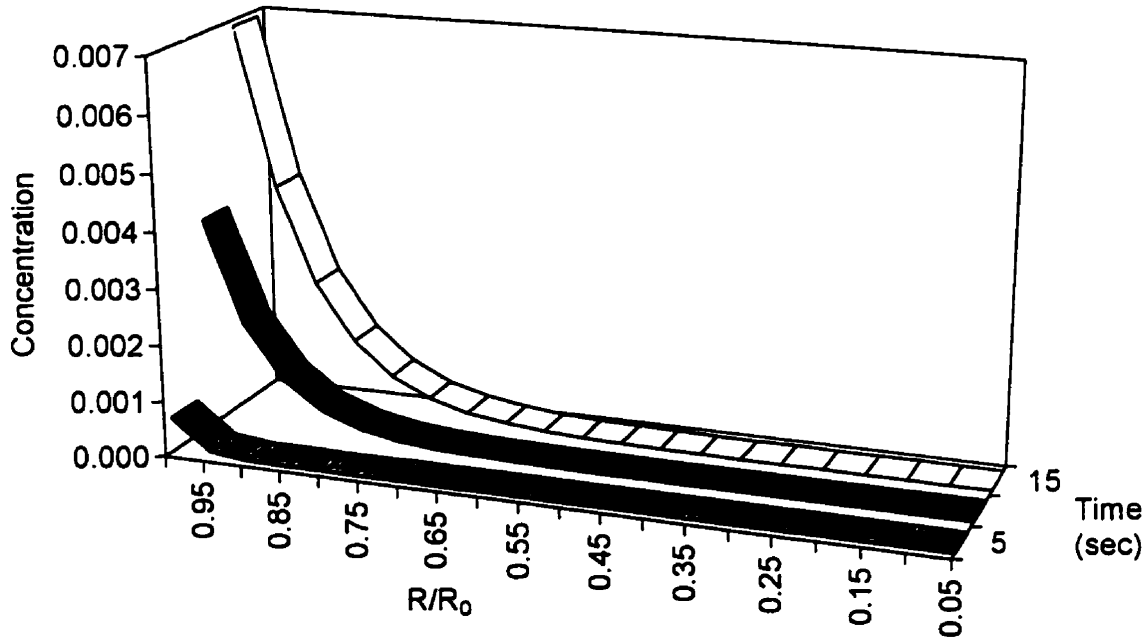

Figure 7.6 Initial concentration profile : $D_s = 10^{-10}$, $D_l = 5 \cdot 10^{-8}$

Fig. 7.7 shows how monomer concentration varies across the macroparticle at different time intervals. Although it is plotted in the same scale of x-axis, it should be remembered that x-axis is only the relative position within the macroparticle and the actual particle sizes are not the same. However, Fig. 7.7 shows the trends of monomer concentration gradients more clearly than its three-dimensional illustrations.

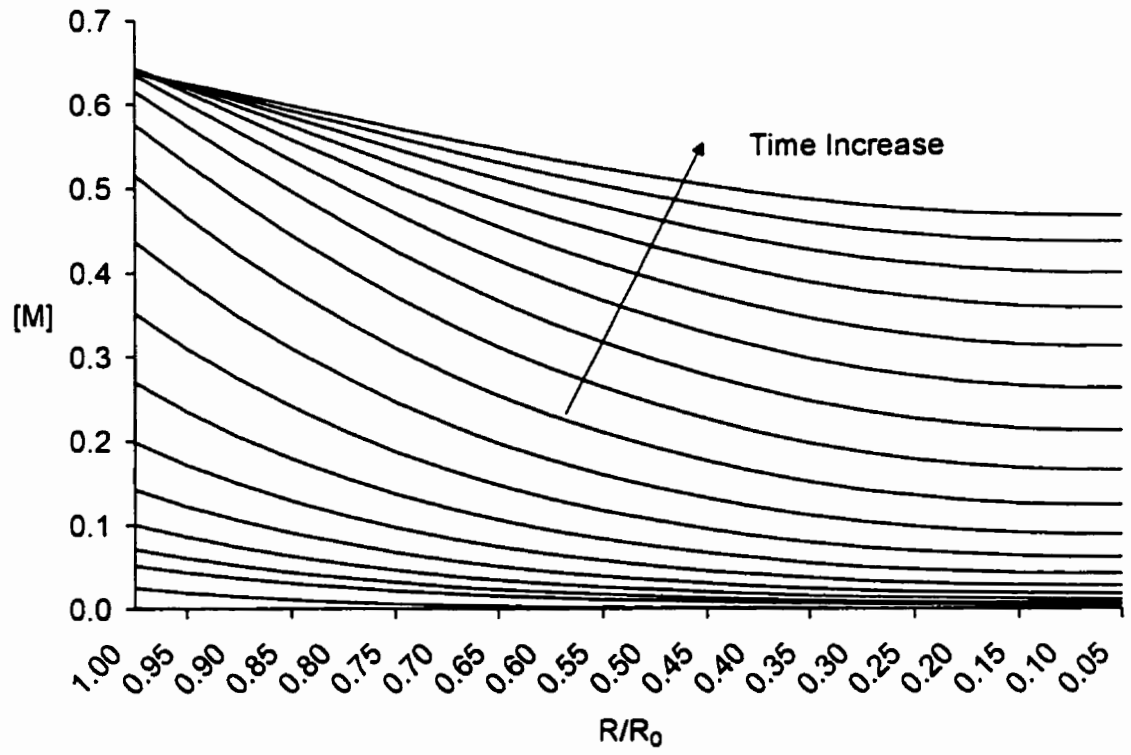

Figure 7.7 Monomer concentration in 2-dimensional plot : $D_S = 10^{-10}$, $D_L = 5 \cdot 10^{-8}$

Fig. 7.8 describes the monomer concentration at the surface of solid catalyst cores when mass transfer resistances are extremely high both in micro and macroparticles. Initially the catalyst is free of monomer and as soon as monomer is introduced in the system the monomer concentration in the particle starts to build up. However, as the monomer concentration builds up, even very thin layers of produced polymer start hindering further monomer diffusion into the particle. Although monomer is still slowly diffusing into the catalyst surface, it is less than the amount of monomer consumed by polymerization. Therefore, the overall monomer concentration starts decreasing. As polymerization continues, the monomer diffuses toward the center of the macroparticle reducing the differences in monomer concentration between the outer shells and the inner shells. Throughout the polymerization, the concentration gradient in the macroparticle is less significant compared to the two previous cases. However, the absolute monomer concentration at the active site of the catalyst is the lowest due to significant mass transfer resistance.

In all the three cases, even after reaching apparent steady state, monomer concentration gradients across macroparticle were observed. Therefore, it can be concluded that mass transfer resistant alone can cause some broadness in the distributions. The extent of the broadening will be described in sections 7.3.2 and 7.3.3. It is very important to note that when relative polymerization rate is higher than the one used for this simulation, the same trends can be observed in polymerization systems, which have even much higher diffusivities.

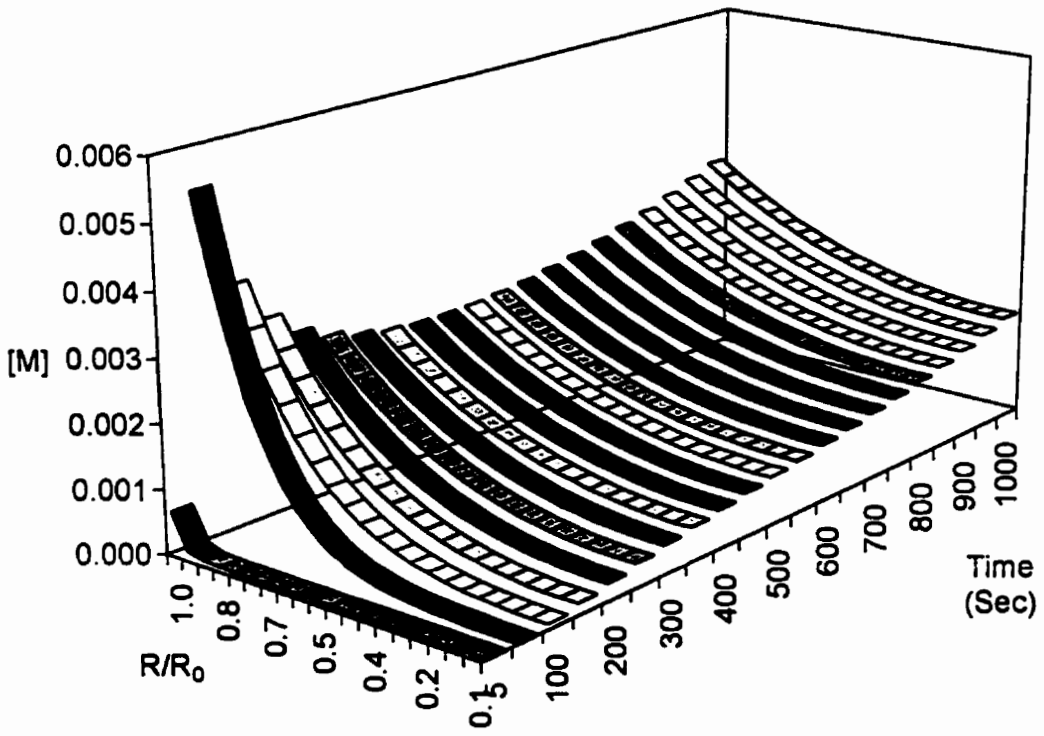

Figure 7.8. Monomer concentration across macroparticle : $D_S = 10^{-12}$, $D_L = 5 \cdot 10^{-12}$

7.3.2. Effect of Mass Transfer Resistance on Molecular Weight Distribution

It was shown that depending on diffusivity or the polymerization rate relative to diffusivity (Thiele modulus), the monomer concentration at the surface of the solid catalyst core varied

significantly. Fig. 7.9 shows the differences in cumulative molecular weights of polymers produced under different diffusion conditions. It seems that until the diffusivities decrease to $D_S = 10^{-7}$ and $D_L = 5 \cdot 10^{-6}$, the molecular weight does not change significantly. Therefore, for the polymerization system modeled in this chapter, the critical point for the Weisz-Prater criterion (Weisz and Prater, 1954), which determines pore diffusion limitations, will lie at the diffusivities around $D_S = 10^{-7}$ and $D_L = 5 \cdot 10^{-6}$, i.e. above these values, there are no diffusion limitations.

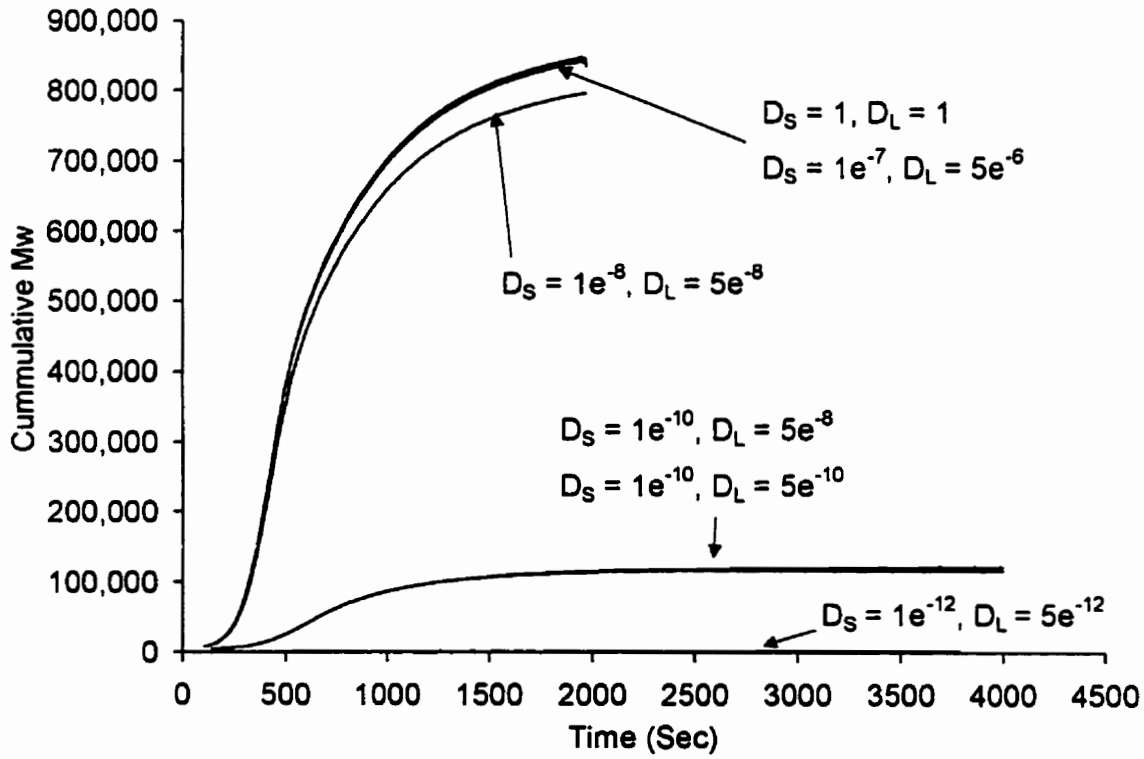

Figure 7.9 Effect of diffusion on cumulative weight average molecular weights

From the previous results, one of the important observations was the fact that even after sufficient polymerization time, the distribution of monomer concentration across the macroparticle becomes narrower but did not disappear completely. The variation of monomer concentration and its gradients across the macroparticle were the greatest at the initial stage in less than 600 seconds, then started reaching a steady state. Therefore, when enough time is

passed the produced polymer chains will have similar molecular weights across the macroparticle compared to the initial stage. Therefore, although the produced MWDs are different (Fig. 7.9), all the polydispersity indexes (PDI) will start decrease as the reaction continues.

Fig. 7.10 shows the PDI of polymers produced under different diffusion limitation conditions. Except for the extremely diffusion limited case ($D_S = 10^{-12}$ and $D_L = 5 \cdot 10^{-12}$), all the PDIs overshoot the theoretical value of two at the initial stage and then start to return to a value closer to two.

According to the simulation, if polymerization time is longer than about 30 minutes (1800 sec), the MWD of the produced polymer will be narrow, independent of diffusion coefficient values. Therefore, it seems that the mass transfer resistance alone cannot explain the broadening of MWD.

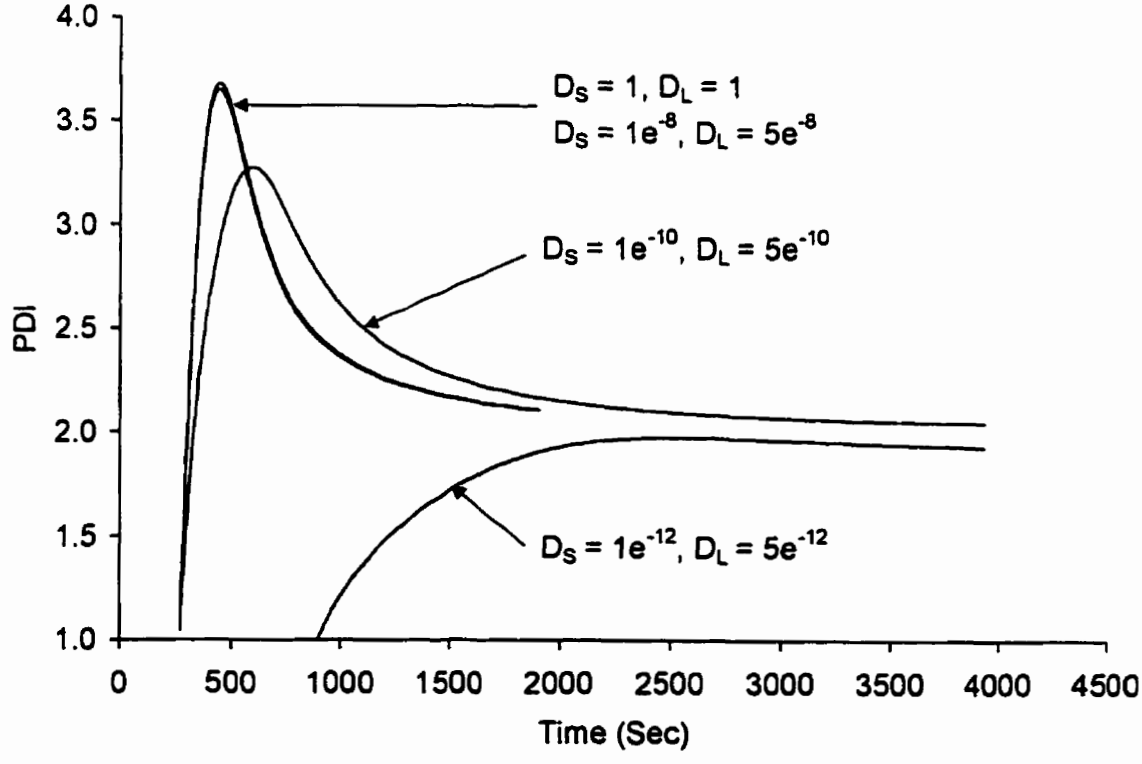

Figure 7.10 Effect of diffusion on polydispersity index

7.3.3. Effect of Mass transfer Resistance on Copolymer Composition

Hoel *et al.* (1994) experimentally measured the copolymer composition at several radial positions in a polymer particle by direct FT-IR analysis of microtomed particles. The results revealed that there was a comonomer content gradient across the polymer particle. However, the variation of copolymer composition along the polymerization time was much greater than the variation across the macroparticle.

Fig. 7.11 shows the mole fraction of ethylene in an ethylene/α-olefin copolymer as a function of radial position and time. It is shown that there are slight copolymer composition gradients across the macroparticle at the initial stage of the polymerization. However, the broadening of CCD will be caused more by the variation of the copolymer composition along the polymerization time according to this simulation result. This trend agrees with the observation by Hoel *et al.* (1994). In Fig. 7.11, the copolymer composition reaches a maximum value and then stabilizes at a lower value after the initial period is over. The fluctuation is caused by different diffusivities of each monomer, of which the effects are more significant at the initial stage of the polymerization, as shown in the previous results.

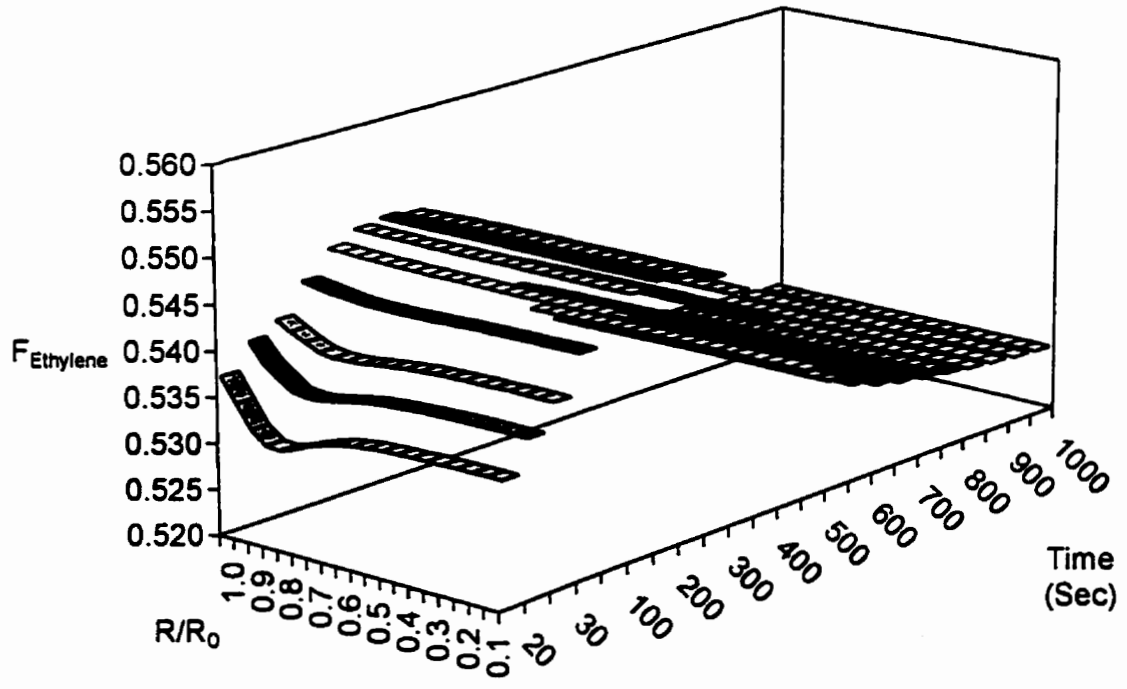

Figure 7.11 Copolymer composition across macroparticle : $D_S = 10^{-8}$ and $D_L = 5 \cdot 10^{-8}$ for both monomers

In Fig. 7.12, it is shown that as the reaction continues, the copolymer composition reaches a steady state value when the diffusivities are high. In this case, the final copolymer composition will be narrow. However, when the diffusivities are low, there will be continuous drifting of copolymer composition, therefore, the copolymer composition of produced polymer will have broad distributions. This trend was not observed in the case of the molecular weight distributions. For molecular weight distributions, the polydispersity index returned near to the theoretical value of two and no significant continuous drifting was observed in any case.

It is interesting to note that the continuous drifting of copolymer composition can also be explained by the presence of multiple active site types, when these active site types have different reactivity ratios and different deactivation rates. Therefore, even for copolymers, the mass transfer resistance cannot be the only source for the broadening of CCDs. It seems that whether it is MWD or CCD, the presence of multiple active site types can explain the behavior of broadening these distributions better. Because even without simulation, it is easy to guess the MWD and CCD will become broader when polymers with different average molecular weights and chemical compositions are mixed together, as they were produced at different active sites. The experimental examples of these broadening by multiple active site type were described in Chapter 5.

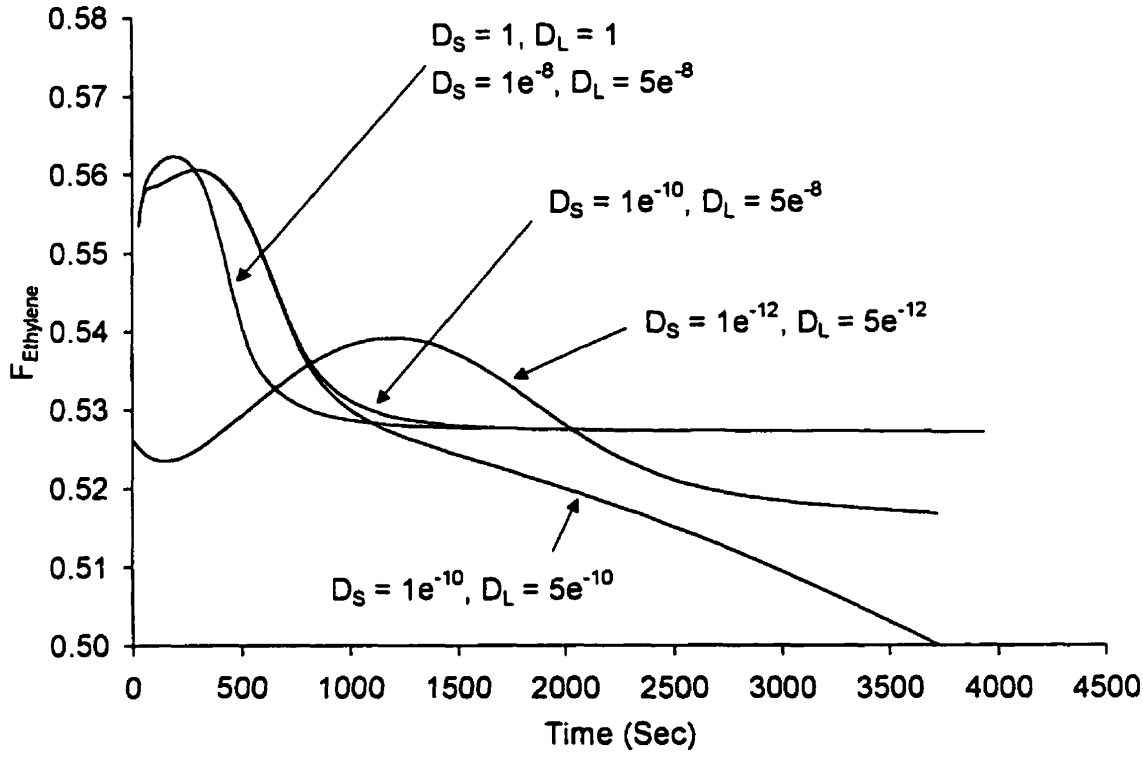

Figure 7.12 Effect of diffusion resistance on cumulative copolymer composition

7.3.4. Effect of Mass Transfer Resistance on Particle Growth and Polymerization Rate

Figs. 7.13 and 7.14 show macroparticle growth and polymerization rates. Since both of them depend on monomer concentration at the catalyst surface in microparticles, they show similar trends. Unlike PDI or comonomer composition simulation results, particle growth rate and the reaction rate show significant dependency on diffusivities of the monomer in the particle.

According to the literature, it is generally accepted that when metallocenes are supported, the activities of the catalyst decrease significantly. Although mass transfer resistance effects were often blamed for the broadening of MWDs, it was not seriously considered as the cause of the reduced polymerization activity. The activity of polymerization catalyst is defined as the amount of polymer produced per amount of catalyst in unit time. It is shown in Fig. 7.13 and 7.14 that when the diffusivities are around 10^{-8}, diffusion resistances of monomer do not significantly affect the rates. However, when lower diffusivities are used, a

significant decrease in polymerization and particle growth rate was observed. Therefore, it seems that the decreased catalyst activity in supported system can be explained at least in part by the mass transfer resistances, when the diffusivities are low or the relative polymerization activities compared to diffusion limitations are high. However, it must be noted that there are many other factors that will reduce the activity of supported catalyst other than the mass transfer resistances. For instance, poisoning of the active sites during catalyst supporting process will reduce the overall catalyst activity. Also, formation of chemically less active catalyst sites due to interaction between the support and catalyst molecules is another possibility.

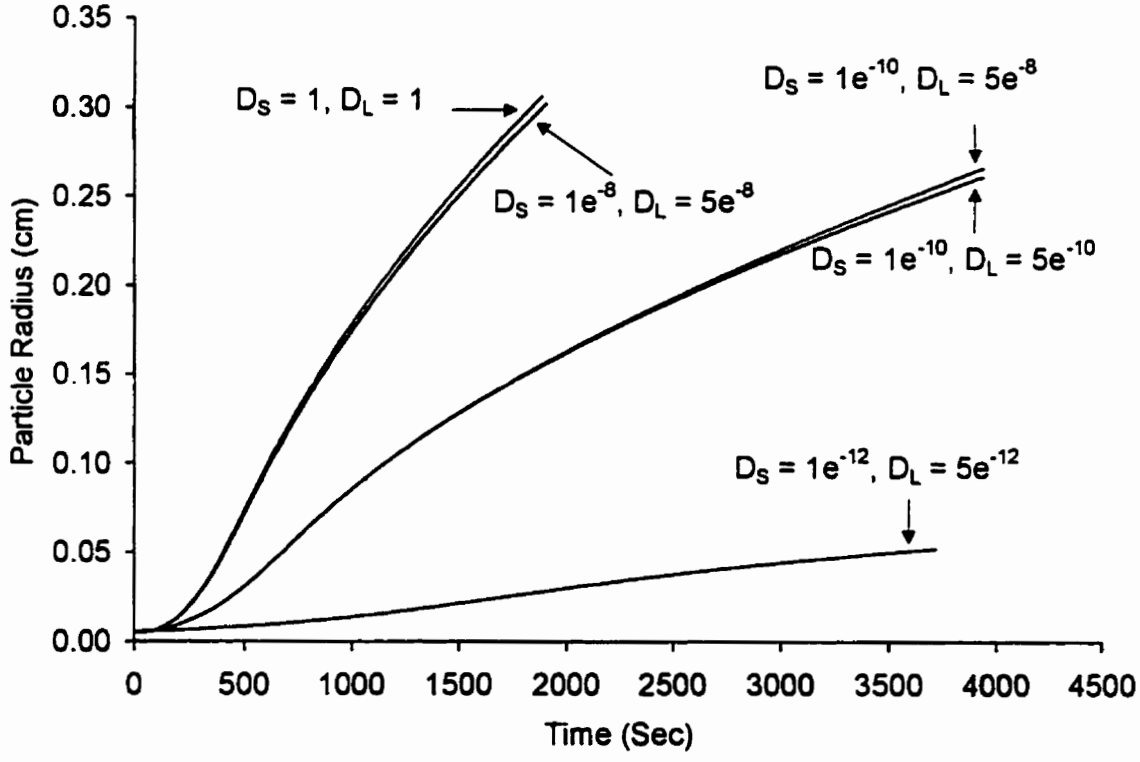

Figure 7.13 Effect of diffusion on particle growth rate

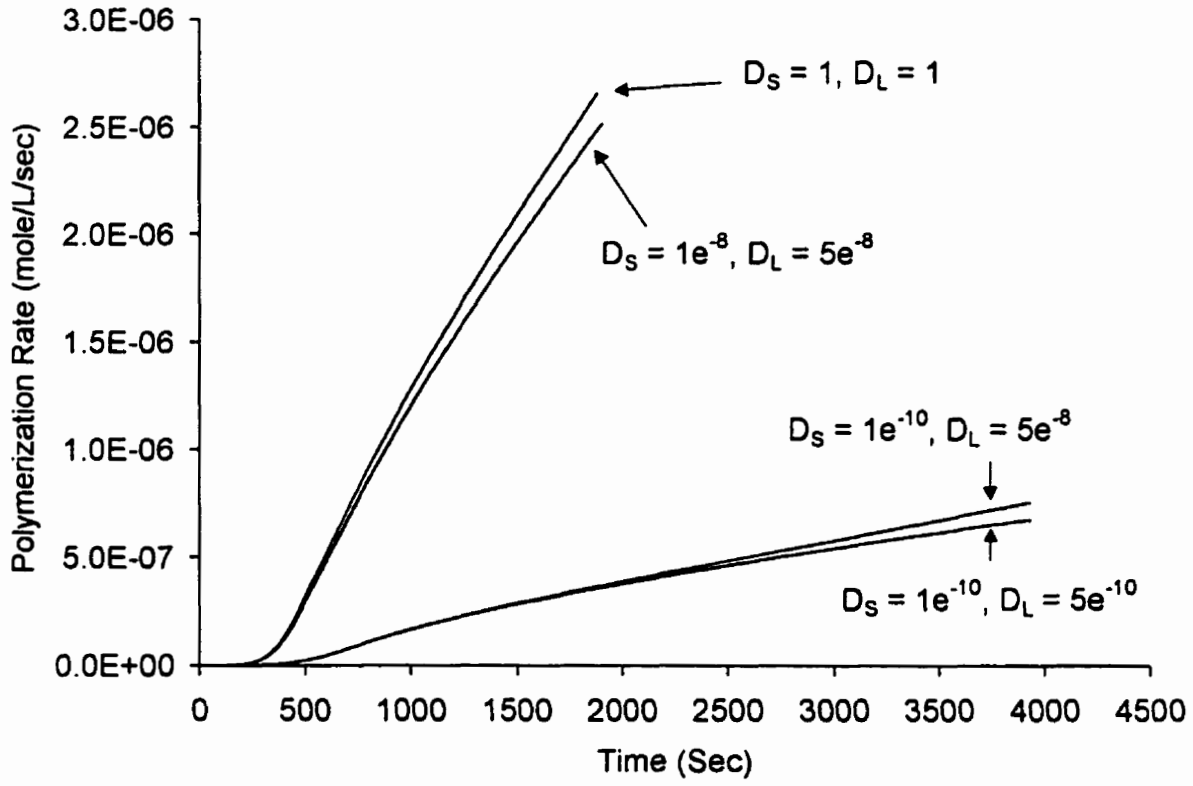

Figure 7.14 Effect of diffusion on polymerization rate (mole/L·s)

7.3.5. Particle Morphology Based on Shell Growth Rates

When the microparticles grow, the volume of each shell in the macroparticle will increase. Depending on the diffusivity differences between microparticle and macroparticle, and the microparticle sizes in each shell, different particle morphologies might be observed during the polymerization.

If the outer shells grow faster all the time, no apparent physical stress will be caused to each shell. However, once the inner shells experience faster growth rate compared to outer shells, some pressure will build up from within the macroparticles. This can happen when the macroparticle mass transfer resistance is small, thus all the microparticles have equal access to monomers across the growing macroparticle. In this event, the microparticles will rearrange their positions to reduce the pressure built inside the macroparticle. If polymerization rate is

slow, it will be easier for the microparticles to move around and for outer shells to stretch to accommodate growing inner shell volume. This may be true in the polymerization catalyzed by conventional Ziegler-Natta catalysts, which has lower polymerization activities. For metallocene catalysts the particle growth rates are much faster compared to conventional Ziegler-Natta catalysts. Therefore, the growing microparticles in outer shells in metallocene catalysts might not have enough time to rearrange their axial positions to absorb the impact caused by expansion of inner shell volume. As a result, the surface of the outer shell might crack, and the formed particles show rough surfaces. Most polymers produced with heterogeneous Ziegler-Natta catalyst have smooth surface. For supported metallocene catalyst, the morphologies of the produced polymers are poor compared to the case of the Ziegler-Natta system. Although leaching of catalyst active sites during polymerization is believed to be the main cause for the poor morphology in metallocene systems, the discussed effect can certainly become an added contributor.

7.4. EFFECT OF PARTICLE RESIDENCE TIME DISTRIBUTION ON MWD

Controlling MWD through combined catalyst systems was demonstrated in the previous chapters. In our system, the polymerization time was usually kept less than a hour, and therefore, the effect of different deactivation rates of each catalyst in bimetallic systems was likely negligible. However, in industrial scale continuous reactors, where some catalysts stay in the reactor for hours depending on the residence time distribution, the effect of different catalyst deactivation rates might be significant. Therefore, in this section, the effect of reactor residence time distribution on MWD of polymer made with a bimetallic supported catalyst is investigated by a simple catalyst decay model.

The decay of active catalyst concentration will be modeled as :

$$[C^*]_i = [C^*]_{i,0}\, e^{-at^b} \tag{7.51}$$

where, $[C^*]_i$ and $[C^*]_{i,0}$ denote the concentration and the initial concentration of the active site type i, t is time, and a and b are adjustable parameters. To consider the worst case scenario, catalysts **A** and **B** are chosen by adjusting the parameters a and b, in a way that their

deactivation rates are very different, as shown in Fig. 7.15. Since one catalyst shows slow decay and the other shows rapid decay, the bimetallic catalyst, which is the combination of these two catalysts, will produce polymers with varying fractions from each site as a function of time. Catalysts **A** and **B** produces polymers with different average chain lengths. Therefore, the MWD of polymer produced with the combined catalyst will vary depending on the age of the catalyst particles in the polymerization reactor. Table 7.3 summarizes the characteristics and parameters used for each catalyst in this study.

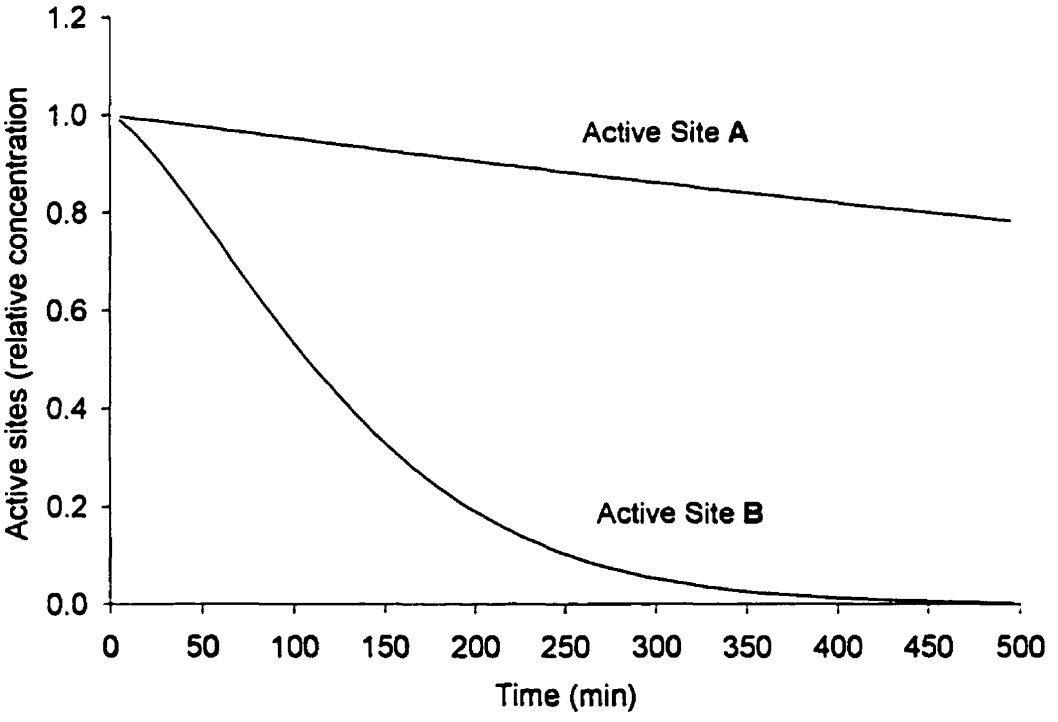

Figure 7.15 Example of multiple active catalyst sites with different deactivation rates

Table 7.3 Catalyst characteristic for a bimetallic supported system

Catalyst	DP_n [1]	a [2]	b [2]	mole-%
A	1000	0.0005	1.0	0.62
B	1250	0.001	1.4	0.38

[1] DP_n : number average degree of polymerization for polymers produced with each catalyst

[2] a, b : catalyst decay constants for Eq. 7.51

The residence time distribution in an ideal continuous stirred tank reactor (CSTR) is expressed as :

$$E(t) = \frac{1}{\theta} e^{-(t/\theta)} \tag{7.52}$$

where θ is the mean residence time in the polymerization reactor.

The instantaneous chain length distribution (CLD) of polymers produced at each active catalyst site at time t can be estimated using Flory's most probable distributions. From the information of the instantaneous CLD and the residence time distribution of the catalyst particles, the overall CLD of the polymer exiting from a polymerization reactor for the bimetallic catalyst system can be estimated as :

$$w_A = \sum [C_i^*](t) E(t) \Delta t \tag{7.53}$$

$$w_B = 1 - w_A \tag{7.54}$$

$$W(n) = w_A n \tau_A^2 \cdot e^{-\tau_A \cdot n} + w_B n \tau_B^2 \cdot e^{-\tau_B \cdot n} \tag{7.55}$$

Fig. 7.16 shows the CLD of polymers produced in an ideal CSTR with different mean residence times. Since catalyst **B** decays rapidly, the peak corresponds to polymers produced at active catalyst site **B** decreases as the mean residence time increases from 30 to 120 minutes.

It seems that the change in the shape of CLD is not drastic considering the fact that each catalyst has significantly different deactivation rates and the mean residence time was doubled or tripled. If it is required to accurately customize the ratios of high and low molecular weight portions of polymers produced in a CSTR with a fixed mean residence time, the initial ratios of the two catalysts in the bimetallic system needs to be adjusted. This simple model can provide an easy way of estimating the initial ratios of catalyst required in a bimetallic system by iterative methods. As can be seen in Fig. 7.16, different residence time do not affect the horizontal position of the peaks. If the catalysts have different reactivity ratios, then mean residence time differences will cause variations in CCD as well.

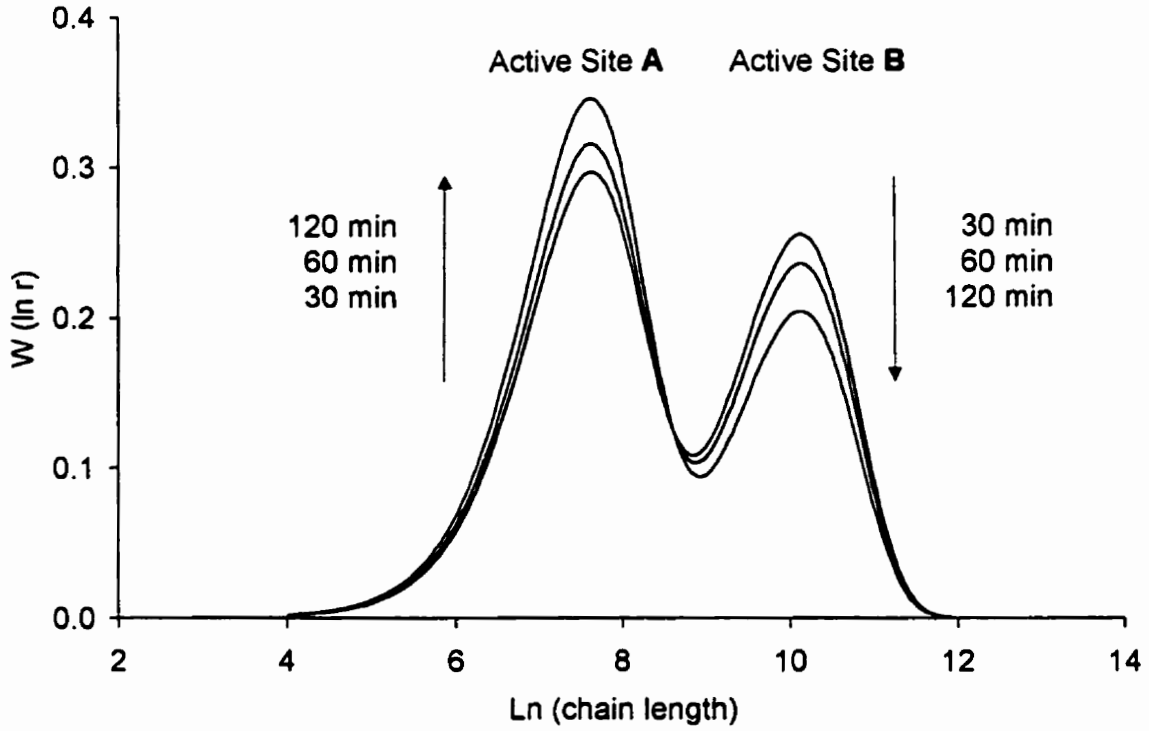

Figure 7.16 Effect of mean residence time on MWD of polymer

7.5. CONCLUSION

These simulation results are useful in predicting general copolymerization behavior in supported metallocene catalysts. From the modeling results, broadening of the molecular weight distribution could not be explained by diffusion controlled kinetics only, although it might account for the reduced activity of supported metallocenes. Based on the results, it is concluded that the mass transfer resistance can be significant if :

(1) Polymerization time is too short

(2) The ratio of polymerization to diffusivity is large (Weisz-Prater criterion >>1)

Other than these cases, it seems that the increase of PDI is mainly caused by multiplicity of catalyst active site types. The broadening of copolymer composition distribution can be

attributed to mass transfer resistances when the diffusivities of monomers are reasonably low compared to polymerization rates.

Particle morphology can be inferred by observing different radial growth rates in different shells of a macroparticle.

And finally, it was shown that in continuous industrial scale polymerization reactors, the residence time distribution could cause further variations in molecular weight and also possibly chemical composition distributions of polyolefins made with binary metallocene catalysts.

CHAPTER 8
CONTRIBUTIONS

For the case of homopolymers, the MWD of polyethylene produced with combined metallocene catalysts was represented as the superposition of the MWD of polymers produced with individually supported catalyst. From the deconvolution results, it was shown that the bimodal MWDs could be deconvoluted into two Flory's most probable distributions with polydispersity index of two for each peak (Soares *et al.*, 1997).

In this research, it was shown for the first time that the molecular weight of polymers produced with $Et[Ind]_2ZrCl_2$ does not change with increasing monomer pressure or hydrogen concentration in the system when monomer pressure is higher than approximately 100 psi at the polymerization temperatures of 40 and 50 °C (Kim *et al.*, 1998, 1999a). When lower monomer pressures were used, the molecular weight of polyethylene produced with $Et[Ind]_2ZrCl_2$ decreased with increasing hydrogen concentration.

This behavior can be used to control the MWD of polymer produced with bimetallic supported catalysts consisting of $Et[Ind]_2ZrCl_2$ and other metallocene catalysts. In our example, the supported catalyst produced by the combination of $Et[Ind]_2ZrCl_2$ and Cp_2HfCl_2 was able to produce polymers with MWDs ranging from bimodal to narrow and unimodal by simply changing ethylene pressure or addition of hydrogen. This result is of significant importance and has been the subject of several invited conference presentations (Kim *et al.*, 1997; Soares and Kim, 1998; and Soares *et al.*, 1998).

For the case of copolymers, it was shown that some supported metallocenes could produce polymers with broad and/or bimodal CCD depending on the method involved in the treatment of the inert carrier (Kim et al., 1997, 1999b). Before this research, the effect of support treatment was examined only in terms of MWD.

Similar trends observed for homopolymerization were also present in copolymerization. Copolymers produced with $Et[Ind]_2ZrCl_2$ showed the least sensitivity toward polymerization conditions. It was demonstrated that the control of CCD and MWD

could be simultaneously achieved to produce the kind of polymers that were available only by reactor cascade technology (Soares and Kim, 1998). This might provide an attractive alternative route for the production of polyethylene with high ESCR in a single polymerization reactor (Soares *et al.*, 1999).

The proposed mathematical model provided useful insights on phenomena taking place in microscopic levels, some of which cannot be observed directly. According to the model, the broadening of MWD or CCD seemed to be caused by the presence of multiple active types rather than mass or heat transfer resistances. However, if polymerization time is too short or the ratio of polymerization rate to diffusivity of monomer in the catalyst particle is very high, mass transfer resistance can further broaden MWD and CCD.

APPENDIX

A. POLYMERIZATION ACTIVITIES

Activity in [kg polymer / (mol metal × atm ethylene × hr)], Reactor Headspace: 100 mL

A.1. HOMOPOLYMERIZATION WITHOUT HYDROGEN

A.1.1. Polymerization Temperature = 40 °C

Catalyst	$P_{Ethylene}$				
	20 psi	30 psi	40 psi	50 psi	70 psi
$Et[Ind]_2ZrCl_2$	2142	1401	1464	2287	2163
Cp_2HfCl_2	169	219	187	150, 329	206
CGCTi	27			35, 55	6
Comb1 (Zr/Hf)	348	836	753	846	1697

Catalyst	$P_{Ethylene}$	
	90 psi	120 psi
$Et[Ind]_2ZrCl_2$	2683	1671
Cp_2HfCl_2	219	186
Comb1 (Zr/Hf)	969	876

A.1.2. Polymerization Temperature = 50 °C

Catalyst	$P_{Ethylene}$			
	20 psi	30 psi	40 psi	50 psi
$Et[Ind]_2ZrCl_2$	3332	3809	3190	1814
Cp_2HfCl_2	484	419	451	227
CGCTi	43			91, 73
Comb1 (Zr/Hf)	1143	1579	2175	1828
Comb2 (Zr/CGCTi)				88

Catalyst	$P_{Ethylene}$				
	70 psi	90 psi	100 psi	120 psi	150 psi
$Et[Ind]_2ZrCl_2$	3224	2074	2143	2574	2918
Cp_2HfCl_2	479	63		311	323
CGCTi	10		24		
Comb1 (Zr/Hf)	2292	164	509	1986	2339
Comb2 (Zr/CGCTi)			528		

A.2. HOMOPOLYMERIZATION WITH HYDROGEN

A.2.1. Polymerization Temperature = 50 °C

Catalyst ($P_{Ethylene}$)	Hydrogen				
	5 mL	25 mL	50 mL	100 mL	150 mL
$Et[Ind]_2ZrCl_2$ (20psi)	3549		914		352
$Et[Ind]_2ZrCl_2$ (30psi)					713
$Et[Ind]_2ZrCl_2$ (40psi)					926
$Et[Ind]_2ZrCl_2$ (50psi)	2626		1295		282
$Et[Ind]_2ZrCl_2$ (70psi)					444
$Et[Ind]_2ZrCl_2$ (100psi)	1450		1057		638
$Et[Ind]_2ZrCl_2$ (150psi)					432
$Et[Ind]_2ZrCl_2$ (200psi)			602		149
Cp_2HfCl_2 (30psi)					27
Cp_2HfCl_2 (50psi)					47
Cp_2HfCl_2 (100psi)					70
Cp_2HfCl_2 (150psi)					34
Cp_2HfCl_2 (200psi)					131
Comb1 (20psi)		142		524	
Comb1 (30psi)					265
Comb1 (50psi)				1021	
Comb1 (100psi)		811	1077	607	1341

Catalyst ($P_{Ethylene}$)	Hydrogen				
	200 mL	10 psi	20 psi	30 psi	100 psi
$Et[Ind]_2ZrCl_2$ (120psi)			258		
Cp_2HfCl_2 (120psi)			71		
Comb1 (50psi)	590				
Comb1 (100psi)	1786	631	326	261	566

A.3. COPOLYMERIZATION

Compared to homopolymerization, copolymerization activities are more reproducible. For $Et[Ind]_2ZrCl_2$, when the monomer pressure is less than 100 psi, it seems that the activity increases as the hydrogen concentration in the polymerization reactor increases. When monomer pressure is greater than 100 psi, the polymerization is very rapid and the reproducibility of the polymerization activity is greatly reduced. For Cp_2HfCl_2, activity decreases as the hydrogen concentration increases in most cases. The highest activity for Cp_2HfCl_2 was observed when ethylene pressure was 50 psi (compared to three other ethylene pressures of 20, 100, and 150 psi). For CGCTi, the activities were always lower than the ones of $Et[Ind]_2ZrCl_2$. However, CGCTi activities were higher compared to Cp_2HfCl_2 except for polymerization temperature of 40 °C and ethylene pressures of 20 psi and 50 psi.

A.3.1. $P_{Ethylene}$ = 20 psi

40 °C	Hydrogen				
1-Hexene = 1 mL	0 mL	5 mL	10 mL	20 mL	30 mL
$Et[Ind]_2ZrCl_2$	3262	3512	3784	2325	485
Cp_2HfCl_2	204	102	101	65	52
CGCTi	73	105		66	40
Comb1 (Zr/Hf)	640	484	351	104	276
Comb2 (Zr/CGCTi)	241	51	703	176	228

50 °C 1-Hexene = 1 mL	Hydrogen				
	0 mL	5 mL	10 mL	20 mL	30 mL
$Et[Ind]_2ZrCl_2$	2336	9383	11923	10220	12827
Cp_2HfCl_2	222	154	212	110	120
CGCTi	725	672	297	206	
Comb1 (Zr/Hf)	2810	4892	3188	3657	2920
Comb2 (Zr/CGCTi)		2310	2170	2750	2026

A.3.2. $P_{Ethylene}$ = 50 psi

40 °C 1-Hexene = 2.5 mL	Hydrogen				
	0 mL	12.5 mL	25 mL	50 mL	75 mL
$Et[Ind]_2ZrCl_2$		3777	3163	3829	2130
Cp_2HfCl_2	2199	1296	908	659	562
CGCTi	145, 108	164	74	105	155
Comb1 (Zr/Hf)	1328	1412	860	547	438
Comb2 (Zr/CGCTi)	646	663	791	461	677

50 °C 1-Hexene = 2.5 mL	Hydrogen				
	0 mL	12.5 mL	25 mL	50 mL	75 mL
$Et[Ind]_2ZrCl_2$	5503	5607	6379	6218	7028
Cp_2HfCl_2	245	214	236	88	149
CGCTi	1193	745	652	379	
Comb1 (Zr/Hf)	1123, 1475	2345	2337	2268	2606
Comb2 (Zr/CGCTi)	640	1317	821	1098	1010

A.3.3. $P_{Ethylene}$ = 100 psi

40 °C 1-Hexene = 5 mL	Hydrogen				
	0 mL	25 mL	50 mL	100 mL	150 mL
$Et[Ind]_2ZrCl_2$	1733	4118	5048	2640	2808
Cp_2HfCl_2	21, 26	26		16	9
CGCTi	142		154	74	181
Comb1 (Zr/Hf)	209, 302	101	444	162	65
Comb2 (Zr/CGCTi)	420	568	626	301	306

50 °C 1-Hexene = 5 mL	Hydrogen				
	0 mL	25 mL	50 mL	100 mL	150 mL
$Et[Ind]_2ZrCl_2$	419	5062, 4303	6769	966	3790
Cp_2HfCl_2	42	74	27	64	72
CGCTi	91, 101	72	145	168	111
Comb1 (Zr/Hf)	724, 890	697	55	490	40
Comb2 (Zr/CGCTi)	1278	1175	920	983	1224

A.3.4. $P_{Ethylene}$ = 150 psi

40 °C	Hydrogen				
1-Hexene = 7.5 mL	0 mL	37.5 mL	75 mL	150 mL	225 mL
$Et[Ind]_2ZrCl_2$	2673	3366	4461	2352	3780
Cp_2HfCl_2	80	73	52	40	38
CGCTi		133	126	120	
Comb1 (Zr/Hf)	1091	1149	1120	406	427
Comb2 (Zr/CGCTi)	504	689	687	697	479

50 °C	Hydrogen				
1-Hexene = 7.5 mL	0 mL	37.5 mL	75 mL	150 mL	225 mL
$Et[Ind]_2ZrCl_2$	8382	13029	7985	5671	9077
Cp_2HfCl_2	72	71	62	51	
CGCTi	63	61	171	284, 296	129, 163
Comb1 (Zr/Hf)	2261	2546	1076	2822	519
Comb2 (Zr/CGCTi)	2510	5169		4754	4989

B. PEAK CRYSTALLIZATION TEMPERATURES MEASURED WITH CRYSTAF [°C]

B.1. $P_{Ethylene}$ = 20 psi

40 °C	Hydrogen				
1-Hexene = 1 mL	0 Ml	5 mL	10 mL	20 mL	30 mL
$Et[Ind]_2ZrCl_2$	77.0				71.1
Cp_2HfCl_2	65.4,78.2	60.6,79.8	66.0,79.8	66.0,80.1	66.8,79.2
Comb1 (Zr/Hf)	41.0,69.5				60.5,72.1
Comb2 (Zr/CGCTi)	30,44.6				30,71.7

50 °C	Hydrogen				
1-Hexene = 1 mL	0 mL	5 mL	10 mL	20 mL	30 mL
$Et[Ind]_2ZrCl_2$	73.4				67.5
Cp_2HfCl_2	67.5,78.6		70.9		58,67,77
Comb1 (Zr/Hf)					72.1
Comb2 (Zr/CGCTi)	30,46.4				

B.2. $P_{Ethylene}$ = 50 psi

40 °C	Hydrogen				
1-Hexene = 2.5 mL	0 mL	12.5 mL	25 mL	50 mL	75 mL
$Et[Ind]_2ZrCl_2$	60.0,74.7				60.0,71.6
Cp_2HfCl_2	52.0,77.6		67.0,80.4		66,80
Comb1 (Zr/Hf)	60.0,72.9				73.7
Comb2 (Zr/CGCTi)	30,66.9				

50 °C	Hydrogen				
1-Hexene = 2.5 mL	0 mL	12.5 mL	25 mL	50 mL	75 mL
$Et[Ind]_2ZrCl_2$	73.9				73.3
Cp_2HfCl_2			71.6,80.5		69,75
Comb1 (Zr/Hf)	76.7				

B.3. $P_{Ethylene}$ = 100 psi

40 °C	Hydrogen				
1-Hexene = 5 mL	0 mL	25 mL	50 mL	100 mL	150 mL
$Et[Ind]_2ZrCl_2$	77.4				75.7
Cp_2HfCl_2	70.2,80.0				72.5,82.2
Comb1 (Zr/Hf)	77.6				76.0
Comb2 (Zr/CGCTi)	57.6,76.6				

50 °C	Hydrogen				
1-Hexene = 5 mL	0 mL	25 mL	50 mL	100 mL	150 mL
$Et[Ind]_2ZrCl_2$	76.5				76.1
Cp_2HfCl_2	71.8,80.0	74.3,80.9			74.1,79.5
Comb1 (Zr/Hf)					79.6
Comb2 (Zr/CGCTi)	40.8,76.0				30,77.3

B.4. $P_{Ethylene}$ = 150 psi

40 °C	Hydrogen				
1-Hexene = 7.5 mL	0 mL	37.5 mL	75 mL	150 mL	225 mL
$Et[Ind]_2ZrCl_2$	76.4				74.7
Cp_2HfCl_2	68.0,81.1	72.2,82.2	72.9,81.5	74.5,79.7	72.3,80.0
CGCTi	37.5				
Comb1 (Zr/Hf)	75.3				77.1
Comb2 (Zr/CGCTi)	50,75.9				30,76.2

50 °C	Hydrogen				
1-Hexene = 7.5 mL	0 mL	37.5 mL	75 mL	150 mL	225 mL
$Et[Ind]_2ZrCl_2$	78.1				74.1
Cp_2HfCl_2	71.8,80.0		74.2,81.6		76.6
Comb1 (Zr/Hf)	76.4				

C. MOLECULAR WEIGHTS [g/mole]

C.1. $P_{Ethylene}$ = 20 psi

40 °C 1-Hexene 1 mL	Hydrogen									
	0 mL		5 mL		10 mL		20 mL		30 mL	
	M_w	PDI	M_w	PDI	M_w	PDI	M_w	PDI	M_w	PDI
$Et[Ind]_2ZrCl_2$	115,100	2.2	133,000	2.1	125,400	2.2	121,900	1.9	73,300	2.1
Cp_2HfCl_2	348,700	1.5	112,200	2.0	70,900	2.0	36,700	1.9	25,700	2.8
CGCTi	404,500	1.6	205,300	1.7	141,900	1.9	80,800	1.9	42,300	1.9
(Zr/Hf)	198,500	2.5	116,500	2.1	105,500	2.0	63,200	2.1	72,300	2.0
(Zr/CGCTi)	164,600	2.2	106,900	3.5	126,800	2.0	105,200	1.9	104,800	2.0

50 °C 1-Hexene 1 mL	Hydrogen									
	0 mL		5 mL		10 mL		20 mL		30 mL	
	M_w	PDI	M_w	PDI	M_w	PDI	M_w	PDI	M_w	PDI
$Et[Ind]_2ZrCl_2$	116,500	2.1	129,000	2.1	118,800	2.2	81,700	2.1	78,100	2.2
Cp_2HfCl_2	631,200	1.7	100,400	1.8	58,300	1.7	26,800	2.0	23,500	1.8
CGCTi	356,100	1.6	274,400	1.6	250,300	1.7	212,000	1.8		
(Zr/Hf)	224,800	2.8	129,400	2.4	109,400	2.1	98,100	2.1	84,500	2.3
(Zr/CGCTi)	166,000	2.5	126,800	2.3	133,800	2.3	125,500	2.3	123,200	2.1

C.2. $P_{Ethylene}$ = 50 psi

40 °C 1-Hexene 2.5 mL	Hydrogen									
	0 mL		12.5 mL		25 mL		50 mL		75 mL	
	M_w	PDI	M_w	PDI	M_w	PDI	M_w	PDI	M_w	PDI
$Et[Ind]_2ZrCl_2$	98,400	2.0	90,700	2.1	83,200	1.9	77,300	2.0	70,200	1.9
Cp_2HfCl_2	596,400	1.6	137,700	1.9	66,700	1.9	35,500	1.9	23,500	2.0
CGCTi	456,000	1.5			295,700	1.9	116,000	2.0	119,100	2.1
(Zr/Hf)	198,900	2.8	101,300	1.9	92,200	1.9	78,700	2.1	72,460	2.1
(Zr/CGCTi)	162,600	2.4	142,200	2.3	124,200	2.0	106,800	2.0	113,600	1.9

50 °C 1-Hexene 2.5 mL	Hydrogen									
	0 mL		12.5 mL		25 mL		50 mL		75 mL	
	M_w	PDI	M_w	PDI	M_w	PDI	M_w	PDI	M_w	PDI
$Et[Ind]_2ZrCl_2$	98,700	2.0	94,900	1.9	91,300	2.0	87,639	2.0	86,600	2.0
Cp_2HfCl_2	762,600	1.6	161,200	1.9	103,000	1.8	34,300	1.8	23,000	2.1
CGCTi	466,600	1.5	448,700	1.5	334,700	1.6	292,700	1.6	281,500	1.7
(Zr/Hf)	202,200	2.7	110,000	2.2	95,200	2.1	80,800	2.0	80,400	2.0
(Zr/CGCTi)	104,800	2.1	115,000	2.1	94,970	2.0	97,800	1.9	96,500	1.9

C.3. $P_{Ethylene}$ = 100 psi

40 °C 1-Hexene 5 mL	Hydrogen									
	0 mL		25 mL		50 mL		100 mL		150 mL	
	M_w	PDI	M_w	PDI	M_w	PDI	M_w	PDI	M_w	PDI
$Et[Ind]_2ZrCl_2$	99,400	2.2	92,500	2.0	96,500	2.1	92,000	2.0	100,500	2.0
Cp_2HfCl_2	501,000	1.6	174,000	2.0	106,400	2.1	57,400	2.1	44,700	2.0
CGCTi	591,400	1.8			311,800	1.7	262,100	1.7	232,000	1.8
(Zr/Hf)	143,000	2.3			103,600	2.1	70,300	9.1	56,000	11.0
(Zr/CGCTi)	114,000	2.2	102,900	2.3	113,000	2.5	100,500	2.3	97,100	2.2

50 °C 1-Hexene 5 mL	Hydrogen									
	0 mL		25 mL		50 mL		100 mL		150 mL	
	M_w	PDI	M_w	PDI	M_w	PDI	M_w	PDI	M_w	PDI
$Et[Ind]_2ZrCl_2$			68,300	2.2	78,500	2.0	73,200	2.1	81,000	1.9
Cp_2HfCl_2	421,000	2.3	204,186	1.8	91,000	1.9	58,000	2.2	27,000	2.3
CGCTi	242,000	1.6	198,000	1.7	241,500	1.8	200,000	1.7	141,200	1.9
(Zr/Hf)	168,200	3.3	99,400	2.8	68,700	2.3			45,000	2.3
(Zr/CGCTi)	114,800	2.4	100,200	2.0	95,800	2.3	94,600	2.2	83,200	2.1

C.4. $P_{Ethylene}$ = 150 psi

40 °C 1-Hexene 7.5 mL	Hydrogen									
	0 mL		37.5 mL		75 mL		150 mL		225 mL	
	M_w	PDI	M_w	PDI	M_w	PDI	M_w	PDI	M_w	PDI
$Et[Ind]_2ZrCl_2$	103,200	2.0	97,600	2.0	92,500	2.0	100,000	1.9	93,700	2.0
Cp_2HfCl_2	628,600	2.3	293,500	2.0	137,500	2.1	96,900	2.1	76,600	2.2
CGCTi	515,000	1.7	455,000	1.7	141,300	1.8	216,300	1.8	216,800	2.1
(Zr/Hf)	136,700	2.4	126,000	2.0	103,900	2.0	90,500	2.0	89,000	2.0
(Zr/CGCTi)	127,700	2.1	124,000	2.2	116,300	2.1	116,700	2.3	11,500	2.1

50 °C 1-Hexene 7.5 mL	Hydrogen									
	0 mL		37.5 mL		75 mL		150 mL		225 mL	
	M_w	PDI	M_w	PDI	M_w	PDI	M_w	PDI	M_w	PDI
$Et[Ind]_2ZrCl_2$	82,700	2.1	85,200	1.9	79,600	2.1	78,900	1.8	76,000	1.9
Cp_2HfCl_2	788,000	2.7	198,400	2.4	120,700	2.0	64,100	1.9	36,100	2.0
CGCTi	198,600	2.1	138,400	2.3	98,900	2.1	145,300	2.2	85,000	2.0
(Zr/Hf)	130,400	2.1	105,100	2.1	91,300	2.1	89,600	1.9	70,100	1.9
(Zr/CGCTi)	80,900	1.9	86,500	1.8	79,900	1.9	88,100	2.0	78,100	2.0

D. ADDITIONAL COPOLYMERIZATION RESULTS

Figs. D.1 and D.2 show CCD and MWD of copolymers produced at 40 °C, with 7.5 mL of 1-hexene and ethylene pressure of 150 psi. The trends observed are very similar to the ones at ethylene pressure of 100 psi. However, compared to Fig. 6.17 in Chapter 6, the CCD of copolymer produced with the combined catalyst in Fig. D.1 does not have the highly crystalline copolymer fractions (T_c > 80 °C). Judging from MWD in Fig. D.2, the fraction of copolymer produced with Cp_2HfCl_2 is significantly smaller than that produced with $Et[Ind]_2ZrCl_2$ because the contribution of the copolymers produced with Cp_2HfCl_2 to MWD of copolymer produced with the combined catalyst is small. Therefore, the small amount of highly crystalline fraction in the bimodal CCD of copolymer produced with Cp_2HfCl_2 becomes less obvious in the CCD of copolymer produced with the combined catalyst. However, the low crystalline fraction, which has significant amount of copolymer, causes the lower crystalline shoulder in the CCD of copolymers produced with the combined catalyst.

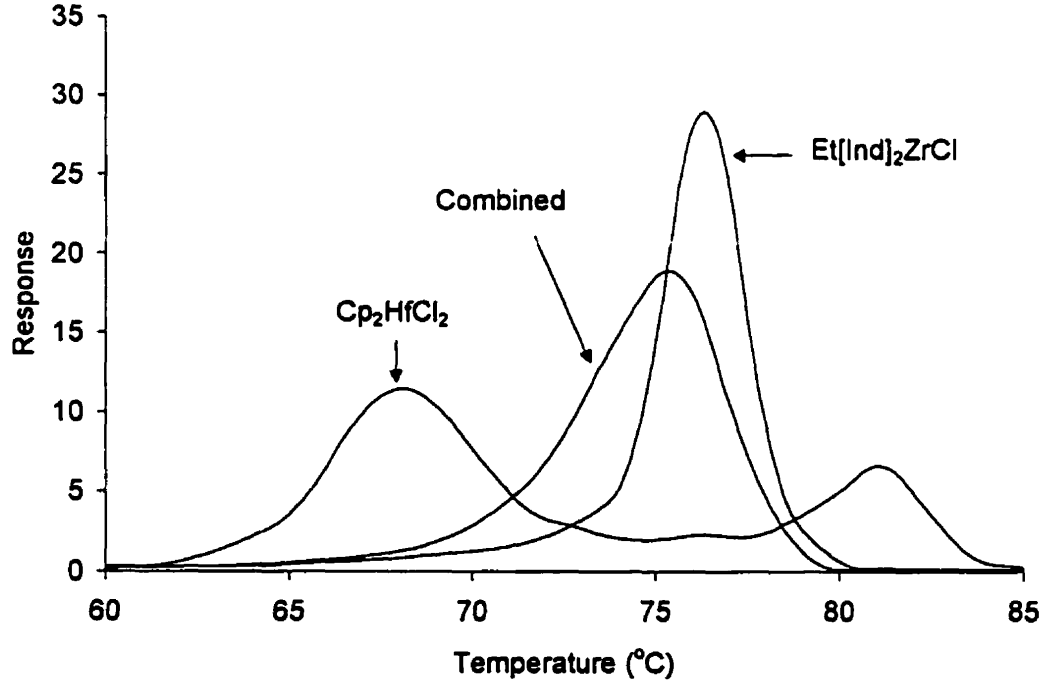

Figure D.1 CRYSTAF results of poly(ethylene-co-1-hexene) produced with a bimetallic supported catalyst ($Et[Ind]_2ZrCl_2$ / Cp_2HfCl_2), 40 °C, $P_{Ethylene}$ = 150 psi, 1-hexene = 7.5 mL

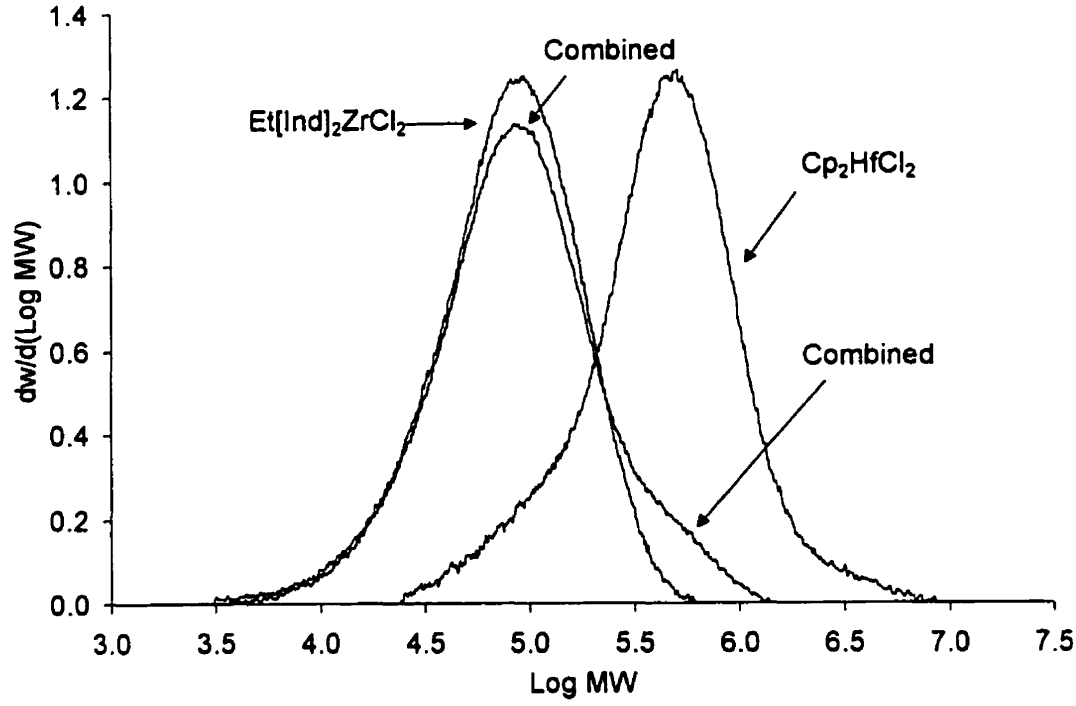

Figure D.2 GPC results of poly(ethylene-co-1-hexene) shown in Fig. D.1

Figs. D.3 and D.4 show CCD and MWD of copolymers produced at 50 °C, with 7.5 mL of 1-hexene and ethylene pressure of 150 psi. Compared to copolymer produced at 40 °C, the shapes of CCD and MWD are similar but less comonomer is incorporated. In Fig. D3, CCD of the copolymer produced with Cp_2HfCl_2 moves toward to higher crystalline region by about 5 °C compared to Fig. D.1, and CCD peak of the copolymer produced with the combined catalyst appears even at slightly higher crystalline region than that of the copolymer produced with $Et[Ind]_2ZrCl_2$.

From the results, it seems that the superposition of distributions in the combined catalyst for copolymerization is still valid. However, in the case of copolymer composition, there might be some bimolecular interaction of catalyst active sites, which causes slight deviations of the CCD in the combined catalyst compared to the individually supported catalyst. One important fact is that there can be significant batch to batch differences in the catalyst's ability to incorporate comonomer into the growing chain. Therefore, the deviation might be caused only by experimental variations during the supporting procedures for each catalyst system.

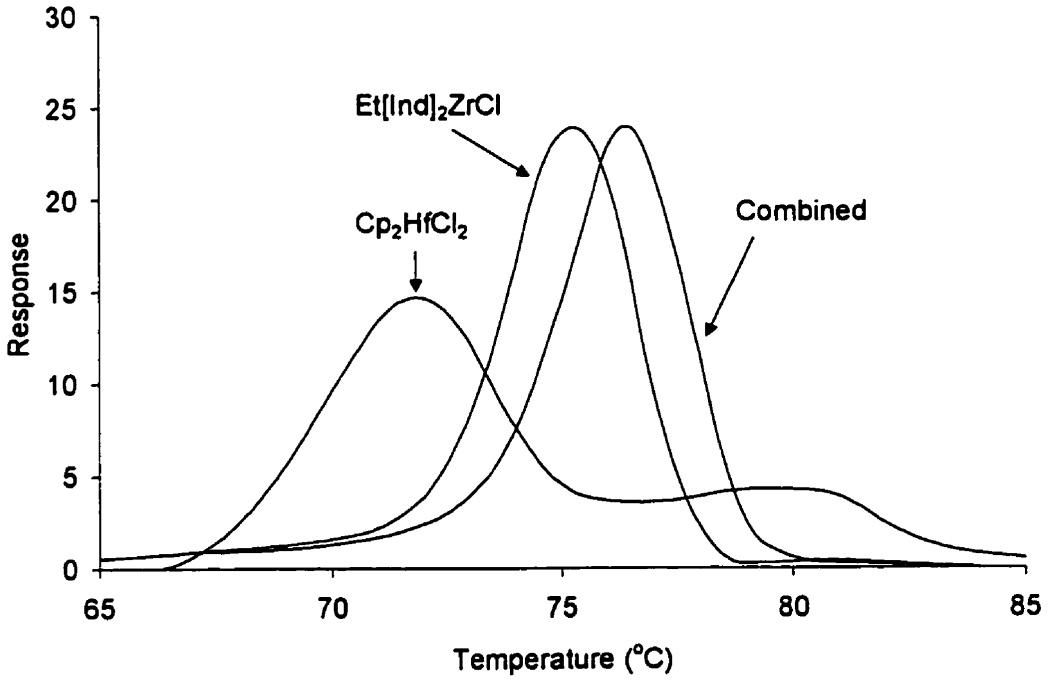

Figure D.3 CRYSTAF results of poly(ethylene-co-1-hexene) produced with a bimetallic supported catalyst ($Et[Ind]_2ZrCl_2$ / Cp_2HfCl_2), 50 °C, $P_{Ethylene}$ = 150 psi, 1-hexene = 7.5 mL

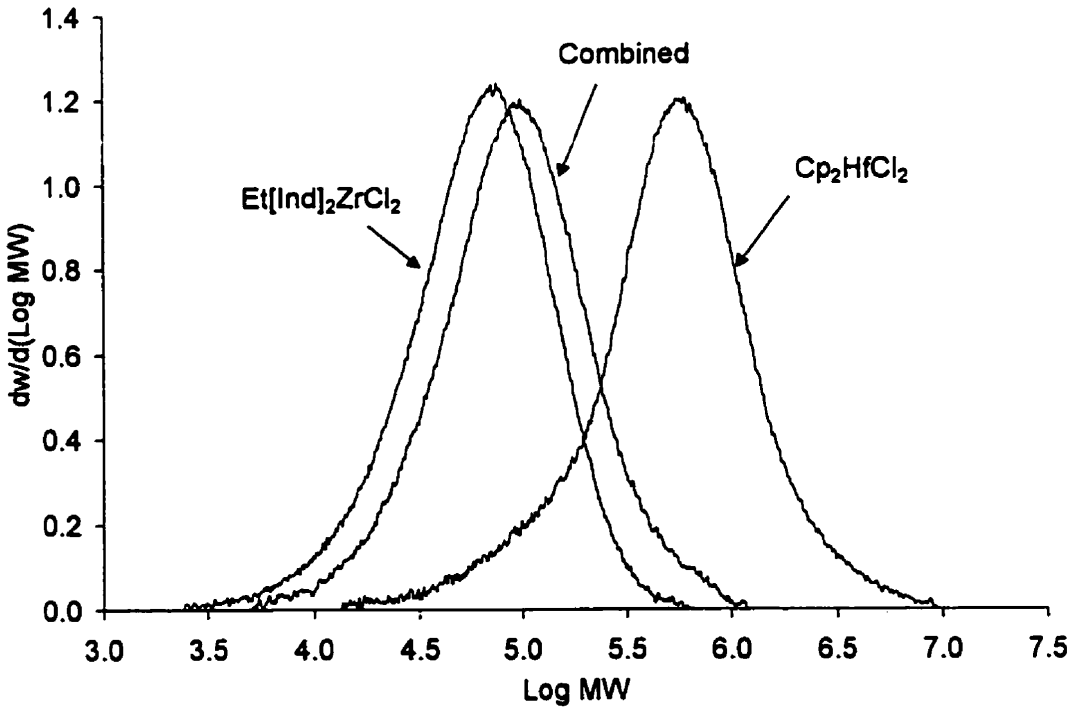

Figure D.4 GPC results of poly(ethylene-co-1-hexene) produced shown in Fig. D.3

E. ^{13}C-NMR ANALYSIS

Table E.1 ^{13}C-NMR chemical shift and assignments (Randall, 1989) for ethylene/1-hexene copolymers with isotactic 1-hexene sequences

Chemical Shift (ppm)	Sequence Assignment
38.13	EHE
35.85	EHH + HHE (m)
35.37	HHH (mm)
35.00	HHEH + HEHH (mm) EHEH + HEHE (m)
34.90	HHEE + EEHH EHH + HHE (mm)
34.54	EHEE + EEHE
34.13	EHE
33.57	HHH (mm)
30.94	HEEH
30.47	HEEE + EEEH
29.98	$(EEE)_n$
29.51	EHE
29.34	EHH + HHE (m)
29.18	HHH (mm)
27.28	EHEE + EEHE
27.09	HHEE + EEHH (m)
24.53	EHEHE (m)
24.39	EHEHH + HHEHE (mm)
24.25	HHEHH (mmm)
23.37	EHE + EHH + HHE + HHH
14.12	EHE + EHH + HHE + HHH

E : Ethylene
H : 1-Hexene
m : isotactic meso dyads of the pairs of adjacent monomer units

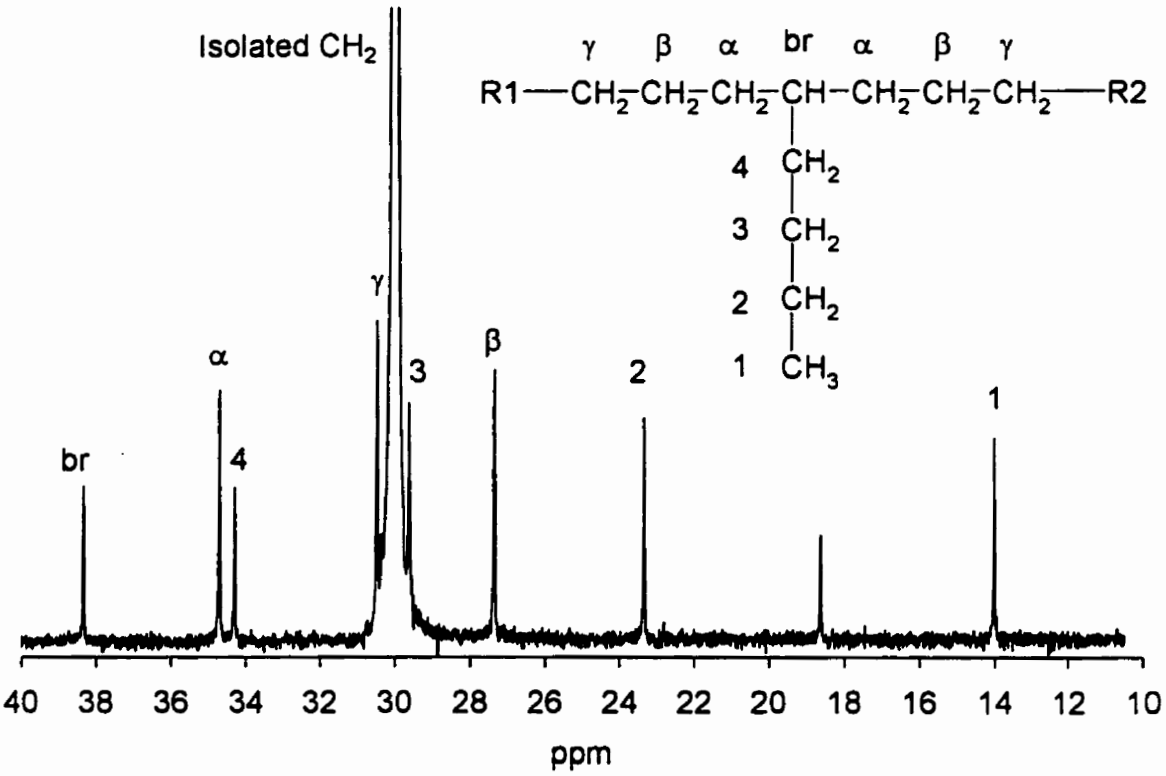

Figure E.1 ^{13}C-NMR spectrum of polymer produced with Et[Ind]$_2$ZrCl$_2$ at 50 °C under 100 psi ethylene pressure with 5 mL of 1-hexene

F. SIMULATION FLOW CHART

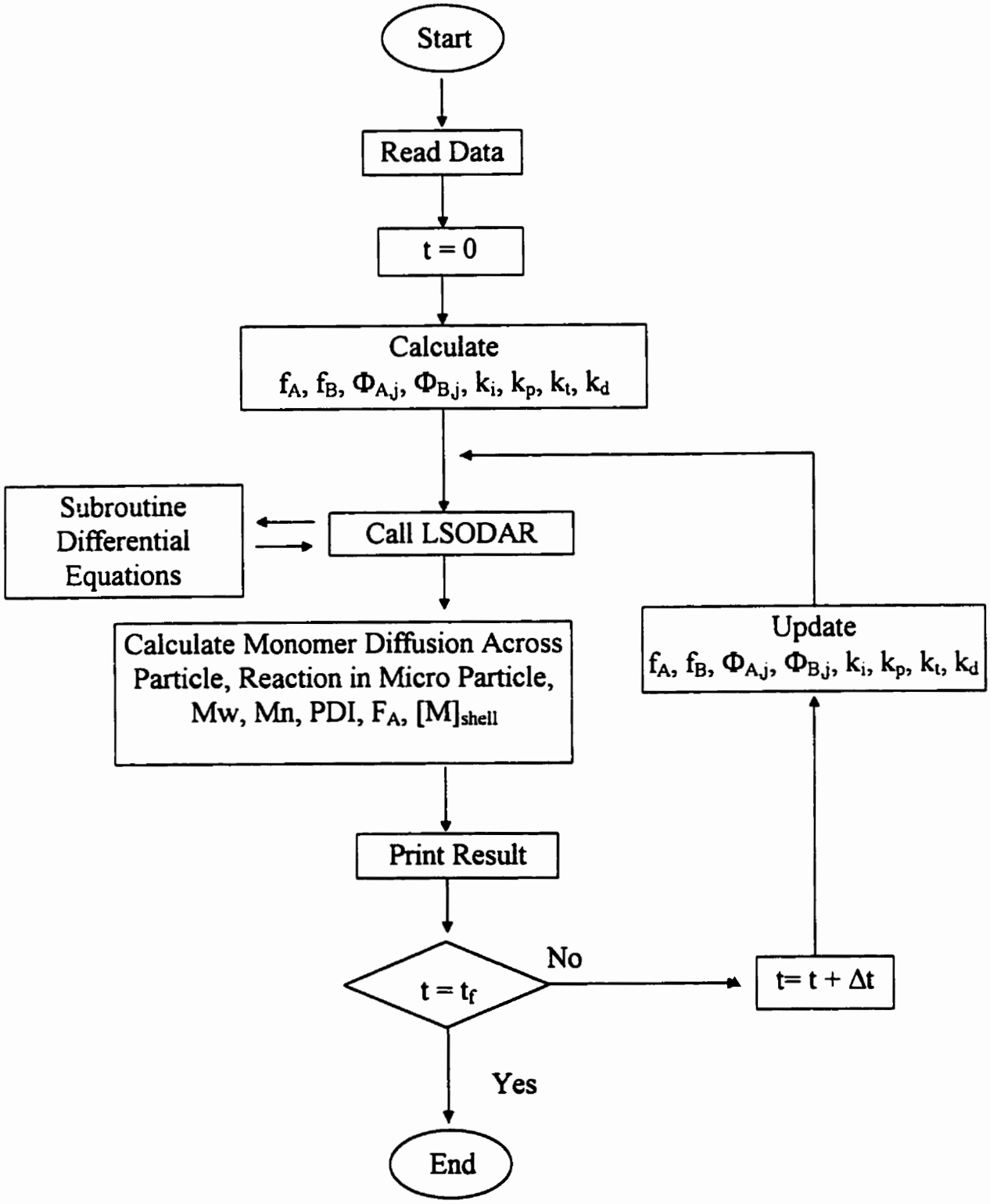

NOMENCLATURE

ε_l	:	porosity of macroparticle
ε_s	:	porosity of microparticle
Φ_A	:	fraction of living polymer chains terminating in monomer A
Φ_B	:	fraction of living polymer chains terminating in monomer B
a_s	:	surface area of growing polymer particle
$C_\bullet^i$	:	active catalyst center of site type *i*
C_d	:	deactivated catalyst
D_L	:	diffusivity in macroparticle
D_r	:	dead polymer of chain length r
D_S	:	diffusivity in microparticle
F_A	:	mole fraction of monomer A in the copolymer
f_A	:	mole fraction of monomer A in the reactor
F_B	:	mole fraction of monomer B in the copolymer
f_B	:	mole fraction of monomer B in the reactor
k_d	:	overall deactivation rate constant
$k_{d,A}$	:	deactivation rate constant for living polymer chain ending with monomer A
$k_{d,B}$	:	deactivation rate constant for living polymer chain ending with monomer B
k_i	:	overall initiation rate constant
$k_{i,A}$	:	initiation rate constant for monomer A
$k_{i,B}$	:	initiation rate constant for monomer B
k_{ls}	:	mass transfer rate constant between bulk liquid phase and polymer particle
k_p	:	overall propagation rate constant
$k_{p,AA}$	:	propagation rate constant between chain ending with A and monomer A
$k_{p,AB}$	:	propagation rate constant between chain ending with A and monomer B
$k_{p,BA}$	:	propagation rate constant between chain ending with B and monomer A
$k_{p,BB}$	:	propagation rate constant between chain ending with B and monomer B
k_t	:	overall transfer rate constant
$k_{t,A}$	:	transfer rate constant for living polymer chain ending with monomer A

$k_{t,B}$: transfer rate constant for living polymer chain ending with monomer B

M : monomer concentration

M_{bulk} : monomer concentration in bulk diluent

$M(r,t)$: monomer concentration in microparticle at radius r and time t

M_n : number average molecular weight

M_w : weight average molecular weight

P_r : living polymer of chain length r

Q_p : heat of polymerization

R : radial position in polymer macroparticle

R_0 : radius of polymer macroparticle

T_c : crystallization temperature in CRYSTAF analysis

X_0' : 0^{th} moment of the distribution for dead polymer chains at site i

X_1' : 1^{st} moment of the distribution for dead polymer chains at site i

X_2' : 2^{nd} moment of the distribution for dead polymer chains at site i

Y_0' : 0^{th} moment of the distribution for living polymer chains at site i

Y_1' : 1^{st} moment of the distribution for living polymer chains at site i

Y_2' : 2^{nd} moment of the distribution for living polymer chains at site i

REFERENCES

Aaltonen, P. and J. Seppälä, **Copolymerization of styrene and ethylene with mono cyclopentadienyl titanium trichloride/MAO catalyst. Characterization of the product**, *Eur. Polym. J.*, **30**(6), 683-688, 1994

Addison, E., M.Ribeiro, A.Deffieux, and M.Fontanille, **Evaluation of the hetrogeneity in linear low-density polyethylene comonomer unit distribution by differential scanning calorimetry characterization of thermally treated samples**, *Polymer*, **33**(20), 4337-4342, 1992

Ahn, T.O., S.C.Hong, J.H.Kim, and D.Lee, **Control of molecular weight distribution in propylene polymerization with Ziegler-Natta/Metallocene catalyst mixtures**, *J. Appl. Polym. Sci.*, **67**, 2213-2222, 1998

Albano, C., G.Sánchez, and A.Ismayel, **Influence of a copolymer on the mechanical properties of a blend of PP and recycled and non-recycled HDPE**, *Polymer Bulletin*, **41**, 91-98, 1998

Arai, T., H.T.Ban, T.Uozumi, and K.Soga, **Syntheses of polysiloxane-supported zirconocene catalysts and application to ethene polymerization**, *Macromol. Chem. Phys.*, **198**, 229-237, 1997

Bailey, A.L., L.T.Kale, and W.J.Tchir, **Investigation of ethylene/1-octene copolymerization models by carbon-13 NMR**, *J. Appl. Polym. Sci.*, **51**, 547-554, 1994

Ban, H.T., T.Uozumi, and K.Soga, **Polymerization of olefins with a novel dinuclear ansa-zirconocene catalyst having a biphenyl bridge**, *J. Polym. Sci.: Polym. Chem.*, **36**, 2269-2274, 1998

Barron, A.R., **A new understanding of the co-catalytic activity of alumoxanes: the opening of a black box!**, *Macromol. Symp.*, **97**, 15-25, 1995

Beigzadeh, D., J.B.P.Soares, T.A.Duever, **Modeling of fractionation in CRYSTAF using Monte Carlo simulation of crystallizable sequence length: Ethylene/1-octene copolymers synthesized with single-site-type catalysts**, *J. Appl. Polym. Sci.*, Submitted, 1998

Bergström, C.H., T.L.J.Väänänen, and J.V.Seppälä, **Influence of polymerization conditions on microstructure of norbornene-ethylene copolymers made using metallocene catalysts and MAO**, *J. Appl. Polym. Sci.*, **63**, 1071-1076, 1997

Bonini, F., V.Fraaije, and G.Fink, **Propylene polymerization through supported metallocene/MAO catalysts: Kinetic analysis and modeling**, *J. Polym. Sci.: Polym. Chem.*, **33**, 2393-2402, 1995

Boor, J., Ziegler-Natta catalysts and polymerizations, Academic Press, New York, 1979

Borrajo, J., C.Cordon, J.M.Carella, S.Toso, and G.Goizueta, **Modeling the fraction process in TREF systems: Thermodynamic simple approach**, *J. Polym. Sci.: Polym. Phys.*, **33**, 1627-1632, 1995

Böhm, L.L., H.F.Enderle, and M.Fleissner, **The industrial synthesis of bimodal polyethylene grades with improved properties**, in Catalyst design for tailor-made polyolefins, K. Soga and M. Terano, Eds., Elsevier, Amsterdam-London-New York-Tokyo, 1994, p. 351

Brintzinger, H.H., D.Fischer, R.Mülhaupt, B.Rieger, and R.M.Waymouth, **Stereospecific olefin polymerization with chiral metallocene catalysts**, *Angew. Chem. Int. Ed. Engl.*, **34**, 1143-1170, 1995

Burkhard, E., and F.J.Karol, **Aspects of polymer growth with silica-supported polyethylene catalysts**, Conference proceeding, Society of Plastics Engineers, RETEC Meeting, Houston TX, USA, February 1989 p. 77

Cam, D. and U.Giannini, **Concerning the reaction of zirconocene dichloride and methylalumoxane: homogeneous Ziegler-Natta catalytic system for olefin polymerization**, *Makromol. Chem.*, **193**, 1049-1055, 1992

Chan, W. and C.A.O.Nascimento, **Use of neural networks for modeling of olefin polymerization in high pressure tubular reactors**, *J. Appl. Polym. Sci.*, **53**, 1277-1289, 1994

Chen, Y., M.D.Rausch, J.C.W.Chien, **Heptane-soluble zirconocene catalyst: synthesis of a single diastereomer, polymerization catalysts, and effect of silica support**, *J. Polym. Sci.: Polym. Chem.*, **33**, 2093-2108, 1995

Chiantore, O., P.Cinquina and M.Guaita, **Fractionation and molecular characterization of EPDM rubbers**, *Eur. Polym. J.*, **30**, 1043-1046, 1994

Chien, J.C.W. and D.He, **Olefin copolymerization with metallocene catalysts. III Supported metallocene/methylaluminoxane catalyst for olefin copolymerization**, *J. Polym. Sci.: Polym. Chem.*, **29**, 1603-1607, 1991

Chien, J.C.W., W.Song and M.D.Rausch, **Polymerization of propylene by zirconocenium catalysts with different counter-ions**, *J. Polym. Sci.: Polym. Chem.*, **32**, 2387-2394, 1994

Choi, K.Y., X.Zhao and S.Tang, **Population balance modelling for a continuous gas phase olefin polymerization reactor**, *J. Polym. Sci.: Polym. Chem.*, **53**, 1589-1597, 1994

Ciardelli, F., A.Altomare, G.Arribas, G.Conti, F.Masi, and F.Menconi, **Effect of ligand and inorganic support on polymerization performances of Ti and Zr catalyst**, Catalyst design for tailor-made polyolefins, K. Soga and M. Terano, Eds., Elsevier, Amsterdam-London-New York-Tokyo, 1994, p. 257

Cihlar, J., J.Mejzlik, and O.Hamrik, **Influence of water on ethylene polymerization catalyzed by titanocene systems**, *Makromol. Chem.*, **179**, 2553-2558, 1978

Cihlar, J., J.Mejzlik, O.Hamrik, P.Hudec, and J.Majer, **Polymerization of ethylene catalyzed by titanocene systems,1. Catalytic systems $Cp_2TiEtCl/AlEtCl_2$ and $Cp_2TiEtCl/(AlEtCl_2+H_2O)$**, *Makromol. Chem.* **181**, 2549-2561, 1980

Collins, S., W.M.Kelly, and D.A.Holden, **Polymerization of propylene using supported, chiral, ansa-metallocene catalysts: production of polypropylene with narrow molecular weight distributions**, *Macromolecules*, **25**, 1780-1785, 1992

Crank, J., The mathematics of diffusion, Oxford Science Publications, 1990

Dayal, U., **High-temperature SEC coupled with MALLS detector for evaluating the end-use performance of LDPE**, *J. Appl. Polym. Sci.*, **53**, 1557-1562, 1994

Defoor, F., G.Groeninckx, P.Schouterden, and B.Heijden, **Molecular, thermal and morphological characterization of narrowly branched fractions of 1-octene linear low-density polyethylene: 1. Molecular and thermal characterization**, *Polymer*, **33**, 3878-3883, 1992

Drushel, H.V. and F.A.Iddings, **Infrared spectrophotometric analysis of ethylene-propylene copolymers**, *Analytical Chem.*, **35**, 28-33,1963

Eisch, J.J., S.I.Pombrik, S.Gürtzgen, R. Rieger, and W.Uzick, **The role of ion-pair equilibria on the activity and stereoregularity of soluble metallocene Ziegler-Natta catalysts**, Catalyst design for tailor-made polyolefins, K. Soga and M. Terano, Eds., Elsevier, Amsterdam-London-New York-Tokyo, 1994, p. 221

Ernst, E., J.Reussner, and W.Neissl, **A new concept for supporting metallocenes**, MetCon '96, Houston, TX, USA, June 1996

Fierro, R., J.C.W.Chien and M.D.Rausch, **Asymmetric zirconocene precursors for catalysis of propylene polymerization**, *J. Polym. Sci.: Polym. Chem.*, **32**(15), 2817-2824, 1994

Floyd, S., T.Heiskanen, T.W.Taylor, G.E.Mann, and W.H.Ray, **Polymerization of olefins through heterogeneous catalysis. VI. Effect of particle heat and mass transfer on polymerization behavior and polymer properties**, *J. Appl. Polym. Sci.*, **33**, 1021-1065, 1987

Frauenrath, H., H.Keul, H.Höcker, **Polymerization of 1-hexene catalyzed by bis(cyclopentadienyl)zirconium dichloride/methylaluminoxane; effect of temperature on the molecular weight and the microstructure of poly(1-hexene)**, *Macromol. Rapid Commun.*, 19, 391-395, 1998

Galli, P., G.Collina, P.Sgarzi, G.Baruzzi, E.Marchetti, **Combining Ziegler-Natta and metallocene catalysis: New heterophasic propylene copolymers from the novel multicatalyst reactor granule technology**, *J. Appl. Polym. Sci.*, **66**, 1831-1837, 1997

Galvan, R. and M.Tirrell, **Molecular weight distribution predictions for heterogeneous Ziegler-Natta polymerization using a two-site model**, *Chem. Eng. Sci.*, **41**, 2385-2393, 1986

Giz A., **An error-in-variables method for use when the reactivity ratios in copolymerization are close to one**, *Macromol. Theory Simul.*, 7, 391-397, 1998

Han, T.K., B.W.Woo, J.T.Park, Y.Do, Y.S.Ko, and S.I.Woo, **Ethylene and propylene polymerization over chrial ansa-dichloro[o-phenylenedimethylenebis(5-1-indenyl)] zirconium**, *Macromolecules*, **28**, 4801-4805, 1995a

Han, T.K., H.K.Choi, D.W.Jeung, Y.S.Ko, and S.I.Woo, **Control of molecular weight and molecular weight distribution in ethylene polymerization with metallocene catalysts**, *Macromol. Chem. Phys.*, **196**, 2637-2647, 1995b

Harrison, D., I.M.Coulter, S.Wang, S.Nistala, B.A.Kuntz, M.Pigeon, J.Tian, and S.Collins, **Olefin polymerization using supported meallocene catalysts: development of high activity catalysts for use in slurry and gas phase ethylene polymerizations**, *J. Mole. Cat.: Chem.*, **128**, 65-77, 1998

Heiland, K. and W.Kaminsky, **Comparison of zirconocene and hafnocene catalysts for the polymerization of ethylene and 1-butene**, *Makromol. Chem.*, **193**, 601-610, 1992

Herfert, N., P.Montag, and G.Fink, **Elementary processes of the Ziegler catalysis, 7; Ethylene, α-olefin and norbornene copolymerization with the stereorigid catalyst systems iPr[FluCp]$ZrCl_2$/MAO and $Me_2Si[Ind]_2ZrCl_2$/MAO**, *Makromol. Chem.*, **194**, 3167-3182, 1993

Hlatky, G.G. and D.J.Upton, **Supported ionic metallocene polymerization catalysts**, *Macromolecules*, **29**, 8019-8020, 1996

Hoel, E.L., C.Cozewith, and G.D.Byrne, **Effect of diffusion on heterogeneous ethylene propylene copolymerization**, *AIChE J.*, **40**, 1669-1684, 1994

Hosoda, S., A.Uemura, Y.Shigematsu, I.Yamamoto, and K.Kojima, **Structure and properties of ethylene/α-olefin copolymers polymerized with homogeneous and heterogeneous catalysts**, Catalyst design for tailor-made polyolefins, K. Soga and M. Terano, Eds., Elsevier, Amsterdam-London-New York-Tokyo, 1994, p. 365

Huang, J., Ph.D. Thesis, University of Waterloo, Waterloo, Ontario, Canada, 1995

Hutshinson, R.A., C.M.Chen, and W.H.Ray, **Polymerization of olefins through heterogeneous catalysis. X : Modeling of particle growth and morphology**, *J. Appl. Polym. Sci.*, **44**, 1389-1414, 1992

Iiskola, E.I., S.Timonen, T.T.Pakkanen, O.Härkki, P.Lehmus, and J.V.Seppälä, **Cyclopentadienyl surface as a support for zirconimum polyethylene catalysts**, *Macromol.*, **30**, 2853-2859, 1997

Janiak, C., B.Rieger, R.Voelkel, and H.G.Braun, **Polymeric aluminoxanes : A possible cocatlytic support material for Ziegler-Natta-type metallocene catalyst**, *J. Polym. Sci.: Polym. Chem.*, **31**, 2959-2968, 1993

Janiak, C. and B.Rieger, **Silica gel supported zirconocene dichloride/MAO catalysts for ethylene polym. Effects of heterogenation of activity, polymer microstructure and product morphology**, *Angew. Makromol. Chem.*, **215**, 47-58, 1994

Janiak, C., T.G.Scharmamm, K.C.H.Lange, **Zirconium beta-diketonate/ methylaluminoxane systems as single-site catalysts for the preparation of high-molecular-weight polyethylene**, *Macromol. Rapid Commun.*, **15**, 655-658, 1994

Jin, J., T.Uozumi, and K.Soga, **Ethylene polymerization initiated by SiO_2-supported neodymocene catalysts**, *Macromol. Rapid Commun.*, **16**, 317-322, 1995

Jin, J., T.Uozumi, T.Sano, T.Teranishi, K.Soga, and T.Shiono, **Alternating copolymerization of ethylene and propene with the [ethylene(1-indenyl)(9-fluorenyl)]zirconium dichloride-methylaluminoxane catalyst system**, *Macromol. Rapid Commun.*, **19**, 337-339, 1998

Jüngline, S., R.Mülhaupt, U.Stephling, H.Brintzinger, D.Fischer, and F.Langhauser, **Propene polymerization using homogeneous MAO- activated metallocene catalysts: $Me_2Si(Benz[e]Indenyl)_2ZrCl_2$/MAO vs. $Me_2Si(2\text{-}Me\text{-}Benz[2]\ Indenyl)_2ZrCl_2$/MAO**, *J. Polym. Sci.: Polym. Chem.*, **33**, 1305-1317, 1995

Kamfjord, T., T.S.Wester, and E.Rytter, **Supported metallocene catalysts prepared by impregnation of MAO modified silica by a metallocene/monomer solution**, *Macromol. Rapid Commun.*, **19**, 505-509, 1998

Kaminaka, M. and K.Soga, **Polymerization of propene with the catalyst systems composted of Al_2O_2- or $MgCl_2$-supported $Et[IndH_2]_2ZrCl_2$ and AlR_2 ($R=CH_2$, C_2H_2)**, *Makromol. Chem., Rapid Commun.*, **12**, 367-372, 1991

Kaminaka, M. and K.Soga, **Polymerization of propene with catalyst systems composed of Al_2O_2 or $MgCl_2$ supported zirconocene and $Al(CH_2)_2$**, *Polymer*, **33**(5), 1105-1107, 1992

Kaminsky, W. and F.Renner, **High melting polypropenes by silica-supported zirconocene catalysts**, *Makromol. Chem., Rapid Commun.*, **14**, 239-243, 1993

Kaminsky, W, F.Renner, and H.Winkelbach, **High melting polypropylene by supported metallocene catalysts**, Proc. Worldwide Metallocene Conference - MetCon '94, Houston, TX, USA, May 1994

Kaminsky, W., **How to reduce the ratio MAO/metallocene**, *Macromol. Symp.*, **97**, 79-89, 1995

Kashiwa, N., Feature of metallocene-catalyzed polyolefins, , Catalyst design for tailor-made polyolefins, K. Soga and M. Terano, Eds., Elsevier, Amsterdam-London-New York-Tokyo, 1994, p. 381

Katayama, H., H.Shiraishi, T.Hino, T.ogane, and A.Imai, **The effect of aluminium compounds in the copolymerization of ethylene/α-olefins**, *Macromol. Symp.*, **97**, 109-118, 1995

Kim, J.D., J.B.P.Soares, G.L.Rempel, and B.Monrabal, **Control of molecular weight and chemical composition distributions of polyolefins with supported metallocene catalysts**, *MetCon'97:Polymers in Transition*, Houston, TX, June 1997

Kim, J.D., J.B.P.Soares, and G.L.Rempel, **Use of hydrogen for the tailoring of the molecular weight distribution of polyethylene in bimetallic supported metallocene catalyst system**, *Macromol. Rapid Commun.*, **19**, 197-200, 1998

Kim, J.D., J.B.P.Soares, and G.L.Rempel, **Synthesis of tailor-made polyethylene through the control of polymerization conditions using selectively combined metallocene catalysts in a supported system**, *J. Polym. Sci.: Polym. Chem.*, **37**, 331-339, 1999a

Kim, J.D. and J.B.P.Soares, **Copolymerization of ethylene and 1-hexene with supported metallocene catalysts: effect of support treatment**, *Macromol. Rapid Commun.*, Accepted, 1999b

Kim, Y, C.Kim, J.Park, J.Kim, and T.Min, **Short chain branching distribution and thermal behavior of high density polyethylene**, *J. Appl. Polym. Sci.*, **60**, 2469-2479, 1996

Kissin, Y.V., **Ethylene polymerization kinetics with heterogeneous Ziegler-Natta catalysts**, Makromol. Chem., *Macromol. Symp.*, **66**, 83-94, 1993

Ko, Y.S., T.K.Han, J.W.Park, and S.I.Woo, **Propene polymerization catalyzed over MCM-41 and VPI-5-supported $Et[Ind]_2ZrCl_2$ catalysts**, *Macromol. Rapid Commun.*, **17**, 749-758, 1996

Koivumäki, J., M.Lahti, and J.V.Seppälä, **Polymerization of ethylene and 1-hexene with Cp_2ZrCl_2/methylaluminoxane catalyst in a heat balance reaction calorimeter,** *Angew. Makromol. Chem.*, **221**, 117-125, 1994

Langhauser, F., J.Kerth, M.Kersting, P.Kolle, D.Lilge, and P.Muller, **Propylene polymerization with metallocene catalysts in industrial processes,** *Angew. Makromol. Chem.*, **223**, 155-164, 1994

Lee, I.M., W.J.Gauthier, J.M.Ball, B.Iyengar, and S.Collins, **Electronic effects in Ziegler-Natta polymerization of propylene and ethylene using soluble metallocene catalysts,** *Organometallics*, **11**, 2115-2122, 1992

Lee, D. and K.Yoon, **Ethylene polymerization initiated with the Cp_2ZrCl_2-MAO catalyst system supported on -cyclodextrin,** *Macromol. Rapid Commun.*, **15**, 841-844, 1994

Lee, D., S.Shin, and D.Lee, **Ethylene polymerization with metallocene and trimethylaluminum-treated silica,** *Macromol. Symp.*, **97**, 195-203, 1995

Lee, D, K.Yoon, and S.Noh, **Polymerization of ethylene by using zirconocene catalyst anchored on silica with trisiloxane and pentamethylene spacers,** *Macromol. Rapid Commun.*, **18**, 427-431, 1997

Lee, T., S.Nitirahardjo, and S.Lee, **An analytic approach in kinetic modelling of Ziegler-Natta polymerization of butadiene,** *J. App. Polym. Sci.*, **53**, 1605-1613, 1994

Mara, J.J. and K.P.Menard, **Characterization of linear low density polyethylene by temperature rising elution fractionation and by differential scanning calorimetry,** *Acta polymer.*, **45**, 378-380, 1994

McKenna, T.F., J.Dupuy, and R.Spitz, **Modeling of transfer phenomena on heterogeneous Ziegler catalysts. III. Modeling of intraparticle mass transfer resistance,** *J. Appl. Polym. Sci.*, **63**, 315-322, 1997

McKenna, T.F. and D.Schwelch, **Copolymerization of olefins on Ziegler-type catalysts: Heat and mass transfer during particle growth,**

Michiels, W. and A.Munoz-Escalona, **Mixed cocatalyst systems in metallocene ethylene polymerization,** *Macromol. Symp.*, **97**, 171-183, 1995

Monrabal, B., J.Blanco, J.Nieto, and J.B.P.Soares, **Characterization of homogeneous ethylene/1-octene copolymers made with a single-site catalyst. CRYSTAF analysis and calibration**, *J. Polym. Sci.: Polym. Chem.*, **37**, 89-93, 1999

Montagna, A.A., **Designed polyolefins**, *Chemtech*, October, 44-47, 1995

Mori, H., M.Yamahiro, K.Tashino, K.Ohnishi, K.Nitta, and M.Terano, **Synthesis of polypropene-block-poly(ethylene-co-propene) by short-period polymerization with $MgCl_2$-supported Ziegler catalyst**, *Macromol. Rapid Commun.*, **16**, 247-252, 1995

Mori, H., K.Tashino, and M.Terano, **Study of the chain transfer reaction by hydrogen in the I stage of propene polymerization**, *Macromol. Rapid Commun.*, **16**, 651-657, 1995

Naga, N., K.Mizunuma, **Effect of co-catalyst system on α-olefin polymerization with rac- and meso-[dimethylsilylenebis(2,3,5-trimethyl-cyclopentadienyl)]Zirconium dichloride**, *Macromol. Rapid Commun.*, **18**, 581-589, 1997

Nishida, H., U.Toshiya, T.Arai, and K.Soga, **Polystyrene-supported metallocene catalysts for olefin polymerizations**, *Macromol. Rapid Commun.*, **16**, 821-830, 1995

Nowlin, T.E., Y.V.Kissin, and K.P.Wagner, **High activity Ziegler-Natta catalysts for the preparation of ethylene copolymers**, *J. Polym. Sci.: Polym. Chem.*, **26**, 755-764, 1988

Pasynkiewicz, S., **Some reactions of alumoxanes**, *Macromol. Symp.*, **97**, 1-13, 1995

Pieters, P.J.J., J.A.M.Beek, and M.F.H.Tol, **A method for the prediction of metallocene-type catalyst activity in olefin (co)polymerisation reactions**, *Macromol. Rapid Commun.*, **16**, 463-467, 1995

Pietikainen, P. and J.V.Seppälä, **Low molecular weight ethylene/propylene copolymers. Effect of process parameters on copolym. with homogeneous Cp_2ZrCl_2 catalyst**, *Macromolecules*, **27**(6), 1325-1329, 1994

Podzimek, S., **The use of GPC coupled with a multiangle laser light scattering photometer for the characterization of polymers. On the determination of molecular weight, size, and branching**, *J. Appl. Polym. Sci.*, **54**, 91-103, 1994

Pooter, M, P.B.Smith, K.K.Dohrer, K.F.Bennett, M.D.Meadows,C.G.Smith, H.P.Schouwenaars, and R.A.Geerards, **Determination of the composition of common**

linear low density polyehtylenen copolymers by ^{13}C-NMR spectroscopy, *J. Appl. Polym. Sci.*, **42**, 399-406, 1991

Quijada, R., J.Dupont, D.C.Silveira, M.S.L.Miranda, and R.B.Scipioni, **The influence of the transition metal and the heteroatomicbridge on the action of metallocene/methyl aluminoxane catalysts in ethylene polymerization and on the properties of the polymer**, *Macromol. Rapid Commun.*, **16**, 357-362, 1995

Quijada, R., R.Rojas, L.Alzamora, J.Retuert, and F.M.Rabagliati, **Study of metallocene supported on porous and nonporous silica for the polymerization of ethylene**, *Catalysis letters*, **46**, 107-112, 1997

Randall, J.C., **A review of high resolution liquid 13Carbon nuclear magnetic resonance characterizations of ethylene-based polymers**, *JMS-Rev. Macromol. Chem. Phys.*, **C29**, 201-317, 1989

Reddy, S.S. and S.Sivaram, **Homogeneous metallocene-methylaluminoxane catalyst systems for ethylene polymerization**, *Prog. Polym. Sci.*, **20**, 309-367, 1995

Repo, T., M.Klinga, P.Pietikäinen, M.Leskelä, A.Uusitalo, T.Pakkanen, K.Hakala, P.Anltonen, and B. Löfgren, **Ethylenebis(salicylideneiminato)zirconium dichloride: Crystal structure and use as a heterogeneous catalyst in the polymerization of ethylene**, *Macromolecules*, **30**, 171-175, 1997

Ribeito, M.R., A.Deffieus, and M.F.Portela, **Supported metallocene complexes for ethylene and propylene polymerizations: preparation and activity**, *Ind. Eng. Chem. Res.*, **36**, 1224-1237, 1997

Rieger, B. and C.Janiak, **Concentration effects of methylalumoxane, zirconocene dichloride and trimethyl-aluminum in ethylene polymerization**, *Angew. Makromol. Chem.*, **215**, 35-46, 1994

Rincon-Rubio, L.M., C.E.Wilen, and L.E.Lindfors, **A kinetic model for the polymerization of propylene over a Ziegler-Natta catalyst**, *Eur. Polym. J.*, **26**, 171-176, 1990

Roos, P., G.B. Meier, J.J.C. Samson, G. Weickert, K.R. Westerterp, **Gas phase polymerization of ethylene with a silica supported metallocene catalyst: influence of temperature on deactivation**, *Macromol. Rapid Commun.*, **18**, 319-324, 1997

Sacchi, M.C., D.Zucchi, I.Tritto, P.Locatelli, and T.dall'Occo, **Silica-supported metallocenes : Stereochemical comparison between homogeneous and heterogeneous catalysis**, *Macromol. Rapid Commun.*, **16**, 581-590, 1995

Sau, M. and S.K.Gupta, **Modeling of a semibatch polypropylene slurry reactor**, *Polymer*, **34**(21), 4417-4426, 1993

Santos, J.H.Z., S.Dorneles, F.C.Stedile, J.Dupont, M.M.C.Forte, and I.J.R.Baumvol, **Silica supported zirconocenes and Al-based cocatalysts: surface metal loading and catalytic activity**, *Macromol. Chem. Phys.*, **198**, 3529-3537, 1997

Satyanarayana, G. and S.Sivaram, **An unusually stable supported bis(cyclopentadienyl)titanium dichloride-trialkyaluminum catalyst system for ethylene polymerization**, *Macromolecules*, **26**, 4712-4714, 1993

Scheirs, J., L.L.Böhm, J.C.Boot, and P.S.Leevers, **PE100 resins for pipe applications: continuing the development into 21st century**, *Trends in Polym. Sci.*, **4**(12), 408-415, 1996

Seborg, D.E., T.F. Edgar, and D.A. Mellichamp, Process Dynamics and Control, John Wiley & Sons Inc., New York, Chichester, Brisbane, Toronto, Singapore, 1989

Siedle, A.R., W.M.Lamanna, R.A.Newmark, J.Stevens, D.E.Richardson, and M.Ryan, **The role of non-coordinating anions in homogeneous olefin polymerization**, *Makromol. Chem., Macromol. Symp.*, **66**, 215-224, 1993

Soares, J.B.P, Dynamic mathematical modeling of polymerization of olefins using heterogeneous and homogeneous Ziegler-Natta catalysts, Ph.D. Thesis, McMaster University, Hamilton, Ontario, Canada, 1994

Soares, J.B.P. and A.E.Hamielec, **Deconvolution of chain-length distributions of linear polymers made by multiple-site-type catalysts**, *Polymer*, **36**(11), 2257-2263, 1995a

Soares, J.B.P. and A.E.Hamielec, **Temperature rising elution fractionation of linear polyolefins**, *Polymer*, **36**(8), 1639-1654, 1995b

Soares, J.B.P. and A.E.Hamielec, **Analyzing TREF data by Stockmayer's bivariate distribution**, *Macromol. Theory Simul.*, **4**, 305-32, 1995c

Soares, J.B.P., R.F.Abbott, J.N.Willis, and X.Liu, **A new methodology for studying multiple-site-type catalysts for the copolymerization of olefins**, *Macromol. Chem. Phys.*, **197**, 3383-3396, 1996

Soares, J.B.P., J.D.Kim, and G.L.Rempel, **Analysis and control of molecular weight and chemical composition distributions of polyolefins made with metallocene and Ziegler-Natta catalysts**, *Ind. Eng. Chem. Res.*, **36**, 1144-1150, 1997

Soares, J.B.P., and J.D. Kim, **Manufacturing of polyolefins with combined metallocene catalysts**, *SPO'98, The 8th International Business Forum on Specialty Polyolefins*, Houston, TX, September 1998

Soares, J.B.P., J.D.Kim, and G.L.Rempel, **Analysis and control of the molecular weight distribution of polyethylene made with a two-site-type metallocene catalyst**, *AIChE Spring Meeting*, New Orleans, LA, March 1998

Soga, K. and M.Kaminaka, **Polymerization of propene with the heterogeneous catalyst system Et[IndH$_4$]$_2$ZrCl$_2$/MAO/SiO$_2$ combined with trialkylaluminium**, *Makromol. Chem., Rapid Commun.*, **13**, 221-224, 1992

Soga, K., H.J.Kim, and T.Shiono, **Polymerization of ethylene with homogeneous metallocene catalysts activated by common trialkylaluminiums and Si(CH$_3$)$_3$OH**, *Makromol. Chem., Rapid Commun.*, **14**, 765-770, 1993

Soga, K. and M.Kaminaka, **Copolymerization of olefins with SiO$_2$-, Al$_2$O$_3$-, and MgCl$_2$-supported metallocene catalysts activated by trialkylaluminiums**, *Macromol. Chem. Phys.*, **195**, 1369-1379, 1994

Soga, K., H.J.Kim, and T.Shiono, **Highly isospecific SiO$_2$-supported zirconocene catalyst activated by ordinary alkylaluminiums**, *Macromol. Rapid Commun.*, **15**, 139-144, 1994

Soga, K., T.Uozumi, and N.Kishi, **A metallocene catalyst system for olefin polymerization using a heteropolyacid as the counter-anion**, *Macromol. Rapid Commun.*, **16**, 793-798, 1995a

Soga, K., T.Uozumi, T.Arai, and S.Nakamura, **Heterogeneity of active species in metallocene catalysts**, *Macromol. Rapid. Commun.*, **16**, 379-385, 1995b

Soga, K., T.Arai, H. Nozawa, and T.Uozumi, **Recent development in heterogeneous metallocene catalysts**, *Macromol. Symp.*, **97**, 53-62, 1995c

Soga, K., T.Arai, B.T.Hoang, and T.Uozumi, **Olefin polymerization with metallocene catalysts supported on polysiloxane derivatives**, *Macromol. Rapid Commun.*, **16**, 905-911, 1995d

Spaleck, W., F.Kuber, A.Winter, J.Rohrmann, B.Bachmann, M.Antberg, V.Dolle, and E.F.Paulus, **The influence of aromatic substituents on the polymerization behavior of bridged zirconocene catalysts**, *Organometallics*, **13**, 954-963, 1994

Spaleck, W., M.Aulbach, B.Bachmann, F.Kuber, and A.Winter, **Stereospecific metallocene catalysts: Scope and limits of rational catalyst design**, *Macromol. Symp.*, **89**, 237-247, 1995

Starck P., **Studies of the comonomer distributions in low density polyethylenes using temperatre rising elution fraction and stepwise crystallization by DSC**, *Polymer International*, **40**, 111-122, 1996

Steinmetz, B, B.Tesche, C.Przybyla, J.Zechlin, and G.Fink, **Polypropylene growth on silica-supported metallocene catalysts: A microscopic study to explain kinetic behavior especially in early polymerization stages**, *Acta Polymer.*, **48**, 392-399, 1997

Stevens, J., **Insite™ catalysts structure/activity relationships for olefin polymerization**, Catalyst design for tailor-made polyolefins, K. Soga and M. Terano, Eds., Elsevier, Amsterdam-London-New York-Tokyo, 1994, p. 277

Subramanian, P.S. and K.J.Chou, **Molecular-modeling studies of the metallocene-catalyzed polymerization reaction, Reviews**, *Trend in Polym. Sci.*, **3**(10), 324-329, 1995

Sun, L, A.Shariati, J.C.Hsu, and D.W.Bacon, **A new polymer-supported catalysts for olefin polymerization**, Catalyst design for tailor-made polyolefins, K. Soga and M. Terano, Eds., Elsevier, Amsterdam-London-New York-Tokyo, 1994, p. 81

Swogger, K.W., **Novel molecular structure opens up new applications for Insite® based polymers**, Catalyst design for tailor-made polyolefins, K. Soga and M. Terano, Eds., Elsevier, Amsterdam-London-New York-Tokyo, 1994, p. 285

Tait, P.J.T. and M.G.K.Monteiro, **Comparative studies on ethylene polymerization using homogeneous and supported metallocene catalysts**, MetCon'95, Houston, TX, USA, May 1995

Tait, P.J.T., M.G.K.Monteiro, M.Yang, and J.L.Richardson, **Some recent advances in supported metallocene catalysts**, MetCon '96, Houston, TX, USA, June 1996

Thorshaug, K. E.Rytter, and M.Ystenes, **Pressure effects on termination mechanisms during ethene polymerization catalyzed by dicyclopentadienylzirconium dichloride/methylaluminoxane**, *Macromol. Rapid Commun.*, **18**, 715-722, 1997

Wagner, B.E. and F.J.Karol, **Aspects of polymer growth with silica-supported polyethylene catalysts**, Society of Plastics Engineers RETEC Meeting, Huston, Texas, 77-92, February, 1989

Wang, L., L.X.Feng, J.T.Xu, and S.L.Yang, **Studies on $VOCl_3/MgCl_2/Nay/Al_2Et_3Cl_3$ complex support catalysts for the copolymerization of ethylene and propylene**, *J. Appl. Polym. Sci.*, **54**, 1403-1408, 1994

Weisz, P.B. and C.D.Prater, *Adv. Catal.*, **6**, 143, 1954

Woo, S.I., Y.S.Ko, and T.K.Han, **Polymerization of ethylene over metallocenes confined inside the supercage of NaY zeolite**, *Macromol. Rapid Commun.*, **16**, 489-494, 1995

Xu, J., Y.Deng, L.Feng, C.Cui, and W.Chen, **Temperature Rising Elution Fractionation of syndiotactic polypropylene prepared by homogeneous and supported metallocene catalysts**, *Polym. J.*, **30**, 824-827, 1998

Ystenes, M., *Makromol. Chem., Macromol. Symp.*, **66**, 71, 1993

Yoon, J.S., H.S.Yoo, and K.S.Kang, **Solubility of α-olefins in linear low density polyethylenes**, *Eur. Polym. J.*, **32**(11), 1333-1336, 1996